Tweaking Epigenetics in EMT Signaling Regulation of Triple-Negative Breast Cancer Cells

A Thesis

Submitted in Partial Fulfilment of the Requirements for the award of the degree of

DOCTOR OF PHILOSOPHY

by

Shilpi Sarkar

(Roll No. - 196106022)

Indian Institute of Technology Guwahati

Department of Biosciences and Bioengineering

Indian Institute of Technology Guwahati

Guwahati, 781039, Assam, India

December 2024

TH-3600_196106022

TH-3600_196106022

Dedicated to my Family

TH-3600_196106022

TH-3600_196106022

DECLARATION

I hereby declare that the results and discussions embodied in the thesis titled **"Tweaking Epigenetics in EMT Signaling Regulation of Triple-Negative Breast Cancer Cells"** are the outcome of research work carried out by me under the supervision of Prof. Siddhartha Sankar Ghosh, Department of Biosciences & Bioengineering, Indian Institute of Technology Guwahati, Guwahati, Assam, India for the award of the degree of Doctor of Philosophy. To the best of my knowledge and belief, the present thesis has not been submitted for any degree, diploma, associateship etc. of any Institute or University elsewhere.

Date: 06.12.2024
Place: Guwahati

Shilpi Sarkar
Roll number: 196106022

TH-3600_196106022

TH-3600_196106022

INDIAN INSTITUTE OF TECHNOLOGY GUWAHATI

Department of Biosciences and Bioengineering

CERTIFICATE

This is to certify that this thesis entitled **"Tweaking Epigenetics in EMT Signaling Regulation of Triple-Negative Breast Cancer Cells"** has been submitted by **Shilpi Sarkar** (Roll No. 196106022) to Indian Institute of Technology Guwahati for the award of the degree of Doctor of Philosophy. This thesis is a record of the bonafide research work carried out by her during her degree tenure. The findings presented here are purely derived from her own research work. She has meticulously performed the research and has been ardently adherent of lab protocols. This work in parts or as a whole is novel and is not been produced in any previous diploma or degree.

Date: 06.12.2024
Place: Guwahati

Prof. Siddhartha Sankar Ghosh
(Thesis Supervisor)

TH-3600_196106022

TH-3600_196106022

ACKNOWLEDGEMENT

Pursuing a doctoral degree is a journey filled with challenges, learning, and immense personal growth, and it would not have been possible without the support and encouragement of many individuals. It gives me immense pleasure to take this opportunity to express my heartfelt gratitude to all those who have been a part of this journey.

First and foremost, I would like to express my heartfelt gratitude to my supervisor, Prof. Siddhartha Sankar Ghosh, for giving me the opportunity to join his lab and for ensuring access to all the necessary facilities to carry out my research work. His constant encouragement, thoughtful guidance, and insightful advice have been invaluable, profoundly shaping not only this thesis but also in fostering my growth as a researcher.

I am also enormously grateful to my doctoral committee members- Dr. Biplab Bose, Dr. Priyadarshi Satpati and Dr. Lal Mohan Kundu for providing me critical inputs in every stage. I am grateful to the Department of Biosciences and Bioengineering, Centre for Nanotechnology, DBT Program Support Facility and Param Ishan, IIT Guwahati, for providing me with all the facilities required to conduct my thesis work.

I am heavily indebted to my senior lab members- Dr. Anil P. Bidkar, Dr. Srirupa Bhattacharya, Dr. Rajib Shome, Dr. Anitha T. Simon, Dr. Muktashree Saha, Dr. Debashree Debasmita, Dr. Plaboni Sen, Dr. Konika Choudhury, and Dr. Arupam Patra for sharing their gathered knowledge and experience with me.

My heartfelt thanks to my lab members, Thiru, Arisha, Hirak, Sayantani, Sawna, Sujisha, Basab, Sayantani, Dheepika, Pijush, Haseena, and Pratik, for their support, and teamwork that made this journey not only productive but also memorable. A special mention goes to Thiru and Arisha for always being there for me and providing constant encouragement. I feel incredibly fortunate to have found wonderful friends like Thiru, Surabhi, Payal, and Satyam, whose friendship has been a source of immense joy and comfort throughout this journey.

TH-3600_196106022

I owe my deepest gratitude to my parents, whose unconditional love, sacrifices, and blessings have been the foundation of everything I have achieved. My sisters, Suity and Kakoli, have been my constant cheerleaders, and I am forever grateful for their support and belief in me.

Finally, I would like to thank Dheerendra, for his endless patience, understanding, and encouragement throughout this journey. His love and support have been a source of strength during the challenging times. Moreover, I am deeply grateful to Almighty God for providing me with the blessings and strength needed to accomplish this achievement.

- Shilpi Sarkar

TH-3600_196106022

Table of Contents

TH-3600_196106022

TH-3600_196106022

TH-3600_196106022

Abstract

Triple-negative breast cancer (TNBC), a distinct and aggressive subtype of breast cancer, poses a major clinical challenge due to its lack of specific therapeutic targets and pronounced drug resistance. Accumulating evidence has shown breast cancer initiation and progression happen through a multifaceted and intricate process that involves numerous genetic and epigenetic alterations. The modulation of gene expression through epigenetic modifications, encompassing DNA methylation, histone alterations, and non-coding RNA regulation, has emerged as a fascinating field that represents a new avenue for breast cancer therapy. Further, epigenetic modifications are also closely associated with the regulation of various signaling pathways, epithelial-to-mesenchymal transition (EMT), cancer stemness, drug resistance, and autophagy. Thus, emerging information regarding epigenetic regulation in cancer provides many therapeutic prospects for breast cancer therapy.

This thesis emphasizes identifying and targeting various epigenetic regulators implicated in the onset and advancement of breast cancer. Understanding the role of these regulators in EMT and related signaling pathways provides valuable insights for developing potential therapeutic strategies. Strategies like drug repurposing and combination therapies were explored to enhance therapeutic outcomes. Therefore, it was hypothesized that harnessing epigenetic regulation represents a promising approach in the realm of TNBC therapy and management.

The present study primarily focuses on exploring the role of epigenetic regulators in the EMT and different signaling pathways associated with TNBC progression. **Chapter 1** comprises the **Introduction and Review of Literature** part, which describes the major epigenetic alterations linked to the development and advancement of breast cancer. Further, the critical epigenetic modifications that are closely associated with the regulation of various signaling pathways, EMT, cancer stemness, and drug resistance have been discussed extensively. The objectives of the thesis have been fabricated to regulate the aberrant epigenetic dynamics of breast cancer via different therapeutic approaches.

Histone acetylation is the most common epigenetic modification, which typically leads to the activation of transcription and is also associated with cancer progression. Histone acetyltransferase p300 is a critical epigenetic regulator that acts as a transcription co-activator and regulates various cellular processes. p300 is overexpressed in breast cancer and promotes cellular invasion and survival, making it a promising druggable target. In **chapter2** the relevance of p300 in different cancer pathways was established through an initial bioinformatic study. Several *in silico* approaches (virtual screening, MDS, and binding free energy studies) have been utilized to screen the potential drugs from the library of FDA-approved drugs against p300. Subsequently, a tyrosine kinase inhibitor, Imatinib, was selected as a model drug from *in silico* studies for *in vitro* validation. Further, the anti-cancer properties of Imatinib were investigated on the breast cancer cell lines (MCF-7 and MDA-MB-231). Imatinib

TH-3600_196106022

treatment activates the intrinsic pathway of apoptosis via generation of intracellular reactive oxygen species (ROS), and depolarization of mitochondrial membrane. Findings from the present study reveal that Imatinib treatment leads to a significant reduction in cancer cell stemness, invasiveness, and migration potential, alongside decreased colony-forming ability. EMT reversal was marked by increase in E-cadherin expression, with concurrent downregulation of mesenchymal markers, including Fibronectin and Slug. Mechanistically, Imatinib was found to inhibit p300 acetyltransferase activity, resulting in reduced levels of H3K18Ac and H3K27Ac, which in turn led to the downregulation of key Notch pathway proteins such as HES1, AKT, and p21. Overall, these findings highlight the ability of Imatinib to suppress EMT through modulation of the Notch signaling pathway, offering a novel therapeutic avenue for breast cancer treatment.

In **chapter 3**, the role of histone methyltransferase, mixed lineage leukemia 1 (MLL1) was explored in the context of TNBC progression. Histone methylation is a key epigenetic modulation that regulates gene expression and is often associated with the pathogenesis of various cancers, including TNBC. Histone methyltransferase, MLL1-WDR5 complex regulates gene transcription by catalyzing trimethylation of lysine 4 on histone H3 (H3K4me3) and promotes carcinogenesis. EMT induction in TNBC cells is shown to facilitate upregulation of MLL1 and WDR5 expression, thereby establishing the association of these proteins in EMT dynamics. Therefore, the effect of inhibiting MLL1-WDR5 interaction was established using the small molecule inhibitor MM-102 in TNBC cell lines. MLL1 inhibition significantly reduced H3K4me3 levels and enhanced the apoptotic population in TNBC cells, demonstrating its cytotoxic potential. Notably, MM-102 treatment reverses the EMT process by upregulating the expression of epithelial markers (such as E-cadherin and claudin) and downregulating the expression of mesenchymal markers (such as β-catenin, Slug, caveolin 1, and fibronectin). In addition, MLL1 inhibition caused a metabolic shift as indicated by enhanced glycolysis. Further reduction in the fatty acid uptake and lipid droplet accumulation by MM-102 treatment signifies that targeting MLL1 also rewires the metabolic network in TNBC cells. Collectively, inhibiting MLL1 represents a promising therapeutic strategy for managing EMT-driven metastasis, reshaping metabolic reprogramming, and ultimately improving therapeutic outcomes in aggressive breast cancer.

Over time, the use of combination therapies involving multiple chemotherapeutic agents has shown significant promise in the treatment of TNBC. Therefore, in **chapter 4**, the efficacy of a novel combination therapy on TNBC cells was determined using Budesonide with Salinomycin. Budesonide, a DNA methyltransferase activator, which is also known for its anti-inflammatory properties. It has been shown to prevent DNA hypomethylation in mouse lung tumors and inhibit lung cancer cell metastasis by suppressing EMT. However, its anti-cancer activity in TNBC remains largely unexplored. This study evaluates the potential of a co-therapeutic module involving Budesonide and Salinomycin, which targets cancer stem cells. Co-administration of the drugs demonstrated a synergistic effect in inhibiting TNBC cell growth by activating the intrinsic apoptosis pathway. It induced intracellular ROS generation and a prominent rise in mitochondrial membrane depolarization. Additionally, extensive signaling studies revealed that the co-treatment specifically targeted multiple signaling nodes, limiting downstream crosstalk. The combination also enhanced autophagic activity by inhibiting the

TH-3600_196106022

AKT/mTOR pathway and reduced cell migration and stemness by suppressing the EMT process. Therefore, the combination of Budesonide and Salinomycin offers a novel therapeutic approach for TNBC.

Chapter 5 comprises the **Conclusion and Future prospects**, which summarize the key findings of the current thesis. Conclusively, the insights gained in the present study reveal that the advancement of breast cancer is significantly influenced by epigenetic regulators, encompassing DNA methylation and histone modifications. Altogether, the findings of the present study incur strong therapeutic potential for targeting and annihilation of breast cancer in future.

TH-3600_196106022

TH-3600_196106022

Abbreviations

Ac	Acetylated
ADCC	Antibody-dependent cellular cytotoxicity
ADCP	Antibody-dependent cellular phagocytosis
AKT	Ak strain transforming
ALDH1A3	Aldehyde dehydrogenase 1 family member A3
BCSC	breast cancer stem cell
BRD4	Bromodomain protein 4
CBP	CREB-binding protein
CDH	Cadherin
CDKN	Cyclin-dependent kinase inhibitor
c-MYC	Cellular myelocytomatosis oncogene
CpG	Cytosine-guanine
CSC	Cancer stem cell
CSL	Suppressor of hairless
DCFDA	2',7' –dichlorofluorescin diacetate
DKK1	Dickkopf-related protein 1
DMEM	Dulbecco's modified eagles medium
DMSO	Dimethyl sulfoxide
DNA	Deoxyribonucleic acid
DNMT	DNA methyltransferases
DOT1L	Disrupter of telomere silencing protein 1
DVL	Dishevelled segment polarity protein
EGF	Epidermal growth factor
EMT	Epithelial to mesenchymal transition
EMT-TF	Epithelial to mesenchymal transition transcription factor
EpCAM	Epithelial cell adhesion molecule
ER	Estrogen receptor
ERbB	Erythroblastic oncogene B
ESR1	Estrogen receptor 1
EZH2	Enhancer of zeste homolog 2
FBS	Fetal bovine serum

TH-3600_196106022

FDA	Food and drug administration
FOXO3	Forkhead box O3
GAS5	Growth arrest-specific 5
H3K18	Histone 3 lysine 18
H3K27	Histone 3 lysine 27
H3K4	Histone 3 lysine 18
HAT	Histone acetyltransferase
HDAC	Histone deacetylase
HDM	Histone demethylases
HER2	Human epidermal growth factor receptor 2
HES1	Hairy and enhancer of split-1
HMT	histone methyltransferase
HR	Hormone receptor
IGF	Insulin-like growth factor
IGF1R	insulin like growth factor 1 receptor
IRF4	Interferon regulatory factor-4
KDM	Lysine specific demethylase
KMT2	lysine methyltransferase 2
LINE	Long interspersed nuclear elements
LRP	Low-density lipoprotein receptor related protein
LSD	lysine-specific demethylase
MALAT1	metastasis associated lung adenocarcinoma transcript 1
MAML	Mastermind-like protein
MAPK	Mitogen-activated protein kinase
MCL1	Myeloid cell leukemia 1
MDR	Multidrug resistance
MDS	Molecular dynamics simulation
Me	Methylated
MLL1	Mixed lineage leukemia 1
MMP	Mitochondrial membrane potential
ncRNAs	non-coding RNAs
NICD	Notch intracellular domain;
Notch	Notch signaling pathway
p21	Cyclin-dependent kinase inhibitor 1
p300	Histone acetyltransferase p300
PAD4	Peptidyl arginine deiminase 4

TH-3600_196106022

PARP	Poly ADP-ribose polymerase;
PCAF	p300/CBP-associated factor
PDGF	Platelet derived growth factor
PD-L1	protein-programmed cell death ligand 1
PI3K	Phosphatidylinositol-3-Kinase
PKC θ	Protein kinase C θ
PR	Progesterone receptor
PTEN	Phosphatase and tensin homolog
PTM	Post-translational modifications
PVDF	Polyvinylidene fluoride
RNA	Ribonucleic Acid
ROS	Reactive oxygen species
SDS-PA GE	Sodium dodecyl sulfate polyacrylamide gel electrophoresis
SFRP	several frizzled-related protein
SHH	Sonic hedgehog signaling molecule
SNGG	Synuclein-γ gene
SOD2	Superoxide dismutase 2
STAT3	Signal transducer and activator of transcription 3
TAZ	Transcriptional co-activator with PDZ-binding motif
TEAD	TEA domain transcription factor
TGF-β	Transforming growth factor β
TIMP3	Tissue inhibitor of metalloproteinases 3
TME	Tumor microenvironment
TNBC	Triple-negative breast cancer
TP	Thymidine phosphorylase
TP53	Tumor protein 53
TS	Thymidylate synthase
uPA	Urokinase-type plasminogen activator
VEGF	Vascular endothelial growth factor
WIF1	Wnt inhibitory factor 1
WNT	Wingless/integrated pathway
YAP	Yes-associated Protein
ZEB1	Zinc finger E-box binding homeobox

TH-3600_196106022

Guwahati • IIT

TH-3600_196106022

List of Figures

TH-3600_196106022

TH-3600_196106022

TH-3600_196106022

TH-3600_196106022

TH-3600_196106022

TH-3600_196106022

TH-3600_196106022

TH-3600_196106022

List of Tables

TH-3600_196106022

TH-3600_196106022

Chapter 1

Introduction and Review of Literature

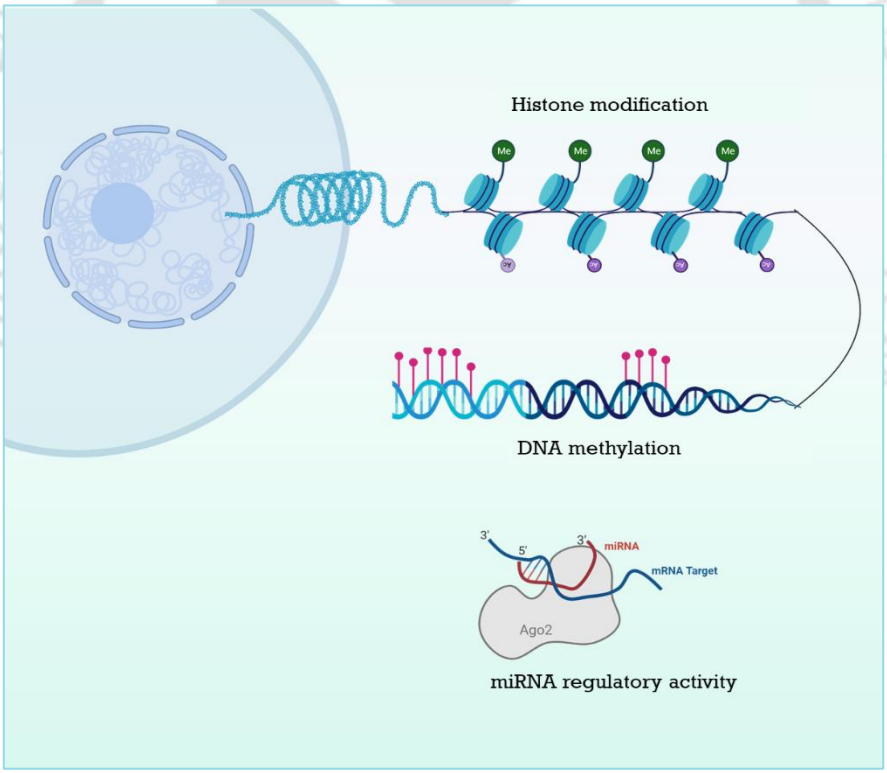

Frontiers in Bioscience–Landmark, 29(8), 287.
https://doi.org/10.31083/j.fbl2908287

TH-3600_196106022

Introduction and Review of Literature

Cancer encompasses a range of diseases characterized by uncontrolled cell growth and the ability of abnormal cells to invade nearby tissues and metastasize to distant organs. It arises from genetic mutations, epigenetic changes, and environmental factors that disrupt normal cellular growth and division. Breast cancer is one of the prevalent types of cancer and a leading cause of cancer-related mortality among women worldwide [1]. Owing to its heterogeneous nature, it represents a major therapeutic challenge. Breast cancer is classified into multiple categories based on molecular subtypes. Major subtypes include hormone receptor-positive (HR+), human epidermal growth factor receptor 2 (HER2+) positive, and triple-negative breast cancer (TNBC). The hormone receptor-positive (HR+) subtype comprises cancer cells expressing estrogen receptor (ER) and progesterone receptor (PR), which promotes the growth of cancer cells. Targeting these receptors via hormonal therapy is often an effective treatment strategy for this subtype [2]. In the case of the HER2-positive subtype, overexpression of the HER2 receptor is prominent, which makes the cancer more aggressive [3]. TNBC is characterized by the lack of estrogen, progesterone, and HER2/neu receptors. The absence of these receptors makes TNBC resistant to conventional hormonal therapy and drugs targeting these receptors. This subtype is characterized by poor differentiation, high invasiveness, an increased tendency for local and distant metastasis, poor prognosis, and elevated recurrence rates. Gene expression profiling reveals that TNBC is associated with mesenchymal characteristics, stem cell markers, and dysregulated metabolic pathways. Transcriptome analysis further categorizes TNBC into six distinct subtypes: basal-like 1, basal-like 2, mesenchymal stem-like, immunomodulatory, mesenchymal, and luminal androgen receptor **(Figure 1.1)** [4].

A comprehensive approach combining radiotherapy, surgery, hormonal, and targeted therapy is generally used for breast cancer. Even though the efficacy of different treatment strategies has increased and mortality has decreased, numerous challenges remain to be solved. These include severe side effects, development of multidrug resistance, intratumoral heterogeneity, and metastatic illness [5]. In addition to the extensively studied genetic alterations, epigenetic changes play a significant role in driving the development of breast cancer by inducing abnormal gene expression. The emerging information regarding epigenetic regulation in cancer provides many therapeutic prospects for breast cancer therapy [6]. The successful use of epigenetic inhibitors or epi-drugs in managing hematological malignancies has generated interest in their potential application for treating solid tumors including breast cancer [7][8].

TH-3600_196106022

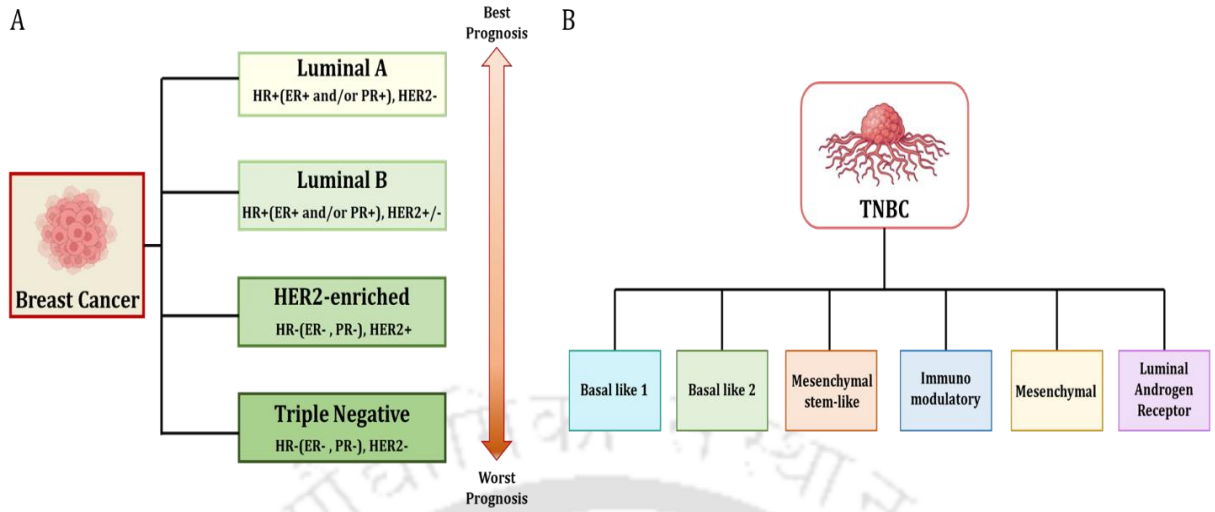

Figure 1.1: *(A) Molecular subtypes of breast cancer and (B) Classification of Triple Negative Breast Cancer. (Concept source: adapted and redrawn from http://dx.doi.org/10.3390/medicina57010062)*

1.1. Epigenetic regulation in breast cancer

Hereditary breast cancer accounts for approximately 10% of all cases. Mutations in tumor suppressor genes such as TP53, BRCA1, and BRCA2 are linked to the development of breast cancer [9]. Alongside genomic alterations, a series of epigenetic modifications contribute to the development and progression of breast cancer. Epigenetic changes are heritable DNA modifications that impact gene expression without altering the DNA sequence. Epigenetic modifications primarily include DNA methylation, histone tail modifications, nucleosomal remodelling, and non-coding RNAs mediated regulatory activity. These mechanisms are crucial for regulating gene transcription and genomic stability, as well as maintaining cellular growth, development, and differentiation **(Figure 1.2)**. Furthermore, epigenetic modifications have a significant impact on the development and progression of multiple malignancies, including breast cancer [10]. These alterations are believed to be involved in the early stages of breast cancer carcinogenesis and often serve as biomarkers for early identification, prognostic assessment, and therapy response. Moreover, a thorough grasp of the epigenetic alteration in breast cancer provides an alternative avenue for drug development [11].

1.1.1. DNA methylation

DNA methylation is the primary epigenetic mechanism extensively studied for its significant role in regulating gene expression. The process of DNA methylation entails the covalent addition of methyl group to the C-5 position of the cytosine in cytosine-guanine (CpG) dinucleotides by DNA methyltransferases (DNMTs). DNMT1 maintains the pre-existing methylation patterns during replication, while DNMT3A and DNMT3B govern *de novo* methylation [12]. Methylation of CpGs at the promoters of genes leads to suppression of gene expression, whereas methylation levels in the gene body positively correlate with expression. DNA methylation is critical in maintaining chromosome stability, X chromosome inactivation, transposable element suppression, aging, and genomic

TH-3600_196106022

imprinting. Moreover, it influences several disease conditions, including cancer and autoimmune disorders [12].

Breast cancer cells often exhibit disruptions of normal methylation patterns. The hypermethylation of promoter region leads to inactivation of tumor suppressor genes, such as BRCA1, APC, CDH1, CCND2, and CTNNB1. On the other hand, breast cancer exhibits global DNA hypomethylation, with up to 50% of instances exhibiting lower 5-methylcytosine content than their counterparts in normal tissue [13]. Hypomethylation in repetitive sequences and pericentromeric satellite DNA is prominent in cancer cells, and it generally remains highly methylated in normal breast cells. For example, retrotransposons, including long interspersed nuclear elements (LINEs), are hypomethylated in breast cancer [14]. In addition, Sat2 and Satα repeats are frequently hypomethylated in a variety of malignancies, including breast cancer. Hypomethylation of these transposable elements leads to their transcriptional activation, further contributing to genomic instability [14, 15]. Moreover, several lines of evidence demonstrated gene-specific hypomethylation in breast cancer, such as hypomethylation of Urokinase-type plasminogen activator (uPA), synuclein-γ gene (SNCG), and multidrug resistance 1 gene (MDR1) [16, 17, 18].

1.1.2. Role of non-coding RNA

Another key epigenetic mechanism is the function of non-coding RNAs (ncRNAs), which constitute approximately 62-75 % of the genome [19, 20]. To date, numerous ncRNAs have been found, including circular RNA (circRNA), short hairpin RNA (shRNA), small nucleolar RNA (snoRNA), piwi-interacting RNA (piRNA), small-interfering RNA (siRNA), and long non-coding RNA (lncRNA). These ncRNAs have emerged as an essential source of biomarkers and targeted therapies due to a growing understanding of their role in various diseases [21].

The dysregulation of miRNAs, one of the crucial ncRNAs, has come to light in the emergence of multifactorial disorders, including breast cancer. miRNAs are short (18–22 nucleotides) endogenous single-stranded RNA molecules that attach to the target mRNA to limit translation. Aberrant miRNA activities are associated with breast cancer onset and progression [22]. For instance, metastatic breast cancer has been associated with overexpression of miR-21 and miR-155 [23]. Similarly, patients with higher expression levels of miR-1307-3p, miR-940, and miR-340-3p were observed to experience decreased overall survival rates [24]. Furthermore, miR-497 regulates cell growth and invasion of breast cancer cells through inhibiting the expression of cyclin E1 [25].

LncRNAs, another important class of non-coding RNAs ranging from 200 nucleotides to 100 kilobases in length, can regulate gene expression at various levels by interacting with DNA, RNA, and proteins [26]. Dysregulation in lncRNA regulatory activity facilitates breast cancer development and dissemination. For example, growth arrest-specific 5 (GAS5) remains highly downregulated in breast cancer and regulates the expression of several tumor-associated genes. Employing various pathways, such as mitochondrial signaling pathways and cell death receptors, GAS5 can induce apoptosis in breast cancer. Moreover, it plays a critical role in regulating PI3K/AKT/mTOR, NF-κB, and Wnt/β-catenin pathway [27]. Another crucial lncRNA, metastasis associated lung adenocarcinoma transcript

TH-3600_196106022

1 (MALAT1), is aberrantly expressed in several kinds of breast cancer types, potentiates metastasis and a poor prognosis [28].

1.1.3. Alteration of histone modifications

Histones serve as essential DNA packaging proteins, thereby maintaining chromatin structure. Histone proteins (H2A, H2B, H3, and H4) assist in generating nucleosomes by wrapping octamers around 147 bp of DNA. Post-translational modifications (PTMs) of histone cause changes in the state of chromatin, subsequently leading to gene expression regulation [29]. Specific residues of the amino and carboxy ends of the histone tails undergo several modifications, including acetylation, phosphorylation, methylation, sumoylation, ubiquitination, ADP-ribosylation, glycosylation, and carbonylation. Different enzymes, such as histone acetyltransferases (HATs), histone deacetylases (HDACs), histone methyltransferases (HMTs), and histone demethylases (HDMs), catalyze these modifications. Alterations in the expression of these enzymes also implicate the onset and advancement of cancer [29]. Numerous alterations have been identified in breast cancer, including the upregulation of p300, HBO1, HDAC1, HDAC2, HDAC3, and HDAC6 [30].

HMTs are the key epigenetic enzymes, which catalyses the addition of methyl groups to the histone residues. HMTs are categorized into two groups based on the residue they target for methyl group transfer: lysine-specific methyltransferases (KMTs) and arginine-specific methyltransferases (PRMTs). lysine methyltransferase 2 (KMT2), were found to be linked with the proliferation and metastasis of breast cancer cells. KMT2 activates oncogenes and pro-metastatic genes by methylating H3K4 at both enhancer and promoter regions [31]. Amplification and overexpression of a crucial histone methyltransferase enhancer of zeste homolog 2 (EZH2) are prominent in breast cancer. By catalyzing H3K27 methylation, EZH2 facilitates transcriptional silencing of several genes and persuades EMT and metastasis in breast cancer [32, 33]. Another prominent HMT, disruptor silencing 1 like (DOT1L), is also known to potentiate metastatic behavior of breast cancer cells [34].

Several histone demethylases, including Lysine-specific demethylase 4A (KDM4A), Lysine-specific demethylase 4B (KDM4B), and Lysine-specific demethylase 4C (KDM4C) are also associated with breast cancer. ERα positive subtype cells exhibit overexpression of KDM4A and KDM4B, whereas in the case of TNBC, enhanced levels of KDM4C are observed [35]. KDM4A triggers a Notch1-NICD-dependent signaling pathway to promote breast cancer growth and metastasis [36]. KDM4B regulates estrogen signaling, and downregulation in KDM4B expression limits breast cancer growth [37]. KDM4C acts as a co-activator of HIF-1α /VEGF signaling, thereby promoting breast cancer progression [38].

TH-3600_196106022

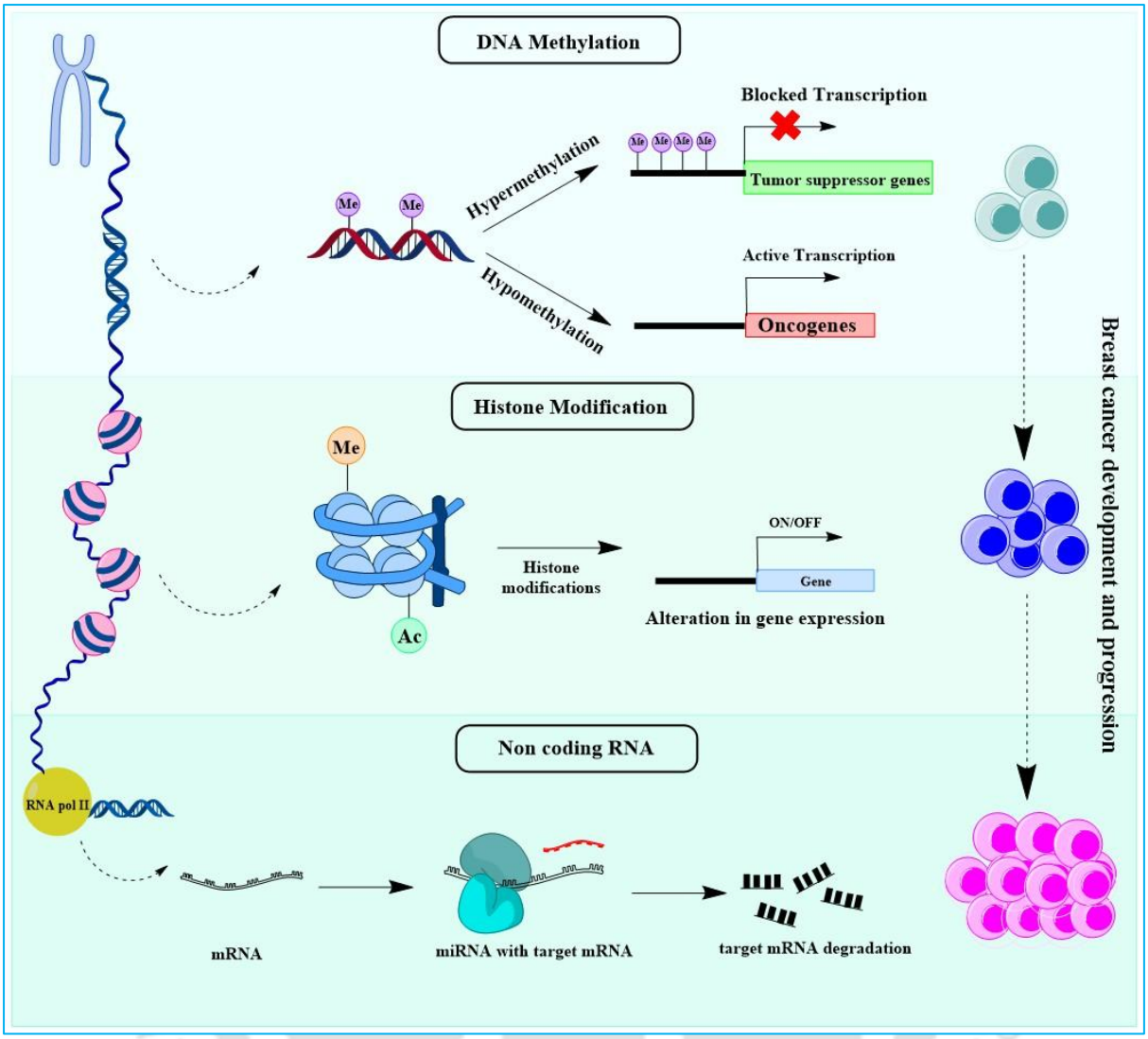

Figure 1.2: *Schematic illustration of fundamental epigenetic mechanisms involved in breast cancer development and progression (Concept source: https://doi.org/10.31083/j.fbl2908287).*

1.2. Estrogen-related epigenetic mechanism

Estrogens, the predominant sex hormones in women, play a crucial role in reproductive maturity, bone growth, and energy homeostasis. The five primary subtypes of estrogen are estrone (E1), 17-β estradiol (E2), estriol (E3), estetrol (E4), and estrone-sulfate (E1s) [39]. Among them, E1 and E2 constitute the majority of estrogens in the body. Besides, E1 primarily functions as a reservoir for estrogen undergoes a reversible conversion to E2, which is the more physiologically active form. Whereas, E3 and E4 are found only during pregnancy, with E3 being the most prevalent. Actions of estrogens are facilitated through two primary types of intracellular estrogen receptors (ERs), namely ERα and ERβ, encoded by the genes ESR1 and ESR2, respectively [40]. ERα positive subtype, which constitutes around 75% of breast tumors, exhibits a better prognosis due to their sensitivity towards hormonal therapy. Conversely, poor prognosis and aggressive tumor growth are observed in the case of ERα negative subtypes [41]. Epigenetic silencing via abnormal methylation of the ERα promoter is one mechanism

TH-3600_196106022

implicated in the suppression of ERα expression **(Figure 1.3)**. Recruitment of ZEB1/ DNMT 3B/ HDAC 1 complex on the ESR1 promoter contributes to hypermethylation of ESR1 **(Figure 1.3)**. Likewise, enhancement in histone deacetylation also suppresses ESR1 transcription by inducing condensation of the nucleosome structure [42].

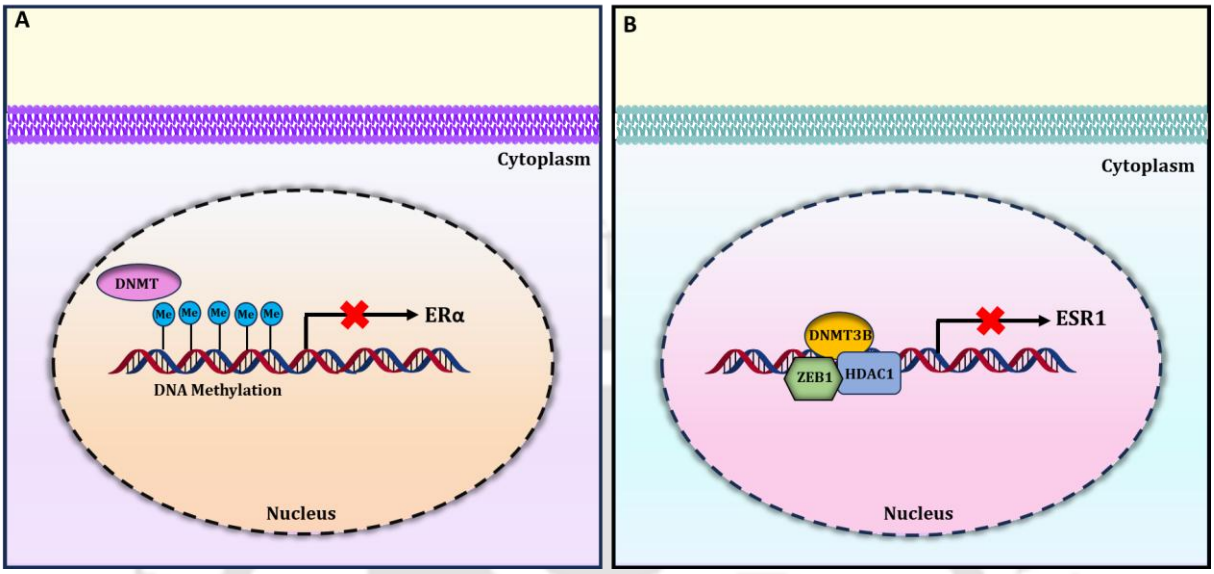

Figure 1.3: *Epigenetic mechanisms regulating the expression of ERα and ESR1in breast cancer (A) DNA methylation mediated suppression of ERα expression, (B) suppression of ESR1 expression by ZEB1/ DNMT 3B/ HDAC1 complex. (Concept source: https://doi.org/10.31083/j.fbl2908287)*

Upon binding of E2, dimerization of ERα monomers takes place, which further translocates to the nucleus and serves as a transcription factor regulating the expression of various genes [43]. E2-ERα dimers recruit ATP-dependent chromatin remodeling complexes (SWI/SNF) and HATs, including p300, p160, CBP, and pCAF, to estrogen-responsive promoters. Eventually, it facilitates breast cancer cell proliferation and promotes tumor growth [44].

Several studies demonstrated a significant role of miRNAs in suppressing ER expression [45, 46]. For instance, overexpression of miR-221 and miR-222 results in post-transcriptional suppression of ERα. Therefore, miR-221 and miR-222 facilitate downregulation in the expression of several tumor suppressors, including PTEN, CDKN1B, CDKN1C, BIM, TIMP3, and FOXO3, as well as lead to estrogen-independent uncontrolled proliferation [45, 46].

1.3. Epigenetic modulation during EMT

Epithelial to mesenchymal transition (EMT) is a cellular process wherein cells transform, losing their epithelial traits and adopting mesenchymal characteristics. EMT plays a pivotal role in wound healing, development, and progression of cancer. It makes cancer cells more migratory and endows drug resistance, stemness, and recurrence. Different growth factors (TGF-β, EGF, FGF, IGF, and PDGF) trigger signaling pathways to instigate EMT transcription factors (SNAI, ZEB, and TWIST) and eventually orchestrate EMT. These TFs have been demonstrated to form regulatory complexes with

TH-3600_196106022

various proteins involved in transcriptional regulation, including epigenetic regulators [47]. In different cancer conditions, including breast cancer, the collaboration between the transcription factors of EMT and epigenetic regulators is prominent, which leads to EMT induction by regulating the expression of genes involved in EMT [48].

For example, in breast cancer, DOT1L collaborates with c-Myc and p300 to promote the methylation and acetylation of H3K79 in the promoter areas of EMT transcription factors, which leads to increased expression of these genes **(Figure 1.3)**. Consequently, this process promotes EMT-associated cancer stemness characteristics [47]. Furthermore, invasive breast cancer cells exhibit aberrantly high levels of methylation in CDH1, which is associated with downregulation in the expression of E-cadherin [48]. E-cadherin is a tumor suppressor that facilitates cell-to-cell adhesion between neighboring cells [49]. G9a silences transcription at the E-cadherin promoter in breast cancer by interacting with Snail **(Figure 1.4)** [50].

Histone deacetylase inhibitor Trichostatin A (TSA) reverses EMT in breast cancer by inhibiting Slug expression [51]. Additionally, inhibiting BRD4 leads to suppression of Gli1, which is necessary for the transcriptional activation of Snail. This suggests that BRD4 regulates the aggressiveness of breast cancer cells through both transcriptional regulation of Snail and post-translational mechanisms [52]. Another study suggests that the combined effect of TGF-β and TNF-α increases MMP-9 expression in breast cancer cells through Smad/p38/H3K36me2 signaling, potentially playing a key role in cancer invasion and metastasis [53]. A recent study found that Sirtinol, a SIRT1 inhibitor, suppresses EMT and metastasis in 4T1 breast cancer cells while also influencing the immune microenvironment [54]. Furthermore, according to another report, metformin inhibits breast cancer proliferation and regulates EMT by modulating the miR-125a/HER2/Vimentin axis through DNMT1-mediated epigenetic regulation [55]. Thus, understanding the interplay between EMT and epigenetics offers new avenues for cancer treatment.

TH-3600_196106022

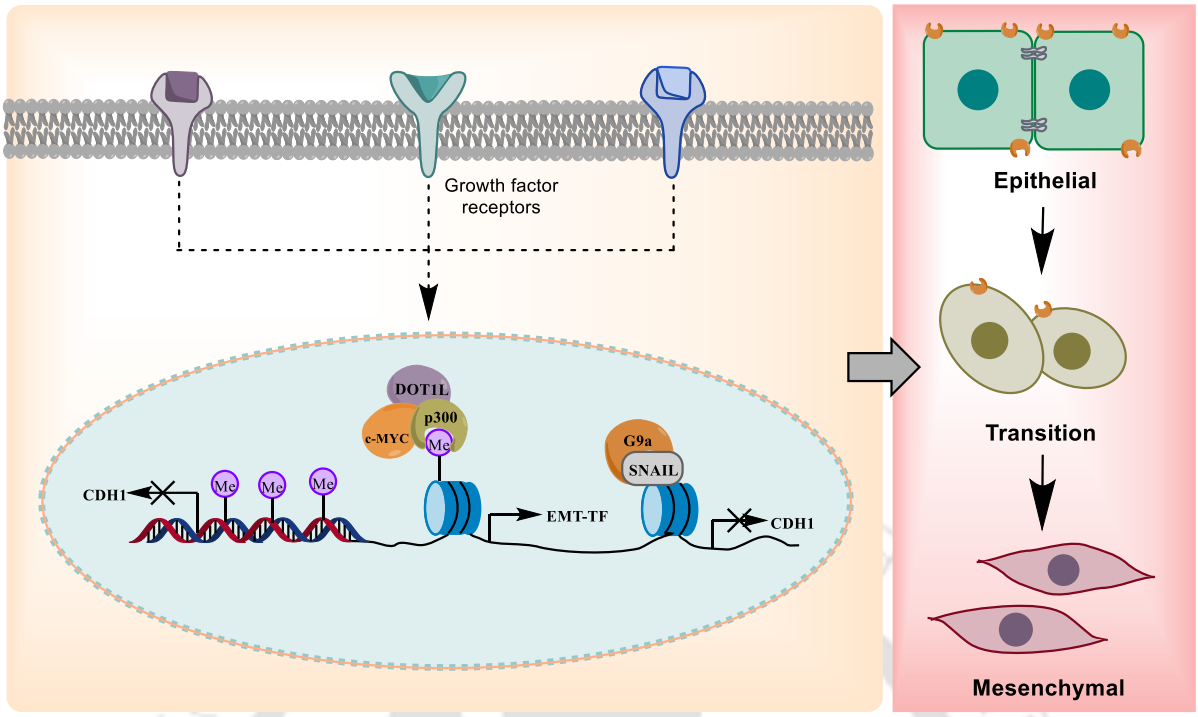

Figure 1.4: *Role of epigenetic mechanisms in EMT dynamics of breast cancer (Concept source: https://doi.org/10.31083/j.fbl2908287).*

1.4. Cancer stemness and epigenetics

Emerging evidence suggests that a tiny population of cancer cells promotes the recurrence and dissemination of the disease known as cancer stem cells (CSC). Like other CSCs, breast cancer stem cells (BCSCs) comprise a subset of diverse breast cancer cells with substantial potential for proliferation and self-renewal. Several studies demonstrated that BCSCs are the main contributory factor of drug resistance, recurrence, metastasis, and the onset of the disease [56]. During development, epigenetic machinery is crucial in reprogramming stem cells to facilitate differentiation into specific cellular and tissue lineages. In several malignancies, including breast cancer, aberrant epigenetic alterations often potentiate the generation of CSCs, which lack differentiation capacity [57].

Epigenetic mechanisms are pivotal in regulating the expression of numerous genes involved in signaling pathways associated with cancer stemness, including Wnt, Notch, Hedgehog, and Hippo/YAP [55]. In breast cancer cells, the promoters of genes involved in Wnt/β-catenin signaling pathways are often found to be hypermethylated [56]. Furthermore, the prominent downregulation of DNA methylation leads to decreased expression of Wnt inhibitors, such as Wnt inhibitory factor 1 (WIF-1), several frizzled-related proteins (SFRP1-5), and Dickkopf-Related Protein 1 (DKK1), in cancer cells **(Figure 1.4)**. Consequently, this enhances Wnt/β-catenin signaling activity in breast cancer stem cells compared to non-CSCs [58, 59]. Another study unveiled an abundance of H3K27me3 and decreased H3K4me2 levels in triple-negative breast cancer stem cells (TNBCSCs) [60]. These epigenetic alterations significantly impact various stemness-associated signaling pathways, including Wnt and human gonadotropin-releasing hormone (GNRH), consequently fostering aggressiveness and drug resistance in TNBCSCs [58]. Epigenetic alterations can also regulate Hedgehog pathway machinery and

TH-3600_196106022

instigate the onset and advancement of several tumors. In breast and gastric cancer, hypomethylation of the promoter region of the SHH gene results in increased expression of the ligand **(Figure 1.5)**. Overexpression of SHH leads to the expression of hedgehog pathway downstream genes, thus facilitating cancer progression and self-renewal capacity [61, 62]. Hyperactivation of Notch signaling, particularly Notch 1 and 4, enhances metastatic and self-renewal traits of BCSCs [55]. In BCSCs, EZH2 serves as a Notch 1 activator, correspondingly regulating Notch signaling to potentiate the growth of CSC populations and cancer development [63]. Histone acetylases and deacetylases are recruited by HES **(Figure 1.4)**, a Notch effector and transcriptional repressor, one of the epigenetic processes controlling Notch signaling [64]. Furthermore, in breast cancer and pancreatic adenocarcinomas, downregulation of miR-200 members leads to activation of the Notch pathway and consequences cell survival, CSC maintenance, and therapeutic resistance [65]. Dysregulation in Hippo signaling has been linked to increased stem cell proliferative and self-renewal capacities of cancer cells. It has been reported that by altering LIFR expression, miRNA-125a indirectly regulates the activity of TAZ, an effector molecule in the Hippo pathway [63]. Furthermore, another crucial miRNA, miR- 520b, activates Hippo/YAP signaling by targeting LATS2, thereby promoting stemness in breast cancer patients **(Figure 1.5)** [67].

TH-3600_196106022

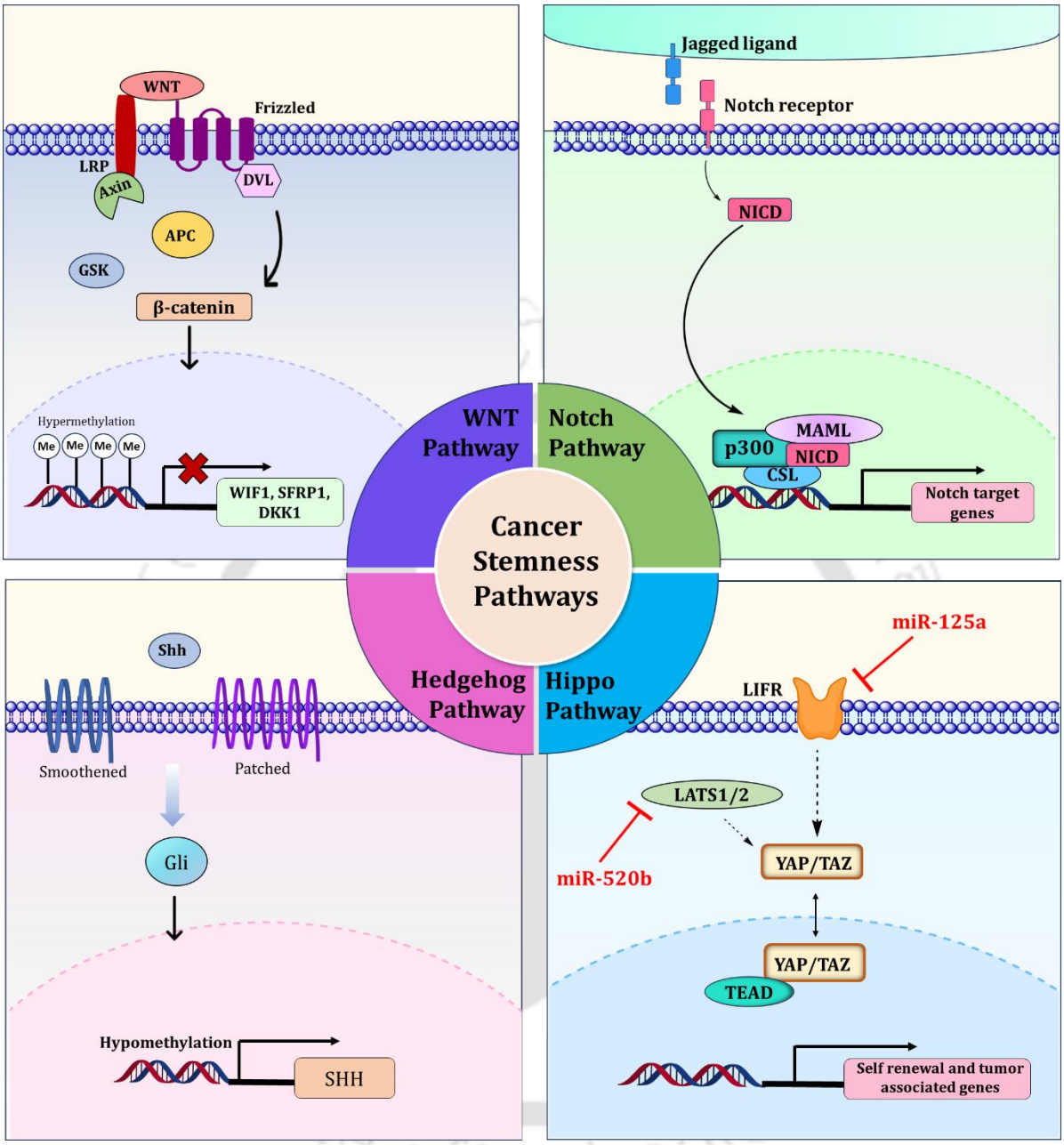

Figure 1.5: *Regulation of signaling pathways associated with cancer stemness, including WNT, Notch Hedgehog, and Hippo pathways by epigenetic mechanisms (Concept source: https://doi.org/10.31083/j.fbl2908287).*

1.5. Drug resistance and epigenetics

Innate and acquired resistance towards conventional chemotherapeutic drugs facilitates cancer recurrence and poor prognosis. The occurrence of cancer stem cells (CSCs) and the EMT process are thought to be the leading causes of cancer therapeutic resistance. According to accumulating evidence, drug resistance in several cancers, including breast cancer, is also influenced by aberrant epigenetic

TH-3600_196106022

regulation [68]. Tamoxifen resistance in breast tumors is caused by EZH2-mediated suppression of GREB1 expression, an ERα cofactor [69]. In breast cancer cells, loss of ten-eleven translocation 2 (TET2) resulted in decreased expression of ERα, leading to endocrine resistance [70]. Through reducing p53 stability and enhancing the expression of AIB1, Histone acetyltransferase KAT2A promotes tamoxifen resistance in breast cancer [71]. Another study reported that inhibition of CBP/p300 activity suppresses ERα function and eventually restricts breast cancer cell growth [72]. Histone demethylase LSD1 is involved in the regulation of self-renewal of breast CSCs, which contributes to the development of chemoresistance in breast cancer [73]. Additionally, in breast cancer, LSD1 regulates EMT by interacting with PKC-θ and induces drug resistance [74]. According to Metzger et al., KDM4A governs the growth and self-renewal of breast CSCs, which facilitates therapeutic resistance [75]. Moreover, IGF1R and ErbB signaling can also be triggered by KDM5A, which then activates the PI3K/AKT/mTOR pathway and tamoxifen resistance [76]. Zhou et al. showed that the overexpression of peptidyl arginine deiminase 4 (PAD4) induced apoptosis and elevated the levels of GSK3β and p53, making cells more susceptible to Adriamycin [77]. Overall, epigenetic machinery is implicated in therapeutic failure, and targeting epigenetic regulators shows significant potential for overcoming breast cancer drug resistance.

1.6. Autophagy and epigenetics

Autophagy is a self-degradative mechanism which is crucial in maintaining energy supply concerning to nutrient stress and helps in sustaining cellular homeostasis. It has been implicated in cancer as an entity governing cancer progression, invasion, and metastasis. Accumulating evidences highlight the complex regulatory networks governing autophagy in breast cancer, where epigenetic mechanisms contribute to autophagy suppression or activation. [78].

Promoter hypermethylation is a key factor in the repression of autophagy associated genes; for example, hypermethylation of BECN1 gene. In primary sporadic breast tumors, monoallelic loss of BECN1 was found in 45% of tumors and this loss was accompanied with significant promoter hypermethylation [79]. Similarly, promoter hypermethylation of ATG2B, ATG4D, ATG9A and ATG9B has been found in invasive ductal carcinoma specimens. These genes play crucial roles in autophagy: ATG2 homologs function as peripheral membrane proteins essential for cellular nucleation, ATG4D is part of the ATG4 family involved in the ATG8-LC3 conjugation system, and ATG9 proteins act as functional orthologs interacting with the phagophore [80].

Studies indicate that core autophagy-related genes can be silenced or activated through histone modifiers. For example, in differentiated breast cancer cells, silencing HDAC6 results in autophagy downregulation and promotes apoptosis [78]. Further, treatment of MCF-7 breast cancer cells with the histone methyltransferase, G9a inhibitor BIX0124 recruits NF-κB to the BECN1 promoter, raising intracellular ROS levels. This process reduces H3K9me2 marks, creating an open chromatin structure that enhances BECN1 expression and autophagy. Notably, breast tumors with high G9a and low BECN1 expression are linked to poor prognosis, suggesting BECN1 as a tumor suppressor regulated by G9a [81]. Similarly, GA001, a G9a antagonist, induces autophagy in breast cancer cells via the AMPK-mTOR-ULK1 pathway [78].

TH-3600_196106022

Additionally, metastatic breast cancer cells in lymph nodes show elevated miR-224-5p levels, which correlate with reduced LC3B protein and increased SQSTM1 expression, indicating autophagy suppression via a SMAD4-dependent mechanism. miR-101 also suppresses basal and Rapamycin-induced autophagy in breast cancer cells by targeting the autophagy-related genes ATG4D, RAB5A, and STMN1 [78]. Therefore, targeting epigenetic modifiers may offer promising therapeutic strategies to regulate autophagy and improve outcomes in breast cancer patients. Overall, these findings unveiled the convergence of autophagy and epigenetics in breast cancer cells.

Notably, the interplay between autophagy and EMT is highly complex. While increased autophagic flux can promote cancer cell survival and enhance metastatic potential in renal cell carcinoma, other studies suggest that autophagy activation can also suppress EMT. This dual role highlights the intricate regulation of cancer progression by autophagy, which may vary depending on the tumor type and microenvironment [82].

Autophagy and EMT signaling pathways share a complex interplay, with mTOR serving as a key regulator. Inhibiting the mTOR pathway induces autophagy while simultaneously suppressing EMT, thereby reducing cancer cell invasion and metastasis. Conversely, activation of the PI3K/Akt/mTOR pathway promotes EMT by upregulating transcription factors such as Twist, Snail, and ZEB-1, leading to E-cadherin suppression. A positive feedback loop between Twist and Akt further reinforces EMT and metastasis. Growth factors like TGF-β also activate PI3K/Akt/mTOR signaling, driving EMT progression [83,84]. Recent studies have highlighted the role of autophagy in modulating EMT in TNBC. Inhibition of autophagy has been shown to upregulate the epithelial marker E-cadherin, thereby suppressing migration and metastasis in TNBC cells. Similarly, Atg7 has been reported to inhibit EMT by increasing E-cadherin levels while reducing the expression of N-cadherin, SMA, and Vimentin [85]. Conversely, EMT can be induced in TNBC cells through the Wnt/β-catenin pathway via Beclin 1 overexpression, which enhances autophagic activity. Furthermore, cancer-associated fibroblast autophagy has been implicated in triggering EMT in TNBC cells through the Wnt/β-catenin pathway, further underscoring the intricate relationship between autophagy and EMT in breast cancer progression [83,86].

1.7. Epigenetic drug advancements

Epidrugs or epigenetic drugs represent a promising field of medicine that focuses on the chemical compounds utilized to rectify epigenetic modifications by targeting epigenetic modulators. These drugs open up new avenues for personalized medicine and have the potential for precise targeting [6]. They can regulate gene activity by correcting aberrant gene expression associated with cancer, neurodegenerative diseases, and autoimmune conditions [10]. Epidrugs can be broadly classified as DNA methyl transferase (DNMT) inhibitors, Histone Acetyltransferase (HAT) inhibitors, Histone deacetylase (HDAC) inhibitors, Histone methyltransferase (HMT) inhibitors, and Histone Demethylase (HDM) inhibitors **(Figure 1.6)** [6]. The need for effective epigenetic inhibitors led to the development of the first generation of epi-drugs, which includes DNMT inhibitors such as pyridine analogs and HDAC inhibitors that target specific histone classes. The first-generation epidrugs fall short in terms of poor pharmacokinetic properties, selectivity, and bioavailability, which paves the way for the

TH-3600_196106022

advancement of second-generation epidrugs with a long half-life, lower cytotoxicity, side effects, and potent inhibitory action. The third-generation epidrugs target epigenetic factors categorized as writers, erasers, and readers. Writers add methyl or acetyl groups to DNA or histones, erasers remove these modifications, and readers recognize and regulate the binding interactions [87]. The list of epidrugs used for breast cancer therapy is provided in **Table 1.1**.

1.7.1. DNA modifying agents

DNA methylation entails the transfer of a methyl group to the fifth carbon of cytosine, orchestrated by a set of enzymes known as DNA methyltransferases (DNMTs), comprising DNMT1, DNMT3A, DNMT3B, and DNMT3L. DNA methylation leads to the silencing of gene expression by impeding the binding of transcription factors to the DNA [12]. The DNMT inhibitors work by incorporating themselves between the DNA base pairs and preventing the methylation of the promoter sequence (CpG islands). Decitabine and Azacitidine are well-known first-generation DNMT inhibitors that follow this mechanism [88].

DNMT inhibitors are of three types, namely non-nucleosidic, nucleosidic, and natural compounds. Natural compounds such as Epigallocatechin-3-gallate (EGCG), catechin, and quercetin demonstrated the ability to inhibit the activity of DNMT1. This inhibition leads to the demethylation of DNA, reactivation of tumor suppressor genes, and reduction of breast cancer cell proliferation [89]. A non-nucleosidic compound called hydralazine is conventionally used as an antihypertensive drug but serves to reduce the expression of DNMTs in mammals [90]. Hydralazine, combined with valproic acid, a mild demethylating drug, decreases cancer cell survival dose-dependently [91]. Zebularine, a potent nucleoside DNMT inhibitor, upregulates p21 expression, downregulates cyclin-D expression, induces apoptosis, and arrests MCF-7 and MDA-MB-231 cells in the S-phase [92]. Procainamide, an antiarrhythmic drug, is a non-nucleoside DNMT analog that sensitizes the ERα positive breast cancer cells to tamoxifen therapy by upregulating ERβ expression [93]. An anti-inflammatory compound used to treat ulcerative colitis, called Olsalazine, is found to escalate the expression of the CDH1 gene, which encodes for E-cadherin; thereby, it abridges EMT in MDA-MB-231 cells [94]. Liraglutide, a type II diabetes drug, has been found to function as a DNMT inhibitor by curtailing the methylation of ESR1, CDH1, and ADAM33 promoter regions in MCF-7, MDA-MB-231, and MDA-MB-436 cell lines [95]. In addition, five potential candidates, namely C-7756, C-5769, C-1723, C-2129, and C-2140, were reported as potential DNMT1 inhibitors as per the *in-silico* studies [96].

1.7.2. Histone Acetyltransferase (HAT) and Histone Deacetylase (HDAC) inhibitors

Histone acetyltransferases (HATs) and Histone Deacetylases (HDACs) are essential enzymes involved in the regulation of gene expression and chromatin remodeling [97]. HATs mediate the addition of an acetyl group from acetyl-CoA to the lysine residues, resulting in the neutralization of the charge of lysine. This process results in the transcriptional activation of the underlying DNA sequence due to the slackened chromatin structure [97]. On the contrary, HDACs catalyze the acetyl group removal from the histones, leading to a more stable and condensed chromatin structure contributing to transcriptional repression [98]. Any dysregulation in the dynamic interplay between these enzymes may result in life-threatening diseases like cancer [87].

TH-3600_196106022

p300 acetyltransferase promotes expression of oncogenes and serves as a critical tumorigenic driver in breast cancer. Several HAT inhibitors from natural sources such as Carnosol, Garcinol, Anacardic acid, and Curcumin are investigated in breast cancer. Carnosol, a polyphenol abundant in rosemary, oregano, and sage plants, serves as a potential inhibitor of p300. It blocks the acetyltransferase activity of p300 by impeding the acetyl CoA binding site, which impels histone hypoacetylation in MDA-MB-231 cells [99]. Another natural compound, Garcinol, is reported to be an effective inhibitor of CBP/p300 mediated acetylation of p53 in MCF-7 cells. Furthermore, a significant decrease in H3K18 methylation was observed, thereby hindering the MCF-7 cell growth by arresting the cells at the G1 phase. Curcumin also inhibits the activity of p300/CBP, which blocks the MCF-7 cells at the G2/M phase [100, 101]. Anacardic acid is predominantly found in Anacardiaceae members like *Amphipterygium adstringens*, cashew, ginko, etc. It is a non-selective HAT inhibitor with HSP90 ATPase inhibitory potential to suppress HSP90 oncoproteins overexpressed in TNBC cells [102]. Pentamidine is a chemical compound used to treat protozoal infection. It has been shown to repress DNA and protein synthesis by targeting Tip60, a HAT from the MYST family, thereby dwindling the H2A acetylation [103]. In addition, bisubstrate inhibitor A is more capable of restraining the HAT activity by resembling the HAT substrate possessing a lysine peptide and an acetyl-CoA group [104]. Some other notable HAT inhibitors include NU9056, MG-149, TH1834, and Lys-CoA [103].

The HDAC inhibitors can be subdivided into three groups, namely, Hydroxyamates (Vorinostat, Belinostat, Dacinostat, Panobinostat, CUDC-10, Quisinostat, and Tefinostat), Benzamides (Tacedinaline, Entinostat, Mocetinostat, and Chidamide) and Carboxylic acid HDAC inhibitors (Butyric acid, Pivanex, Phenylbutyric acid, and Valproic acid). Electrophilic ketones and cyclic peptides are recently explored for their HDAC inhibitory activity [105]. Vorinostat, commonly known as suberoylanilide hydroxamic acid (SAHA), is one of the most prevalent first-generation HDAC inhibitors to be discovered first. It functions by inhibiting the class I and II family of HDAC and requires a Zn2+ ion for the catalytic binding. Vorinostat is known to deplete the ERα expression in breast cancer cells by channeling it to the ubiquitin-proteasome degradation pathway, which mitigates cell proliferation, migration, and invasion [106]. Quisinostat, a second-generation class I and II HDAC inhibitor, disrupts the self-renewability of cancer stem cells by inducing the expression of histone H1, which acts as a tumor suppressor without affecting the normal stem cells [107]. Tacedinaline, a class I and II HDAC inhibitor, yielded promising outcomes by suppressing the BIRC5 gene, which is typically overexpressed in TNBC and inhibits the expression of apoptotic proteins [108]. Mocetinostat, a class I and IV HDAC inhibitor, was found to trigger apoptotic cell death in 4T1 breast cancer cells in combination with capecitabine [109]. Chidamide, an inhibitor of HDAC 1, 2, 3, and 10, belongs to the benzamide class of HDAC inhibitors exhibited promising efficacy in the treatment of HER+ breast cancer patients along with exemestane [110]. Following the failure of CDK4/6 inhibitor administration in HR+ and HER2-negative advanced breast cancer patients, Tucidinostat combined with endocrine therapy was an emphatic strategy for such patients [111].

TH-3600_196106022

1.7.3. Histone Methyltransferase (HMT) and Histone Demethyltransferase (HDMT) inhibitors

Histone methyltransferases are essential for adding methyl groups to specific lysine or arginine residues on histone proteins. This process is catalyzed by lysine methyltransferases (KMTs) or arginine methyltransferases (RMTs), which derive the methyl groups from S-adenosyl-l-methionine (SAM). KMTs append 1, 2, or 3 methyl groups to the lysine residues, while RMTs add 1 or 2 methyl groups to the arginine residues. It is further classified based on the presence or absence of SET domain as SET domain lysine methyltransferases and DOT1 domain lysine N-methyltransferase [87]. A few histone methyltransferases include EZH2, G9a, DOT1L, and PRMT. Chaetocin, derived from Chaetomium fungi, explicitly targets the H3K9 tri-methylation mediated by SUV39H1. In MDA-MB-231 cells, it inhibited cell proliferation and induced apoptosis by activating caspase 3 and PARP proteins [112]. A PRMT5 inhibitor, GSK3326595, is in a phase II clinical trial for treating early-stage HR+ breast cancer. JNJ-64619178 is one of the potent inhibitors of PRMT5, and it is currently under clinical trial for advanced tumors [113]. Pemrametostat is an oral small molecule inhibitor under investigation, which inhibits PRMT5 and reduces the arginine methylation levels of histones H2A, H3, and H4, thus downregulating the cancer cell proliferation. Sinefungin is a natural inhibitor of EHMT1/2 derived from *Streptomyces incamatus* and *S. Griseolus* [114]. EZH2 specific inhibitors that inhibit its activity by competing with SAM are 3-deazaneplanocin A hydrochloride (DZNep), GSK2816126, EPZ005687, GSK343, GSK926, Tazemetostat, CPI-1205, etc. Some inhibitors broadly curb the activity of both EZH1/2, like UNC1999, ORS1/ORS2, and DS-3201b, while the others target the EZH2 degradation, such as GNA022, ANCR, FBW7, ZRANB1 [115].

Histone demethylases are divided into two classes based on their specificity as FAD dependant lysine-specific demethylases (LSDs) and 2-oxoglutarate- ferrous iron and oxygen-dependent demethylases, which encompasses the Jumonji C domain-containing family. The former can demethylate mono and dimethylated substrates, while the latter can demethylate mono, di, and trimethylated substrates [116]. Phenelzine, a monoamine oxidase inhibitor, inhibits the activity of LSD1 irreversibly by downregulating the mesenchymal markers alongside nab-paclitaxel in metastatic breast cancer patients. It was also found to inhibit the cancer stem cells and reduce the number of circulating tumor cells that give rise to metastasis [117]. Pargyline is a monoamine oxidase inhibitor that blocks the activity of LSD1, exhibits a dose-dependent decrease in cell proliferation, and elevated expression of cleaved PARP proteins that consequences apoptosis [118]. The MAO-A gene is primarily associated with depression but is often found to be overexpressed in breast cancer cells, contributing to poor prognosis. Clorgyline, an MAO-A inhibitor, facilitates the mesenchymal to epithelial transition (MET) in metastatic MDA-MB-231 cells by promoting the expression of epithelial markers such as E-cadherin while concurrently altering the expression of mesenchymal markers like vimentin. In addition, it suppresses cell proliferation, anchorage-independent growth, and invasiveness [119]. ORY-1001(Iadademstat) is another LSD1 inhibitor that suppresses androgen receptor expression in TNBC cells like MDA-MB-231 and BT549. It also abridges the multiplication of cells and provokes apoptosis [120]. 4SC-202, also referred to as Domatinostat is a potent inhibitor targeting both HDAC class I and LSD1[121]. It demonstrates cytostatic and cytotoxic effects, making it a promising candidate for cancer

TH-3600_196106022

therapy. Treatment of MDA-MB-231 and 4T1 TNBC cells with 4SC-202 led to cytotoxic effects, prohibited migration, invasion, and mitigated lung metastasis [121].

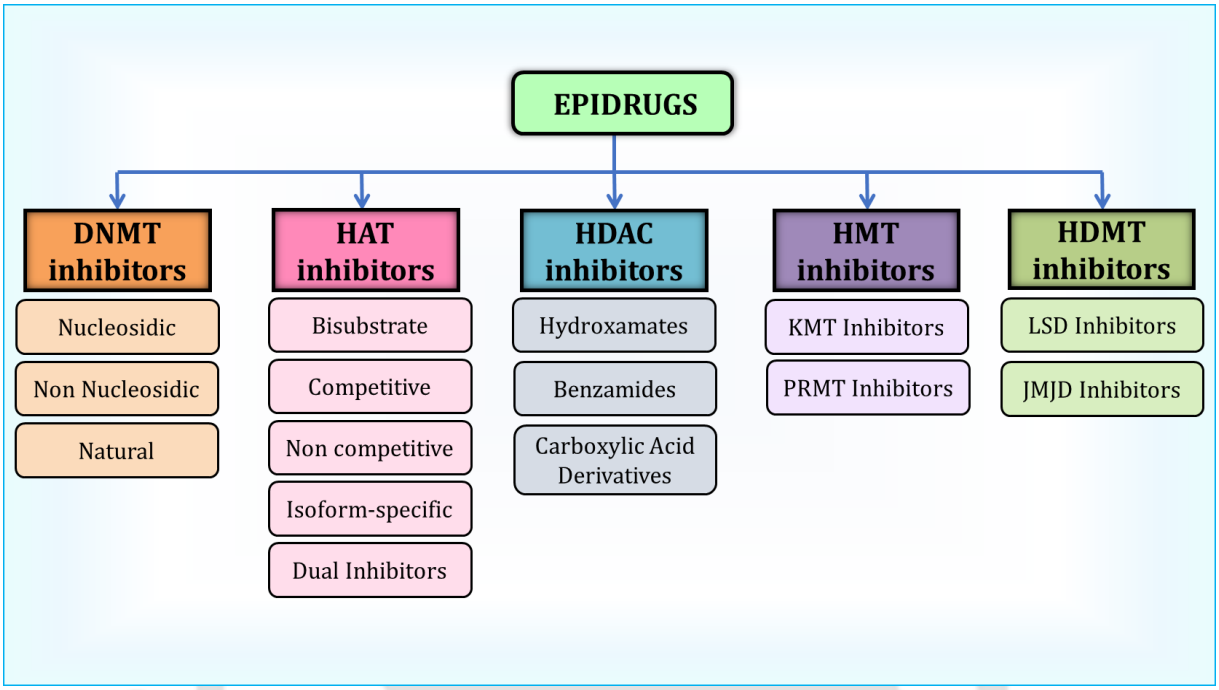

Figure 1.6: *Classification of Epidrugs used in breast cancer therapy (Concept source: https://doi.org/10.31083/j.fbl2908287).*

Table 1.1: *List of epi-drugs used in breast cancer therapy*

Generation	Type of epidrug	Name	Reference
First generation epidrugs	DNMT inhibitor	Decitabine, Azacitidine	[122, 123, 87]
	HDAC inhibitor	Vorinostat, Trichostatin A, Trapoxin A, Romidepsin	[122, 123, 87]
Second generation epidrugs	DNMT inhibitors	Zebularine, CP-4200, Guadecitabine, Hydralazine	[122, 123]
	HDAC inhibitors	Belinostat, Dacinostat, Panobinostat, CUDC-101, Quisinostat, Tefinostat,	[122, 123]

TH-3600_196106022

		Tacedinaline, Entinostat, Mocetinostat, Chidamide, Butyric acid, Pivanex, Phenylbutyric acid, Valproic acid	
Third generation epidrugs	KDM inhibitors	Tranylcypromine, ORY-101, GSK2879552, 4SC-202, Clorgyline, Pargyline, Bizine, KDM5-C70, JIB-04	[122, 123]
	KMT inhibitors	Sinefungine, Pinometostat, GSK2816126, Tazemetostat, GSK3326595, JNJ64619178, GSK3368715, EPZ-6438, CPI360, DZNep, GSK343, EI1, BIX-01294, UNC0638, EPZ004777, UNC0224	[122, 123]
	Bromodomain ligands	I-BET762, CPI-0610, OTX015, RVX-280	[122, 123]

1.7.4. Combination therapy with epidrugs in breast cancer

Combining epidrugs with chemotherapy or immunotherapy offers potential benefits such as reduced drug resistance and improved overall treatment outcomes [124, 125]. This integrated strategy holds immense potential to fight against breast cancer, paving the way for personalized and effective therapeutic interventions. Several such combinations are under clinical trial to optimize the dosage and evaluate long-term safety and efficacy **(Table 1.2)**. Combining HDAC inhibitors has proven to be more efficient than using them individually [124, 126]. The co-administration of Estrogen Related Receptor α (ERRα) inhibitor C29 with DNMT inhibitor like 5-aza-2'deoxycytidine (decitabine) inhibits the crosstalk between DNMT1 and ERRα, which contributes to the stability of ERRα that in turn contributes to DNA methylation. The conjunction of these drugs helps to reactivate the tumor suppressor gene Interferon Regulatory Factor-4 (IRF4), which mitigates the proliferation of breast cancer cells [127]. Panobinostat, an HDAC inhibitor in combination with Trastuzumab, is under clinical trials for treating HER+ metastatic breast cancer [128]. Vorinostat and Valproic acid intensified Trastuzumab mediated antibody dependent cell-mediated phagocytosis and cytotoxicity. As well as it decreased the expression of anti-apoptotic protein myeloid leukemia cell differentiation 1 (MCL1) in HER+ SKBR3 cells [129]. Entinostat, along with Lapatinib, was found to reduce the colony-forming potential by inhibiting phosphorylated AKT and FOXO3 mediated Bim expression that triggers

TH-3600_196106022

apoptosis [130]. In the case of Vorinostat and Olaparib combined treatment, Vorinostat inhibits HDAC while Olaparib blocks polyadenosine 5' diphosphoribose polymerase (PARP). Together, it affects the ability of cancer cells to repair DNA damage, which results in tumor cell death [106]. Valproic acid, a popular HDAC inhibitor, has shown to fuel up the anti-cancer activity of Capecitabine by upregulating the expression of thymidine phosphorylase (TP). TP is a key enzyme involved in the conversion of 5′-deoxy-5-fluorouridine (5′-DFUR) to 5-FU, which is further metabolized to 5-fluoro-2-deoxyuridine monophosphate (FdUMP). Further, FdUMP curbs the thymidine synthesis by interfering with DNA replication by inhibiting thymidylate synthase (TS). These two drugs synergistically induced apoptosis, RNA, and DNA damage in the breast cancer cell lines, including MCF-7, MDA-MB-231, MDA-MB-468, and SKBR3 [131]. Azacitidine and Entinostat combination, under phase 2 clinical trial, was synergistically found to inhibit DNA synthesis and class I HDAC activity [132]. Another HDAC inhibitor, Panobinostat, was proven to enhance the efficacy of Trastuzumab by evoking NK-cell mediated immune response in a CXC3 and IFNγ dependant manner in HER+ breast cancer patients [133]. Combining Entinostat and Atezolizumab mutually targeted the HDAC activity and protein-programmed cell death ligand 1 (PD-L1) in TNBC cells [134].

Moreover, Letrozole, a widely recognized aromatase inhibitor, when paired with Panobinostat, successfully reinstated ERα expression and enhanced cell sensitivity to endocrine therapy. This effect was characterized by elevated acetylation of H3 and H4 histones and resulted in the inhibition of tumor progression in ER-negative breast cancer cells [135]. Vorinostat has been shown to augment the anti-apoptotic effect of paclitaxel through acetylation of histone and α-tubulin. It also deterred the interaction of Hsp90 with AKT, c-RAF, and HER2 through proteasomal degradation of Hsp90 and exhibited antiangiogenic activity by altering the VEGF signaling pathway [136]. Hydralazine, a DNA demethylating agent, in combination with an HDAC inhibitor like magnesium valproate, synergistically induced gene reactivation and reduction in global C5 methylation in locally advanced breast cancer patients along with Doxorubicin and Cyclophosphamide [137]. A combination therapy using Romidepsin, an HDAC inhibitor, Gemcitabine, a DNA synthesis inhibitor, and DNA damaging agent, Cisplatin, was found to induce cell death in TNBC cells like MDA-MB-231, MDA-MB-468, and MCF-7 by the generation of reactive oxygen species (ROS) and proteolytic cleavage of PARP [130]. DNMT inhibitor Decitabine successfully abridged the cancer cell proliferation, DNA methylation, and DNMT1 activity along with Doxorubicin [6].

TH-3600_196106022

Table 1.2: *Details of epi-drugs used in combination with different chemotherapeutic drugs in breast cancer therapy*

Serial No.	Drugs	Target/ Effect of the drug	Reference
1.	Decitabine + C29	Inhibits DNMT1 and ERRα	[127]
2.	Vorinostat & Valproic acid + Trastuzumab	Reduction in MCL1, heightens ADCC and ADCP	[129]
3.	Entinostat + Lapatinib	Transcriptional activation of FOXO3 and Bim	[130]
4.	Vorinostat + Olaparib	HDAC, PARP	[106]
5.	Valproic acid + Capecitabine	Upregulation of TP, downregulation of TS enzyme, reduction in thymidine synthesis	[131]
6.	Azacitidine + Entinostat	Blocks DNA synthesis and HDAC class I activity	[132]
7.	Panobinostat + Trastuzumab	Triggers NK-cell mediated immune response	[133]
8.	Entinostat + Atezolizumab	Inhibits HDAC activity and PD	[134]
9.	Letrozole + Panobinostat	Sensitizes BC cells to endocrine therapy, enhances H3, H4 acetylation, inhibits aromatase activity	[135]
10.	Vorinostat + Paclitaxel	Acetylation of histone, α-tubulin, proteasomal degradation of Hsp90, and antiangiogenic activity	[136]

TH-3600_196106022

11.	Entinostat + Exemestane	HDAC class I inhibitor and Aromatase inhibitor	[87]
12.	Tacedinaline + UNC0638	Targets class I HDAC and G9a, suppresses BIRC5 and upregulates GADD45A	[108]
13.	Capecitabine + Mocetinostat	Triggers apoptotic pathway by downregulating BCl2, Akt, HDAC1, PI3K, c-myc and upregulating Bax, Pten, C-Parp, Cas-7, Cas-9, p53 and Cas-3	[109]
14.	Chidamide + Exemestane	Targets HDAC 1,2,3&10 and aromatase activity	[110]
15.	Hydralazine + Magnesium valproate + doxorubicin + cyclophosphamide	Demethylates DNA and inhibits HDAC activity, global decrease in C_5me content	[137]
16.	Phenelzine + Nab-Paclitaxel	Suppresses the generation of CSCs by inhibition of mesenchymal markers	[117]
17.	Romidepsin + Gemcitabine + Cisplatin	TNBC cell death via ROS generation	[138]
18.	Decitabine + Doxorubicin	Mitigates tumor proliferation, DNMT1 activity, and DNA methylation	[139]
19.	Zebularine + Decitabine/Vorinostat	Dysregulation of cell proliferation and colony formation potential	[92]
20.	Liraglutide + Paclitaxel/Methotrexate	Induction of global demethylation through the abrogation of DNMTs and transcription of CDH1, ESR1, and	[95]

TH-3600_196106022

		ADAM33 genes, resulting in reduced migration and viability	

1.7.5. Epigenetic drug repurposing

Given the limitations of conventional chemotherapies and the low success rate of newly synthesized drugs, drug repurposing has gained attention as a viable therapeutic strategy. Drug repurposing involves applying approved drugs to new therapeutic uses, offering a faster and more cost-effective alternative to drug development [140]. The availability of large amounts of data frequently minimizes the need for additional research to examine the pharmacokinetic characteristics and toxicity of approved drugs, which is a significant benefit of this approach [141]. Drug repurposing offers a new approach for more rapid and potentially more affordable development of therapies aimed at addressing the widespread epigenetic alterations in human cancer.

Some widely recognized epidrugs used in cancer therapy, impacting epigenetic targets, and are either FDA-approved or undergoing clinical trials. The first anticancer epidrugs developed through repurposing were 5-azacytidine and 5-aza-2′-deoxycytidine (decitabine). Initially, the FDA approved these drugs for treating myelodysplastic syndromes due to their antimetabolic effects observed in *in vitro* cancer cell assays. Later, it was discovered that both azacytidine and decitabine could inhibit DNA methylation, making them effective in tumor cells and in myelodysplastic syndromes [142]. Several drugs such as Hydralazine (antihypertensive drug), Olsalazine (anti-inflammatory agent), Mithramycin A (antibiotic), Nanaomycin A (anthracycline antibiotic), Disulfiram (alcohol aversive drug) were repurposed as a DNMT Inhibitors for cancer therapy. Further, some repurposed drugs were identified to inhibit HDAC enzymes such as Valproic acid (anticonvulsant), Apicidin (antimalarial drug) and Artemisin (antimalarial drug). Ribavirin (antiviral drug) and hydroxychloroquine (antimalarial drug) has been found to be effective as HMT Inhibitor [143]. Overall, repurposing drugs provides a valuable opportunity to explore their hidden potential, especially those with epigenetic remodelling effects beneficial for cancer treatment. This approach can significantly shorten drug development times and offers promising prospects for advancing precision medicine.

1.8. Gaps in the Literature

Despite significant advancements in understanding the role of epigenetic modifications in breast cancer, several knowledge gaps remain.

1.8.1. Epigenetic Regulation of EMT

Although epigenetic regulators such as DOT1L, p300, and G9a have been implicated in EMT, the precise mechanisms through which epigenetic modifications dynamically regulate EMT transcription factors in different breast cancer subtypes remain unclear. Moreover, the context-dependent nature of these modifications, their reversibility, and their contribution to EMT plasticity warrant further exploration.

TH-3600_196106022

1.8.2. Epigenetic Control of Cancer Stemness

While histone modifications and DNA methylation have been linked to the maintenance of BCSCs, the specific epigenetic signatures distinguishing BCSCs from non-stem-like cancer cells remain insufficiently characterized. The precise role of epigenetic modulators in shaping stemness-related signaling pathways, such as Notch, Wnt, Hedgehog, and Hippo/YAP, remains an active area of investigation [58].

1.8.3. Epigenetics and Drug Resistance

Although epigenetic dysregulation has been linked to therapeutic resistance in breast cancer, the exact mechanisms underlying resistance to endocrine therapy and chemotherapy remain incompletely defined. The interplay between the epigenetic factors and other resistance mechanisms, such as metabolic reprogramming and immune evasion, remains unexplored. Additionally, the role of histone acetyltransferases and deacetylases in modulating drug response and their potential as combinatorial therapeutic targets requires further investigation.

1.8.4. Epigenetic Crosstalk with Autophagy

Epigenetic regulation of autophagy in breast cancer is an emerging field, yet gaps remain in understanding how histone modifications and DNA methylation influence key autophagy-related genes such as BECN1, ATG2B, and ATG4D. The relationship between tumor-specific epigenetic changes and autophagy modulation in response to stress, therapy, and metastasis is not well-characterized.

1.8.5. Translational and Therapeutic Implications

Although epigenetic inhibitors including, BRD4 inhibitors, HDAC inhibitors, and G9a inhibitors have demonstrated promise in preclinical models, their clinical translation remains limited. A deeper understanding of the specificity, long-term effects, and potential resistance mechanisms against epigenetic therapies is crucial. Furthermore, the combinatorial potential of epigenetic drugs with conventional chemotherapy, immunotherapy, and targeted therapies in TNBC remains underexplored.

Addressing these gaps will provide deeper insights into the epigenetic landscape governing EMT, cancer stemness, drug resistance, and autophagy. This will pave the way for more precise therapeutic interventions, ultimately improving clinical outcomes for breast cancer patients.

1.9. Key features and Scope of Research

A comprehensive literature review on epigenetic mechanisms and their role in breast cancer progression highlights the following potential research avenues:

- Identifying the critical epigenetic regulators involved in EMT regulation and metastasis in TNBC cells.
- Exploring potential drugs or inhibitors to address epigenetic aberrations in TNBC cells.
- Assessing FDA-approved drugs for their potential to target epigenetic proteins and EMT pathways in TNBC therapy.

TH-3600_196106022

- Exploring the role of epigenetic regulators in several cellular processes such as autophagy, stemness and metabolism.
- Developing suitable combination therapeutic module to modulate key oncogenic signalling pathways.
- Investigating the interplay between epigenetic regulators and other cellular pathways, such as wnt, MAPK, PI3K-AKT and Notch signalling to provide valuable insights into TNBC pathogenesis.

1.10. Thesis Objectives

- Identification and experimental validation of potential repurposed drugs against histone acetyltransferase p300.
- Studying the role of histone methyltransferase MLL1 in EMT and Metabolic pathways in TNBC cells.
- Co-therapeutic strategy to modulate epigenetic and autophagy pathways in TNBC cells.

1.11. Salient Outcome

- The present study reveals key epigenetic mechanisms driving EMT progression and TNBC aggressiveness.
- Identification of novel therapeutic targets and potential therapeutic strategy to address epigenetic alterations in TNBC.
- The crosstalk between epigenetic mechanisms and EMT signalling pathways was established.
- Leveraging epigenetic alterations to regulate EMT, stemness, metabolism and autophagy, provides therapeutic interventions to annihilate TNBC progression.

TH-3600_196106022

1.12. References

1. Bray, F., Ferlay, J., Soerjomataram, I., Siegel, R. L., Torre, L. A., & Jemal, A. (2018). Global cancer statistics 2018: GLOBOCAN estimates of incidence and mortality worldwide for 36 cancers in 185 countries. *CA: a cancer journal for clinicians*, 68(6), 394–424. https://doi.org/10.3322/caac.21492

2. Turner, K. M., Yeo, S. K., Holm, T. M., Shaughnessy, E., & Guan, J. L. (2021). Heterogeneity within molecular subtypes of breast cancer. *American journal of physiology. Cell physiology*, 321(2), C343–C354. https://doi.org/10.1152/ajpcell.00109.2021

3. Douganiotis, G., Kontovinis, L., Markopoulou, E., Ainali, A., Zarampoukas, T., Natsiopoulos, I., & Papazisis, K. (2022). Prognostic Significance of Low HER2 Expression in Patients with Early Hormone Receptor Positive Breast Cancer. *Cancer diagnosis & prognosis*, 2(3), 316–323. https://doi.org/10.21873/cdp.10111

4. Obidiro, O., Battogtokh, G., & Akala, E. O. (2023). Triple negative breast cancer treatment options and limitations: future outlook. *Pharmaceutics*, 15(7), 1796. https://doi.org/10.3390%2Fpharmaceutics15071796

5. Moo, T. A., Sanford, R., Dang, C., & Morrow, M. (2018). Overview of Breast Cancer Therapy. *PET clinics*, 13(3), 339–354. https://doi.org/10.1016/j.cpet.2018.02.006

6. Lu, Y., Chan, Y. T., Tan, H. Y., Li, S., Wang, N., & Feng, Y. (2020). Epigenetic regulation in human cancer: the potential role of epi-drug in cancer therapy. *Molecular cancer*, 19(1), 79. https://doi.org/10.1186/s12943-020-01197-3

7. Morel, D., Jeffery, D., Aspeslagh, S., Almouzni, G., & Postel-Vinay, S. (2020). Combining epigenetic drugs with other therapies for solid tumours - past lessons and future promise. Nature reviews. *Clinical oncology*, 17(2), 91–107. https://doi.org/10.1038/s41571-019-0267-4

8. VD, P., & V, V. (2022). Targeting epigenetic alterations in cancer stem cells. Frontiers in *Molecular Medicine*, 2, 1011882. https://doi.org/10.3389/fmmed.2022.1011882

9. Taylor, A., Brady, A. F., Frayling, I. M., Hanson, H., Tischkowitz, M., Turnbull, C., Side, L., & UK Cancer Genetics Group (UK-CGG) (2018). Consensus for genes to be included on cancer panel tests offered by UK genetics services: guidelines of the UK Cancer Genetics Group. *Journal of medical genetics*, 55(6), 372–377. https://doi.org/10.1136/jmedgenet-2017-105188

10. Chen, J. F., & Yan, Q. (2021). The roles of epigenetics in cancer progression and metastasis. *The Biochemical journal*, 478(17), 3373–3393. https://doi.org/10.1042/BCJ20210084

TH-3600_196106022

11. Schröder R, Illert A-L, Erbes T, Flotho C, Lübbert M, Duque-Afonso J. (2021) The epigenetics of breast cancer – Opportunities for diagnostics, risk stratification and therapy. *Epigenetics*; 17:612–24. https://doi.org/10.1080/15592294.2021.1940644 .

12. Okano, M., Bell, D. W., Haber, D. A., & Li, E. (1999). DNA methyltransferases Dnmt3a and Dnmt3b are essential for de novo methylation and mammalian development. *Cell*, 99(3), 247–257. https://doi.org/10.1016/s0092-8674(00)81656-6

13. Ruiz-Flores, L., Ebuoma, L. O., Benveniste, M. F., Nagi, C., OrtizPerez, T., & Benveniste, A. P. (2018). Case Report: Metastatic Phyllodes Tumor. *Seminars in ultrasound, CT, and MR*, 39(1), 122–126. https://doi.org/10.1053/j.sult.2017.05.011

14. Veeck, J., & Esteller, M. (2010). Breast cancer epigenetics: from DNA methylation to microRNAs. *Journal of mammary gland biology and neoplasia*, 15(1), 5–17. https://doi.org/10.1007/s10911-010-9165-1

15. Costa, F. F., Paixão, V. A., Cavalher, F. P., Ribeiro, K. B., Cunha, I. W., Rinck, J. A., Jr, O'Hare, M., Mackay, A., Soares, F. A., Brentani, R. R., & Camargo, A. A. (2006). SATR-1 hypomethylation is a common and early event in breast cancer. *Cancer genetics and cytogenetics*, 165(2), 135–143. https://doi.org/10.1016/j.cancergencyto.2005.07.023

16. Guo, Y., Pakneshan, P., Gladu, J., Slack, A., Szyf, M., & Rabbani, S. A. (2002). Regulation of DNA methylation in human breast cancer. Effect on the urokinase-type plasminogen activator gene production and tumor invasion. *The Journal of biological chemistry*, 277(44), 41571–41579. https://doi.org/10.1074/jbc.M201864200

17. Sharma, G., Mirza, S., Parshad, R., Srivastava, A., Datta Gupta, S., Pandya, P., & Ralhan, R. (2010). CpG hypomethylation of MDR1 gene in tumor and serum of invasive ductal breast carcinoma patients. *Clinical biochemistry*, 43(4-5), 373–379. https://doi.org/10.1016/j.clinbiochem.2009.10.009

18. Gupta, A., Godwin, A. K., Vanderveer, L., Lu, A., & Liu, J. (2003). Hypomethylation of the synuclein gamma gene CpG island promotes its aberrant expression in breast carcinoma and ovarian carcinoma. *Cancer research*, 63(3), 664–673. (PMID: 12566312)

19. Djebali, S., Davis, C. A., Merkel, A., Dobin, A., Lassmann, T., Mortazavi, A., Tanzer, A., Lagarde, J., Lin, W., Schlesinger, F., Xue, C., Marinov, G. K., Khatun, J., Williams, B. A., Zaleski, C., Rozowsky, J., Röder, M., Kokocinski, F., Abdelhamid, R. F., Alioto, T., ... Gingeras, T. R. (2012). Landscape of transcription in human cells. *Nature*, 489(7414), 101–108. https://doi.org/10.1038/nature11233

TH-3600_196106022

20. Serviss, J. T., Johnsson, P., & Grandér, D. (2014). An emerging role for long non-coding RNAs in cancer metastasis. *Frontiers in genetics*, 5, 234. https://doi.org/10.3389/fgene.2014.00234

21. Palazzo, A. F., & Lee, E. S. (2015). Non-coding RNA: what is functional and what is junk?. *Frontiers in genetics*, 6, 2. https://doi.org/10.3389/fgene.2015.00002

22. Iorio, M. V., Ferracin, M., Liu, C. G., Veronese, A., Spizzo, R., Sabbioni, S., Magri, E., Pedriali, M., Fabbri, M., Campiglio, M., Ménard, S., Palazzo, J. P., Rosenberg, A., Musiani, P., Volinia, S., Nenci, I., Calin, G. A., Querzoli, P., Negrini, M., & Croce, C. M. (2005). MicroRNA gene expression deregulation in human breast cancer. *Cancer research*, 65(16), 7065–7070. https://doi.org/10.1158/0008-5472.CAN-05-1783

23. Yan, L. X., Huang, X. F., Shao, Q., Huang, M. Y., Deng, L., Wu, Q. L., Zeng, Y. X., & Shao, J. Y. (2008). MicroRNA miR-21 overexpression in human breast cancer is associated with advanced clinical stage, lymph node metastasis and patient poor prognosis. *RNA* (New York, N.Y.), 14(11), 2348–2360. https://doi.org/10.1261/rna.1034808

24. Wang, N., Zhang, H., Li, D., Jiang, C., Zhao, H., & Teng, Y. (2021). Identification of novel biomarkers in breast cancer via integrated bioinformatics analysis and experimental validation. *Bioengineered*, 12(2), 12431–12446. https://doi.org/10.1080/21655979.2021.2005747

25. Luo, Q., Li, X., Gao, Y., Long, Y., Chen, L., Huang, Y., & Fang, L. (2013). MiRNA-497 regulates cell growth and invasion by targeting cyclin E1 in breast cancer. *Cancer cell international*, 13(1), 95. https://doi.org/10.1186/1475-2867-13-95

26. Statello, L., Guo, C. J., Chen, L. L., & Huarte, M. (2021). Gene regulation by long non-coding RNAs and its biological functions. *Nature reviews. Molecular cell biology*, 22(2), 96–118. https://doi.org/10.1038/s41580-020-00315-9

27. Filippova, E. A., Fridman, M. V., Burdennyy, A. M., Loginov, V. I., Pronina, I. V., Lukina, S. S., Dmitriev, A. A., & Braga, E. A. (2021). Long Noncoding RNA GAS5 in Breast Cancer: Epigenetic Mechanisms and Biological Functions. *International journal of molecular sciences*, 22(13), 6810. https://doi.org/10.3390/ijms22136810

28. Arun, G., & Spector, D. L. (2019). MALAT1 long non-coding RNA and breast cancer. *RNA biology*, 16(6), 860–863. https://doi.org/10.1080/15476286.2019.1592072

TH-3600_196106022

29. Khan, S. A., Reddy, D., & Gupta, S. (2015). Global histone post-translational modifications and cancer: Biomarkers for diagnosis, prognosis and treatment?. *World journal of biological chemistry*, 6(4), 333–345. https://doi.org/10.4331/wjbc.v6.i4.333

30. Hosseini A, Minucci S. (2018). Alterations of Histone Modifications in Cancer. *Epigenetics in Human Disease* :141–217. https://doi.org/10.1016/b978-0-12-812215-0.00006-6

31. Ansari, K. I., Kasiri, S., & Mandal, S. S. (2013). Histone methylase MLL1 has critical roles in tumor growth and angiogenesis and its knockdown suppresses tumor growth in vivo. *Oncogene*, 32(28), 3359–3370. https://doi.org/10.1038/onc.2012.352

32. Yang, X., Karuturi, R. M., Sun, F., Aau, M., Yu, K., Shao, R., ... & Yu, Q. (2009). CDKN1C (p57KIP2) is a direct target of EZH2 and suppressed by multiple epigenetic mechanisms in breast cancer cells. PloS one, 4(4), e5011. https://doi.org/10.1371/journal.pone.0005011

33. Ma, J., Zhang, J., Weng, Y. C., & Wang, J. C. (2018). EZH2-mediated microRNA-139-5p regulates epithelial-mesenchymal transition and lymph node metastasis of pancreatic cancer. *Molecules and Cells*, 41(9), 868–880. https://doi.org/10.14348/molcells.2018.0109

34. Byun, W. S., Kim, W. K., Han, H. J., Chung, H. J., Jang, K., Kim, H. S., ... & Lee, S. K. (2019). Targeting histone methyltransferase DOT1L by a novel psammaplin A analog inhibits growth and metastasis of triple-negative breast cancer. Molecular Therapy-Oncolytics, 15, 140-152.https://doi.org/10.1016/j.omto.2019.09.005

35. Thakur, C., Qiu, Y., Fu, Y., Bi, Z., Zhang, W., Ji, H., & Chen, F. (2022). Epigenetics and environment in breast cancer: New paradigms for anti-cancer therapies. Frontiers in Oncology, 12, 971288.https://doi.org/10.3389/fonc.2022.971288

36. Pei, J., Zhang, S., Yang, X., Han, C., Pan, Y., Li, J., ... & Zhang, J. (2023). Epigenetic regulator KDM4A activates Notch1-NICD-dependent signaling to drive tumorigenesis and metastasis in breast cancer. Translational Oncology, 28, 101615. https://doi.org/10.1016/j.tranon.2022.101615

37. Gaughan, L., Stockley, J., Coffey, K., O'Neill, D., Jones, D. L., Wade, M., Wright, J., Moore, M., Tse, S., Rogerson, L., & Robson, C. N. (2013). KDM4B is a master regulator of the estrogen receptor signalling cascade. *Nucleic Acids Research*, 41(14), 6892–6904. https://doi.org/10.1093/nar/gkt469

38. Wu, X., Deng, Y., Zu, Y., & Yin, J. (2022). Histone demethylase KDM4C activates HIF1α/VEGFA signaling through the costimulatory factor STAT3 in NSCLC. *American Journal of Cancer*

TH-3600_196106022

Research, 12(2), 5692. PMID: 36628291. https://www.ncbi.nlm.nih.gov/pmc/articles/PMC9827078/

39. Fuentes, N., & Silveyra, P. (2019). Estrogen receptor signaling mechanisms. *Advances in Protein Chemistry and Structural Biology*, 116, 135–170. https://doi.org/10.1016/bs.apcsb.2019.01.001

40. Yaşar, P., Ayaz, G., User, S. D., Güpür, G., & Muyan, M. (2016). Molecular mechanism of estrogen–estrogen receptor signaling. *Reproductive Medicine and Biology*, 16, 4–20. https://doi.org/10.1002/rmb2.12006

41. Zattarin, E., Leporati, R., Ligorio, F., Lobefaro, R., Vingiani, A., Pruneri, G., & Vernieri, C. (2020). Hormone receptor loss in breast cancer: molecular mechanisms, clinical settings, and therapeutic implications. Cells, 9(12), 2644. https://doi.org/10.3390/cells9122644

42. Zhang, J., Zhou, C., Jiang, H., Liang, L., Shi, W., Zhang, Q., Sun, P., Xiang, R., Wang, Y., & Yang, S. (2017). ZEB1 induces ER-α promoter hypermethylation and confers antiestrogen resistance in breast cancer. *Cell Death & Disease*, 8(4), e2732. https://doi.org/10.1038/cddis.2017.154

43. Gourdy, P., Guillaume, M., Fontaine, C., Adlanmerini, M., Montagner, A., Laurell, H., Lenfant, F., & Arnal, J. F. (2018). Estrogen receptor subcellular localization and cardiometabolism. *Molecular Metabolism*, 15, 56–69. https://doi.org/10.1016/j.molmet.2018.05.009

44. Hervouet, E., Cartron, P.-F., Jouvenot, M., & Delage-Mourroux, R. (2013). Epigenetic regulation of estrogen signaling in breast cancer. *Epigenetics*, 8, 237–245. https://doi.org/10.4161/epi.23790

45. Di Martino, M. T., Arbitrio, M., Caracciolo, D., Cordua, A., Cuomo, O., Grillone, K., Riillo, C., Caridà, G., Scionti, F., Labanca, C., & Romeo, C. (2022). miR-221/222 as biomarkers and targets for therapeutic intervention on cancer and other diseases: A systematic review. *Molecular Therapy-Nucleic Acids*, 27, 1191–1224. https://doi.org/10.1016/j.omtn.2022.02.005

46. Di Leva, G., Gasparini, P., Piovan, C., Ngankeu, A., Garofalo, M., Taccioli, C., Iorio, M. V., Li, M., Volinia, S., Alder, H., & Nakamura, T. (2010). MicroRNA cluster 221-222 and estrogen receptor α interactions in breast cancer. *JNCI: Journal of the National Cancer Institute*, 102(10), 706–721. https://doi.org/10.1093/jnci/djq102

47. Cho, M. H., Park, J. H., Choi, H. J., Park, M. K., Won, H. Y., Park, Y. J., ... & Kong, G. (2015). DOT1L cooperates with the c-Myc-p300 complex to epigenetically derepress CDH1 transcription factors in breast cancer progression. Nature communications, 6(1), 7821.https://doi.org/10.1038/ncomms8821

TH-3600_196106022

48. Liu, J., Sun, X., Qin, S., Wang, H., Du, N., Li, Y., ... & Ren, H. (2016). CDH1 promoter methylation correlates with decreased gene expression and poor prognosis in patients with breast cancer. Oncology letters, 11(4), 2635-2643. https://doi.org/10.3892/ol.2016.4274

49. Pećina-Šlaus, N. (2003). Tumor suppressor gene E-cadherin and its role in normal and malignant cells. *Cancer Cell International*, 3, 1–7. https://doi.org/10.1186/1475-2867-3-17

50. Dong, C., Wu, Y., Yao, J., Wang, Y., Yu, Y., Rychahou, P. G., ... & Zhou, B. P. (2012). G9a interacts with Snail and is critical for Snail-mediated E-cadherin repression in human breast cancer. The Journal of clinical investigation, 122(4), 1469-1486. https://doi.org/10.1172/jci57349

51. Wang, X., Chen, S., Shen, T., Lu, H., Xiao, D., Zhao, M., ... & Cheng, Z. (2020). Trichostatin A reverses epithelial-mesenchymal transition and attenuates invasion and migration in MCF-7 breast cancer cells. *Experimental and therapeutic medicine*, 19(3), 1687-1694. https://doi.org/10.3892/etm.2020.8422

52. Lu, L., Chen, Z., Lin, X., Tian, L., Su, Q., An, P., ... & Wang, H. (2020). Inhibition of BRD4 suppresses the malignancy of breast cancer cells via regulation of Snail. Cell Death & Differentiation, 27(1), 255-268. https://doi.org/10.1038/s41418-019-0353-2

53. Kochumon, S., Al-Sayyar, A., Jacob, T., Bahman, F., Akhter, N., Wilson, A., ... & Al-Mulla, F. (2024). TGF-β and TNF-α interaction promotes the expression of MMP-9 through H3K36 dimethylation: implications in breast cancer metastasis. Frontiers in Immunology, 15, 1430187. https://doi.org/10.3389/fimmu.2024.1430187

54. Satam, S., Palekar, N., Premkumar, K., & Shankar, B. S. (2024). Sirtinol, a SIRT1 inhibitor, inhibits the EMT and metastasis of 4T1 breast cancer cells and impacts the tumor microenvironment. Immunopharmacology and Immunotoxicology, 46(6), 829-842. https://doi.org/10.1080/08923973.2024.2412110

55. Ahmadpour, F., Igder, S., Eftekhari Moghadam, A. R., Moradipoodeh, B., Sepahdar, A., Mokarram, P., Fallahi, J., & Mohammadzadeh, G. (2024). Metformin as a Potential Therapeutic Agent in Breast Cancer: Targeting miR-125a Methylation and Epigenetic Regulation. International journal of molecular and cellular medicine, 13(3), 272–285. https://doi.org/10.22088/IJMCM.BUMS.13.3.272

56. Zhang, X., Powell, K., & Li, L. (2020). Breast cancer stem cells: Biomarkers, identification and isolation methods, regulating mechanisms, cellular origin, and beyond. *Cancers*, 12(3765). https://doi.org/10.3390/cancers12123765

TH-3600_196106022

57. Toh, T. B., Lim, J. J., & Chow, E. K.-H. (2017). Epigenetics in cancer stem cells. *Molecular Cancer*, 16. https://doi.org/10.1186/s12943-017-0596-9

58. Keyvani-Ghamsari, S., Khorsandi, K., Rasul, A., & Zaman, M. K. (2021). Current understanding of epigenetics mechanism as a novel target in reducing cancer stem cells resistance. *Clinical Epigenetics*, 13. https://doi.org/10.1186/s13148-021-01107-4

59. Klarmann, G. J., Decker, A., & Farrar, W. L. (2008). Epigenetic gene silencing in the Wnt pathway in breast cancer. *Epigenetics*, 3(59–63). https://doi.org/10.4161/epi.3.2.5899

60. Li, G., Wang, D., Ma, W., An, K., Liu, Z., Wang, X., ... & Sun, Y. (2018). Transcriptomic and epigenetic analysis of breast cancer stem cells. Epigenomics, 10(6), 765-783. https://doi.org/10.2217/epi-2018-0008

61. Cui, W., Wang, L. H., Wen, Y. Y., Song, M., Li, B. L., Chen, X. L., ... & Wang, E. H. (2010). Expression and regulation mechanisms of Sonic Hedgehog in breast cancer. Cancer science, 101(4), 927-933.https://doi.org/10.1111/j.1349-7006.2010.01495.x

62. Samadani, A. A., Norollahi, S. E., Rashidy-Pour, A., Mansour-Ghanaei, F., Nemati, S., Joukar, F., ... & Gatei, M. (2018). Cancer signaling pathways with a therapeutic approach: An overview in epigenetic regulations of cancer stem cells. Biomedicine & Pharmacotherapy, 108, 590-599.https://doi.org/10.1016/j.biopha.2018.09.048

63. Gonzalez, M. E., Moore, H. M., Li, X., Toy, K. A., Huang, W., Sabel, M. S., ... & Kleer, C. G. (2014). EZH2 expands breast stem cells through activation of NOTCH1 signaling. Proceedings of the National Academy of Sciences, 111(8), 3098-3103.https://doi.org/10.1073/pnas.1308953111

64. Ponnusamy, L., Mahalingaiah, P. K. S., Chang, Y. W., & Singh, K. P. (2019). Role of cellular reprogramming and epigenetic dysregulation in acquired chemoresistance in breast cancer. *Cancer Drug Resistance*, 2(2), 297. https://doi.org/10.20517/cdr.2018.11

65. Brabletz, S., Bajdak, K., Meidhof, S., Burk, U., Niedermann, G., Firat, E., ... & Brabletz, T. (2011). The ZEB1/miR-200 feedback loop controls Notch signalling in cancer cells. The EMBO journal, 30(4), 770-782. https://doi.org/10.1038/emboj.2010.349

66. Nandy, S. B., Arumugam, A., Subramani, R., Pedroza, D., Hernandez, K., Saltzstein, E., & Lakshmanaswamy, R. (2015). MicroRNA-125a influences breast cancer stem cells by targeting leukemia inhibitory factor receptor which regulates the Hippo signaling pathway. *Oncotarget*, 6(19), 17366–17376). https://doi.org/10.18632/oncotarget.3953

TH-3600_196106022

67. Zhang, H., Lang, T. Y., Zou, D. L., Zhou, L., Lou, M., Liu, J. S., ... & Li, L. (2019). miR-520b promotes breast cancer stemness through Hippo/YAP signaling pathway. OncoTargets and therapy, 11691-11700. https://doi.org/10.2147/ott.s236607

68. Wang, N., Ma, T., & Yu, B. (2023). Targeting epigenetic regulators to overcome drug resistance in cancers. *Signal Transduction and Targeted Therapy*, 8. https://doi.org/10.1038/s41392-023-01341-7

69. Wu, Y., Zhang, Z., Cenciarini, M. E., Proietti, C. J., Amasino, M., Hong, T., ... & Xu, K. (2018). Tamoxifen resistance in breast cancer is regulated by the EZH2–ERα–GREB1 transcriptional axis. Cancer research, 78(3), 671-684. https://doi.org/10.1158/0008-5472.can-17-1327

70. Kim, M. R., Wu, M.-J., Zhang, Y., Yang, J.-Y., & Chang, C. J. (2020). TET2 directs mammary luminal cell differentiation and endocrine response. *Nature Communications*, 11. https://doi.org/10.1038/s41467-020-18129-w

71. Oh, J. H., Lee, J. Y., Kim, K. H., Kim, C. Y., Jeong, D. S., Cho, Y., ... & Kim, M. H. (2020). Elevated GCN5 expression confers tamoxifen resistance by upregulating AIB1 expression in ER-positive breast cancer. Cancer Letters, 495, 145-155. https://doi.org/10.1016/j.canlet.2020.09.017

72. Waddell, A., Mahmud, I., Ding, H., Huo, Z., & Liao, D. (2021). Pharmacological inhibition of CBP/p300 blocks estrogen receptor alpha (ERα) function through suppressing enhancer H3K27 acetylation in luminal breast cancer. *Cancers*, 13(2799). https://doi.org/10.3390/cancers13112799

73. Verigos, J., Karakaidos, P., Kordias, D., Papoudou-Bai, A., Evangelou, Z., Harissis, H. V., ... & Magklara, A. (2019). The histone demethylase LSD1/KDM1A mediates chemoresistance in breast cancer via regulation of a stem cell program. Cancers, 11(10), 1585. https://doi.org/10.3390/cancers11101585

74. Boulding, T., McCuaig, R. D., Tan, A., Hardy, K., Wu, F., Dunn, J., ... & Rao, S. (2018). LSD1 activation promotes inducible EMT programs and modulates the tumour microenvironment in breast cancer. Scientific reports, 8(1), 73.https://doi.org/10.1038/s41598-017-17913-x

75. Metzger, E., Stepputtis, S. S., Strietz, J., Preca, B. T., Urban, S., Willmann, D., ... & Schüle, R. (2017). KDM4 inhibition targets breast cancer stem–like cells. Cancer research, 77(21), 5900-5912.https://doi.org/10.1158/0008-5472.can-17-1754

76. Choi, H. J., Joo, H. S., Won, H. Y., Min, K. W., Kim, H. Y., Son, T., ... & Kong, G. (2018). Role of RBP2-induced ER and IGF1R-ErbB signaling in tamoxifen resistance in breast cancer. JNCI: Journal of the National Cancer Institute, 110(4), 400-410.https://doi.org/10.1093/jnci/djx207

TH-3600_196106022

77. Zhou, Q., Song, C., Liu, X., Qin, H., Miao, L., & Zhang, X. (2019). Peptidylarginine deiminase 4 overexpression resensitizes MCF-7/ADR breast cancer cells to adriamycin via GSK3β/p53 activation. *Cancer Management and Research*, 11(625–636). https://doi.org/10.2147/cmar.s191353

78. Mandhair, H. K., Novak, U., & Radpour, R. (2021). Epigenetic regulation of autophagy: A key modification in cancer cells and cancer stem cells. *World Journal of Stem Cells*, 13(6), 542–567. https://doi.org/10.4252/wjsc.v13.i6.542

79. Li, Z., Chen, B., Wu, Y., Jin, F., Xia, Y., & Liu, X. (2010). Genetic and epigenetic silencing of the beclin 1 gene in sporadic breast tumors. *BMC cancer*, 10, 98. https://doi.org/10.1186/1471-2407-10-98

80. Zhang, X., Li, C., Wang, D., Chen, Q., Li, C. L., & Li, H. J. (2016). Aberrant methylation of ATG2B, ATG4D, ATG9A and ATG9B CpG island promoter is associated with decreased mRNA expression in sporadic breast carcinoma. *Gene*, 590(2), 285–292. https://doi.org/10.1016/j.gene.2016.05.036

81. Park, S. E., Yi, H. J., Suh, N., Park, Y. Y., Koh, J. Y., Jeong, S. Y., Cho, D. H., Kim, C. S., & Hwang, J. J. (2016). Inhibition of EHMT2/G9a epigenetically increases the transcription of Beclin-1 via an increase in ROS and activation of NF-κB. *Oncotarget*, 7(26), 39796–39808. https://doi.org/10.18632/oncotarget.9290

82. Lyu, L., Li, H., Lu, K., Jiang, S., & Li, H. (2024). PAK inhibitor FRAX486 decreases the metastatic potential of triple-negative breast cancer cells by blocking autophagy. British journal of cancer, 130(3), 394-405.https://doi.org/10.1038/s41416-023-02523-4

83. Babaei, G., Aziz, S. G. G., & Jaghi, N. Z. Z. (2021). EMT, cancer stem cells and autophagy; The three main axes of metastasis. Biomedicine & Pharmacotherapy, 133, 110909. https://doi.org/10.1016/j.biopha.2020.110909

84. Chen, H. T., Liu, H., Mao, M. J., Tan, Y., Mo, X. Q., Meng, X. J., ... & Jiang, G. M. (2019). Crosstalk between autophagy and epithelial-mesenchymal transition and its application in cancer therapy. Molecular cancer, 18, 1-19. https://doi.org/10.1186/s12943-019-1030-2

85. Li, M., Liu, J., Li, S., Feng, Y., Yi, F., Wang, L., ... & Cao, L. (2019). Autophagy-related 7 modulates tumor progression in triple-negative breast cancer. Laboratory Investigation, 99(9), 1266-1274. https://doi.org/10.1038/s41374-019-0249-2

TH-3600_196106022

86. Huang, M., Fu, M., Wang, J., Xia, C., Zhang, H., Xiong, Y., ... & Liu, F. (2021). TGF-β1-activated cancer-associated fibroblasts promote breast cancer invasion, metastasis and epithelial-mesenchymal transition by autophagy or overexpression of FAP-α. Biochemical Pharmacology, 188, 114527. https://doi.org/10.1016/j.bcp.2021.114527

87. Montalvo-Casimiro, M., González-Barrios, R., Meraz-Rodriguez, M. A., Juárez-González, V. T., Arriaga-Canon, C., & Herrera, L. A. (2020). Epidrug repurposing: Discovering new faces of old acquaintances in cancer therapy. *Frontiers in Oncology, 10*. https://doi.org/10.3389/fonc.2020.605386

88. Chovanec, M., Taza, F., Kalra, M., Hahn, N., Nephew, K. P., Spinella, M. J., & Albany, C. (2018). Incorporating DNA methyltransferase inhibitors (DNMTis) in the treatment of genitourinary malignancies: A systematic review. *Targeted Oncology, 13*(1), 49–60. https://doi.org/10.1007/s11523-017-0546-x

89. Juárez-Mercado, K. E., Prieto-Martínez, F. D., Sánchez-Cruz, N., Peña-Castillo, A., Prada-Gracia, D., & Medina-Franco, J. L. (2020). Expanding the structural diversity of DNA methyltransferase inhibitors. *Pharmaceuticals, 14*(1), 17. https://doi.org/10.3390/ph14010017

90. Szyf, M. (2012). DNA methylation signatures for breast cancer classification and prognosis. *Genome Medicine, 4*, 26. https://doi.org/10.1186/gm325

91. Candelaria, M., Gallardo-Rincón, D., Arce, C., Cetina, L., Aguilar-Ponce, J. L., & Arrieta, Ó., et al. (2007). A phase II study of epigenetic therapy with hydralazine and magnesium valproate to overcome chemotherapy resistance in refractory solid tumors. *Annals of Oncology, 18*(9), 1529–1538. https://doi.org/10.1093/annonc/mdm204

92. Billam, M., Sobolewski, M. D., & Davidson, N. E. (2009). Effects of a novel DNA methyltransferase inhibitor zebularine on human breast cancer cells. *Breast Cancer Research and Treatment, 120*(3), 581–592. https://doi.org/10.1007/s10549-009-0420-3

93. Altundag, O., Altundag, K., & Gunduz, M. (2004). DNA methylation inhibitor, procainamide, may decrease the tamoxifen resistance by inducing overexpression of the estrogen receptor beta in breast cancer patients. *Medical Hypotheses, 63*(4), 684–687. https://doi.org/10.1016/j.mehy.2004.03.017

94. Naghitorabi, M., Asl, M., & Asl, J. (2021). Comparison of the effects of olsalazine and decitabine on the expression of CDH1 and uPA genes and cytotoxicity in MDA-MB-231 breast cancer cells. *Research in Pharmaceutical Sciences, 16*(3), 278. https://doi.org/10.4103/1735-5362.314826

TH-3600_196106022

95. Chequin, A., Costa, L. E., de Campos, F. F., Moncada, A. D., de Lima, L. T., Sledz, L. R., ... & Klassen, G. (2021). Antitumoral activity of liraglutide, a new DNMT inhibitor in breast cancer cells in vitro and in vivo. Chemico-Biological Interactions, 349, 109641.https://doi.org/10.1016/j.cbi.2021.109641

96. Alkaff, A. H., Saragih, M., Imana, S. N., Nasution, M. A. F., & Tambunan, U. S. F. (2021). Identification of DNA methyltransferase-1 inhibitor for breast cancer therapy through computational fragment-based drug design. *Molecules, 26*(2), 375. https://doi.org/10.3390/molecules26020375

97. Demetriadou, C., Koufaris, C., & Kirmizis, A. (2020). Histone N-alpha terminal modifications: Genome regulation at the tip of the tail. *Epigenetics & Chromatin, 13*(1), 29. https://doi.org/10.1186/s13072-020-00352-w

98. Verza, F. A., Das, U., Fachin, A. L., Dimmock, J. R., & Marins, M. (2020). Roles of histone deacetylases and inhibitors in anti-cancer therapy. *Cancers, 12*(6), 1664. https://doi.org/10.3390/cancers12061664

99. Alsamri, H., Hasasna, H. E., Baby, B., Alneyadi, A., Dhaheri, Y. A., Ayoub, M. A., ... & Iratni, R. (2021). Carnosol is a novel inhibitor of p300 acetyltransferase in breast cancer. Frontiers in Oncology, 11, 664403. https://doi.org/10.3389/fonc.2021.664403

100. Collins, H. M., Abdelghany, M. K., Messmer, M., Yue, B., Deeves, S. E., Kindle, K. B., ... & Heery, D. M. (2013). Differential effects of garcinol and curcumin on histone and p53 modifications in tumour cells. BMC cancer, 13, 1-11. https://doi.org/10.1186/1471-2407-13-37

101. Kopytko, P., Piotrowska, K., Janisiak, J., & Tarnowski, M. (2021). Garcinol—a natural histone acetyltransferase inhibitor and new anti-cancer epigenetic drug. *International Journal of Molecular Sciences*, 22(6), 2828. https://doi.org/10.3390/ijms22062828

102. Zhao, Q., Zhang, X., Cai, H., Zhang, P., Kong, D., Ge, X., & Dong, W. (2018). Anti-cancer effects of plant-derived anacardic acid on human breast cancer MDA-MB-231 cells. *American Journal of Translational Research, 10*(8), 2424. PMID: 30210681

103. Brown, J. A. L., Bourke, E., Eriksson, L. A., & Kerin, M. J. (2016). Targeting cancer using KAT inhibitors to mimic lethal knockouts. *Biochemical Society Transactions, 44*(3), 979–986. https://doi.org/10.1042/bst20160081

104. Fiorentino, F., Mai, A., & Rotili, D. (2018). Lysine acetyltransferase inhibitors: Structure–activity relationships and potential therapeutic implications. *Future Medicinal Chemistry, 10*(9), 1067–1091. https://doi.org/10.4155/fmc-2017-0244

TH-3600_196106022

105. Bondarev, A. D., Attwood, M. M., Jonsson, J., Chubarev, V. N., Tarasov, V. V., & Schiöth, H. B. (2021). Recent developments of HDAC inhibitors: Emerging indications and novel molecules. *British Journal of Clinical Pharmacology, 87*(12), 4577–4597. https://doi.org/10.1111/bcp.14889

106. Wawruszak, A., Borkiewicz, L., Okon, E., Kukula-Koch, W., Afshan, S., & Halasa, M. (2021). Vorinostat (SAHA) and breast cancer: An overview. *Cancers, 13*(18), 4700. https://doi.org/10.3390/cancers13184700

107. Morales Torres, C., Wu, M. Y., Hobor, S., Wainwright, E. N., Martin, M. J., Patel, H., ... & Scaffidi, P. (2020). Selective inhibition of cancer cell self-renewal through a Quisinostat-histone H1. 0 axis. Nature communications, 11(1), 1792. https://doi.org/10.1038/s41467-020-15615-z

108. Chu, P.-Y., Lai, J.-C., Hou, M.-F., & Lin, C.-S. (2019). Combination of tacedinaline and EHMT2 inhibition increases breast cancer cell death involving BIRC5 repression and GADD45A induction. *Cancer Research, 79*(13 Supplement), 4715–4715. https://doi.org/10.1158/1538-7445.am2019-4715

109. Çakir, H. K., & Eroglu, O. (2021). In vitro anti-proliferative effect of Capecitabine (Xeloda) combined with mocetinostat (MGCD0103) in 4T1 breast cancer cell line by immunoblotting. *Iranian Journal of Basic Medical Sciences*, 24(11), 1515. https://doi.org/10.22038/ijbms.2021.58393.12971

110. Zhang, Q., Wang, T., Geng, C., Zhang, Y., Zhang, J., Ning, Z., & Jiang, Z. (2018). Exploratory clinical study of chidamide, an oral subtype-selective histone deacetylase inhibitor, in combination with exemestane in hormone receptor-positive advanced breast cancer. Chinese Journal of Cancer Research, 30(6), 605. https://doi.org/10.21147/j.issn.1000-9604.2018.06.05

111. Zhou, J., Wu, X., Zhang, H., Wang, X., Yuan, Y., Zhang, S., ... & Wang, T. (2022). Clinical outcomes of tucidinostat-based therapy after prior CDK4/6 inhibitor progression in hormone receptor-positive heavily pretreated metastatic breast cancer. The Breast, 66, 255-261.https://doi.org/10.1016/j.breast.2022.10.018

112. Jiang, H., Li, Y., Xiang, X., Tang, Z., Liu, K., Su, Q., ... & Li, L. (2021). Chaetocin: A review of its anticancer potentials and mechanisms. European Journal of Pharmacology, 910, 174459.https://doi.org/10.1016/j.ejphar.2021.174459

113. Brehmer, D., Beke, L., Wu, T., Millar, H. J., Moy, C., Sun, W., ... & Laquerre, S. (2021). Discovery and pharmacological characterization of JNJ-64619178, a novel small-molecule inhibitor of PRMT5 with potent antitumor activity. Molecular cancer therapeutics, 20(12), 2317-2328.https://doi.org/10.1158/1535-7163.mct-21-0367

TH-3600_196106022

114. Devkota, K., Lohse, B., Liu, Q., Wang, M. W., Stærk, D., Berthelsen, J., & Clausen, R. P. (2014). Analogues of the natural product sinefungin as inhibitors of EHMT1 and EHMT2. ACS medicinal chemistry letters, 5(4), 293-297. https://doi.org/10.1021/ml4002503

115. Duan, R., Du, W., & Guo, W. (2020). EZH2: A novel target for cancer treatment. *Journal of Hematology & Oncology*, 13(1), 104. https://doi.org/10.1186/s13045-020-00937-8

116. McAllister, T. E., England, K. S., Hopkinson, R. J., Brennan, P. E., Kawamura, A., & Schofield, C. J. (2016). Recent progress in histone demethylase inhibitors. *Journal of Medicinal Chemistry*, 59(4), 1308–1329. https://doi.org/10.1021/acs.jmedchem.5b01758

117. Prasanna, T., Malik, L., McCuaig, R. D., Tu, W. J., Wu, F., Lim, P. S., ... & Yip, D. (2022). A phase 1 proof of concept study evaluating the addition of an LSD1 inhibitor to nab-paclitaxel in advanced or metastatic breast cancer (EPI-PRIMED). Frontiers in Oncology, 12, 862427.https://doi.org/10.3389/fonc.2022.862427

118. Lee, H. T., Jung, K. H., Kim, S. K., Choi, M. R., & Chai, Y. G. (2012). Effects of pargyline on cellular proliferation in human breast cancer cells. *Molecular & Cellular Toxicology*, 8(4), 393–399. https://doi.org/10.1007/s13273-012-0048-y

119. Satram-Maharaj, T., Nyarko, J. N., Kuski, K., Fehr, K., Pennington, P. R., Truitt, L., ... & Mousseau, D. D. (2014). The monoamine oxidase-A inhibitor clorgyline promotes a mesenchymal-to-epithelial transition in the MDA-MB-231 breast cancer cell line. Cellular signalling, 26(12), 2621-2632. https://doi.org/10.1016/j.cellsig.2014.08.005

120. Wang, T., Zhang, F., & Sun, F. (2021). ORY-1001, a KDM1A inhibitor, inhibits proliferation and promotes apoptosis of triple negative breast cancer cells by inactivating androgen receptor. *Drug Development Research*, 83(2), 208–216. https://doi.org/10.1002/ddr.21860

121. Zylla, J. L., Hoffman, M. M., Plesselova, S., Bhattacharya, S., Calar, K., Afeworki, Y., ... & Messerli, S. M. (2022). Reduction of metastasis via epigenetic modulation in a murine model of metastatic triple negative breast cancer (TNBC). Cancers, 14(7), 1753.https://doi.org/10.3390/cancers14071753

122. Kim, A., Mo, K., Kwon, H., Choe, S., Park, M., Kwak, W., & Yoon, H. (2023). Epigenetic regulation in breast cancer: insights on epidrugs. Epigenomes, 7(1), 6.https://doi.org/10.3390/epigenomes7010006

TH-3600_196106022

123. Yang, T., Yang, Y., & Wang, Y. (2021). Predictive biomarkers and potential drug combinations of epi-drugs in cancer therapy. Clinical Epigenetics, 13. https://doi.org/10.1186/s13148-021-01098-2

124. Pan, C. H., Chang, Y. F., Lee, M. S., Wen, B. C., Ko, J. C., Liang, S. K., & Liang, M. C. (2016). Vorinostat enhances the cisplatin-mediated anti-cancer effects in small cell lung cancer cells. *BMC Cancer*, 16(1). https://doi.org/10.1186/s12885-016-2888-7

125. Xia, C., Leon-Ferre, R., Laux, D., Deutsch, J., Smith, B. J., Frees, M., & Milhem, M. (2014). Treatment of resistant metastatic melanoma using sequential epigenetic therapy (decitabine and panobinostat) combined with chemotherapy (temozolomide). *Cancer Chemotherapy and Pharmacology*, 74(3), 691–697. https://doi.org/10.1007/s00280-014-2501-1

126. Voso, M. T., Santini, V., Finelli, C., Musto, P., Pogliani, E., Angelucci, E., ... & Leone, G. (2009). Valproic acid at therapeutic plasma levels may increase 5-azacytidine efficacy in higher risk myelodysplastic syndromes. Clinical cancer research, 15(15), 5002-5007.https://doi.org/10.1158/1078-0432.CCR-09-0494

127. Vernier, M., McGuirk, S., Dufour, C. R., Wan, L., Audet-Walsh, E., St-Pierre, J., & Giguère, V. (2020). Inhibition of DNMT1 and ERRα crosstalk suppresses breast cancer via derepression of IRF4. Oncogene, 39(41), 6406-6420. https://doi.org/10.1038/s41388-020-01438-1

128. Conte, P., Campone, M., Pronzato, P., Amadori, D., Frank, R., Schuetz, F., ... & Elias, A. (2009). Phase I trial of panobinostat (LBH589) in combination with trastuzumab in pretreated HER2-positive metastatic breast cancer (mBC): Preliminary safety and tolerability results. Journal of Clinical Oncology, 27(15_suppl), 1081-1081. https://doi.org/10.1200/jco.2009.27.15_suppl.1081

129. Laengle, J., Kabiljo, J., Hunter, L., Homola, J., Prodinger, S., Egger, G., & Bergmann, M. (2020). Histone deacetylase inhibitors valproic acid and vorinostat enhance trastuzumab-mediated antibody-dependent cell-mediated phagocytosis. Journal for immunotherapy of cancer, 8(1), e000195.https://doi.org/10.1136/jitc-2019-000195

130. Lee, J., Bartholomeusz, C., Mansour, O., Humphries, J., Hortobagyi, G. N., Ordentlich, P., & Ueno, N. T. (2014). A class I histone deacetylase inhibitor, entinostat, enhances lapatinib efficacy in HER2-overexpressing breast cancer cells through FOXO3-mediated Bim1 expression. Breast cancer research and treatment, 146, 259-272. https://doi.org/10.1007/s10549-014-3014-7

131. Terranova-Barberio, M., Roca, M. S., Zotti, A. I., Leone, A., Bruzzese, F., Vitagliano, C., ... & Di Gennaro, E. (2015). Valproic acid potentiates the anticancer activity of capecitabine in vitro and

TH-3600_196106022

in vivo in breast cancer models via induction of thymidine phosphorylase expression. Oncotarget, 7(7), 7715. https://doi.org/10.18632/oncotarget.6802

132. Connolly, R. M., Li, H., Jankowitz, R. C., Zhang, Z., Rudek, M. A., Jeter, S. C., ... & Stearns, V. (2017). Combination epigenetic therapy in advanced breast cancer with 5-azacitidine and entinostat: a phase II National Cancer Institute/Stand Up to Cancer Study. Clinical cancer research, 23(11), 2691-2701. https://doi.org/10.1158/1078-0432.CCR-16-1729

133. Medon, M., Vidacs, E., Vervoort, S. J., Li, J., Jenkins, M. R., Ramsbottom, K. M., ... & Haynes, N. M. (2017). HDAC inhibitor panobinostat engages host innate immune defenses to promote the tumoricidal effects of trastuzumab in HER2+ tumors. Cancer research, 77(10), 2594-2606.https://doi.org/10.1158/0008-5472.CAN-16-2247

134. Won, K., & Spruck, C. (2020). Triple negative breast cancer therapy: Current and future perspectives (Review). *International Journal of Oncology*, 57(6), 1245–1261. https://doi.org/10.3892/ijo.2020.5135

135. Tan, W. W., Allred, J. B., Moreno-Aspitia, A., Northfelt, D. W., Ingle, J. N., Goetz, M. P., & Perez, E. A. (2016). Phase I study of panobinostat (LBH589) and letrozole in postmenopausal metastatic breast cancer patients. Clinical breast cancer, 16(2), 82-86.https://doi.org/10.1016/j.clbc.2015.11.003

136. Ramaswamy, B., Fiskus, W., Cohen, B., Pellegrino, C., Hershman, D. L., Chuang, E., ... & Sparano, J. A. (2012). Phase I–II study of vorinostat plus paclitaxel and bevacizumab in metastatic breast cancer: evidence for vorinostat-induced tubulin acetylation and Hsp90 inhibition in vivo. Breast cancer research and treatment, 132, 1063-1072. https://doi.org/10.1007/s10549-011-1928-x

137. Arce, C., Perez-Plasencia, C., Gonzalez-Fierro, A., de la Cruz-Hernandez, E., Revilla-Vazquez, A., Chavez-Blanco, A., ... & Dueñas-Gonzalez, A. (2007). A proof-of-principle study of epigenetic therapy with hydralazine and magnesium valproate plus doxorubicin cyclophosphamide as neoadjuvant therapy for locally advanced breast cancer. BMC Cancer, 7, 1-2. https://doi.org/10.1186/1471-2407-7-s1-a23

138. Pattarawat, P., Wallace, S., Pfisterer, B., Odoi, A., & Wang, H.-C. R. (2019). Formulation of a triple combination gemcitabine plus romidepsin + cisplatin regimen to efficaciously and safely control triple-negative breast cancer tumor development. *Cancer Chemotherapy and Pharmacology*, 85(1), 141–152. https://doi.org/10.1007/s00280-019-04013-y

139. Buocikova, V., Longhin, E. M., Pilalis, E., Mastrokalou, C., Miklikova, S., Cihova, M., ... & Smolkova, B. (2022). Decitabine potentiates efficacy of doxorubicin in a preclinical

TH-3600_196106022

trastuzumab-resistant HER2-positive breast cancer models. Biomedicine & Pharmacotherapy, 147, 112662. https://doi.org/10.1016/j.phrs.2022.106501

140. Krishnamurthy, N., Grimshaw, A. A., Axson, S. A., Choe, S. H., & Miller, J. E. (2022). Drug repurposing: a systematic review on root causes, barriers and facilitators. *BMC health services research*, 22(1), 970. https://doi.org/10.1186%2Fs12913-022-08272-z

141. Weth, F. R., Hoggarth, G. B., Weth, A. F., Paterson, E., White, M. P., Tan, S. T., ... & Gray, C. (2023). Unlocking hidden potential: advancements, approaches, and obstacles in repurposing drugs for cancer therapy. *British Journal of Cancer*, 1-13. https://doi.org/10.1038/s41416-023-02502-9

142. Montalvo-Casimiro, M., González-Barrios, R., Meraz-Rodriguez, M. A., Juárez-González, V. T., Arriaga-Canon, C., & Herrera, L. A. (2020). Epidrug Repurposing: Discovering New Faces of Old Acquaintances in Cancer Therapy. *Frontiers in oncology*, 10, 605386. https://doi.org/10.3389/fonc.2020.605386

143. Moreira-Silva, F., Camilo, V., Gaspar, V., Mano, J. F., Henrique, R., & Jerónimo, C. (2020). Repurposing Old Drugs into New Epigenetic Inhibitors: Promising Candidates for Cancer Treatment? *Pharmaceutics*, 12(5), 410. https://doi.org/10.3390/pharmaceutics12050410

TH-3600_196106022

TH-3600_196106022

CHAPTER 2

Targeting p300 acetyltransferase activity using repurposed drug

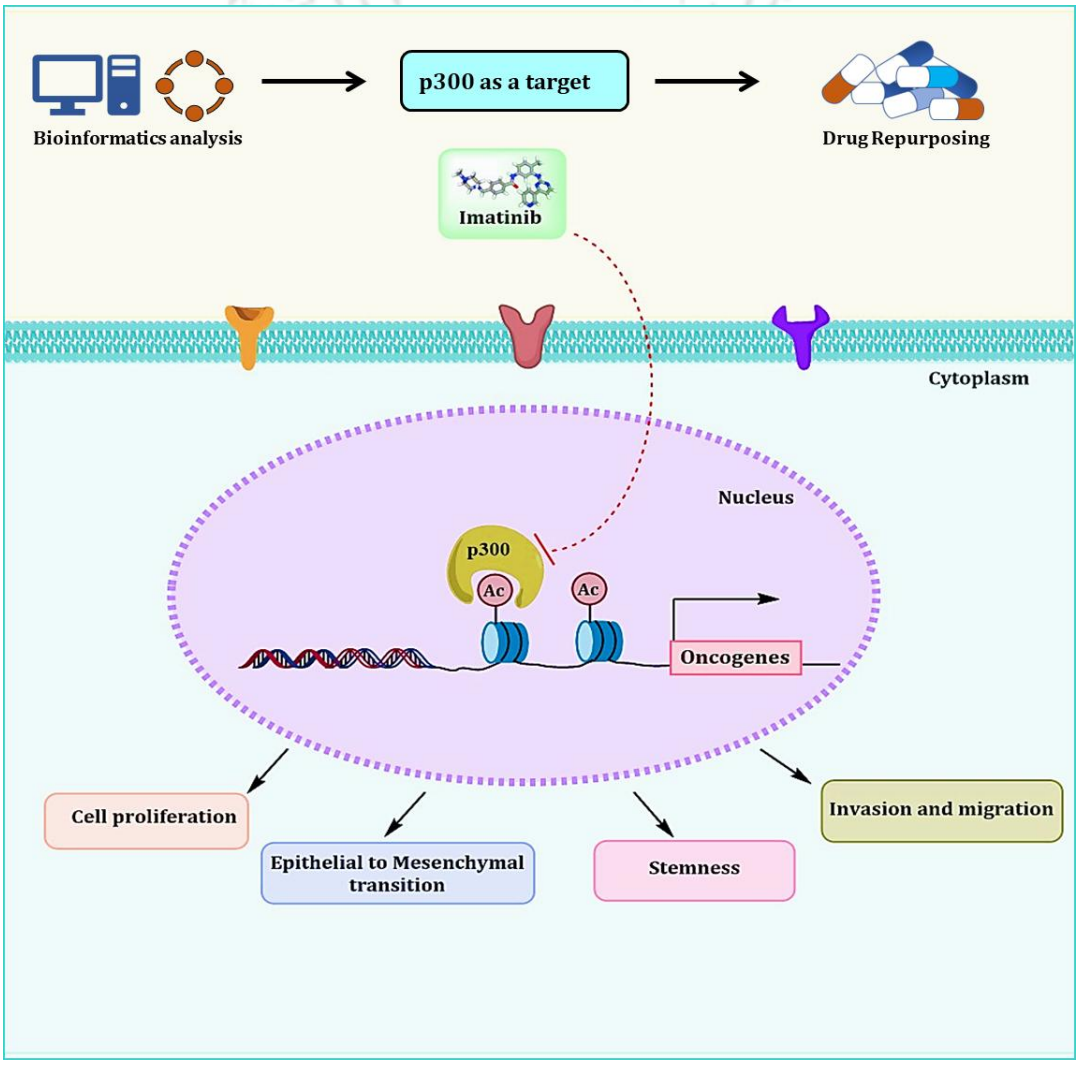

Journal of Biomolecular Structure and Dynamics, 2023,1-12.

https://doi.org/10.1080/07391102.2023.2270086

Molecular Carcinogenesis, *10.1002/mc.23848*, 2023,1-12.

https://doi.org/10.1002/mc.23848

TH-3600_196106022

Chapter 2

2.1. Introduction

The E1A binding protein p300 (KAT3B) serves a pro-cancer role in breast cancer and involves multiple cellular processes, including proliferation, apoptosis, and metastasis. It serves a crucial role in gene regulation primarily through catalyzing H3K27 and H3K18 acetylation [1,2]. In breast cancer, overexpression of p300 is observed, which further correlates with a low survival rate and aggressive features [3]. Furthermore, it has been observed that p300 promotes invasion of cells and survival, which contributes to the advancement of breast cancer [4]. Moreover, recent studies revealed the intricate association of p300 with epithelial-mesenchymal transition (EMT), a dynamic mechanism involved in the metastatic cascade [5, 6]. During EMT, epithelial cells lose their adherence to one another, and the extracellular matrix transforms into mesenchymal cells. Acquired mesenchymal features facilitate the dissociation of cancer cells from their primary site, eventually leading to their localization in distant organs. Moreover, EMT enables cancer cells to acquire resistance to apoptosis and stem cell features. During this process, cells cease to express epithelial markers such as E-cadherin, cytokeratins, and claudins, whereas considerably overexpress mesenchymal markers, namely N-cadherin, vimentin, and Fibronectin. EMT transcription factors like Twist, Snail, and Zeb also trigger EMT, contributing to cancer cell growth, invasion, and migration [7]. In lung cancer, p300 activates Snail through acetylation, thereby reducing E-cadherin expression and promoting EMT [8]. In addition, p300 promotes EMT progression in pancreatic cancer through the SNAI2-mediated pathway [9]. Another study reported that interaction between p300 and SnoN regulates EMT in mammary organoids [10]. Furthermore, in breast cancer, p300 forms a complex with DOT1L and c-Myc to activate different EMT transcription factors [11]. Additionally, recent studies have highlighted the critical role of the Notch signalling pathway in regulating EMT, with p300 acting as a key mediator of this interaction. The Notch pathway, which governs cell fate determination, stemness, and differentiation, has been shown to promote EMT when aberrantly activated [12]. Consequently, targeting p300 in breast cancer can be a viable strategy for the creation of new anti-cancer therapies.

Further, the current clinical attrition rate of cancer drugs can be alleviated through drug repurposing approach. The repurposing approach utilizes the poly pharmacological properties of an approved drug to target multiple proteins in disease conditions instead of developing new molecules. Repurposing provides several advantages over the standard drug development method; the two most significant ones are a lower probability of failure owing to safety and a quicker development period. Drug repurposing utilizing target-based approaches has proven to be more effective when combined with intensive *in-vitro* validations [13]. Targeting p300 using drug repurposing is a promising and alternative method in breast cancer treatment. To achieve this, library of FDA approved drugs was collected through the server named Guide to Pharmacology and screened against p300. Further

TH-3600_196106022

utilizing binding free energy (MM-PBSA method) and molecular dynamics simulation, Imatinib, a tyrosine kinase inhibitor, was repurposed as a very effective p300 HAT domain inhibitor. Further, the anti-cancer effect of the repurposed drug on breast cancer cells was investigated, with a particular focus on its ability to inhibit EMT and Notch signalling pathway.

2.2. Materials and methods

2.2.1. Expression analysis

Gene Expression Profiling Interactive Analysis (GEPIA2) server was utilized to determine the p300 expression profile across all tumor samples and paired normal tissues. Overall survival probability based on p300 expression levels of breast cancer patients was acquired from the GEPIA2 server (http://gepia2.cancer-pku.cn/). GEPIA 2 uses The Cancer Genome Atlas (TCGA) database to generate survival plot through Kaplan–Meier analysis.

2.2.2 Construction of functional network

The functional and physical interconnection between p300 and other proteins was confirmed through STRING v9.1 database (https://string-db.org). This database portrays physical and functional association between two proteins through analyzing co-expressed genes, literature, high throughput experimental data, and database mining. Herein, p300 was queried in the database using the search tool, and as the organism, *Homo sapiens* was chosen. The score of interaction was selected to 0.7 (high confidence), and the maximum number of interactors was set to no more than 50 interactors. Further, cluster analysis was performed using K-means clustering algorithm with number of clusters 5.

2.2.3. Pathway enrichment analysis

The involvement of the interactors of p300 obtained from the STRING database in different biological pathways was analyzed using the Enrichr database (https://maayanlab.cloud/Enrichr/enrich#). Enrichr allows the user to explore the involvement of query protein (s) in pathways, ontology, diseases/drugs, and expression in different cell lines. The list of 50 primary interactors of p300 was given as a query in the Enrichr server. Then, their role in different pathways was studied through KEGG 2021 Human (Hunam cell signaling and metabolic pathways manually curated database. 2021 version.) as pathways option in the Enrichr database. The bar graph of the top 10 pathways was downloaded based on the p-value ranking from the Enrichr save option. The table format of all the pathways associated with p300 and its interactors was retrieved in CSV format.

2.2.4. Preparation of protein and drugs for molecular docking

The three-dimensional structural coordinates of p300 were obtained in PDB format from the RCSB PDB database (https://www.rcsb.org/). Followed by the 3D coordinates of FDA-approved drugs (1293 drugs) were acquired in SDF format from Guide to pharmacology server (https://www.guidetopharmacology.org/GRAC/LigandListForward?database=all) and the 3D structure of C646 (Control inhibitor of p300) was acquired from PubChem database (

TH-3600_196106022

https://pubchem.ncbi.nlm.nih.gov/). The 3D structure of p300 was prepared for virtual screening by changing the atom type to AD4 type and removing water molecules, other ions, adding charges using Autodock4 and PyMol 2.3 (Schrodinger, LLC. 2010. The PyMOL Molecular Graphics System, Version 2.3.). The final structure was saved as pdbqt format for Vina docking. Similarly, SDF formatted drug library was modified into pdbqt format by Open Bable version 2.4.0.

2.2.5. Virtual Screening of FDA Approved Drug library

The screening of potent FDA approved drug against P300 virtually carried out using Autodock Vina 1.1.2. It makes use of a flexible docking algorithm for ligands while screening against rigid protein.

The grid box center was set to coordinates X, Y, Z (0.138, -24.105, -5.989) based on the structural data of P300, ensuring that the entire protein, including known active sites and potential allosteric regions, is encompassed. The grid dimensions (72, 80, 68) were determined by assessing the overall size and shape of P300. These dimensions guarantee that all potential binding regions are accessible for the ligands during docking, reducing the risk of missing critical interactions. The box was sized to cover the full extent of the protein's binding domain, allowing for an unbiased exploration of binding modes.

Post-docking, interactions between P300 and the ligands were analyzed using PyMol 2.3 and Discovery Studio Visualizer v20.1.0.19195. These tools enabled detailed visualization of binding poses, hydrogen bonds, hydrophobic interactions, and other key contacts. This step is essential for validating docking results and ensuring that the predicted interactions are biologically plausible.

2.2.6. Molecular dynamics simulation

The dynamic behaviours of p300 with selected FDA approved drugs were performed in a solvent rich environment using molecular dynamics simulation (MDS) methods. MDS has been successfully used over a decade to understand the behaviours of biological molecules like nucleic acid, proteins, and lipids in solvent-rich environments. In this study, MDS of P300-drug complexes were performed using CHARMM27 force field in GROMACS 2019.6. Parameter files of selected docked complexes were prepared as per gromacs tutorial [14]. p300-drug complex systems were positioned inside a dodecahedron box by keeping 1.0 nanometre edge distance and solvated using the model of TIP3P water. Then the neutralization of system was carried out using Na^+ and Cl^- and energy was minimized up to 10KJ/mol with "genion" module of gromacs and steepest descent algorithm, respectively. The system was equilibrated with the canonical ensemble and Isobaric-isothermal ensemble for 100 picoseconds before the final MD run which is of 100 nanoseconds. The structural stability and strength of the protein-drug complexes were analyzed from the MD trajectory using RMSD, RMSF, pair distance, and H-bond analysis.

2.2.7. Binding free energy analysis:

The binding free energy of p300-drug complexes was further recalculated after MD using Molecular Mechanics Poisson-Boltzmann Surface Area (MMBPSA) method. Gromacs function "g_mmpbsa" was

TH-3600_196106022

utilized to calculate the binding free energy of P300-drug complexes with 1 ns time interval [15]. The binding free energy ($\triangle G_{\text{bind}}$) of drug molecules with P300 was calculated using the following formula.

$$\triangle G_{\text{bind}} = \triangle E_{MM} + \triangle G_{PBSA} - T\triangle S_{MM}$$

Where $\triangle G_{\text{bind}}$ - average binding free energy of protein–drug complex, $\triangle E_{MM}$ - average molecular mechanics' energy, $\triangle G_{PBSA}$ - solvation free energy, and $T\triangle S_{MM}$ - solute configuration entropy.

2.2.8. Cell lines and culture conditions

Human breast cancer cell lines MCF-7 (luminal breast cancer cell line) and MDA-MB-231 (Triple-negative Breast Cancer cell line) were obtained from the National Centre for Cell Science (NCCS) Pune, India. All cell lines were cultured in Dulbecco's Modified Eagle's Medium (DMEM) added with sodium bicarbonate (Sigma-Aldrich), 10% Fetal Bovine Serum (FBS) (Thermo Fisher Scientific), Antibiotic-Antimycotic (Thermo Fisher Scientific) in a moistened environment at 37°C provided with 5% CO_2.

2.2.9. Cell viability assay

The anti-proliferative activity of the drugs was evaluated using MTT [3-(4,5-dimethylthiazol-2-yl)-2,5-diphenyltetrazolium-bromide] assay (HiMedia). The tetrazolium salt is converted into the purple formazan by the active mitochondria of the living cells. At a density of 5 $\times 10^3$ cells/well, MCF-7 and MDA-MB-231 cells were seeded in 96 well tissue culture plate(s). Following attachment, increasing concentrations of drugs were added to the cells. After 48h of treatment, 0.5 mg/ml MTT solution was added and incubated for 2h. After that, the formed formazan crystals were dissolved in dimethyl sulfoxide (DMSO), and a microplate reader (Thermo Fisher Scientific) was used to measure the absorbance at 570 nm with a reference wavelength of 630 nm. Inhibitory concentration-50 (IC_{50}) was determined through GraphPad Prism software (www.graphpad.com).

2.2.10. Detection of cellular Reactive Oxygen Species (ROS)

The study utilized Dichlorodihydrofluorescein diacetate (DCFDA) dye (Sigma-Aldrich) to quantify the ROS generation following treatment with inhibitors. DCFDA generates green fluorescence in the presence of intracellular ROS. To quantity ROS production, 3 $\times 10^5$ cells/well, MCF-7 and MDA-MB-231 cells were seeded in 6 well plate(s). Following treatment with inhibitors for 24h, cells were incubated with 10 µM DCFDA for 30 min. This allowed the dye to enter the cells and react with any ROS present, resulting in green fluorescence that could be detected and measured. After incubation, cells were trypsinized and used for flow cytometry (Cytoflex, Beckman Coulter) to evaluate the green fluorescence.

2.2.11. Detection of the mitochondrial membrane potential

To evaluate the alteration in membrane potential of mitochondria, a cationic dye 5,5′,6,6′-tetrachloro-1,1′,3,3′-tetraethylbenzimi- dazolylcarbocyanine iodide (JC-1) was utilized. JC 1 distinguishes energized mitochondria from de-energized mitochondria because it turns red when

TH-3600_196106022

concentrated within energized mitochondria. This occurs due to the dye generating red fluorescent aggregates due to the higher membrane potential. For this study, 3 ×10^5 cells/well, MCF-7 and MDA-MB-231 cells were seeded in 6 well plate(s). After 48 h of treatment, 10 µM JC-1 was added to the cells and incubated for 30 min. In the case of positive control cells, 50 µM carbonyl cyanide m-chlorophenylhydrazone (CCCP) was added and incubated for 30 min. Following trypsinization, cells were examined by flow cytometer (Cytoflex, Beckman Coulter). Red and green channels were used to acquire fluorescence intensity data.

2.2.12. Apoptosis assay

Using Alexa fluor 488 Annexin V/dead Kit (Invitrogen), the apoptotic cell population was estimated. For this study, 3 ×10^5 cells/well, MCF-7 and MDA-MB-231 cells were seeded in 6 well plate(s). After 48h of treatment, samples were prepared in accordance with the instructions of the manufacturer and analysed through flow cytometry (CytoFLEX, Beckman Coulter). Data processing and fluorescence compensation were carried out through Cytexpert software.

2.2.13. Western blot analysis

Radio Immuno Precipitation Assay (RIPA) buffer (Sigma Aldrich) was used to isolate total protein from the cells after 48 h treatment. Protein concentration quantification was performed using the BCA Protein Assay Kit (Thermo Fisher Scientific). Afterward, in SDS-PAGE, the protein samples were loaded in equal amounts and transferred to PVDF membranes. Further, the blots were incubated with blocking buffer (4% BSA in PBST) and primary antibodies for overnight **(Table 2.1).** After washing, the blots were incubated for 2h with secondary antibodies conjugated to HRP (Cell Signaling Technology). Applying chemiluminescent reagent (Bio-Rad), images were developed using ChemiDoc (Bio-Rad). The image analysis was done using ImageJ software. To evaluate gene expression at the protein level, the data were normalized to β-actin.

Table 2.1: *The list of antibodies used for protein expression study*

Antibodies	Catalog No	Manufacture
β-actin	8457S	Cell Signaling Technology, USA
AKT	8200	Cell Signaling Technology, USA
HES1	68309	Cell Signaling Technology, USA
p21	68309	Cell Signaling Technology, USA
H3K18AC	9927T	Cell Signaling Technology, USA
H3K27AC	9927T	Cell Signaling Technology, USA
Anti-Rabbit IgG, HRP linked	7074S	Cell Signaling Technology, USA

TH-3600_196106022

2.2.14. RNA isolation and quantitative real-time PCR

Following 48 h of treatment, total RNA from breast cancer cells was isolated utilizing TRI reagent (Sigma Aldrich), followed by phenol-chloroform-based separation and ethanol precipitation of RNA. iScript cDNA synthesis kit (Bio-Rad) was used to convert RNA into Complementary DNA (cDNA). Further, Real-time PCR was employed to amplify the target cDNA using a Rotor-Gene Q real-time PCR cycler (Qiagen) and SYBR Green Master Mix (Bio-Rad). The results were normalized against β-actin and calculated by ΔΔCt process using LinReg PCR software. Primers used for gene expression quantification are listed in **Table 2.2**.

Table 2.2: *List of primers used for real-time PCR experiments*

Sl.No	Gene name	Forward primer	Reverse primer
1	E-cadherin	TGGGTGAATTCGGGCTTGTT	TGAAGGTGACAGAGCCTCTGGAT
4	Fibronectin	AACATGTAACCACCAGTCTCATGTG	GGTGACACTTATGAGCGTCCTAAA
5	SNAI2	ATGAGGAATCTGGCTGCTGT	CAGGAGAAAATGCCTTTGGA
6	p300	TTCAAACGCCGAGTCTTCTT	GTTGAGCTGCTGTTGGCATA
4	β-actin	AAGGGACTTCCTGTAACAATGCA	CTGGAACGGTGAAGGTGACA

2.2.15. Live-dead cell imaging

MCF-7 and MDA-MB-231 cells were treated with Imatinib and C646 at their respective IC_{50} concentration for 48 h to image live-dead cell populations. Following the treatment, 2 µM Calcein-AM and 4 µM PI cells were added to the cells and incubated for 30 min. Afterward, images were captured using ZOE Fluorescent Cell Imager (Bio-Rad).

2.2.16. Colony formation assay

MCF-7 and MDA-MB-231 cells were treated with C646 and Imatinib for 48 h in 6-well plates. Following treatment, cells were trypsinized and resuspended in fresh DMEM media. Subsequently, 2 mL of cell suspension with a cell density of 5000 cells/ml was added to 6 well plates and kept in cell culture conditions for 10 days. Ultimately, the produced colonies were stained using 0.5% crystal violet solution after fixing with 4% formaldehyde solution.

2.2.17. Sphere formation assay

Breast cancer cells were treated with the drugs according to their respective IC_{50} concentrations for 48h. Then, using 8000 cells/well, the spheroids of the untreated, C646, and Imatinib-treated cells were generated. Spheroids were produced using a forced floatation approach and allowed to grow for 72h under cell culture conditions. Subsequently, the images were acquired by the Nikon Eclipse Ti microscope.

TH-3600_196106022

2.2.18. Matrigel invasion assay

In 1mg/ml concentration, matrigel (Sigma Aldrich) was diluted in serum-free media. After that, it was transferred into transwell inserts (Corning) and incubated for 6h to solidify. 5×10^4 cells in serum-free media were added to the upper chambers, whereas media with 10% FBS (as a chemoattractant) was kept in the lower chambers. After 18h of incubation, cells from the upper sides of the chambers were removed and washed with PBS. Subsequently, 16% formaldehyde was used to fix the cells. After that, the cells were stained with DAPI and rewashed with PBS to remove the excess stain. Subsequently, the images were captured through a Zeiss LSM 880 confocal microscope and analyzed using the ImageJ Software.

2.2.19. Migration assay

Scratch wound-healing assay was employed to measure the difference in TNBC cell migratory potential after treatment. MDA-MB-231 cells were grown until 60–70% confluency. Subsequently, cells were incubated in 1% serum medium for 24h, and linear wounds were generated. Cellular debris was removed through PBS washing. Subsequently, cells were treated for 48h with inhibitors equivalent to their IC_{50} concentrations. Before and after treatment, images of the wound area were acquired using ZOE Fluorescent Cell Imager (Bio-Rad). Using the ImageJ Software, the wound distance was measured at three different positions inside each wound region, and the average of those measurements was then calculated.

2.2.20. Statistical Analysis

GraphPad Prism software was used for all statistical analysis. All the experimental data are presented as mean ± SEM. In addition, a one-way ANOVA test was carried out to assess the correlations between the groups. The p-value <0.05 (*) is considered to be statistically significant, whereas p<0.001 (***) and p<0.0001 (****) are considered to be highly significant.

TH-3600_196106022

2. 3. Results

2.3.1. p300 and Cancer

The role of p300 in different cancers, including breast cancer, was investigated using gene expression and functional network analysis. The differential gene expression profile of p300 was obtained from the GEPIA2 server. Out of 31 different types of cancer, p300 was upregulated in 15 types, downregulated in 15 types, and unaffected in Kidney renal clear cell carcinoma (KIRC) **(Figure 2.1A)**. p300 was observed to be overexpressed in breast cancer, and this phenomenon correlated with a low survival rate in cancer patients **(Figure 1B)**.

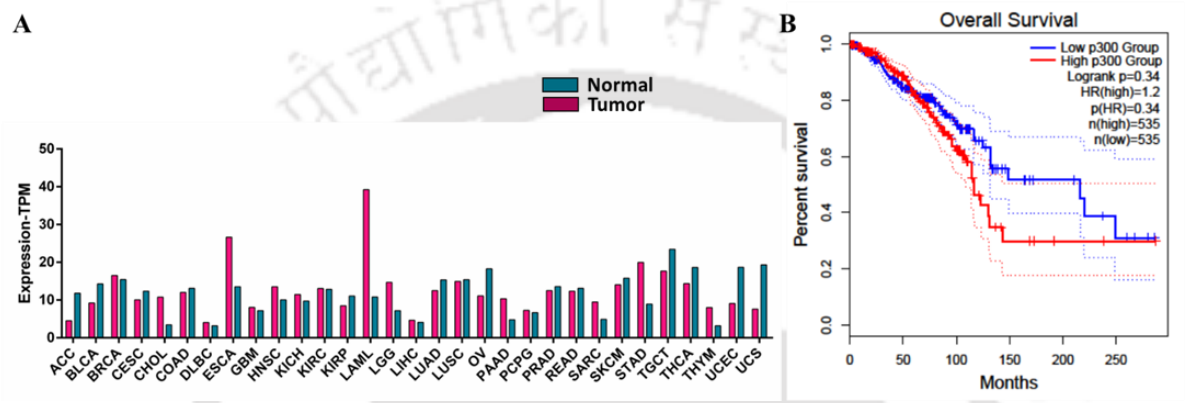

Figure 2.1: *(A) Gene expression profile of p300 in different cancers. (B) The overall rate of survival of breast cancer patients with respect to p300 expression.*

2.3.2. Functional network analysis of p300

In addition, the impact of p300 in different pathways was established with the help of functional network analysis. The interconnection between p300 and 50 different proteins was portrayed in **Figure 2.2**, which impacts overall cancer survival. Further, the functional network of p300 was categorized into 5 different clusters to ease the analysis of their involvement in different pathways. These clusters depict the association of different pathways with p300 **(Figure 2.3)**.

Cluster 1 comprised of 28 proteins which are mostly transcription factors and nuclear proteins that are HDAC2 (Histone deacetylase 2), NR3C1 (Nuclear receptor subfamily 3 group C member 1), NR4A1 (Nuclear receptor subfamily 4 group A member 1), SMAD2 (Mothers against decapentaplegic homolog 2), SMAD3 (Mothers against decapentaplegic homolog 3), RUNX2 (Runt related transcription factor 2), PPARA (Peroxisome proliferator- activated receptor alpha), PPARG (Peroxisome proliferator-activated receptor gamma), CITED2 (Cbp/p300-interacting trans activator 2), JMY (Junction-mediating and regulatory protein), MAML1 (Mastermind like protein 1), STAT1 (Signal transducer and activator of transcription 1), STAT3 (Signal transducer and activator of transcription 3), MYC (Myc proto oncogene protein), STRT1 (NAD dependent protein deacetylase sirtuin 1), ARNT (Aryl hydrocarbon receptor nuclear translocator), CEBPB (CCAAT/enhancer binding protein beta), MYB

TH-3600_196106022

(Transcriptional activator Myb), IRF1 (Interferon regulating factor 1), IRF3 (Interferon regulating factor 3), KAT2B (Histone acetyl transferase), CREB1 (Cyclic AMP-responsive element binding protein 1), MEF2A (Myocyte-specific enhancer factor 2A), YY1 (Transcriptional repressor protein), RELA (Proto ongogene), CARM1 (Histone arginine methyl transferase), GATA4 (Transcriptional factor) and p300 (Histone acetyl transferase). These proteins are mainly involved in molecular functions such as cell cycle progression and development, transcription regulation, energy homeostasis, DNA damage, and apoptosis.

Cluster 2 of the functional network includes 5 proteins that are TP73 (Tumour protein 73), TP53 (Tumour protein 53), MDM2 (E3 ubiquitin protein ligase), HIF1A (Hypoxia-inducible factor 1- alpha), AKT1 (RAC-alpha serine/threonine protein kinase). Cluster 2 proteins are involved in tumor suppressor/activator pathways.

Cluster 3 consists of 8 proteins of FOXO and Notch signalling pathways such as FOXO1 (Fork head box protein O1), FOXO3 (Fork head box protein O3), Noth1 (Neurogenic locus notch homolog protein 1), KLF4 (Krueppel like factor 4), CTNNB1 (Catenin beta 1), CREBBP (CREB Binding Protein), SMAD4 (Mothers against decapentaplegic homolog 4), AR (Androgen receptor). The main cellular functions of these proteins are proliferation, development, and metabolic homeostasis.

TH-3600_196106022

Cluster 4 with 2 proteins such as TCF3 (Transcription factor E2 alpha) and MYOD1 (Myoblast determination protein 1) associated with myogenesis. Finally, Cluster 5 with 8 proteins involved mainly in cell proliferation. The associated proteins are NCOA1 (nuclear receptor co-activator 1), NCOA3 (Nuclear receptor co-activator 3), SP1 (Transcriptional factor), ESR1 (Estrogen receptor 1), FOS (proto-oncogene), JUN (Transcriptional factor AP-1), HDAC1 (Histone deacetylase 1), CCND1 (G1/S specific cyclin D1).

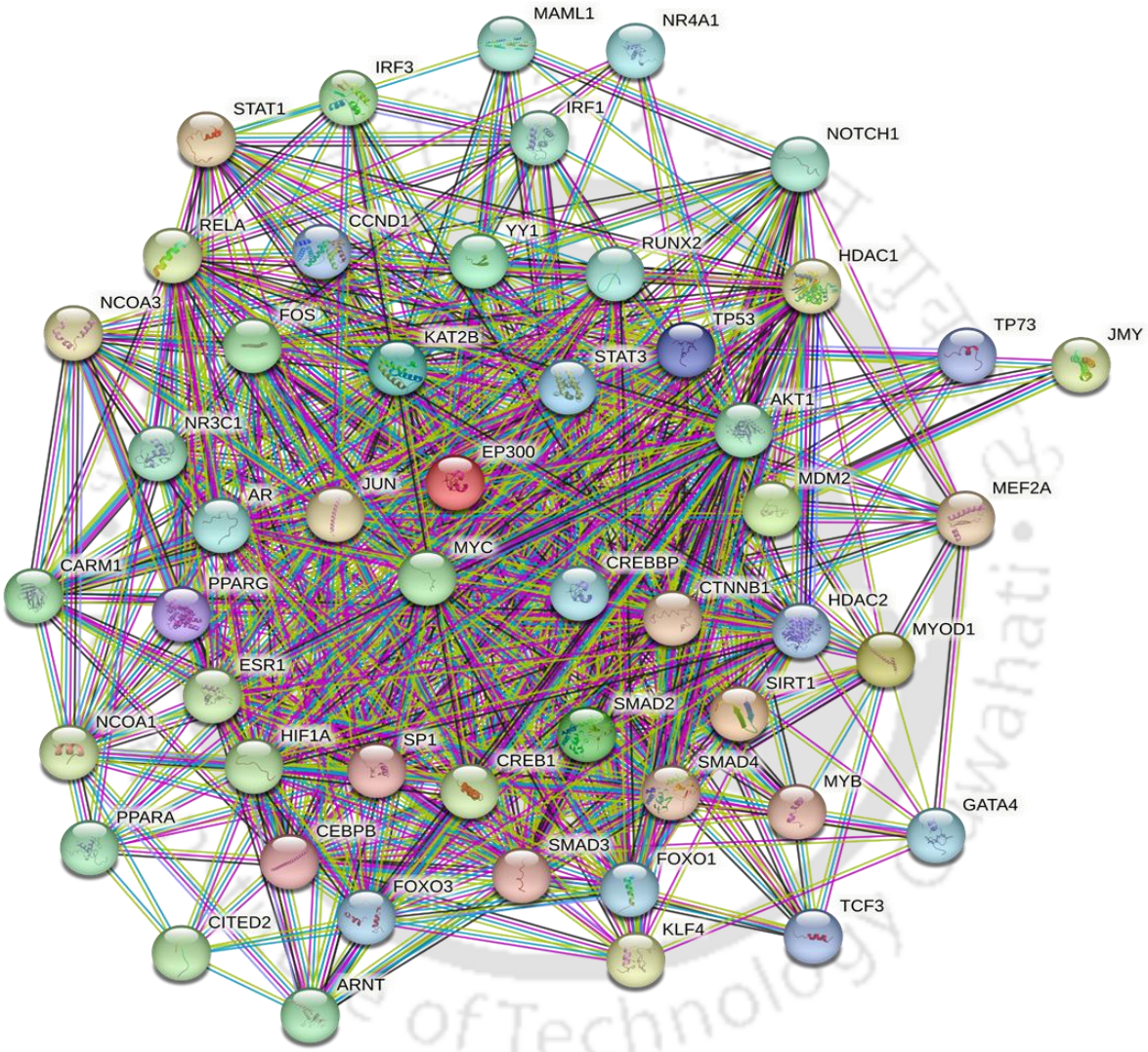

Figure 2.2: *Functional network of p300 depicted by STRING database*

TH-3600_196106022

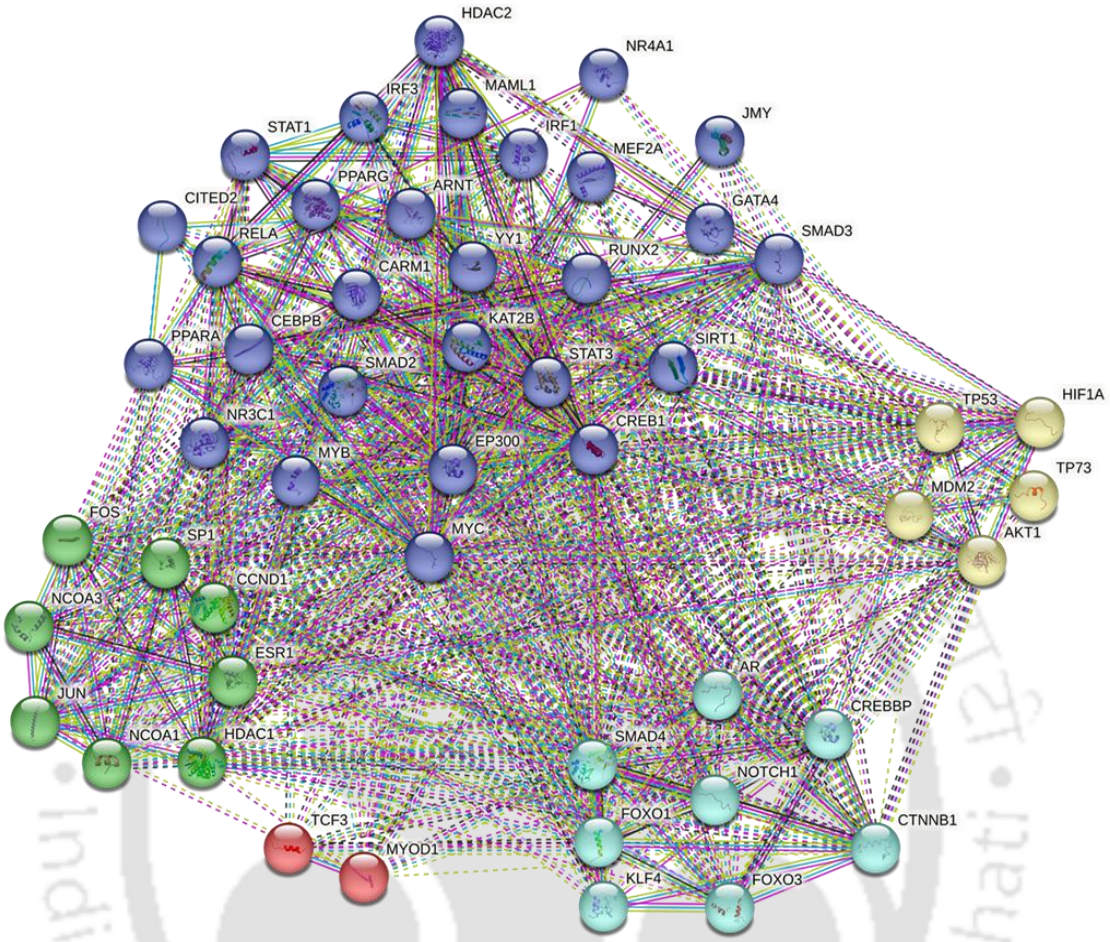

Figure 2.3: *Clusters of p300 primary interactors by K-means clustering.*

2.3.3. Pathway enrichment analysis

In addition to the functional network analysis with different clusters, the pathway enrichment analysis of p300 and its interactors were also performed using the Enrichr database. The involvement of p300 and its interactors in the top 10 pathways were depicted in **Figure 2.4** based on the p-value and the adjusted p-values generated by the Enrichr. p300 interactors mainly played a role in cancer pathways, more specifically breast cancer, prostate cancer, Chronic myeloid leukemia, and thyroid hormone signaling pathways **(Figure 2.4A)**. In the case of p300, out of 10 pathways, three pathways were majorly activated in most cancer, including breast cancer in the different stages that are the Notch signaling pathway, the TGF-beta signaling pathway, and the HIF-1 signaling pathway **(Figure 2.4B)**.

TH-3600_196106022

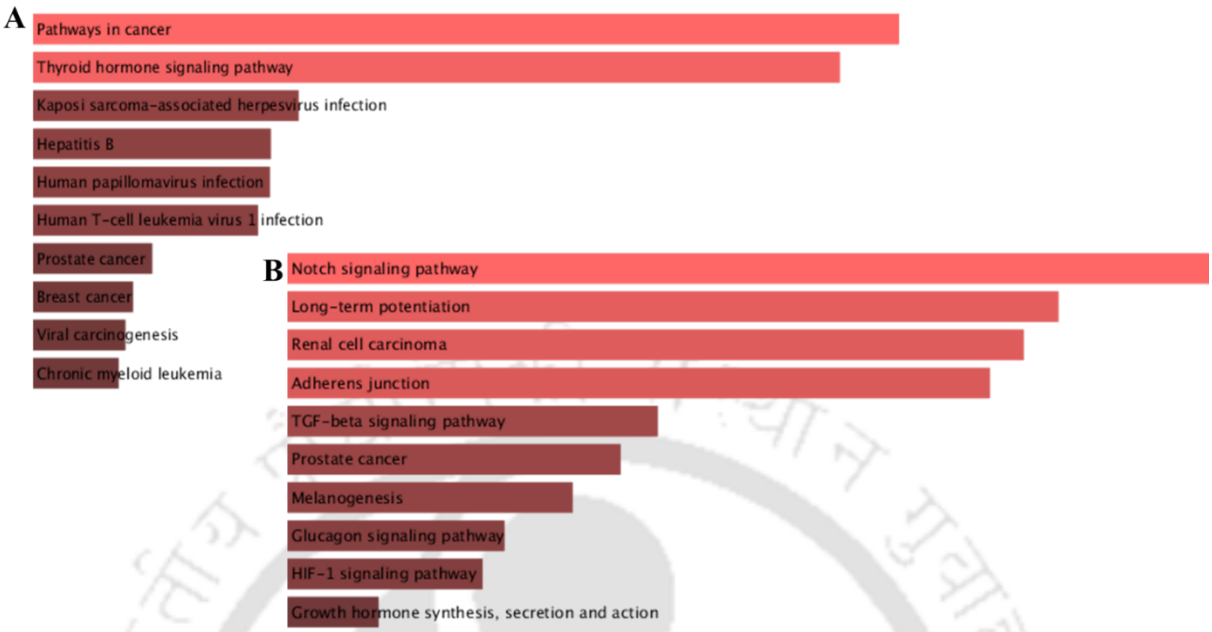

Figure 2.4: *Pathway enrichment analysis of A) p300 interactors, B) p300 by Enrichr server.*

2.3.4. Virtual screening of FDA-approved drug library

The library of 1293 FDA-approved drugs were virtually screened against p300 using Autodock Vina, and C646 (a known inhibitor of p300) was used as a control inhibitor for the screening. As a result, 89 drugs exhibited better binding scores than the control inhibitor (-9.5 Kcal/mol). Among them, the top 10 ranked FDA-approved drugs were chosen based on their binding score for further studies. The details of the binding scores and the interacting residues of P300 with the top 10 drugs were tabulated in **Table 2.3.** The three-dimensional and two-dimensional interacting profiles of the top 10 drugs and the control inhibitor with p300 are shown in **Figure 2.5**. Out of 10 FDA-approved drugs, only one drug is being used for cancer chemotherapy (Imatinib – used to treat Acute lymphoblastic leukemia). However, all these top 10 selected drugs can act as potent inhibitors for p300, and their binding characteristics with p300 were analyzed in detail by further molecular dynamic simulation studies.

TH-3600_196106022

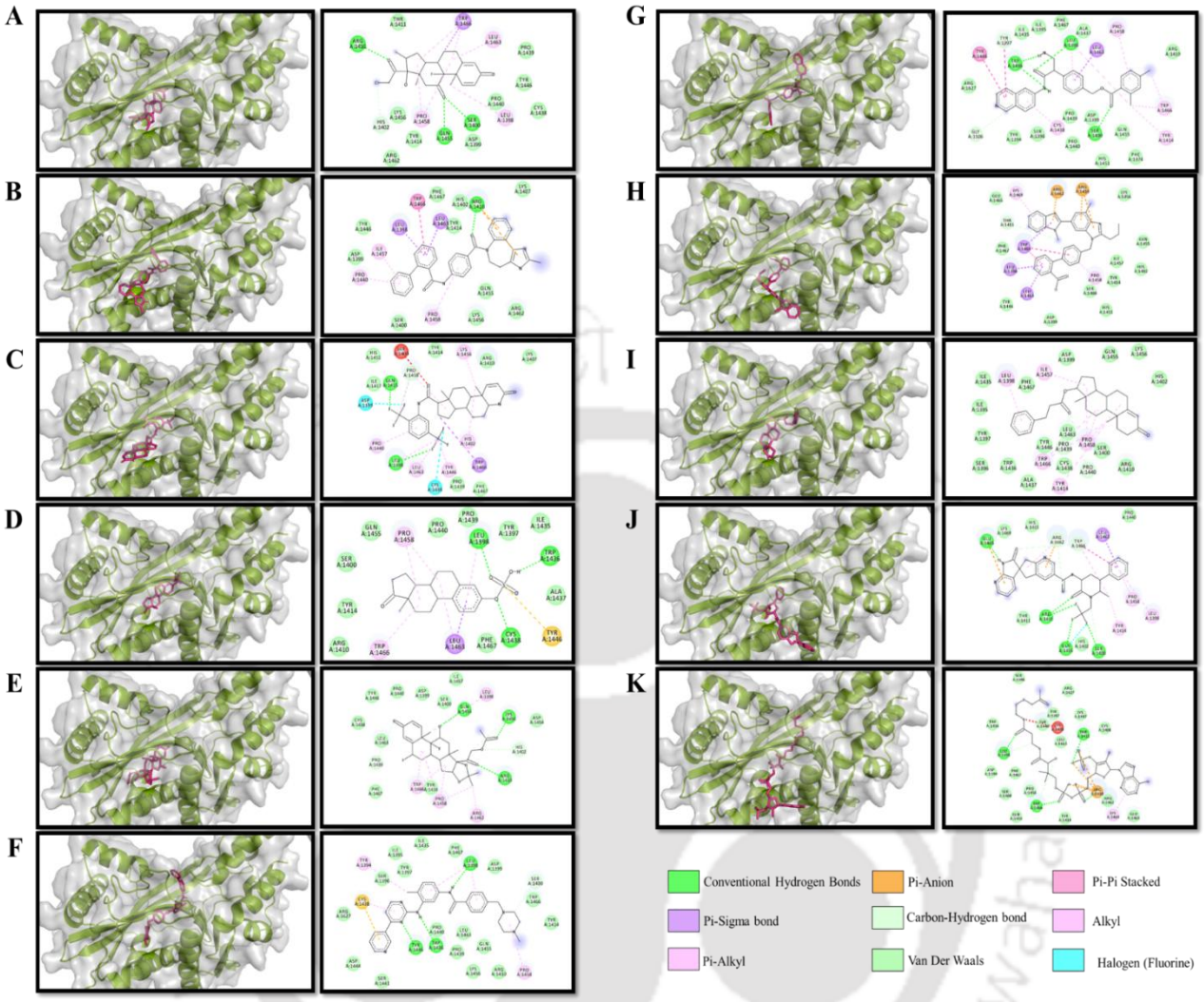

Figure 2.5: *2D interaction profile of top 10 FDA approved drugs with p300. A) Clobetasone, B) Conivaptan, C) Dutasteride, D) Estrone-3-Sulphate E) Fluocinonide, G) Imatinib, H) Telmisartan, I) Testrosterone-phenylpropionate, J) Ubrogepant, H) Control – C646.*

TH-3600_196106022

Table 2.3: Binding energy and interaction profile of top10 FDA approved drugs with p300

Sl. No	Binding energy (kCal/mol)	Drug name	Total no of interaction	No of H-bond	Interacting residues
1	-10.6	Clobatasone	17	3	ARG-1410, THR-1411, TRP-1466 LEU-1463, PRO-1439, TYR-1446 CYS-1438, PRO-1440, LEU-1398 SER-1400, ASP-1399, GLN-1455 PRO-1458, TYR-1414, LYS-1456 HIS-1402, ARG-1462
2	-10.8	Conivaptan	17	1	PRO-1440, ASP-1399, ILE-1457 TYR-1446, LEU-1398, TRP-1466 LEU-1463, PHE-1467, TYR-1414 HIS-1402, ARG-1410, LYS-1407 ARG-1462, GLN-1455, LYS-1456 PRO-1458, SER-1400
3	-11.9	Dutasteride	19	2	ASP-1399, GLN-1455, ILE-145 PRO-1458, HIS-1451, SER-1400 TYR-1414, LYS-1456, ARG-1410 LYS-1407, HIS-1402, TRP-1466 PHE-1467, TYR-1446, PRO-1439 CYS-1438, LEU-1463, LEU-1398 PRO-1440
4	-10.8	Estrone-3-Sulphate	17	3	SER-1400, GLN-1455, PRO-1458 PRO-1440, PRO-1439, LEU-1398 TYR-1397, ILE-1435, TRP-1436 ALA-1437, TYR-1446, CYS-1438 PHE-1467, LEU-1463, TRP-1466 ARG-1410, TYR-1414
5	-10.6	Fluocinonide	19	3	PRO-1439, LEU-1463, PHE-1467 TRP-1466, PRO-1458, TYR-1414 ARG-1462, ARG-1410, HIS-1402 LYS-1456, ASP-1454, SER-1400 LEU-1398, GLN-1455, ILE-1457 ASP-1439, PRO-1440, TYR-1446 CYS-1438
6	-10.7	Imatinib	24	3	ARG-1627, CYS-1438, SER-1396 TYR-1394, TYR-1397, ILE-1395 ILE-1435, PHE-1467, LEU-1398 ASP-1399, SER-1400, TRP-1466 TYR-1414, PRO-1458, ARG-1410 GLN-1455, LYS-1456, PRO-1439 LEU-1463, PRO-1440, TRP-1436 TYR-1446, SER-1441, ASP-1444
7	-10.9	Netarsudil	25	3	ARG-1410, TRP-1466, TYR-1414 ILE-1435, PHE-1374, PHE-1467 ILE-1395, ALA-1437, TRP-1436 CYS-1438, TYR-1394, SER-1396 GLY-1506, ARG-1627, TYR-1397

TH-3600_196106022

					TYR-1446, LEU-1398, PRO-1439 PRO-1440, LEU-1463, ASP-1399 SER-1400, HIS-1451, GUN-1455 PRO-1458
8	-10.5	Telmisartan	19	-	LEU-1463, TYR-1446, LEU-1398 TRP-1466, PHE-1467, THR-1411 GLU-1465, LYS-1469, ARG-1462 ARG-1410, LYS-1456, GLN-1455 HIS-1402, ILE-1457, TYR-1414 HIS-1451, SER-1400, PRO-1458 ASP-1399
9	-10.9	Testrosterone-phenylpropionate	23	-	LEU-1398, PHE-1467, ILE-1457 ASP-1399, GLN-1455, LYS-1456 HIS-1402, ARG-1410, SER-1400 PRO-1458, LEU-1463, PRO-1439 PRO-1440, CYS-1438, TYR-1446 TRP-1466, TYR-1414, ALA-1437 TRP-1436, SER-1396, TYR-1397 ILE-1395, ILE-1435
10	-10.6	Ubrogepant	15	4	GLU-1465, LYS-1469, HIS-1415 ARG-1462, TRP-1466, LEU-1463 PRO-1440, PRO-1458, LEU-1398 TYR-1414, SER-1400, HIS-1402 GLN-1455, ARG-1410, THR-1411
11	-9.5	Control – C646	15	-	PHE-1467, LEU-1398, GLU-1465 LYS-1469, ARG-1462, ARG-1410 HIS-1402, GLN-1455, TYR-1414 SER-1400, TRP-1466, PRO1458 LEU-1463, PRO-1440, TYR-1446

2.3.5. Molecular Dynamics Simulation (MDS)

Virtual screening has the limitation of using only proteins and ligands to predict binding; however, in *in vitro* and *in vivo* studies, the binding of small molecules to target proteins is influenced by several variables, including solvents, ions, temperature, pressure, and concentration. These limitations mentioned above can be overcome with the help of the molecular dynamic simulation method. In this study, the p300 - drug complexes were simulated in a solvated system to mimic the biological environment. The binding free energy of the complex systems was re-calculated using the gromacs function named "g_mmpbsa." The strength and stability of the interactions between drugs and p300 were determined using gromacs parameters: root means square deviation (RMSD), root means square fluctuations (RMSF), pair distance, and number of H-bonds.

2.3.5.1. Binding Free Energy Analysis

Binding energies of p300-drug complexes predicted through Vina were re-calculated after molecular dynamics simulation using the MM-PBSA method. Gromacs function "g-mmpbsa" was applied to

TH-3600_196106022

calculate the binding energy of p300 – drug complexes with a 1 ns time interval for 100 ns simulation. The binding free energies of all p300 – drug complexes were given in terms of Van der Waals force, electrostatic force, SASA, and polar solvation energy in **Table 2.4**. The two main forces of drug binding were the electrostatic force (Strongest force of attraction), which attracts the ligands to the binding pocket, and the Van der Waals force that holds the drugs inside the binding pocket. Among ten, seven drugs such as Conivaptan, Fluocinonide, Imatinib, Netarsudil, Telmisartan, Testosterone phenylpropionate, and Ubrogepant, possessed higher binding energy compared to the control inhibitor (C646) of p300 **(Table 2.4).** The stability and strength of these seven drugs with p300 were further investigated using gromacs parameters.

Table 2.4: Binding free energy analysis of p300-drug complexes using MM-PBSA method.

Sl. NO	Drug Name	Van der Waals energy (kJ/mol)	Electrostatic energy (kJ/mol)	Polar solvation energy (kJ/mol)	SASA energy (kJ/mol)	Binding free energy (kJ/mol)
1	Clobetasone	-150.404	58.370	132.116	-15.852	24.229
2	Conivaptan	-210.414	-19.188	101.675	-20.328	-148.254
3	Dutasteride	-156.646	-8.305	166.703	-17.088	-15.337
4	Estrone-3-sulphate	-156.344	216.094	160.234	-16.665	203.319
5	Fluocinonide	-196.052	-24.559	172.336	-19.713	-67.987
6	Imatinib	-222.890	-523.709	509.730	-23.588	-260.457
7	Netarsudil	-243.282	-349.811	311.262	-23.237	-305.068
8	Telmisartan	-203.062	-84.543	270.406	-21.846	-39.045
9	Testosterone phenylpropionate	-185.598	-51.187	148.703	-19.874	-107.956
10	Ubrogepant	-223.351	-79.499	215.409	-20.752	-108.193
11	C646	-83.0022	-263.156	319.5492	-11.3708	-37.9796

2.3.5.2. Stability Analysis of p300 – Drug Complexes

To determine the structural stability of p300 following the binding of selected FDA-approved drugs, RMSD and RMSF analysis was carried out. The RMSD of the p300 backbone represents the protein stability during molecular dynamics simulation. Drug binding might affect the target protein stability in a solvated environment. Moreover, the deviation in the RMSD of p300 – drug complexes were plotted in **Figure 2.6A**, and the mean values were tabulated in **Table 2.5**. The observed deviation in the backbone RMSD was between 0.2 to 0.3 nm over 100 ns for all p300 – drug complexes as well as unbound p300 **(Figure 2.6A)**, and the mean RMSD of complexes were lesser than the unbound p300 except p300-conivaptan and p300-control complexes. In addition, the deviation in residual level

TH-3600_196106022

(RMSF) was also analyzed for all the complexes to shed light on the residues which affected most by the drug interaction. It was found that the fluctuation of the residues from 240 to 250 was reduced compared to the unbound p300, which indicates the drug interactions with those residues **(Figure 2.6B)**. The mean value of RMSF of the p300 complexes was also lesser compared to unbound p300 except for onivaptan and control; however, the increase in the mean values was less significant. Both RMSD and RMSF studies of p300-drug complexes indicate the binding of chosen drug molecules had no effect on the stability of the p300 backbone.

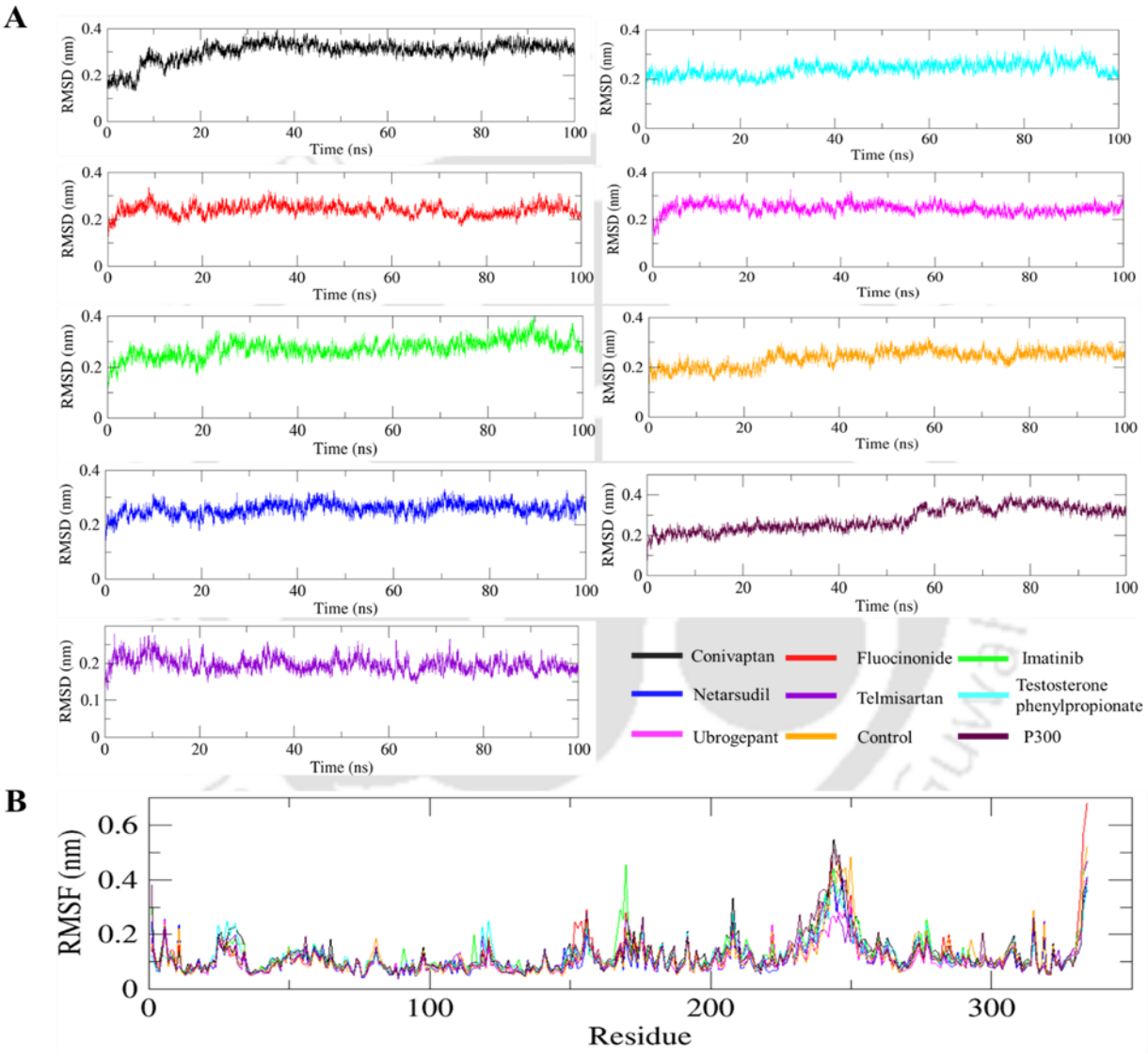

Figure 2.6: *Parameters of molecular dynamics simulation study over 100 ns. (A) RMSD analysis of p300 backbone following the binding of selected drugs. (B) RMSF of each residue of p300 following drug binding.*

TH-3600_196106022

2.3.5.3. Strength Analysis of p300 – Drug Complexes

The interaction strength between the ligand and protein molecules can be measured through the distance and the total number of H-bond established among them over a period of time. In this study, the total number of H-bonds constructed by drug molecules fluctuated in the range of 0 to 6 for 100 ns simulation **(Figure 2.7A)**. The average H-bonds created by drug molecules were calculated for 100 ns and tabulated in **Table 2.5**. The mean pair distance between the drug and p300 **(Table 2.5)** was lower than 0.21 nm, representing the strongest interaction. Pair distance analysis indicates that the formed H-bonds between the drug and protein can hold the drug molecules inside the binding pocket strongly over the simulation period **(Figure 2.7B)**. The snapshot of all p300-drug complexes is also shown in **Figure 2.7C** to check whether all the drugs were inside the same binding pocket over the 100 ns simulation. The 2D interaction profile of selected FDA-approved drugs with p300 after MDS is also depicted in **Figure 2.8**. It seemed as though; all the drug molecules were residing in the same binding site as 0^{th} ns with the conformation changes. Thus, all seven selected drug molecules might show potential inhibitory action against p300; however, based on binding free energy analysis, Netarsudil (used to treat glaucoma) has better binding energy, followed by Imatinib (used to treat Acute lymphoblastic leukemia) among all.

Table 2.5: Mean values of MDS parameters over 100 ns simulation

Sl. No	Drug Name	RMSD (nm)	RMSF (nm)	Pair Distance (nm)	H-bond (nm)
1	**Conivaptan**	0.302378	0.12998	0.176966	0.844516
2	**Fluocinonide**	0.241174	0.121943	0.216745	0.436756
3	**Imatinib**	0.273182	0.127607	0.184332	0.432757
4	**Netarsudil**	0.25783	0.108509	0.179648	0.953005
5	**Telmisartan**	0.196258	0.119409	0.170181	2.381162
6	**Testosterone phenylpropionate**	0.239861	0.120899	0.18486	0.675432
7	**Ubrogepant**	0.247088	0.107847	0.187857	0.146585
8	**C646**	0.284855	0.13695	0.169703	4.312269
9	**p300**	0.279965	0.122393		

TH-3600_196106022

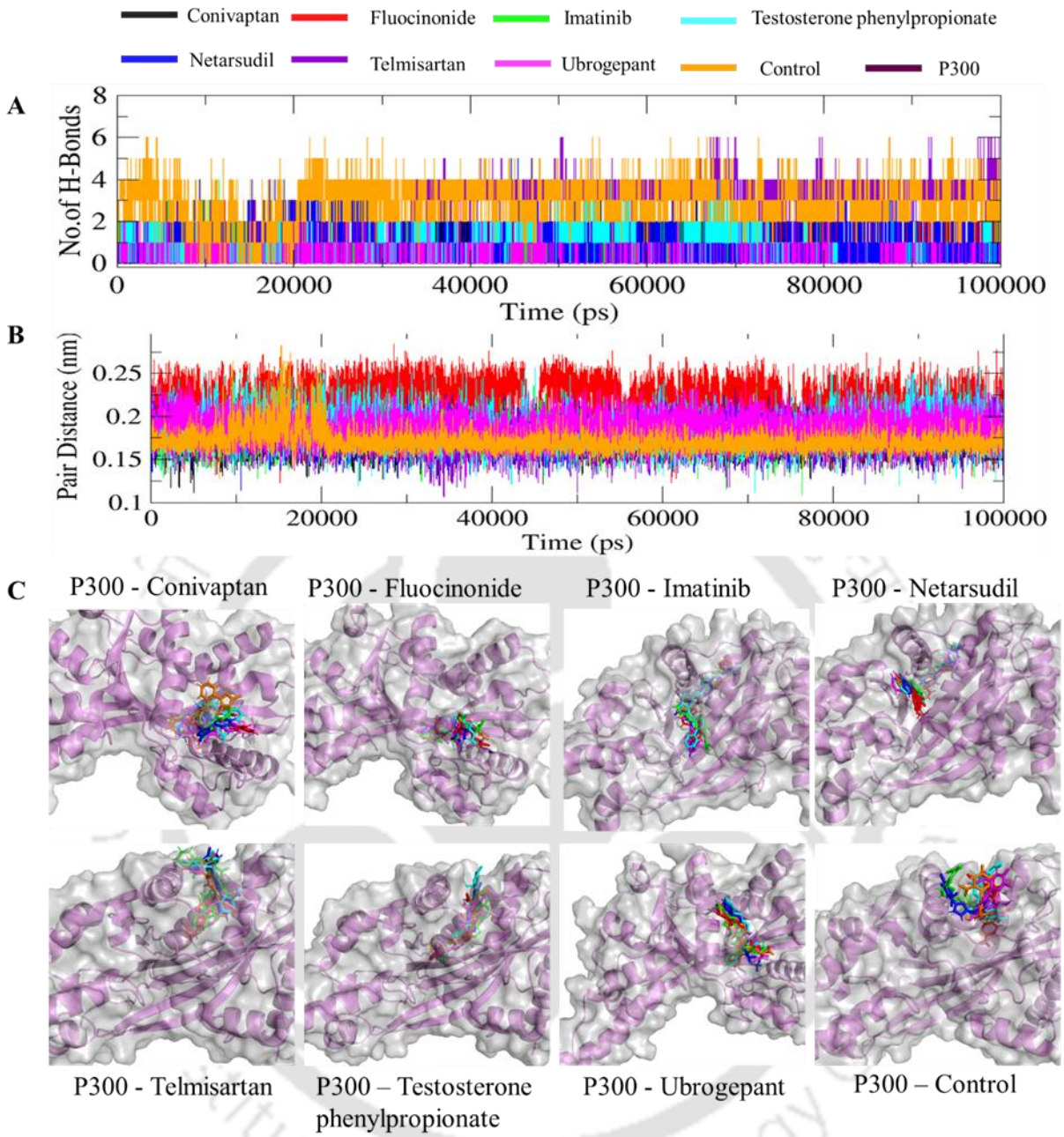

Figure 2.7: *(A) Number of hydrogen bonds were created between p300 and selected drugs (B) Pair distance between the p300 and selected drugs over 100 ns. C) Confirmation changes in drug binding within the p300 binding pocket with 20 ns time interval for 100 ns. Drug molecules were represented in 5 different colours to indicate the time point that are 0th ns- Red, 20th ns- Green, 40th ns- Blue, 60th ns- Magenta, 80th ns- Cyan, 100th ns- Orange.*

TH-3600_196106022

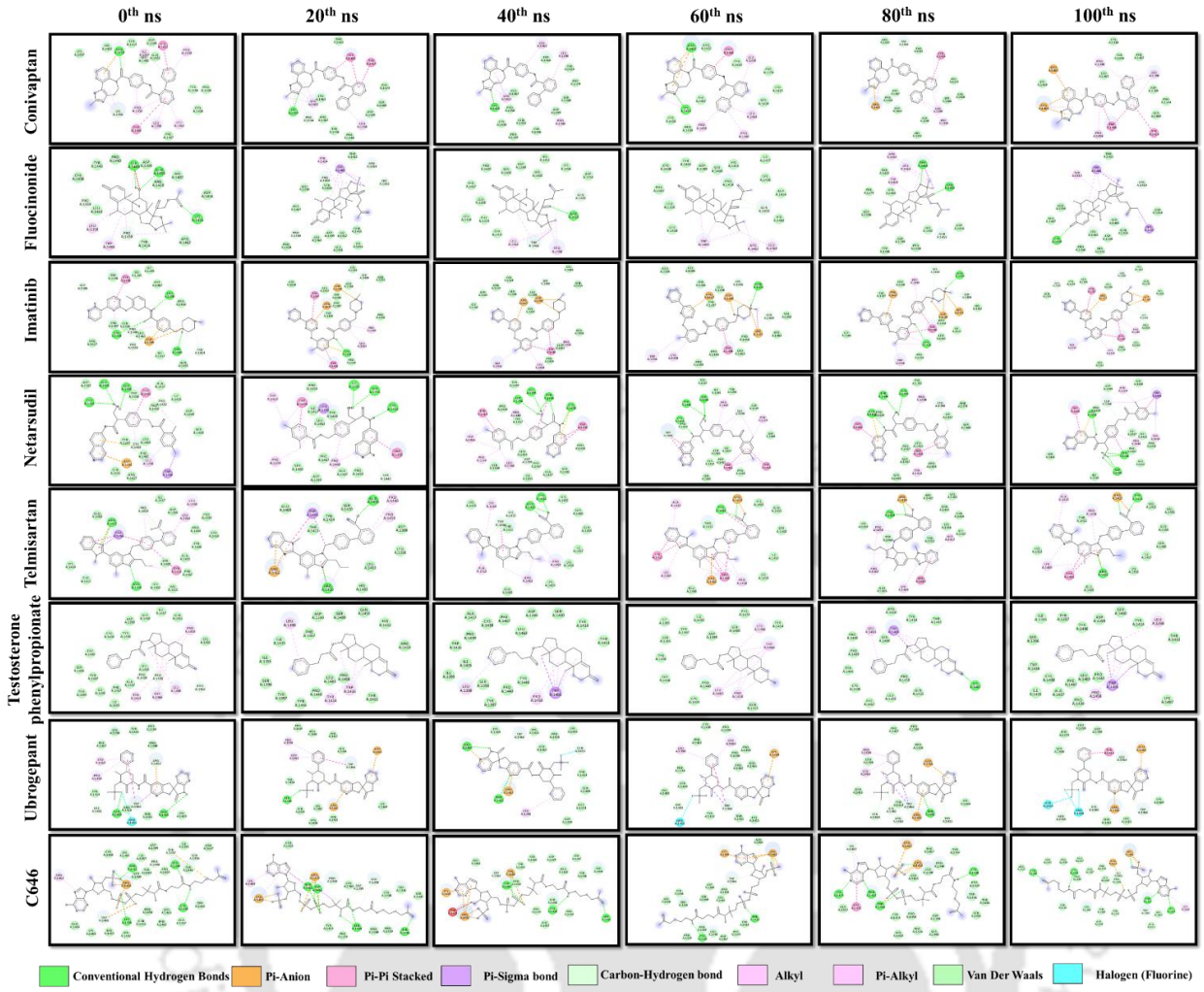

Figure 2.8: *2D interaction profile of selected FDA approved drugs with p300 after MDS.*

2.3.6. Anti-proliferative Activity of Imatinib in breast cancer cells

The MTT assay was utilized to evaluate the therapeutic potential of Imatinib in breast cancer cell lines. Treatment of cells with increasing concentrations of Imatinib was carried out, resulting in a dose-dependent decrease in cell viability in both MCF-7 and MDA-MB-231(**Figure 2.9**). The IC_{50} concentration of Imatinib (16.61 µM in MCF-7 & 24.95 µM in MDA-MB-231) was determined to be significantly less when compared to control inhibitor C646 (35.65 µM in MCF-7 & 46.43 µM in MDA-MB-231). This indicates that Imatinib has higher anti-proliferative properties against breast cancer cells than C646.

TH-3600_196106022

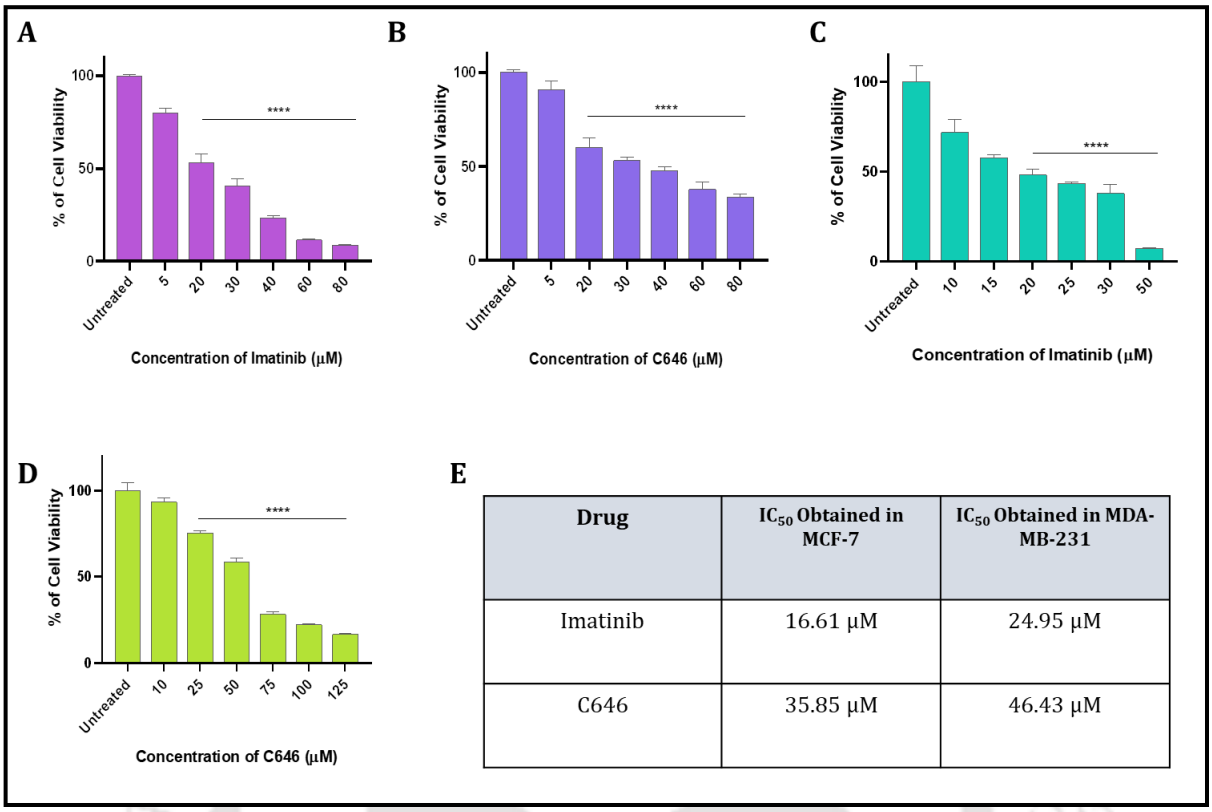

E

Drug	IC_{50} Obtained in MCF-7	IC_{50} Obtained in MDA-MB-231
Imatinib	16.61 µM	24.95 µM
C646	35.85 µM	46.43 µM

Figure 2.9: *Anti-cell proliferative effect of (A) Imatinib in MCF-7, (B) C646 in MCF-7, C) Imatinib in MDA-MB-231and (D) C646 in MDA-MB-231 cells. (E) IC_{50} values of C646 and Imatinib in different breast cancer cell lines.*

TH-3600_196106022

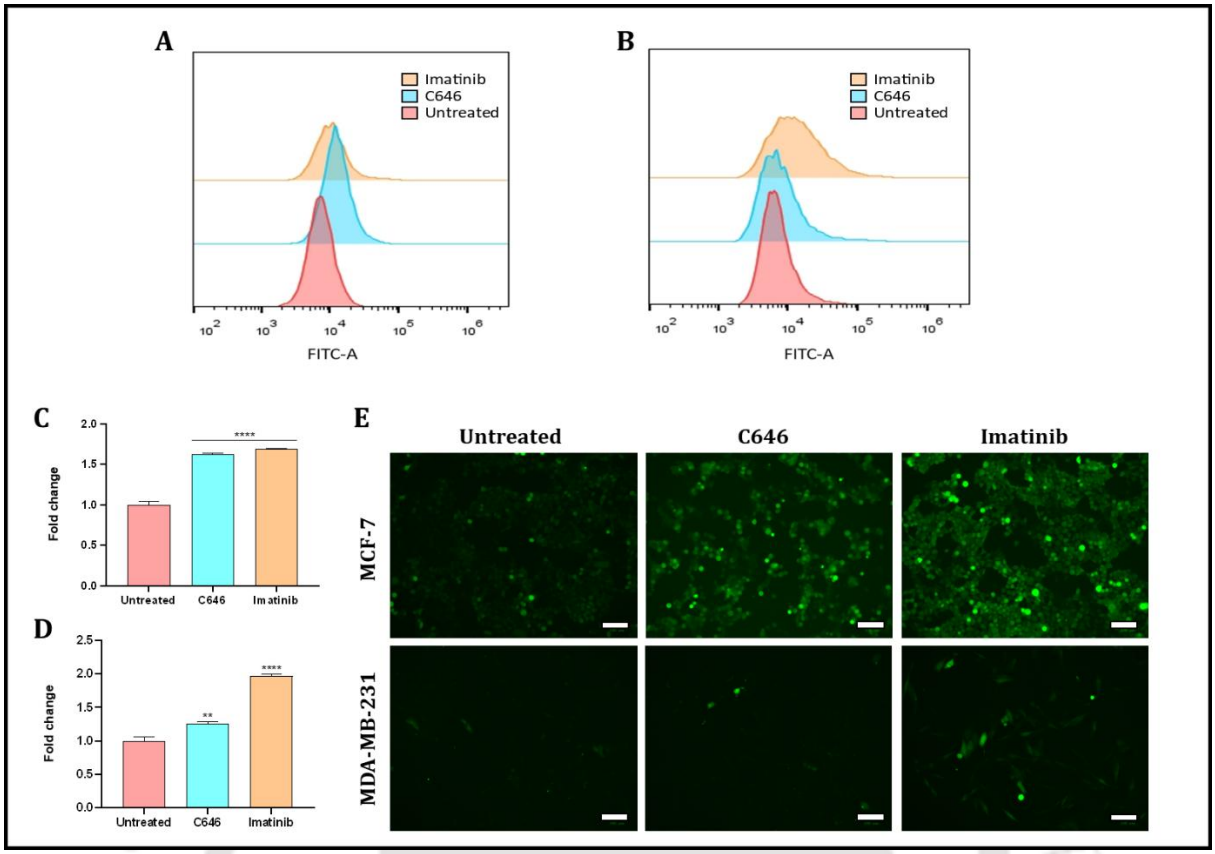

Figure 2.10: *Cellular ROS generation detection using flow cytometry in (A) MCF-7 and (B) MDA-MB-231. Fold change in ROS generation in (C) MCF-7 and (D) MDA-MB-231. (E) Fluorescent microscopy images were acquired after DCFDA staining following 24h of treatment with the drugs.*

2.3.7. Imatinib triggers ROS Generation, depolarizes mitochondrial membrane, and induces apoptosis

The cellular process behind the imatinib-mediated cell death was further elucidated by investigating cellular ROS level, changes in mitochondrial membrane potential, and apoptotic cell population. Following a 24-h treatment with Imatinib and C646 at their respective IC_{50} concentrations, intracellular ROS was quantified in breast cancer cell lines using DCFDA-mediated flow cytometry (**Figure 2.10A and Figure 2.10B**). Compared to untreated cells, ROS generation was increased by 1.62 and 1.68-fold in C646 and Imatinib-treated MCF-7 cells **(Figure 2.10C)**, respectively. Similarly, C646 and Imatinib-treated MDA-MB-231 cells exhibited 1.25 and 1.96-fold increase in ROS generation **(Figure 2.9I)**. Imaging study after DCFDA staining also showed an increase in green fluorescence, depicting enhanced ROS generation following drug treatment for 24h **(Figure 2.10D)**.

Subsequently, flow cytometry using JC-1 staining was employed to evaluate the impact of generated ROS on mitochondrial membrane integrity. In MCF-7, Imatinib and C646 treated cells exhibited a 24.91 and 22.74% increase in green fluorescence compared to the untreated cells, indicating the depolarization of mitochondrial membrane **(Figure 2.11A and 2.11C)**. On the other hand, a 21.4% upsurge in green fluorescence was found in Imatinib-treated MDA-MB-231 cells; however, no

TH-3600_196106022

substantial changes were found in the case of C646 treatment **(Figure 2.11B and 2.11D)**. A rise in intracellular ROS and mitochondrial membrane depolarization is a sign of diverse cellular damage, eventually resulting in programmed cell death. Therefore, the apoptotic population of cells after Imatinib and C646 treatment was analyzed through a flow cytometry-based apoptosis assay. It was determined that treatment with Imatinib for 48h resulted in 50.43 % and 45.74 % rise in the population of apoptotic cells in MCF-7 and MDA-MB-231, respectively **(Figure 2.11E-2.11H)**. In contrast, the C646 treatment increased the apoptotic cell population by 26.53 and 11.54 % in MCF-7 and MDA-MB-231**(Figure 2.11E-2.11H)**. These findings imply that Imatinib is more potent than C646 in inducing apoptosis. Live-dead cell imaging demonstrated enhancement in the PI-stained cells following drug treatment **(Figure 2.12A and 2.12B)**. Overall, these findings portrayed the anti-cancer effect of Imatinib on both cell lines.

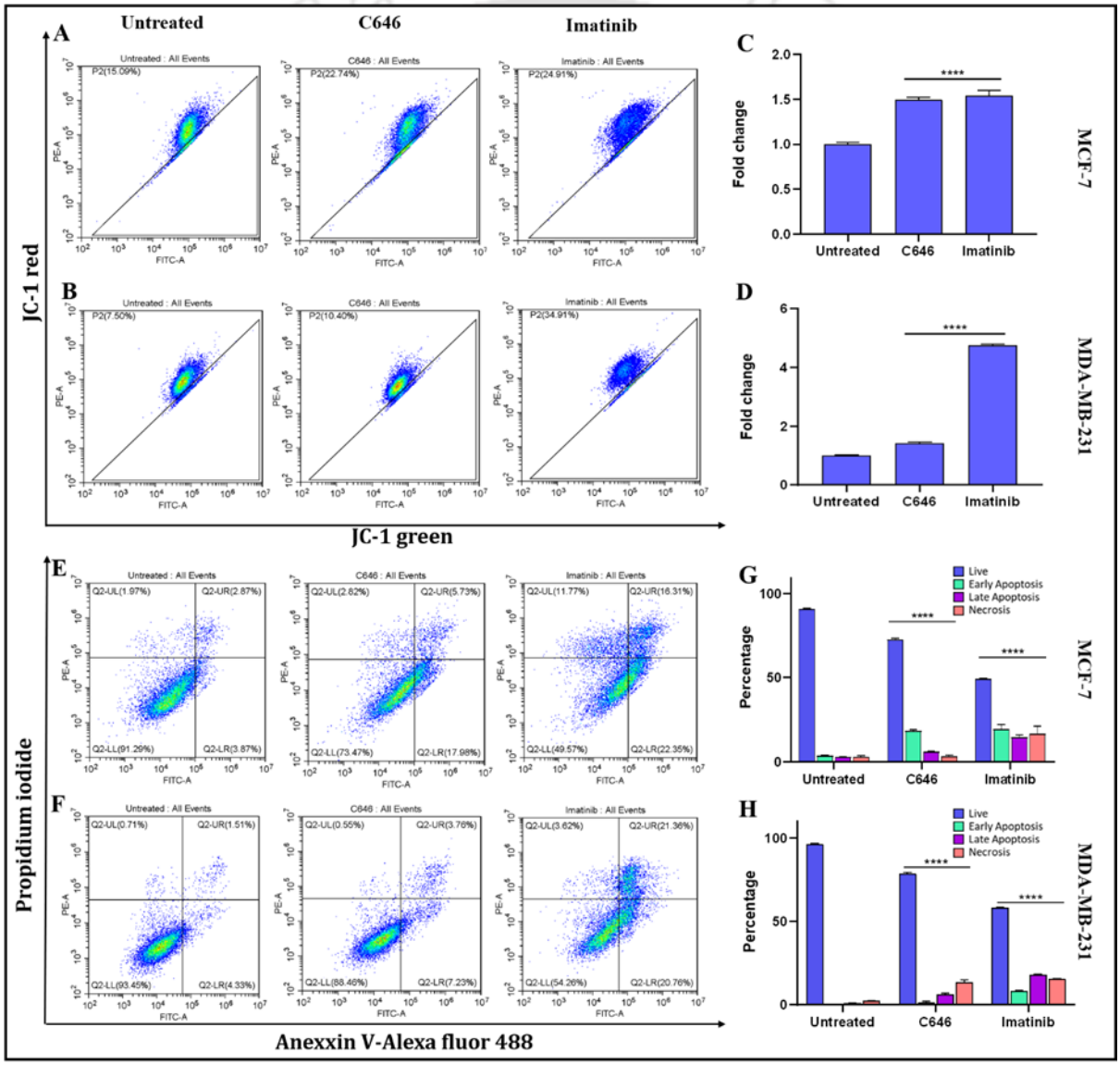

Figure 2.11: *Mitochondrial membrane potential determination of (A) MCF-7 and (B) MDA-MB-231. Graphical illustration of the change in mitochondrial membrane depolarization of (C) MCF-7 and (D) MDA-*

TH-3600_196106022

MB-231 after C646 and Imatinib treatment for 48h. Determination of apoptotic cell population by annexin-V-Alexa fluor 488 and PI-based flow cytometry in (E)MCF-7 and (F) MDA-MB-231. Graphical representation of apoptotic cell population in (G)MCF-7 and (H) MDA-MB-231 following C646 and Imatinib treatment.

2.3.8. Imatinib affects the colony and sphere-forming ability of breast cancer cells

The effect of drugs on the colony-forming capacity of breast cancer cells was evaluated after treatment with the drug and inhibitor at their respective IC_{50} concentration. It was evident that the colony-forming capability of both MCF-7 and MDA-MB-231 cells was reduced substantially due to Imatinib treatment. In contrast, no significant change in colony-forming ability was obtained from the C646 treatment **(Figure 2.12C)**. In addition, the spheroids of the treated MCF-7 and MDA-MB-231 cells were produced using the force flotation approach. In the case of MCF-7, imatinib-treated cells generated significantly smaller spheroids compared to normal cells. Meanwhile, for MDA-MB-231 cells, extremely disordered spheroid formation was observed due to Imatinib treatment **(Figure 2.12D)**. Overall, the substantial reduction in the ability to form spheres was prominent after the Imatinib treatment.

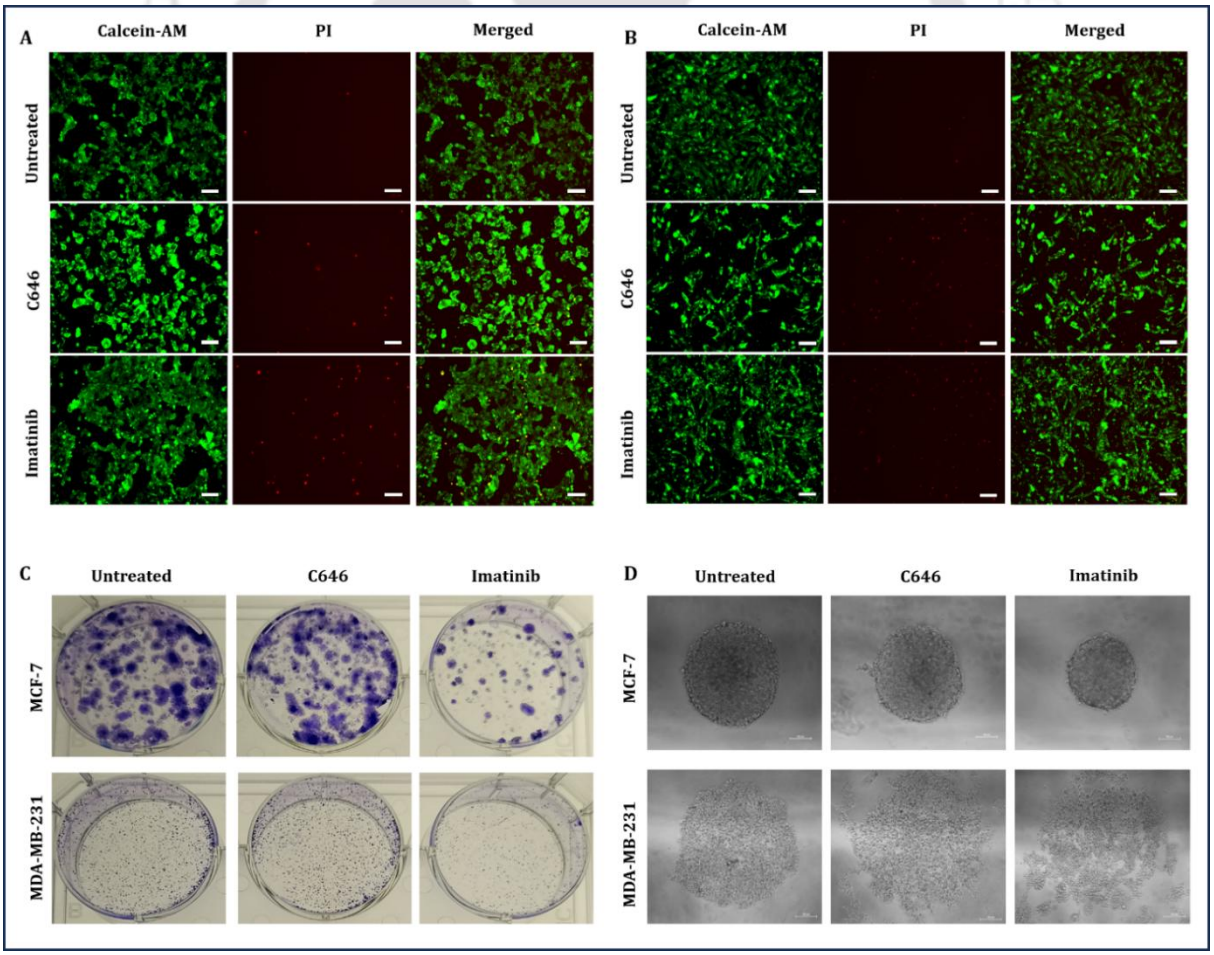

Figure 2.12: *Live/dead cell imaging of (A) MCF-7 and (B) MDA-MB-231 cells after C646 and Imatinib treatment for 48h (scale 100 µm). (C) Colony formation assay and (D) Sphere formation assay (scale 100 µm).*

TH-3600_196106022

2.3.9. Effect of Imatinib on p300 mediated histone acetylation and p300 expression

The acetylation status of H3K18 and H3K27 lysine residues was studied using specific antibodies **(Figure 2.13A and 2.13D)**. Imatinib treatment for 48 h caused distinct effects in the acetylation of particular lysine residues of histone, such as H3K18 acetylation was reduced by 5.78-fold and 2-fold in MCF-7 and MDA-MB-231 cell lines **(Figure 2.13B and 2.13E)**, respectively. Treatment with C646 resulted in a 1.5-fold increase in H3K18 acetylation in MCF-7 cells **(Figure 2.13B)**. Similarly, H3K18 acetylation increased 1.32-fold after treatment with C646 in MDA-MB-231 **(Figure 2.13E)**.

Subsequently, H3K27 acetylation was found to be downregulated by 2.15-fold in MCF-7 and 5-fold in the MDA-MB-231 cell line after Imatinib treatment **(Figure 2.13C and 2.13F)**. However, H3K27 acetylation was upregulated by 1.24-fold in MCF-7 cells following C646 treatment **(Figure 2.13C and 2.13F)**. Treatment with C646 resulted in no substantial effect on H3K27 acetylation in MDA-MB-231 cells. These results suggest that Imatinib induces histone hypoacetylation in breast cancer cell lines by inhibiting the HAT activity of p300.

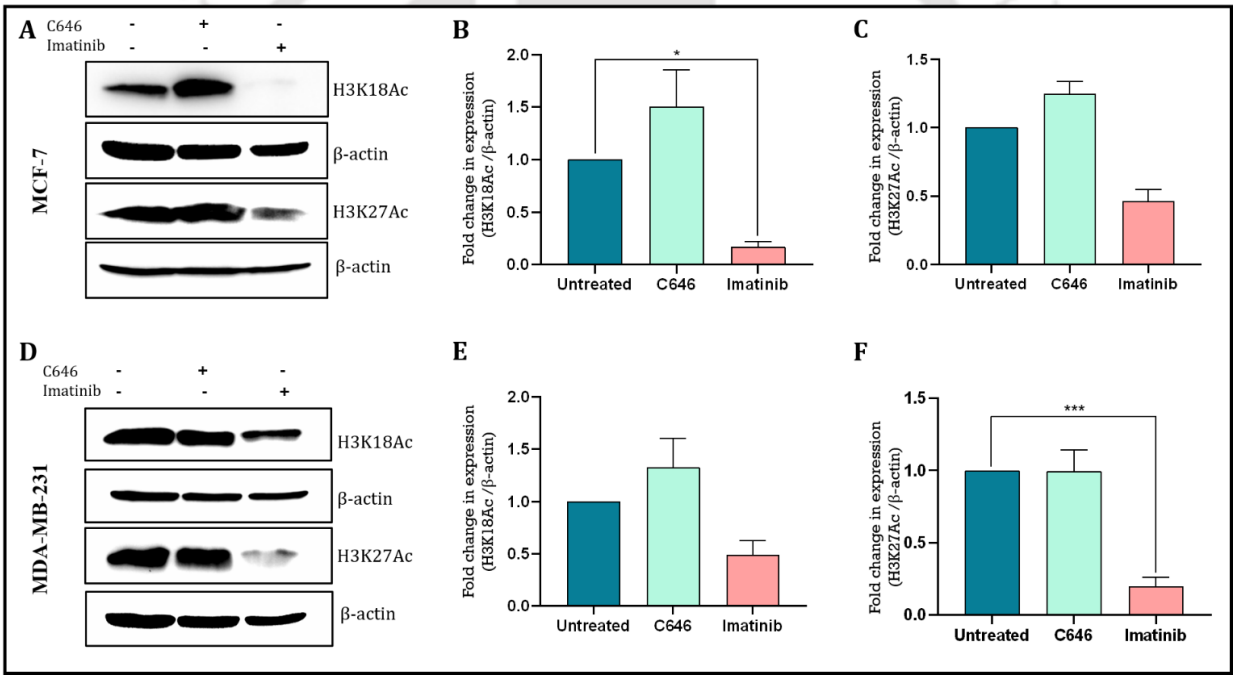

Figure 2.13: *Representative Western blots representing H3K18Ac and H3K27Ac levels in A) MCF-7 and D) MDA-MB-231 cells after C646 and Imatinib treatment for 48h. As a loading control, β-actin was used. Graphical illustration of the difference in the level of (B) H3K18Ac and (C) H3K27Ac in MCF-7 cells and (E) H3K18Ac and (F) H3K27Ac in MDA-MB-231 cells in comparison with the untreated cells. Visualization of the changes in expression was carried out using the ImageJ software.*

2.3.10. Imatinib mediated EMT reversal in TNBC cells

To ascertain the effect of Imatinib in EMT regulation expression of EMT markers was evaluated following 48h of treatment **(Figure 2.14)**. Expression levels of epithelial marker E-cadherin were

TH-3600_196106022

enhanced by 2.71-fold in imatinib-treated cells compared to only EGF-treated cells. Meanwhile, 3.65-fold downregulation in E-cadherin expression was observed due to C646 treatment **(Figure 2.14A)**. Correspondingly, expression of mesenchymal markers such as Fibronectin was reduced by 1.35-fold and 1.78-fold after C646 and Imatinib treatment, respectively **(Figure 2.14B)**. Similarly, Imatinib reduced the expression of the EMT transcription factor, SNAI2, by 2.15-fold compared to untreated cells, while slight upregulation in the expression of SNAI2 was detected in the case of C646 treatment **(Figure 2.14C)**. Overall, these findings imply Imatinib impedes the EGF-induced EMT of TNBC cells, and it is also evident that compared to C646, Imatinib possesses better EMT reversal potential.

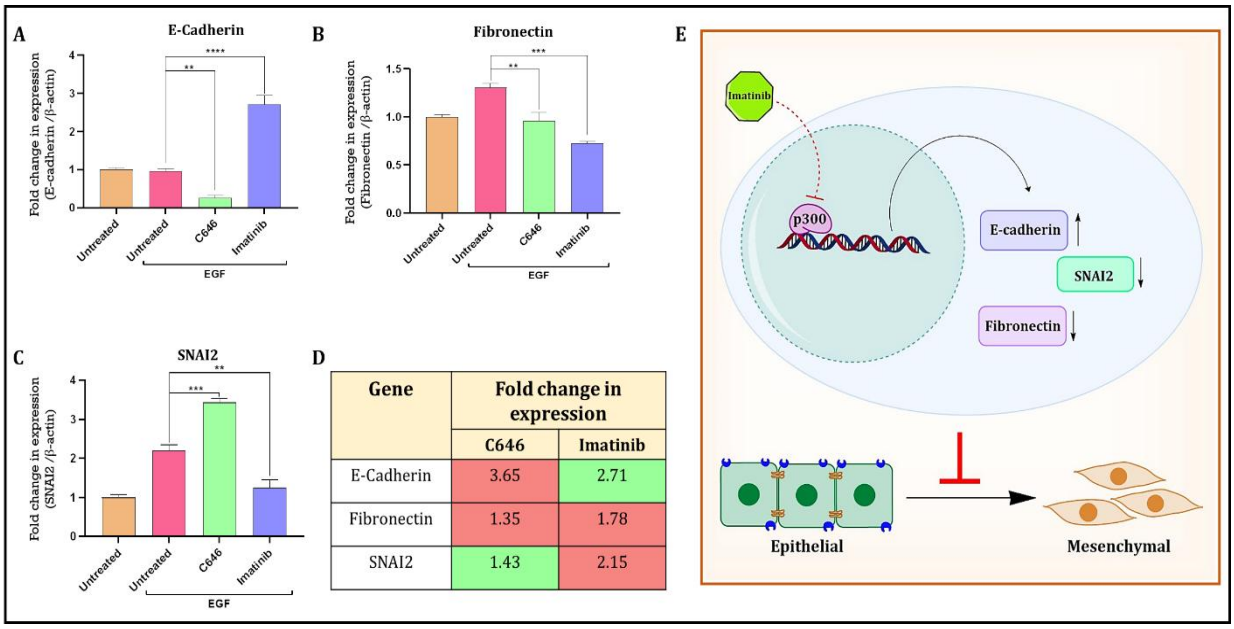

Figure 2.14: *Gene expression analysis of (A) E-cadherin, (B) Fibronectin, and (C) SNAI2 in EMT-induced MDA-MB-231 cells after treatment with C646 and Imatinib for 48h. (D) Fold change in the gene expression level in EMT-induced MDA-MB-231 cells. Red depicts downregulation in the gene expression, while green represents upregulation in the expression level. (E) Schematic illustration of the role of Imatinib in EMT dynamics.*

2.3.11. Imatinib reduces invasion and migration of TNBC cells

A matrigel invasion assay was employed to evaluate the impact of Imatinib on the invasion potential of TNBC cells. After 18h of incubation, cells treated with Imatinib exhibited a 3.03-fold reduction in blue fluorescence compared to untreated cells. However, for C646 treated cells, no significant change was observed **(Figure 2.15A and 2.15B)**. These findings signify that Imatinib decreased the capacity of cells to invade the layer of Matrigel, which resembles the extracellular matrix. The scratch wound-healing experiment was performed to assess the impact of Imatinib and C646 on the migratory ability of the TNBC cells. The capacity of migration of MDA-MB-231 cells was decreased by 1.85-fold and 1.11-fold following Imatinib and C646 treatment, compared to untreated cells **(Figure 2.15C and 2.15D)**, respectively.

TH-3600_196106022

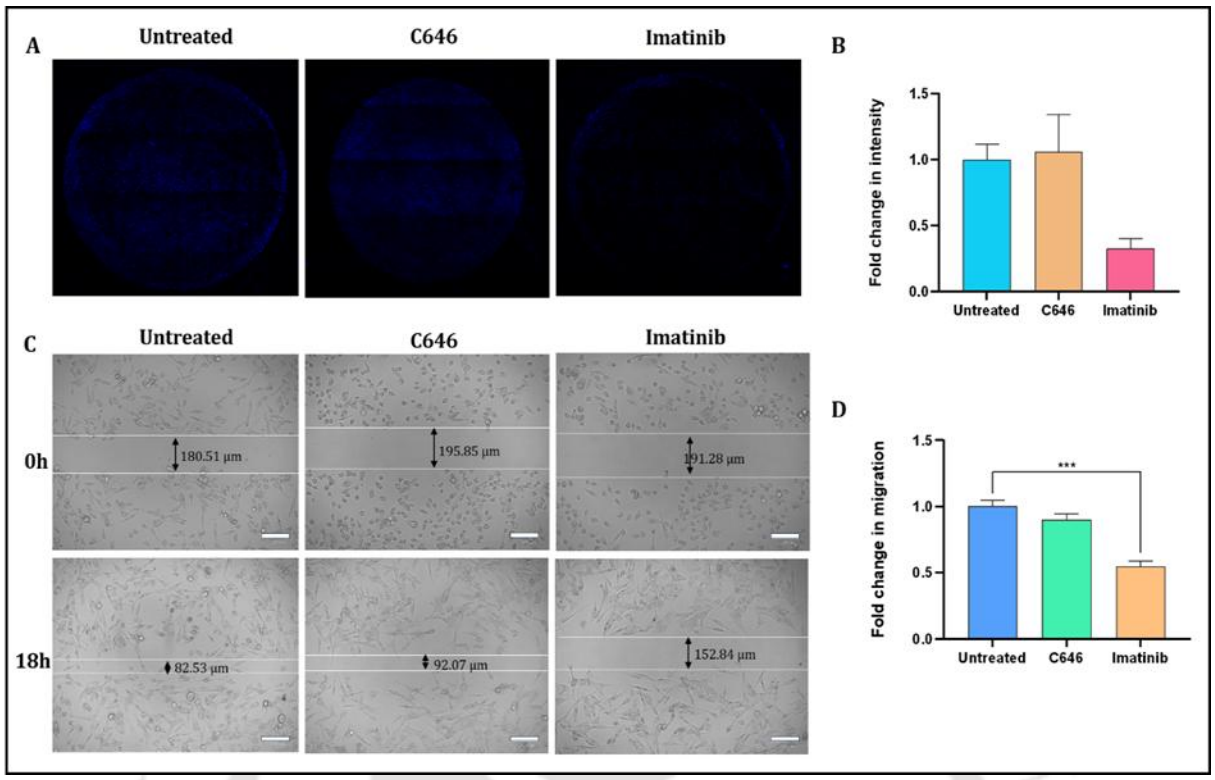

Figure 2.15: *(A) Matrigel invasion assay images of MDA-MB-231 cells treated with C646 and Imatinib (B) Graphical illustration of fold change in blue fluorescence. (C) Scratch wound healing assay to assess the migration ability of the MDA-MB-231 cell line after the treatment of C646 and Imatinib. The gaps were analyzed using ImageJ software (scale 100 µm). (D) Graphical illustration of fold change in migration capacity of MDA-MB-231 cells after treatment with C646 and Imatinib.*

2.3.12. Imatinib inhibits the expression of Notch downstream proteins

Notch signaling is one of the key regulatory pathways for pathogenesis of TNBC, which is involved in tumor development and growth **(Figure 2.16A)**. In fact, several experimental investigations have shown how Notch signaling assists in the promotion of EMT, which allows cancer cells to seed secondary organs, as well as in maintaining the cancer stem cells (CSCs) that give rise to chemoresistance [21]. Protein expression studies were carried out after 48h of treatment for EMT-induced MDA-MB-231 cells to ascertain the impact of Imatinib on the Notch downstream genes. Results showed that protein expression of HES1 was reduced by 2-fold and 2.94-fold after C646 and Imatinib treatment, respectively **(Figure 2.16B and 2.16C)**. Similarly, downregulation in the expression of AKT by 2.85-fold and 2.08-fold was evident following C646 and Imatinib treatment, respectively **(Figure 2.16B and 2.16D)**. Correspondingly, compared to untreated cells, a 1.88-fold reduction in expression of p21 was observed due to Imatinib treatment. Whereas, C646 treated cells exhibited slight upregulation in the p21 expression level compared to untreated cells **(Figure 2.16B and 2.16E)**.

TH-3600_196106022

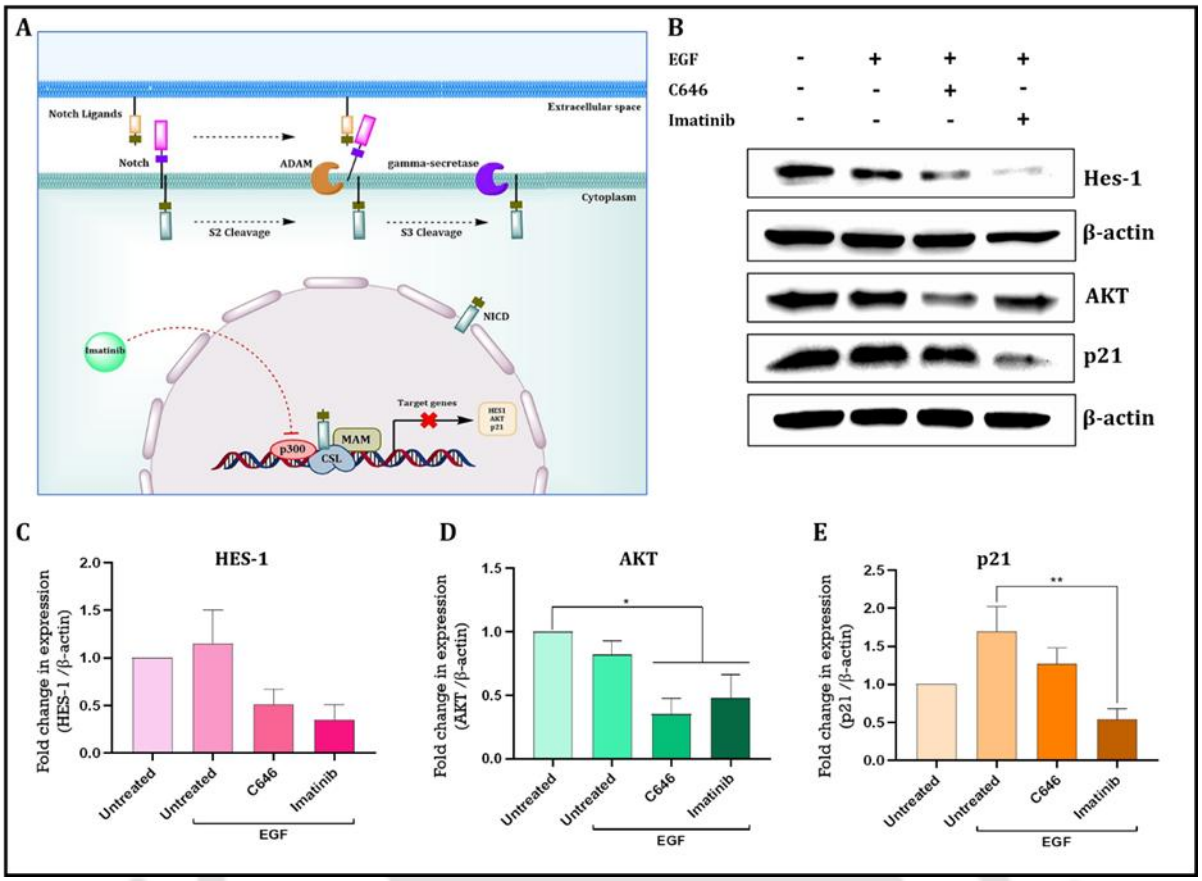

Figure 2.16: *(A) Schematic illustration of the role of Imatinib in Notch pathway regulation. (B)Representative Western blots representing HES1, AKT, and p21 levels in MDA-MB-231 cells treated with C646 and Imatinib for 48h. Graphical illustration of the difference in the level of (C) HES1 and (D)AKT and (E) p21 in MDA-MB-231 cells compared to the untreated cells. Visualization of the changes in expression was carried out using the ImageJ software.*

2.4. Discussion

Alterations in the epigenome are becoming recognized as critical events in the initiation and growth of cancer [16]. Histone acetylation is the most common epigenetic modification, which typically leads to the activation of transcription and is also associated with cancer progression [17]. p300 histone acetyltransferase is one of the important transcription co-activators linked with multiple cellular events and oncogenesis. Data acquired from the GEPIA2 server decipher that the expression of p300 is upregulated and correlates with a low survival rate in breast cancer. In addition, functional network analysis established the association of p300 in different oncogenic signaling pathways, including Notch signaling, TGFβ3, and SMAD2-mediated pathways. The impact of p300 on the initiation and progression of cancer is suggested by these studies, making it a viable target for breast cancer therapeutics. Virtual screening of FDA-approved drugs against the catalytic HAT domain of p300 provided us with 89 possible repurposed drugs out of the top 10 that were selected for further analysis. The binding site of these 10 drugs was the same as the control inhibitor of p300 (C646), which confirms that these drugs can act as a potential inhibitor of the HAT domain. The binding energies of these

TH-3600_196106022

selected drugs were re-calculated using the MM-PBSA method after 100ns MD simulation. MM-PBSA method considers the Van der Waals force of interaction, electrostatic interaction, polar solvation energy, and SASA for the binding free energy calculation. The study exhibited that seven out of ten drugs possessed better binding energy than the control inhibitor (-37.9796 kJ/mol). Further, the dynamic properties of these seven selected drugs were analyzed through molecular dynamic simulation parameters. RMSD and RMSF analysis showed that all these seven drugs formed stable complexes with p300. In addition to that, H-bond and pair distance analysis depicted the strongest interaction of the drugs with p300. Finally, the snapshot of the MD trajectory with a 20 ns time interval confirms that all the drugs remained bound to the HAT domain of p300 as the control inhibitor.

Despite its well-documented efficacy in treating chronic myeloid leukemia, the effects of Imatinib on breast cancer have remained unexplored, motivating its selection as a repurposed drug in this study. Anti-cell proliferative studies revealed that Imatinib significantly decreased breast cancer cell growth in a dose-dependent manner better than the control inhibitor C646. However, the IC_{50} value suggests that Imatinib showed better anti-cell proliferative activity in luminal (MCF-7) compared to the triple negative (MDA-MB-231) breast cancer cells. This differential response suggests that inhibitory effects of Imatinib may vary depending on the molecular subtype of breast cancer.

Further, flow cytometric analysis revealed that Imatinib enhanced intracellular ROS production in both MCF-7 and MDA-MB-231 cells. Numerous reports have indicated that excessive ROS production facilitates mitochondrial membrane depolarization through the oxidation of membrane lipids and the opening of mitochondrial permeability transition pores (mPTP) [18][19]. Flow cytometry studies using JC-1 dye demonstrated the rise in depolarized mitochondria affirms imatinib-induced ROS-driven impairment of the mitochondrial membrane. In addition, imatinib treatment exerted a 50.43 % increase in apoptotic cells in MCF-7 and a 45.74 % increase in MDA-MB-231, confirming the effectiveness of Imatinib in apoptosis induction. Additionally, the reduction in colony-forming and sphere-forming abilities following treatment suggests a decrease in stemness, which is critical for cancer cell survival and relapse.

Moreover, it was found that pharmacological inhibition of the p300 HAT domain using Imatinib reduced TNBC cell migration. p300 plays a pivotal part in the process of transcriptional activation through acetylating histone H3K18 and H3K27 [2]. H3K18Ac is a critical player in the growth of several cancers, including colon, lung, breast, hepatocellular, pancreatic, prostate, and thyroid [20]. Likewise, hematologic cancers are associated with H3K27Ac-enriched enhancers [21]. H3K27Ac remains abundant in the c-Myc promoter and enhances c-Myc expression in Merkel cell carcinoma [22]. In the instance of breast cancer, H3K27ac levels were found to be much greater than normal tissues [23]. These modifications were significantly reduced after treatment with Imatinib in both MCF-7 and MDA-MB-231 cell lines, confirming the hypothesis of imatinib-mediated inhibition of p300 HAT activity.

A critical finding of this study is the reversal of epithelial-mesenchymal transition (EMT) following Imatinib treatment. EMT is a key process that drives metastasis, therapy resistance, and cancer cell

TH-3600_196106022

stemness [24,25]. Several lines of evidence illuminated p300-mediated EMT progression in cancer [8,9,10,11]. Gene expression analysis from the current study portrayed that Imatinib treatment increased the expression of the epithelial marker E-cadherin, while decreasing the expression of mesenchymal markers, including Fibronectin and Slug. This suggests that Imatinib disrupts EMT by inhibiting p300's transcriptional coactivator function, ultimately reducing the invasive and migratory capacities of TNBC cells. Furthermore, p300 is intricately linked with the Notch signaling pathway, which is crucial for cancer progression, particularly in TNBC. The interaction between the Notch intracellular domain (NICD) and p300 facilitates the acetylation of histones at Notch target gene promoters, promoting the transcription of genes involved in angiogenesis, metastasis, and cancer stem cell maintenance [26,27,28]. By inhibiting p300, Imatinib disrupts the formation and function of the NICD–p300 complex. This leads to reduced histone acetylation at Notch target sites, thereby decreasing the transcriptional activation of genes that drive tumor growth and metastasis. As a result, Imatinib treatment significantly lowers the expression of key Notch downstream proteins, which in turn impairs the Notch signaling pathway. Mechanistically, our study indicates that, Imatinib treatment significantly reduced the expression of key Notch downstream proteins, including HES1, AKT, and p21, suggesting that p300 inhibition by Imatinib impedes Notch signaling in breast cancer cells. Given the role of Notch in promoting EMT, metastasis, and therapy resistance, this finding underscores the potential of Imatinib to target both p300 and Notch pathways, thereby hindering TNBC progression.

Overall, the findings from the present study demonstrate that p300 is a crucial oncogenic regulator in breast cancer, particularly in the context of EMT and Notch signaling. Imatinib, through its inhibition of p300 HAT activity, shows significant promise as a therapeutic agent for breast cancer, particularly for targeting the aggressive and metastatic properties of TNBC. These results provide a foundation for further clinical exploration of Imatinib as a repurposed drug for breast cancer therapy.

2.5. Conclusion

Histone acetyltransferase p300 was identified as a crucial tumorigenic protein, and targeting its activity has been considered a very promising approach for breast cancer therapy. Several *in silico* approaches (virtual screening, MDS, and binding free energy studies) have been utilized to screen the potential drugs from the library of FDA-approved drugs against p300. As a result, Imatinib was chosen as a potential repurposed drugs to inhibit p300 HAT activity. Further, the *in vitro* studies have established the inhibitory effects of Imatinib, an FDA-approved tyrosine kinase inhibitor, on p300 acetyltransferase. Findings from the cytotoxicity studies indicated that Imatinib exhibited more significant anti-proliferative activity on breast cancer cells than the control inhibitor of p300. Furthermore, it activates the intrinsic pathway of apoptosis via intracellular ROS generation and mitochondrial membrane depolarization. Concurrently, the colony and sphere-forming ability of the cells were reduced. Furthermore, Imatinib significantly reduced the acetylation of H3K18 and H3K27 by inhibiting the HAT activity of p300. Along with the hindrance in p300 HAT activity, Imatinib treatment decreased the expression of p300 in MCF-7 cells. Elevated expression of Epithelial marker

TH-3600_196106022

and downregulation of mesenchymal markers in TNBC cells reflected perturbation in EMT progression upon treatment. Besides, Imatinib was also effective in reducing the invasion and migration potential of TNBC. Moreover, the reduction in the expression of HES1, AKT, and p21 signifies the hindrance in the Notch signaling pathway. Thus, targeting p300 is a promising clinical strategy for breast cancer treatment, making Imatinib a promising repurposed drug for the targeted therapy of aggressive breast cancer.

TH-3600_196106022

2.6. References

1. Attar, N., & Kurdistani, S. K. (2017). Exploitation of EP300 and CREBBP lysine acetyltransferases by cancer. *Cold Spring Harbor perspectives in medicine*, 7(3), a026534. https://doi.org/10.1101/cshperspect.a026534

2. Ono, H., Basson, M. D., & Ito, H. (2016). P300 inhibition enhances gemcitabine-induced apoptosis of pancreatic cancer. *Oncotarget*, 7(32), 51301. https://doi.org/10.18632%2Foncotarget.10117

3. Xiao, X. S., Cai, M. Y., Chen, J. W., Guan, X. Y., Kung, H. F., Zeng, Y. X., & Xie, D. (2011). High expression of p300 in human breast cancer correlates with tumor recurrence and predicts adverse prognosis. *Chinese Journal of Cancer Research*, 23, 201-207. https://doi.org/10.1007/s11670-011-0201-5

4. Fermento, M. E., Gandini, N. A., Salomon, D. G., Ferronato, M. J., Vitale, C. A., Arevalo, J., ... & Curino, A. C. (2014). Inhibition of p300 suppresses growth of breast cancer. Role of p300 subcellular localization. *Experimental and molecular pathology*, 97(3), 411-424. https://doi.org/10.1016/j.yexmp.2014.09.019

5. Liao, Z. W., Zhao, L., Cai, M. Y., Xi, M., He, L. R., Yu, F., ... & Liu, M. Z. (2017). P300 promotes migration, invasion and epithelial-mesenchymal transition in a nasopharyngeal carcinoma cell line. *Oncology Letters*, *13*(2), 763-769. https://doi.org/10.3892%2Fol.2016.5491

6. Yokomizo, C., Yamaguchi, K., Itoh, Y., Nishimura, T., Umemura, A., Minami, M., ... & Yoshikawa, T. (2011). High expression of p300 in HCC predicts shortened overall survival in association with enhanced epithelial mesenchymal transition of HCC cells. *Cancer letters*, *310*(2), 140-147. https://doi.org/10.1016/j.canlet.2011.06.030

7. Ribatti, D., Tamma, R., & Annese, T. (2020). Epithelial-mesenchymal transition in cancer: a historical overview. *Translational oncology*, *13*(6), 100773. https://doi.org/10.1016%2Fj.tranon.2020.100773

8. Chang, R., Zhang, Y., Zhang, P., & Zhou, Q. (2017). Snail acetylation by histone acetyltransferase p300 in lung cancer. *Thoracic cancer*, *8*(3), 131-137. https://doi.org/10.1111%2F1759-7714.12408

9. Wang, Y., Qin, C., Zhao, B., Li, Z., Li, T., Yang, X., ... & Wang, W. (2023). EGR1 induces EMT in pancreatic cancer via a P300/SNAI2 pathway. *Journal of Translational Medicine*, *21*(1), 201. https://doi.org/10.1186/s12967-023-04043-4

10. Chanda, A., Sarkar, A., Deng, L., Bonni, A., & Bonni, S. (2023). Sumoylated SnoN interacts with HDAC1 and p300/CBP to regulate EMT-associated phenotypes in mammary organoids. *Cell Death & Disease*, *14*(7), 405. https://doi.org/10.1038/s41419-023-05921-x

TH-3600_196106022

11. Cho, M. H., Park, J. H., Choi, H. J., Park, M. K., Won, H. Y., Park, Y. J., ... & Kong, G. (2015). DOT1L cooperates with the c-Myc-p300 complex to epigenetically derepress CDH1 transcription factors in breast cancer progression. *Nature communications*, 6(1), 7821. https://doi.org/10.1038/ncomms8821

12. Popko-Scibor, A. E., Lindberg, M. J., Hansson, M. L., Holmlund, T., & Wallberg, A. E. (2011). Ubiquitination of Notch1 is regulated by MAML1-mediated p300 acetylation of Notch1. *Biochemical and biophysical research communications*, 416(3-4), 300-306. https://doi.org/10.1016/j.bbrc.2011.11.030

13. Jain, A. S., Prasad, A., Pradeep, S., Dharmashekar, C., Achar, R. R., Ekaterina, S., Victor, S., Amachawadi, R. G., Prasad, S. K., Pruthvish, R., Syed, A., Shivamallu, C., & Kollur, S. P. (2021). Everything Old Is New Again: Drug Repurposing Approach for Non-Small Cell Lung Cancer Targeting MAPK Signaling Pathway. *Frontiers in Oncology*, 11(October), 1–15. https://doi.org/10.3389/fonc.2021.741326

14. Lemkul, J. (2019). From Proteins to Perturbed Hamiltonians: A Suite of Tutorials for the GROMACS-2018 Molecular Simulation Package [Article v1.0]. *Living Journal of Computational Molecular Science*, 1(1), 1–53. https://doi.org/10.33011/livecoms.1.1.5068

15. Kumari, R., Kumar, R., & Lynn, A. (2014). G-mmpbsa -A GROMACS tool for high-throughput MM-PBSA calculations. *Journal of Chemical Information and Modeling*, 54(7), 1951–1962. https://doi.org/10.1021/ci500020m

16. Sharma, S., Kelly, T. K., & Jones, P. A. (2009). Epigenetics in cancer. *Carcinogenesis*, 31(1), 27–36. https://doi.org/10.1093/carcin/bgp220

17. Grunstein, M. (1997). Histone acetylation in chromatin structure and transcription. *Nature*, 389(6649), 349–352. https://doi.org/10.1038/38664

18. Kowaltowski, A. J., & Vercesi, A. E. (1999). Mitochondrial damage induced by conditions of oxidative stress. *Free Radical Biology and Medicine*, 26(3–4), 463–471. https://doi.org/10.1016/S0891-5849(98)00216-0

19. Marchi, S., Giorgi, C., Suski, J. M., Agnoletto, C., Bononi, A., Bonora, M., De Marchi, E., Missiroli, S., Patergnani, S., Poletti, F., Rimessi, A., Duszynski, J., Wieckowski, M. R., & Pinton, P. (2012). Mitochondria-Ros Crosstalk in the Control of Cell Death and Aging. *Journal of Signal Transduction*, 2012, 1–17. https://doi.org/10.1155/2012/329635

TH-3600_196106022

20. Hałasa, M., Wawruszak, A., Przybyszewska, A., Jaruga, A., Guz, M., Kałafut, J., Stepulak, A., & Cybulski, M. (2019). H3K18Ac as a marker of cancer progression and potential target of anti-cancer therapy. *Cells*, 8(5), 1–27. https://doi.org/10.3390/cells8050485

21. Raisner, R., Kharbanda, S., Jin, L., Jeng, E., Chan, E., Merchant, M., Haverty, P. M., Bainer, R., Cheung, T., Arnott, D., Flynn, E. M., Romero, F. A., Magnuson, S., & Gascoigne, K. E. (2018). Enhancer Activity Requires CBP/P300 Bromodomain-Dependent Histone H3K27 Acetylation. *Cell Reports*, 24(7), 1722–1729. https://doi.org/10.1016/j.celrep.2018.07.041

22. Sengupta, D., Kannan, A., Kern, M., Moreno, M. A., Vural, E., Stack, B., Suen, J. Y., Tackett, A. J., & Gao, L. (2015). Disruption of BRD4 at H3K27Ac-enriched enhancer region correlates with decreased c-Myc expression in Merkel cell carcinoma. *Epigenetics*, 10(6), 460–466. https://doi.org/10.1080/15592294.2015.1034416

23. Li, Q. L., Wang, D. Y., Ju, L. G., Yao, J., Gao, C., Lei, P. J., Li, L. Y., Zhao, X. L., & Wu, M. (2019). The hyper-activation of transcriptional enhancers in breast cancer. *Clinical Epigenetics*, 11(1), 1–17. https://doi.org/10.1186/s13148-019-0645-x

24. Grasset, E. M., Dunworth, M., Sharma, G., Loth, M., Tandurella, J., Cimino-Mathews, A., ... & Ewald, A. J. (2022). Triple-negative breast cancer metastasis involves complex epithelial-mesenchymal transition dynamics and requires vimentin. *Science translational medicine*, 14(656), eabn7571 https://doi.org/10.1126%2Fscitranslmed.abn7571

25. Thiery, J. P., Acloque, H., Huang, R. Y., & Nieto, M. A. (2009). Epithelial-mesenchymal transitions in development and disease. *cell*, 139(5), 871-890. https://doi.org/10.1016/j.cell.2009.11.007

26. He, H., Wang, D., Yao, H., Wei, Z., Lai, Y., Hu, J., Liu, X., Wang, Y., Zhou, H., Wang, N., Luo, X. G., & Zhang, T. C. (2015). Transcriptional factors p300 and MRTF-A synergistically enhance the expression of migration-related genes in MCF-7 breast cancer cells. *Biochemical and Biophysical Research Communications*, 467(4), 813–820. https://doi.org/10.1016/j.bbrc.2015.10.060

27. Bigas, A., & Espinosa, L. (2016). Notch signaling in cell–cell communication pathways. *Current Stem Cell Reports*, 2, 349-355. https://doi.org/10.1007/s40778-016-0065-1

28. Sen, P., & Ghosh, S. S. (2023). The intricate Notch signaling dynamics in therapeutic realms of cancer. *ACS Pharmacology & Translational Science*, 6(5), 651-670. https://doi.org/10.1021/acsptsci.2c00239

TH-3600_196106022

CHAPTER 3

Studying the role of histone methyltransferase MLL1 in EMT and Metabolic pathways in TNBC cells

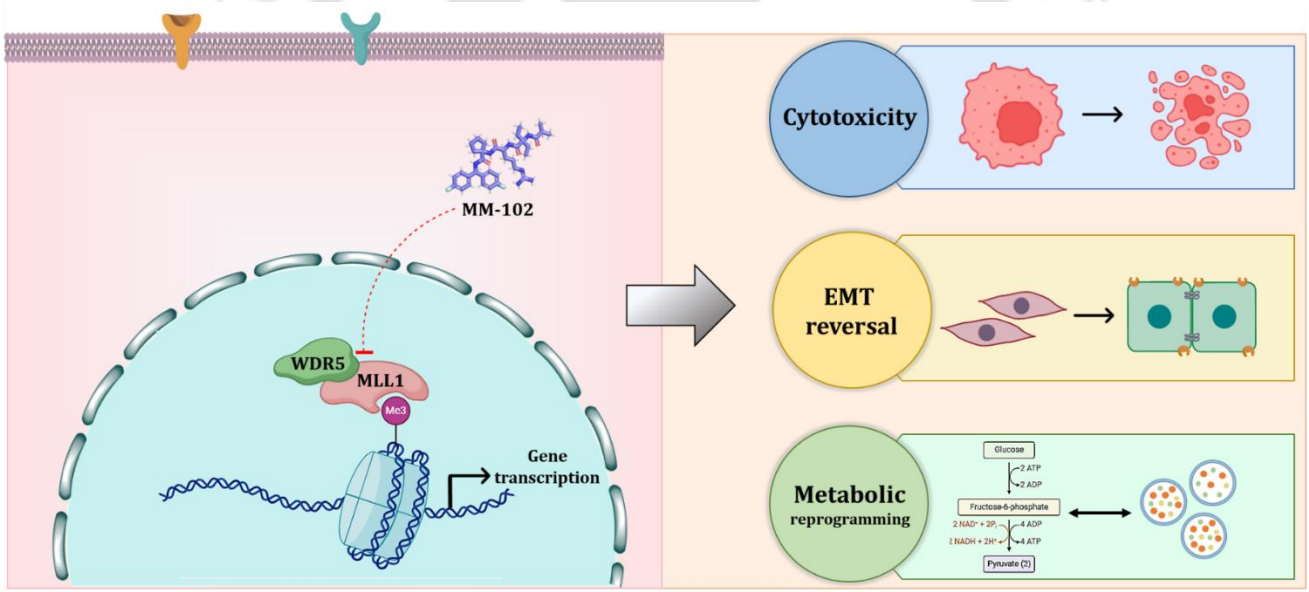

Biochemical and Biophysical Research Communications, Volume 755, 151559

https://doi.org/10.1016/j.bbrc.2025.151559

TH-3600_196106022

TH-3600_196106022

Chapter 3

3.1. Introduction

Histone modifications play an essential role in regulating chromatin structure and gene expression, influencing various biological processes, including cancer progression [1]. Histone modifications such as acetylation, methylation, and ubiquitination affect chromatin architecture and recruit enzymes that regulate transcriptional activity. Among these modifications, histone methylation, particularly on histone H3 lysine 4 (H3K4), has emerged as a crucial marker of active transcription. H3K4 methylation exists in three forms—mono-, di-, and tri-methylation (H3K4me1, H3K4me2, H3K4me3)—each associated with different regions of the genome [1]. While H3K4me1 is commonly found at active enhancers, H3K4me2/3 is associated with gene bodies and promoters, particularly at transcription start sites (TSS). These marks are deposited by a family of histone methyltransferases (HMTs) known as KMT2 (Lysine Methyltransferase 2) or mixed-lineage leukemia (MLL) proteins and are vital for the accurate regulation of gene expression throughout development and in cancer progression [2]. Among the MLL family members, MLL1 (KMT2A) catalyzes the transfer of methyl groups to H3K4 and is part of a larger multiprotein complex. This complex includes WDR5, ASH2L, RbBP5, and DPY30, which are essential for stabilizing the MLL1 complex and enhancing its methyltransferase activity [2]. The primary function of MLL1 is to regulate the expression of genes involved in cell proliferation, differentiation, and other key cellular processes, making it critical for maintaining cellular homeostasis. However, aberrations in MLL1 and other KMT2 family members can lead to dysregulated gene expression, contributing to tumorigenesis [3].

In cancer, dysregulation of histone methylation patterns has been linked to oncogenic transformation and metastasis, with aberrant H3K4 methylation driving the expression of genes that promote tumorigenesis [4]. Breast cancer, in particular, exhibits distinct epigenetic alterations that contribute to its heterogeneity and aggressiveness. It remains the most frequently diagnosed malignancy among women worldwide, with significant variability in its molecular subtypes [5]. Among these, triple-negative breast cancer (TNBC) is characterized by the absence of estrogen receptor (ER), progesterone receptor (PR), and human epidermal growth factor receptor 2 (HER2), making it resistant to targeted therapies that are effective in other breast cancer subtypes. Consequently, TNBC is associated with a poor prognosis, rapid disease progression, and a high propensity for metastasis [5, 6]. A key mechanism driving metastasis in TNBC and other cancers is the epithelial-to-mesenchymal transition (EMT). EMT is a biological process wherein epithelial cells lose their cell-cell adhesion properties and acquire a mesenchymal phenotype, leading to enhanced migratory and invasive capacities. This transition is tightly regulated by a network of transcription factors, including SNAIL, SLUG, and TWIST, which orchestrate the suppression of epithelial markers (such as E-cadherin) and the upregulation of mesenchymal markers (such as N-cadherin and vimentin). EMT often coincides with

TH-3600_196106022

metabolic reprogramming, enabling cancer cells to adopt the metabolic flexibility needed to support the energy and biosynthetic demands of invasion and survival under stress [7]. While EMT is essential for normal tissue development and wound healing, its aberrant activation in cancer is a critical step in facilitating tumor metastasis and drug resistance [6, 7]. Understanding the molecular regulators of EMT in TNBC is crucial for developing therapeutic strategies aimed at curbing metastasis and improving patient outcomes.

Recent studies have highlighted the role of histone methylation in the regulation of EMT, pointing to a significant interplay between epigenetic modifications and transcriptional programs that govern cell plasticity [8, 9]. Within this framework, histone methyltransferases, particularly those of the KMT2/MLL family, have gained attention for their role in cancer-associated gene expression. Of the six KMT2/MLL family members, KMT2A/MLL1 has been recognized for its role in regulating gene-specific H3K4me3, making it a key player in transcriptional control during both development and cancer [2, 3]. MLL1 (encoded by the KMT2A gene) is a large multi-domain protein with a complex architecture. Its C-terminal SET domain harbors the catalytic activity responsible for the methylation of H3K4, while its N-terminal domains mediate DNA binding and interactions with various cofactors. One of the most critical interactions for the functional integrity of the MLL1 complex is its association with WDR5, a WD40-repeat protein that stabilizes the complex and enhances its enzymatic activity [2, 3]. The MLL1-WDR5 interaction is pivotal for the recruitment of the complex to chromatin and the subsequent methylation of H3K4 at promoters of target genes. Interestingly, this interaction has become a target for therapeutic intervention. Small molecule inhibitors, such as MM-102, have been developed to disrupt the MLL1-WDR5 protein-protein interaction, thereby impairing the catalytic activity of the MLL1 complex and reducing H3K4 methylation at oncogenic loci [10].

This study investigates the role of MLL1 in regulating EMT and metabolic reprogramming, exploring its potential as a therapeutic target in TNBC. The effect of disrupting the MLL1-WDR5 interaction axis in the expression of crucial EMT transcription factors, mesenchymal markers, and the migratory and invasive behavior of TNBC cells was demonstrated. By uncovering the molecular mechanisms behind MLL1-mediated EMT modulation and metabolic reprogramming, this study offers new insights for targeting EMT in TNBC, with promising implications for enhancing therapeutic interventions.

3.2. Materials and methods

3.2.1. Cell Lines and Reagents

MDA-MB-468 and MDA-MB-231 cells were obtained from the National Centre for Cell Science (NCCS) in Pune, India. After the initial screening of contaminants, cells were passaged and maintained at 37°C, 5 % CO2 in Dulbecco's Modified Eagle's Medium (Sigma-Aldrich) added with 10 % fetal bovine serum (Gibco) and 1 % antibiotic (Gibco). MM-102 with a purity of ≥98% (HPLC) was purchased from Sigma-Aldrich and was prepared in dimethyl sulfoxide (Sigma-Aldrich). In culture media, drugs were diluted before being employed at the specified concentrations.

TH-3600_196106022

3.2.2. EMT induction

To induce EMT, MDA-MB-231 and MDA-MB-468 cells were treated with 20 ng/ml hEGF (Sigma-Aldrich) for 48 h. Cells were cultured in DMEM media containing 0.5% FBS in order to enhance the effect of hEGF. The same has been followed for all the experiments employing EMT-induced conditions.

3.2.3. Bioinformatics Analysis of MLL1 and WDR5 in Breast Cancer

To investigate the correlation between MLL1 and WDR5 expression and patient survival in breast cancer, the Gene Expression Profiling Interactive Analysis (GEPIA) server was utilized. It is a web-based tool that integrates TCGA and GTEx expression data. GEPIA parameters were set to categorize patients into high- and low-expression groups, with a statistical significance threshold of $p < 0.05$. Further, to explore functional interactions between MLL1 and WDR5, the STRING database was employed. Using the multiprotein interaction query, both MLL1 and WDR5 were input as target proteins. Interacting partners were extended to a maximum of 50 proteins, with a confidence score of 0.7 to ensure high interaction reliability. The STRING database allowed us to visualize the interaction network, providing insights into potential co-regulatory pathways associated with MLL1 and WDR5 in breast cancer.

3.2.4. MTT assay

The anti-proliferative activity of the MM-102 was evaluated using MTT assay (HiMedia) as per manufacturer protocol. Cells were seeded at a density of 5×10^3 cells/well in 96 well tissue culture plate(s). Following attachment, increasing concentrations of MM-102 were added to each well. After 48h of treatment, 0.5 mg/ml MTT solution was added and incubated for 2h. After that, the formed formazan crystals were dissolved in dimethyl sulfoxide (DMSO). The change in the color with respect to the treatment was measured using a microplate reader (Thermo Fisher Scientific) at 570 nm with a reference wavelength of 630 nm. Inhibitory concentration-50 (IC_{50}) was determined through GraphPad Prism software version 6.0.

3.2.5. Cytotoxicity study for spheroids

Cells were seeded with a density of 20×10^3 cells per well, and spheroids were produced utilizing a forced floating approach [11]. Following 72 h of seeding, spheroids were treated with different drugs. After 72 h of treatment, spheroids were incubated with alamarBlue for 4 h at cell culture conditions. Afterward, the respective incubations and absorbance were noted at 570 nm and 600 nm with a microplate reader (Thermo Fisher Scientific) [11]. Determination of the inhibitory concentration-50 (IC_{50}) was performed using GraphPad Prism version 6.0.

3.2.6. Live/dead cell imaging

Cells treated with MM-102 for 48 h were subjected to live and dead cell populations analysis. Subsequent to the treatment period, 2 µM of Calcein-AM and 4 µM of PI were added to the cells for 30 min. Afterward, the cells were visualized using ZOE Fluorescent Cell Imager (Bio-Rad). Similarly,

TH-3600_196106022

MDA-MB-468 and MDA-MB-231 spheroids were treated for 72h. Similarly, the spheroids were also incubated with the same concentrations of Calcein-AM and PI for 1h. Following that, a Zeiss LSM 880 confocal microscope was used for image acquisition of the spheroids after washing with PBS.

3.2.7. Detection of cellular Reactive Oxygen Species (ROS)

The study utilized Dichlorodihydrofluorescein diacetate (DCFDA) dye (Sigma-Aldrich) to quantify the ROS generation following treatment with inhibitors. DCFDA generates green fluorescence in the presence of intracellular ROS. To quantity ROS production, following treatment with inhibitors for 24h, 10 µM DCFDA was added to the cells for 30 min. This allowed the dye to enter the cells and react with any ROS present, resulting in green fluorescence that could be detected and measured. After incubation, cells were trypsinized and used for flow cytometry (Cytoflex, Beckman Coulter) to evaluate the green fluorescence.

3.2.8. Apoptosis assay

Alexa fluor 488 Annexin V/dead Kit (Invitrogen) was used to estimate the apoptotic cell population in treatment conditions. After 48h of MM-102 treatment, samples were prepared in accordance with the manufacturer's instructions and analysed through flow cytometry (BD FACSMelody). Data processing and fluorescence compensation were carried out through FlowJo software.

3.2.9. Glycolysis Assay

The impact of the drug on glucose uptake and metabolism of the cells was ascertained from the glycolysis assay by employing the glucose (HK) assay kit (Sigma Aldrich). Cells were plated in a 35mm dish at a concentration of $0.3x10^6$ cells and exposed to serum deprivation in media containing 0.5% serum overnight. Subsequently, the EMT-induced cells were cultured in DMEM 1mg/ml glucose media and treated with the drug. Following a 6-h incubation period, the media underwent centrifugation to ascertain the residual glucose concentration. The samples were prepared in compliance with the protocol provided by the manufacturer, and the absorbance was determined by harnessing a microplate reader at a wavelength of 340 nm.

3.2.10. Scratch wound-healing migration assay

This assay was executed to assess the variation in TNBC cell migratory capacity following treatment in EMT-induced conditions. Cells were allowed to grow until 60–70% confluency and starved in 0.5% serum media for 24 h prior to the linear wound generation. PBS washing was implemented to remove cellular debris. Subsequently, EGF (20 ng/ml) and drugs were added to the cells and treated for 18h. Pre-and post-treatment image acquisition of the wounded area was carried out by a Nikon Eclipse Ti microscope. The wound distance was measured at three different positions inside each wound region, and the average of those measurements was then calculated using ImageJ.

3.2.11. Colony formation assay

For this assay, cells were plated and treated with respective drug concentrations for 48 h in 6-well plates. After that, trypsinization was performed to resuspend the cells in fresh DMEM media. In 6 well

TH-3600_196106022

plates, 2 mL of cell suspension with a cell density of 5000 cells/ml was added and kept in cell culture conditions for 10 days. Ultimately, the generated colonies were stained using 0.5% crystal violet solution after fixing with 4% formaldehyde solution.

3.2.12. Quantitative real-time PCR

After 48h of treatment with the drugs, total RNA was isolated using TRI reagent (Sigma-Aldrich), and further cDNA synthesis was carried out using the iScript cDNA synthesis kit (Bio-Rad). SYBR Green Master Mix (Bio-Rad) was used to amplify the target cDNA in Rotor-Gene Q real-time PCR cycler (Qiagen). β-actin was normalized, and ΔΔCt values were calculated using LinReg PCR software. Primers utilized for amplification are provided in **Table 3.1**.

Table 3.1: List of primers used for real-time PCR experiments

Sl.No	Gene name	Forward primer	Reverse primer
1	MLL1	GACCTCAGGCACAGGGACTC	CGGAAGAACAGCGACTTGCC
2	WDR5	ATGCGACAGAGACCATCATAG	CGTGAGGATATGGGATGTGAA
3	Caveolin 1	AACACGTAGCTGCCCTTCAG	GGATGGGAACGGTGTAGAGAT
4	Fibronectin	AACATGTAACCACCAGTCTCATGTG	GGTGACACTTATGAGCGTCCTAAA
5	Aldolase A	GACACTCTACCAGAAGGCGGAT	GGTGGTAGTCTCGCCATTTGTC
6	PGK1	CCGCTTTCATGTGGAGGAAGAAG	CTCTGTGAGCAGTGCCAAAAGC
7	ENO1	GGCTTTACGTTCACCTCGG	TCAACCTCAACAGTGGGATTC
8	β-actin	AAGGGACTTCCTGTAACAATGCA	CTGGAACGGTGAAGGTGACA

3.2.13. Western blotting

After 48h of treatment, total protein from the cells was isolated and quantified using RIPA lysis buffer (Sigma Aldrich) and bicinchoninic acid (BCA) protein assay kit (Thermo Fisher Scientific), respectively. Subsequently, the Western blot experiment was performed, as mentioned in the previous study [12]. Antibodies used for the Western blot are enlisted in **Table 3.2**. Further applying chemiluminescent reagent (Bio-Rad) images were developed using ChemiDoc (Bio-Rad). The image analysis was done using ImageJ software. The acquired data were normalized with respect to the expression of β-actin, and protein expressions were estimated.

TH-3600_196106022

Table 3.2: The list of antibodies used for protein expression study

Antibodies	Catalog No	Manufacture
β-actin	8457	Cell Signaling Technology, USA
H3K4Me3	9751	Cell Signaling Technology, USA
E-cadherin	9782	Cell Signaling Technology, USA
Claudin	9782	Cell Signaling Technology, USA
β-catenin	9782	Cell Signaling Technology, USA
Slug	9782	Cell Signaling Technology, USA
Caveolin	3267	Cell Signaling Technology, USA
Fibronectin	26836	Cell Signaling Technology, USA
SOD2	13141	Cell Signaling Technology, USA
Anti-Rabbit IgG (Alexa Flour® 488 Conjugate)	A-11008	Thermo Fisher Scientific, USA
Anti-Rabbit IgG, HRP linked	7074S	Cell Signaling Technology, USA

3.2.14. Proteomics Analysis

A comprehensive proteomic analysis was performed to explore the proteomic changes induced by the inhibition of MLL1 in MDA-MB-468 cells. MDA-MB-468 cells were seeded at a density of 5 x 10^5 cells per 60 mm dishes and treated with the MM-102 for 48 h. After treatment, total cellular proteins were extracted using RIPA buffer (Thermo Fisher Scientific, USA), and the protein concentration was determined using the BCA protein assay kit (Thermo Fisher Scientific, USA) following the manufacturer's instructions.

For mass spectrometry analysis, in-solution trypsin digestion was performed using the standard protocol. The digested peptides were desalted using C18 columns (Thermo Fisher Scientific, USA) and dried in a vacuum centrifuge. The reconstituted peptides were subjected to liquid chromatography-tandem mass spectrometry (LC-MS/MS) using the Q-Exactive Plus Biopharma mass spectrometer (Thermo Scientific, USA). Peptide separation was carried out using a PepMap RSLC C18 analytical column (2 µm, 100 Å, 50 cm) along with an Acclaim PepMap 100 pre-column (100 µm x 2 cm, nanoviper). The mobile phase consisted of solvent A (0.1% formic acid in Milli-Q water) and solvent B (85:15 acetonitrile water with 0.1% formic acid). Peptides were eluted using a gradient program and analyzed in data-dependent acquisition (DDA) mode. Data acquisition was performed using the Thermo Scientific Xcalibur software, Version 4.2.28.14.

Raw MS/MS data were processed using Thermo Proteome Discoverer 2.2 software for data analysis. The data were searched against the UniProt human protein database (uniprot-Homo+sapiens.fasta). Protein identification was achieved with a false discovery rate (FDR) threshold of <1% and proteins were quantified based on at least two unique peptides. Differentially expressed proteins (DEPs) were identified based on a fold-change cutoff of ≥2 and a p-value of <0.05.

TH-3600_196106022

3.2.15. Statistical analysis

All statistical analyses were performed using GraphPad Prism software. Each experiment was conducted in triplicate, with data presented as the mean ± SEM. A one-way ANOVA was employed to evaluate correlations among groups. A p-value of <0.05 (*) indicates statistical significance, while p-values of <0.001 (**) and <0.0001 (****) denote high statistical significance.

3.3. Results

3.3.1 Comparative analysis of MLL1 and WDR5 expression in EMT-induced conditions

The expression levels of MLL1 and WDR5 in EMT-induced conditions of TNBC cell lines were determined to explore their relevance in EMT. In this study, EGF was used to activate the EMT process, a key driver of metastasis in TNBC [13]. EGF treatment induces EMT-like characteristics in both cell lines, providing an ideal condition to assess the role of MLL1 and WDR5 during EMT activation. qRT-PCR analysis revealed a significant upregulation of mRNA levels of MLL1 and WDR5 in response to EGF treatment. In MDA-MB-468 cells, MLL1 expression was upregulated by 4.7-fold, while WDR5 expression increased by 3.84-fold compared to the untreated controls **(Figure 3.1 A-B)**. These findings suggest a marked activation of both genes in EMT-induced MDA-MB-468 cells, indicating a possible functional role of the MLL1-WDR5 complex in the EMT process. Similarly, notable upregulation was observed in MDA-MB-231 cells, with MLL1 expression increasing by 1.7-fold and WDR5 by 1.17-fold under the same conditions **(Figure 3.1 C-D)**. This differential expression pattern between the two cell lines highlights the context-dependent nature of MLL1 and WDR5 involvement in EMT.

To further explore the clinical relevance of MLL1 and WDR5 expression in breast cancer, we utilized the GEPIA server to analyze overall survival rates in patients with high expression of these genes. The study revealed that overexpression of both MLL1 and WDR5 was associated with significantly poorer survival outcomes in breast cancer patients **(Figure 3.1 E-F)**. Specifically, patients with elevated levels of MLL1 and WDR5 demonstrated reduced survival rates, suggesting that these genes may serve as negative prognostic markers in breast cancer, particularly in aggressive subtypes like TNBC. These findings underscore the importance of the MLL1-WDR5 complex in the progression of breast cancer and its potential as a therapeutic target. To gain insights into the functional interactions of MLL1 and WDR5, a network analysis using the STRING database was performed. This analysis revealed a robust interaction network, identifying the top 50 potential interactors of the MLL1-WDR5 complex. Many of these interactors are involved in chromatin modification, gene transcription, and cell cycle regulation, further supporting the role of the MLL1-WDR5 complex in the regulation of EMT-related gene expression **(Figure 3.1G)**. The identification of these interactors provides valuable information for future studies aimed at dissecting the molecular mechanisms by which MLL1 and WDR5 contribute to breast cancer metastasis.

Collectively, these results suggest that MLL1 and WDR5 are significantly upregulated in EMT-induced TNBC cells, and their overexpression correlates with poor patient outcomes. This study highlights the potential of targeting the MLL1-WDR5 complex as a therapeutic strategy in TNBC, particularly in the context of inhibiting EMT-driven metastasis. Therefore, disrupting the MLL1-WDR5 interaction could

TH-3600_196106022

impair the transcriptional regulation of EMT-associated genes, offering a novel therapeutic strategy to inhibit TNBC progression.

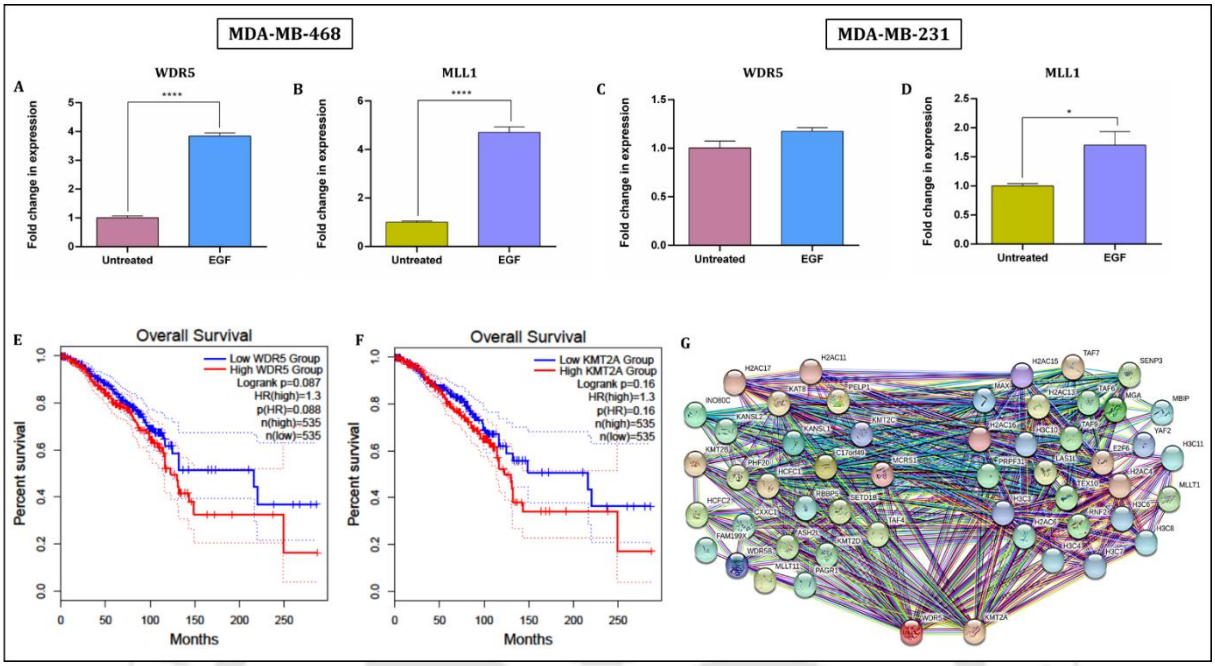

Figure 3.1: *Gene expression analysis of A) WDR5, B) MLL1 in MDA-MB-468, C) WDR5, D) MLL1 in MDA-MB-231, Survival plot of E) WDR5 F) MLL1 in breast cancer from GEPIA, G) functional network of MLL1-WDR5 from STRING.*

3.3.2. Inhibition of MLL1 reduces cell viability in EMT-induced TNBC cells

The therapeutic potential of targeting MLL1 was explored by assessing the effect of MLL1 inhibition on cell viability using the MLL1 inhibitor MM-102 in EMT-induced conditions. This experiment was designed to evaluate whether inhibiting MLL1 can induce cell death in aggressive TNBC cell lines. The MTT assay was performed to determine cell viability after treating MDA-MB-468 and MDA-MB-231 cells with MM-102 for 48 h under EMT-induced conditions. The results indicated a significant reduction in cell viability in both cell lines after treatment with MM-102. The IC_{50} concentration determined for MM-102 was 7.4 µM in MDA-MB-468, while it was notably higher at 21.1 µM in MDA-MB-231 **(Figure 3.2 A-C)**. This difference in IC_{50} values can be attributed to the differential expression of MLL1 in these cell lines under EMT conditions, with MDA-MB-468 exhibiting a higher expression level of MLL1 compared to MDA-MB-231. The lower IC_{50} in MDA-MB-468 suggests greater sensitivity to MLL1 inhibition, likely due to its elevated MLL1 expression in the EMT-induced state.

In addition to the MTT assay, a live/dead cell imaging analysis was performed to validate further the cell death observed with MM-102 treatment. This analysis confirmed increased cell death in MM-102-treated cells, supporting the MTT findings. The live/dead staining results showed a significant increase in dead cells in the MM-102-treated group compared to controls, indicating that MLL1 inhibition effectively induces cell death under EMT conditions in TNBC cells **(Figure 3.2D-3.2E)**. These results

TH-3600_196106022

collectively suggest that targeting MLL1 with MM-102 significantly reduces cell viability and induces cell death, particularly in cells with higher MLL1 expression, such as MDA-MB-468. Given the role of MLL1 in promoting EMT and cancer progression, the findings from the present study support the potential of MLL1 inhibition as a promising therapeutic strategy for aggressive cancers like TNBC.

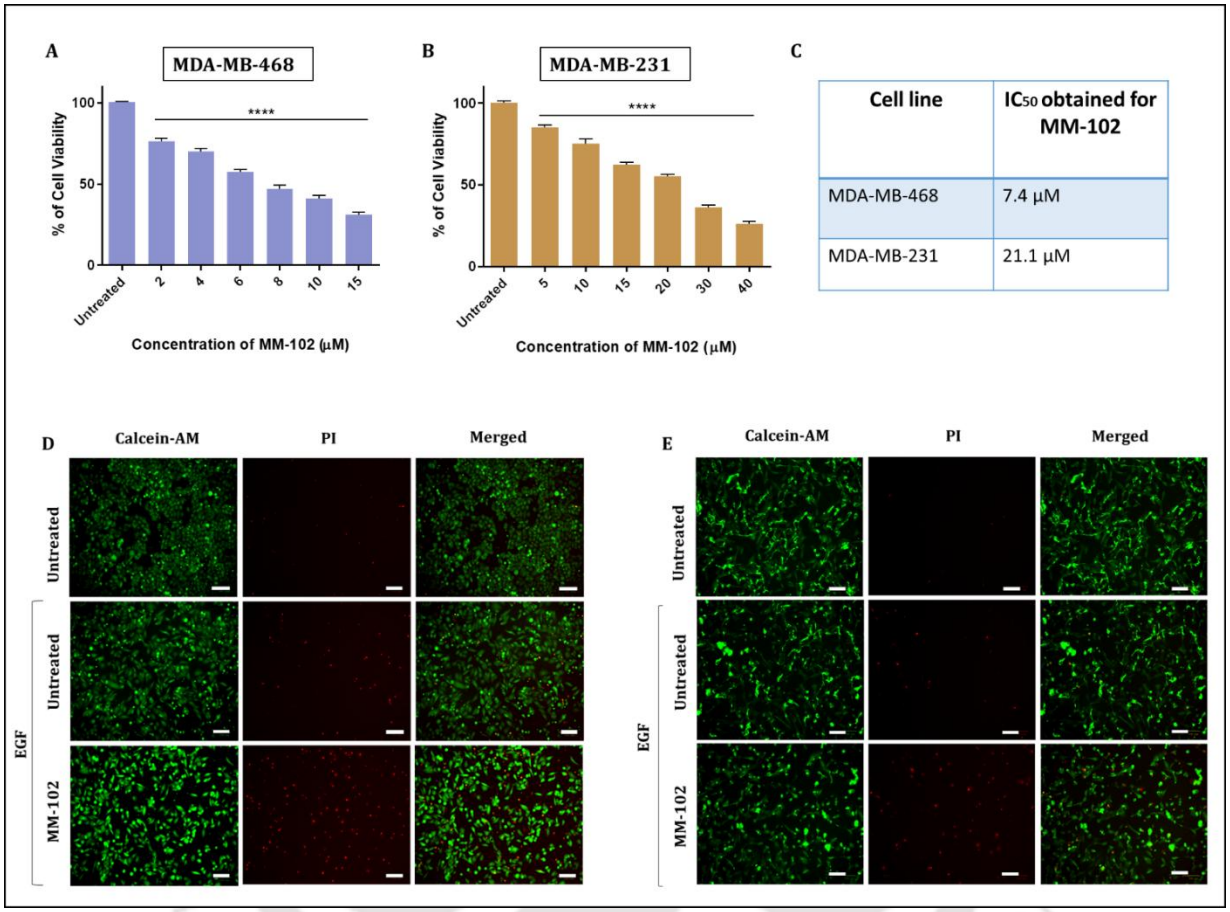

Figure 3.2: *MTT assay showing the reduction in cell viability of A) MDA-MB-468 and B) MDA-MB-23 cells treated with MM-102 under EMT-induced conditions. C) IC_{50} values of MM-102 in MDA-MB-468 and MDA-MB-231 cells. Live/dead assay confirming increased cell death in MM-102 treated D) MDA-MB-468 cells and E) MDA-MB-231 cells.*

3.3.3. Inhibition of MLL1 induces ROS-mediated intrinsic apoptosis in TNBC cells

The cellular mechanism of MLL1-mediated cell death was studied further in EMT-induced TNBC cells. A series of cellular studies were conducted to explore the relationship between MLL1 inhibition, oxidative stress, and apoptosis. The analysis of the generation of intracellular ROS following MM-102 treatment in both MDA-MB-468 and MDA-MB-231 cell lines was carried out. The flow cytometry and fluorescence microscopy-based DCFDA staining revealed a striking increase in ROS levels. Specifically, a 5-fold increase in ROS generation was observed in MDA-MB-468 cells, while MDA-MB-231 cells exhibited a 2-fold increase **(Figure 3.3A-B)**. This heightened ROS production following MM-102

TH-3600_196106022

treatment suggests that MLL1 inhibition leads to oxidative stress, particularly in the highly EMT-prone MDA-MB-468 cell line.

Further, the expression of the antioxidant enzyme superoxide dismutase 2 (SOD2) was assessed after MM-102 treatment. Despite the significant induction of ROS, SOD2 expression was found to be downregulated in both cell lines, as confirmed by western blot analysis **(Figure 3.3C)**. This suggests that MM-102 promotes ROS accumulation by suppressing SOD2, further implicating oxidative stress as a critical mediator of the observed cellular responses. Annexin V and propidium iodide (PI) staining was performed using flow cytometry to determine whether this increase in ROS leads to apoptotic cell death. The findings demonstrated a significant increase in apoptotic populations in both cell lines, with approximately 30% more cells undergoing apoptosis in MM-102-treated groups than controls **(Figure 3.3D)**. This indicates that MLL1 inhibition induces apoptosis, likely through a ROS-mediated intrinsic apoptosis pathway. Overall, the results suggest that MM-102 activates the intrinsic apoptosis pathway via ROS generation and SOD2 downregulation in TNBC cells.

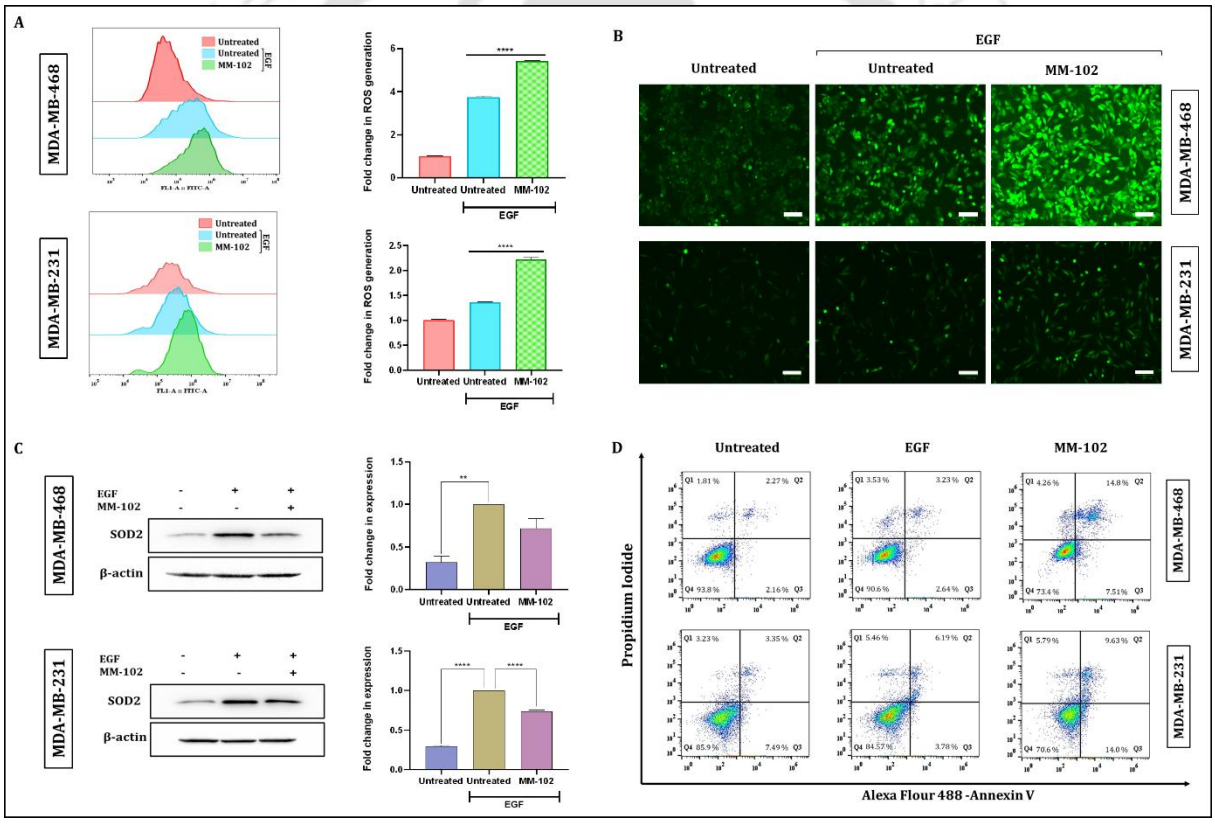

Figure 3.3: *A) Flow cytometric analysis shows increased intracellular ROS generation in MDA-MB-468 and MDA-MB-231 cells treated with MM-102 under EMT-induced conditions. B) Fluorescence microscopy image-based DCFDA staining showing ROS generation in MDA-MB-468 and MDA-MB-231 cells treated with MM-102. C) Western blot analysis showing the downregulation of SOD2 expression in MM-102-treated MDA-MB-468 and MDA-MB-231 cells. D) Flow cytometry analysis of Annexin V/PI staining showing increased apoptotic populations in both cell lines treated with MM-102.*

TH-3600_196106022

3.3.4. MM-102 inhibits H3K4me3 methylation in TNBC

MLL1 is a well-known histone methyltransferase responsible for trimethylation of histone H3 at lysine 4 (H3K4me3), a modification associated with active gene transcription. Several studies have demonstrated the role of MLL1 in maintaining H3K4me3 levels in various cancers, including breast cancer [14]. In the present study, the inhibition of H3K4me3 by MM-102 treatment was further validated in EMT-induced TNBC cells. Western blot analysis was carried out to examine the expression levels of H3K4me3 in both MDA-MB-468 and MDA-MB-231 cell lines after 48 h of treatment with the IC_{50} concentration of MM-102. Western blot results revealed a significant reduction in H3K4me3 levels in both cell lines compared to the EGF-treated EMT-induced condition **(Figure 3.4 A-D)**. This suggests that MM-102 effectively inhibits the methyltransferase activity of MLL1, leading to decreased H3K4me3 methylation in these aggressive cancer cells.

H3K4me3 is known to regulate the transcription of several essential genes involved in EMT and cell survival. For instance, the EMT-associated transcription factors ZEB1 and SNAIL, which promote metastasis and drug resistance, are often regulated by H3K4me3-marked promoters [15, 16]. Decreasing H3K4me3 levels can suppress the expression of these transcription factors, thus attenuating the EMT process. Additionally, the downregulation of H3K4me3 can disrupt the transcription of genes involved in cell survival pathways, such as PI3K/AKT, promoting apoptotic signaling [17]. To further validate the reduction of H3K4me3, confocal microscopy was performed to visualize H3K4me3 levels in MM-102-treated cells. The images confirm a marked decrease in H3K4me3 expression in MM-102-treated MDA-MB-468 cells compared to the EMT-induced controls **(Figure 3.4E)**. These results further support the notion that MLL1 inhibition through MM-102 disrupts critical epigenetic marks, such as H3K4me3, required for EMT maintenance and cell survival, thereby promoting apoptosis.

TH-3600_196106022

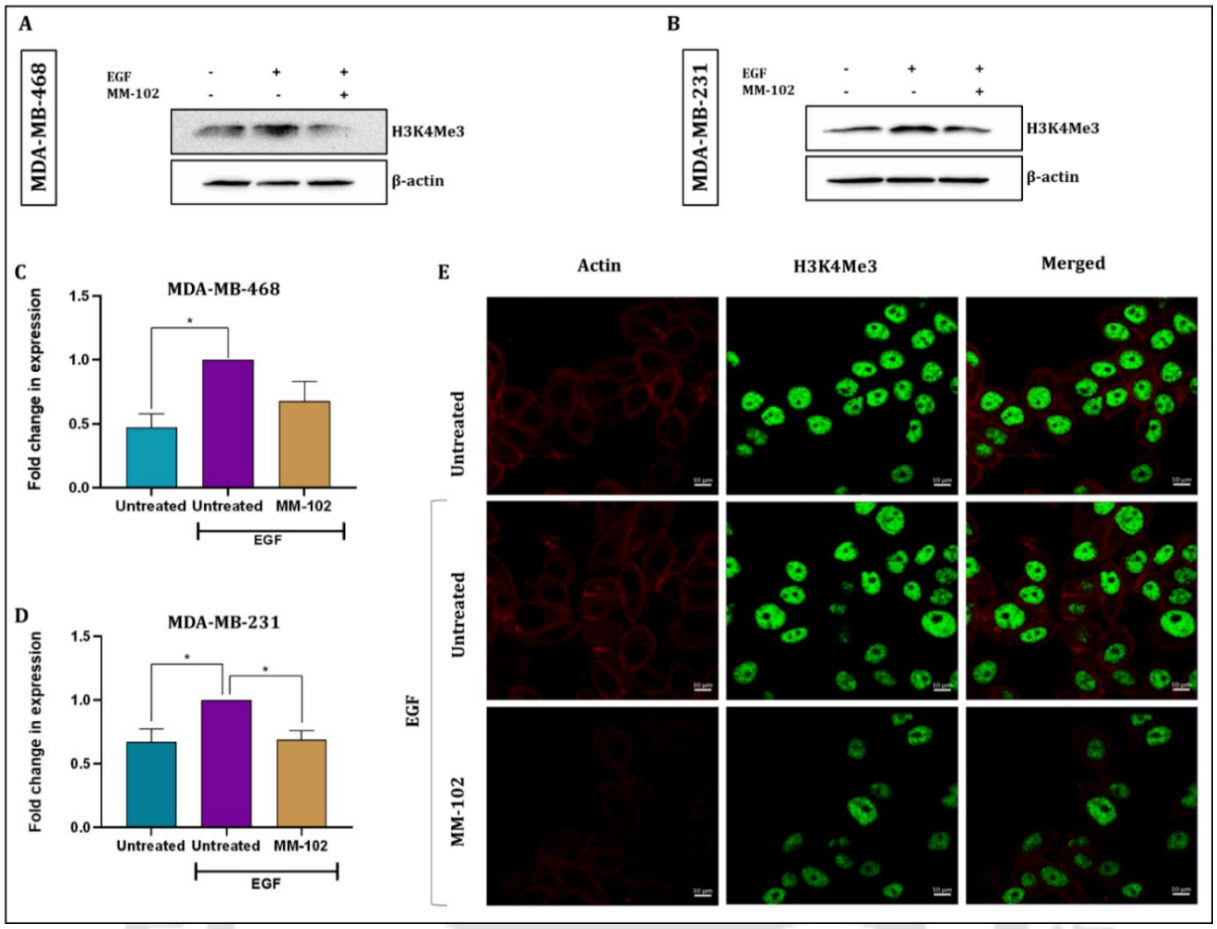

Figure 3.4: *A-D) Western blot analysis showing the reduction in H3K4me3 levels in both MDA-MB-468 and MDA-MB-231 cell lines following treatment with MM-102. The levels are compared to EMT-induced cells treated with EGF. E) Confocal microscopy images showing reduced H3K4me3 expression in MM-102-treated cells compared to EMT-induced control in the MDA-MB-468 cell line (scale 10 µm).*

3.3.5. Inhibition of MLL1 reverses EMT by modulating key EMT markers

The reduction in H3K4me3 levels observed in MM-102-treated cells is closely associated with the reversal of EMT, a process driven by specific EMT transcription factors (EMT-TFs) and the dysregulation of cellular adhesion molecules [16]. To further validate the effect of MLL1 inhibition on EMT, the expression of crucial EMT markers was analysed using Western blot in both MDA-MB-468 and MDA-MB-231 cells. The markers selected are β-catenin, Slug, Claudin, E-cadherin, Caveolin, and fibronectin, well-recognized components of the EMT process. EMT reversal is crucial for reducing the metastatic potential of cancer cells, and the modulation of key EMT markers provides insights into the mechanisms of MLL1 inhibition in this context.

The results showed a significant reduction in the expression of β-catenin and Slug in both cell lines following MM-102 treatment compared to EMT-induced cells treated with EGF **(Figure 3.5)**. β-catenin plays a pivotal role in cell-cell adhesion and EMT regulation, while Slug is a critical EMT-TF that

TH-3600_196106022

represses epithelial markers and promotes mesenchymal transition. The downregulation of these proteins strongly suggests that MM-102 reverses EMT by targeting the transcriptional and signaling mechanisms essential for the mesenchymal phenotype.

Interestingly, cell line-specific variations were observed in the expression of Claudin and E-cadherin. In MDA-MB-468 cells, Claudin levels significantly increased after MM-102 treatment, while E-cadherin expression remained unchanged **(Figure 3.5)**. Conversely, in MDA-MB-231 cells, no significant change in Claudin expression was detected, but E-cadherin levels increased approximately 2-fold compared to EGF-treated controls **(Figure 3.5)**. These differential patterns reflect the intrinsic characteristics of these cell lines and their EMT regulation. The increase in Claudin expression in MDA-MB-468 cells suggests a partial re-establishment of tight junctions, typically lost during EMT. Claudin is a tight junction protein, and its upregulation indicates a shift towards an epithelial phenotype. This is consistent with the reversal of EMT in MDA-MB-468 cells. However, the lack of significant change in E-cadherin, another epithelial marker, in these cells could be due to the aggressive nature of MDA-MB-468, where Claudin restoration may play a more dominant role than E-cadherin in maintaining epithelial characteristics.

On the other hand, in MDA-MB-231 cells, the increase in E-cadherin levels following MM-102 treatment is a clear marker of EMT reversal, as the loss of E-cadherin is one of the hallmark events during EMT. E-cadherin is crucial for the maintenance of epithelial integrity, and its restoration in MDA-MB-231 cells suggests that MM-102 effectively promotes epithelial differentiation in this cell line. The absence of significant changes in Claudin expression in these cells further underscores the heterogeneity in EMT regulation across different TNBC subtypes. In addition to the epithelial markers, the expression of crucial mesenchymal markers, such as Caveolin and Fibronectin, was also examined, using RT-PCR and immunocytochemistry (ICC) to validate EMT reversal further. In MDA-MB-468 cells, RT-PCR results showed a 4.5-fold reduction in Caveolin expression and a 1.21-fold decrease in Fibronectin expression upon MM-102 treatment **(Figure 3.6 A-B)**.

In contrast, in MDA-MB-231 cells, Caveolin expression did not exhibit significant changes, while Fibronectin expression was reduced by 1.5-fold following treatment **(Figure 3.6 C-D)**. The ICC analysis confirmed the RT-PCR results, showing a substantial reduction in Caveolin in MM-102-treated MDA-MB-468 cells compared to EGF-treated cells **(Figure 3.6E)**. However, in MDA-MB-231 cells, there was no significant change in Caveolin levels **(Figure 3.6F)**. Fibronectin expression, on the other hand, was significantly reduced in both cell lines, as visualized through confocal microscopy **(Figure 3.7)**. The differential modulation of EMT markers between MDA-MB-468 and MDA-MB-231 may also be linked to their distinct signaling pathways. For instance, β-catenin, which interacts with cell-cell adhesion proteins and the Wnt signaling pathway, was significantly downregulated in both cell lines. This suggests that MM-102 disrupts the Wnt/β-catenin axis, a key driver of EMT. The inhibition of Slug, a major repressor of E-cadherin and a promoter of mesenchymal markers, also indicates that MM-102 reverses the transcriptional changes underlying EMT. These findings collectively suggest that the inhibition of MLL1 by MM-102 leads to EMT reversal, potentially through the downregulation of H3K4me3 levels and associated EMT-TF expression. The distinct patterns of EMT marker modulation

TH-3600_196106022

between MDA-MB-468 and MDA-MB-231 cells reflect the complexity of EMT regulation in different TNBC subtypes, with both Claudin and E-cadherin playing critical roles in restoring epithelial characteristics in a cell line-specific manner.

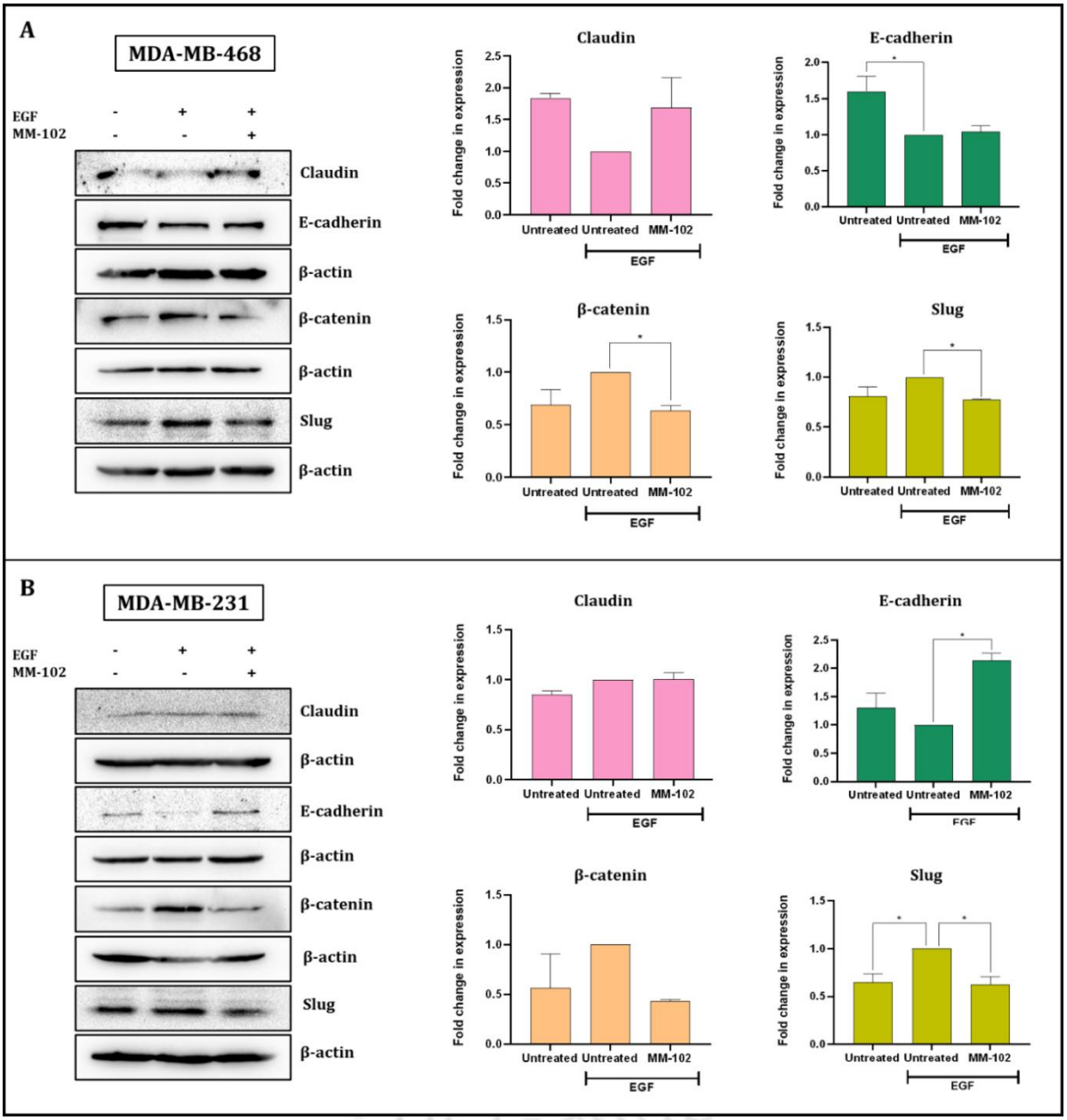

Figure 3.5: *Western blot analysis showing the differential expression of EMT marker proteins Claudin, E-cadherin, β-catenin, and Slug in MM-102-treated* ***A)*** *MDA-MB-468 and* ***B)*** *MDA-MB-231 cells compared to EGF-treated controls.*

TH-3600_196106022

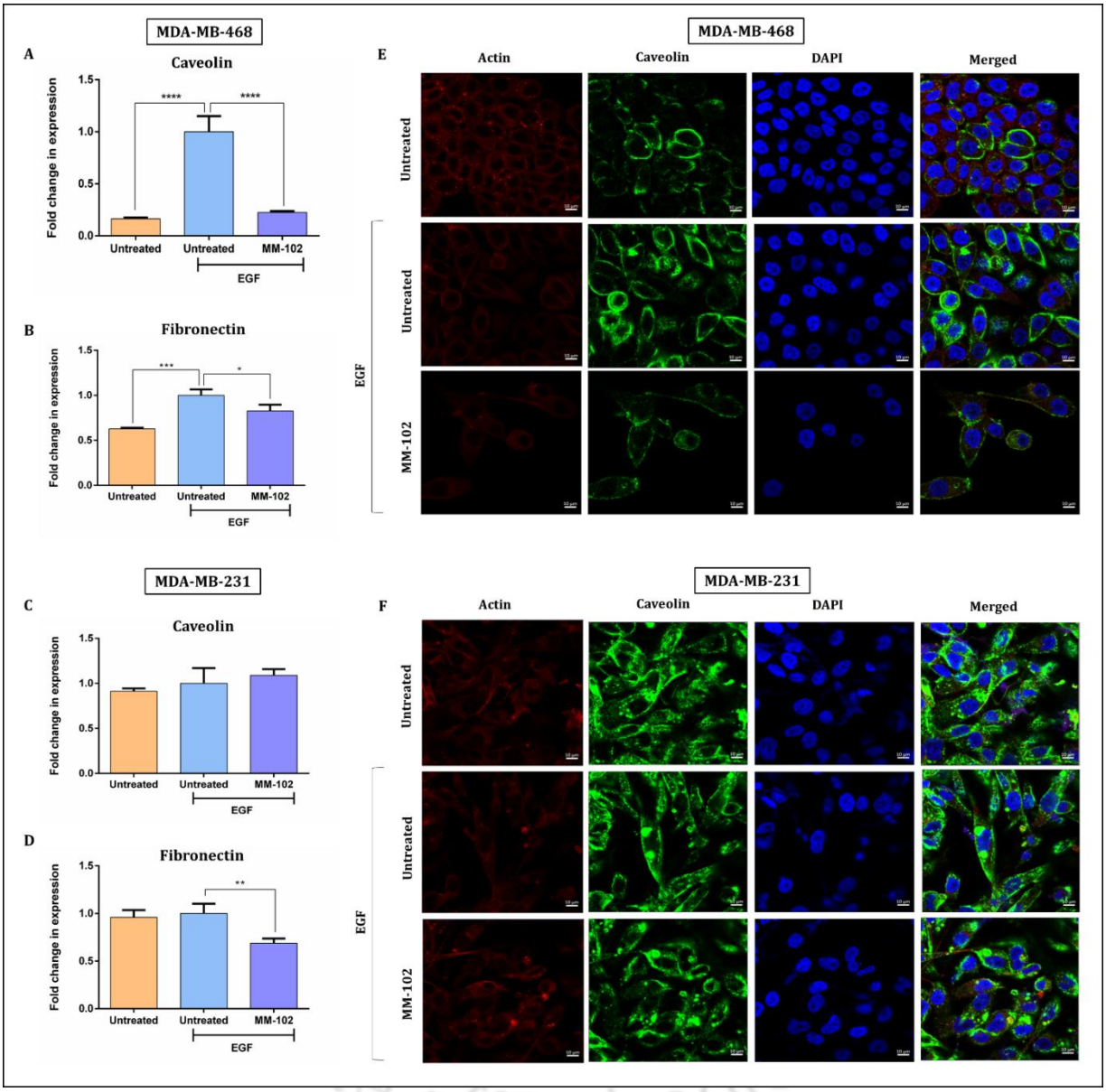

Figure 3.6: *Gene expression analysis by RT-PCR showing the differential expression of mesenchymal marker genes Caveolin and Fibronectin in MM-102-treated A-B) MDA-MB-468 and C-D) MDA-MB-231 cells compared to EGF-treated controls. Immunocytochemistry images showing differential expression of Caveolin in MM-102-treated E) MDA-MB-468 and F) MDA-MB-231 cells compared to EMT-induced control (scale 10 µm).*

TH-3600_196106022

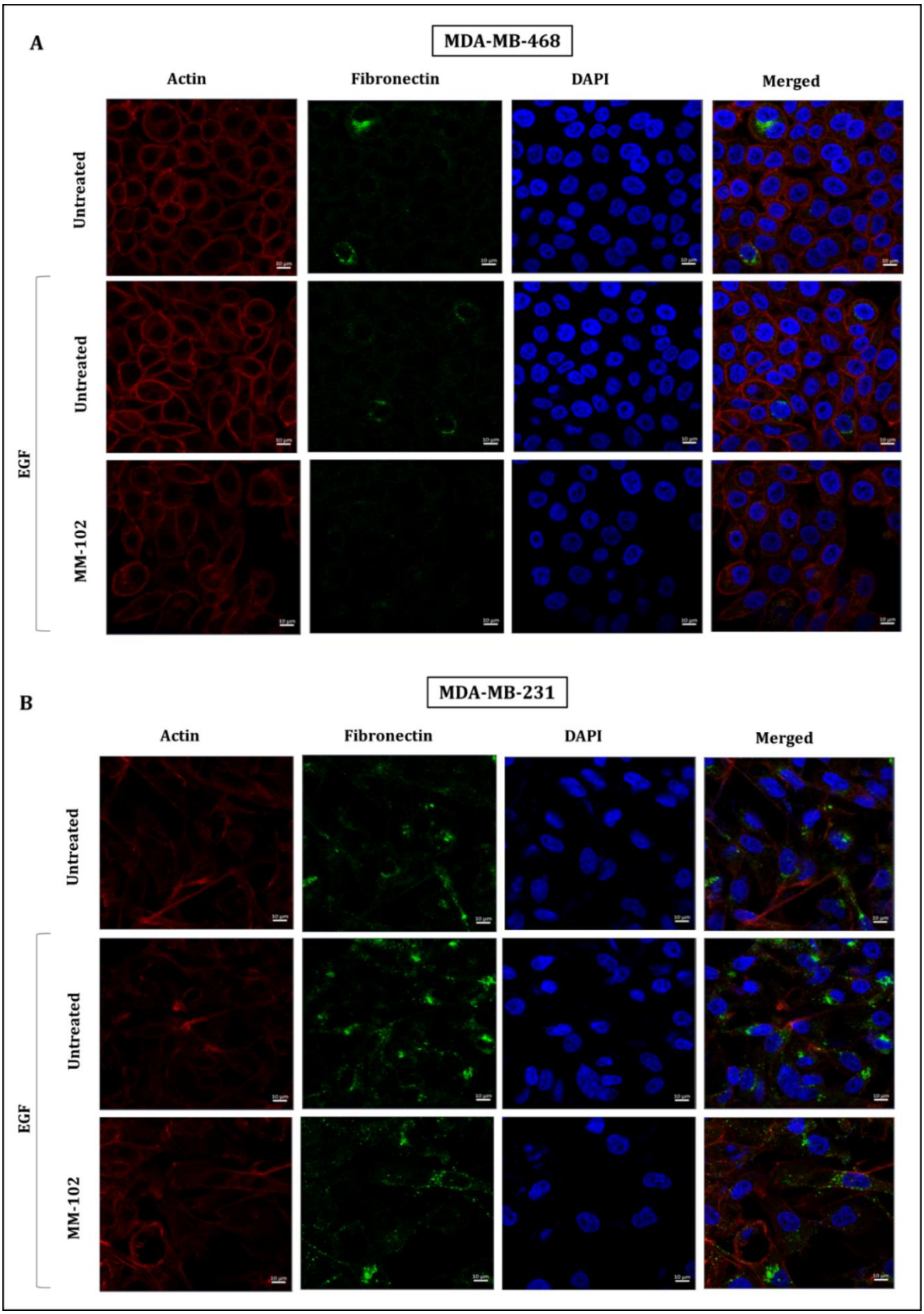

Figure 3.7: *Differential expression of fibronectin after treatment with MM-102 by ICC assay in A) MDA-MB-468 and B) MDA-MB-231 cell line (Scale 10 µm).*

TH-3600_196106022

3.3.6. MM-102 treatment reduces cellular migration and invasion in EMT-induced TNBC cells

In this study, whether the reversal of EMT by MM-102 impacts the migration and invasion capabilities of TNBC cells was further explored, as EMT is a critical process driving these aggressive cellular behaviors. It was hypothesized that inhibiting EMT through MLL1 inhibition with MM-102 would reduce both migration and invasion properties of MDA-MB-468 and MDA-MB-231 cells. The effect of MLL1 inhibition on migration was evaluated using a scratch wound healing assay on both cell lines after treatment with MM-102 and EGF (to induce EMT conditions). After 18 h, the EGF-treated cells displayed a significant reduction in scratch size, indicating enhanced migration. However, in the MM-102-treated groups, there was no substantial reduction in the scratch size. Specifically, the scratch size was 1.9-fold larger in MDA-MB-468 cells and 1.5-fold larger in MDA-MB-231 cells compared to their EGF-treated counterparts **(Figure 3.8 A-B)**. This suggests that inhibition of MLL1 with MM-102 markedly suppresses the migratory capacity of both cell lines.

Further, the invasive properties of the cells were assessed using a transwell migration assay. The number of cells that invaded through the transwell membrane was significantly higher in the EGF-treated cells, indicative of active invasion under EMT conditions. In contrast, cells treated with MM-102 showed a dramatic reduction in invasion. Invaded cells were stained with DAPI, and confocal images revealed a visible decrease in blue-stained cells in both MDA-MB-468 and MDA-MB-231 **(Figure 3.8 C-D)**. This confirms that MM-102 treatment effectively reduces the invasion ability of these TNBC cells under EMT conditions. Taken together, these results demonstrate that inhibiting MLL1 with MM-102 reverses EMT markers and significantly impairs the migration and invasion capacities of TNBC cells, further highlighting its potential as a therapeutic target in the treatment of aggressive breast cancer.

TH-3600_196106022

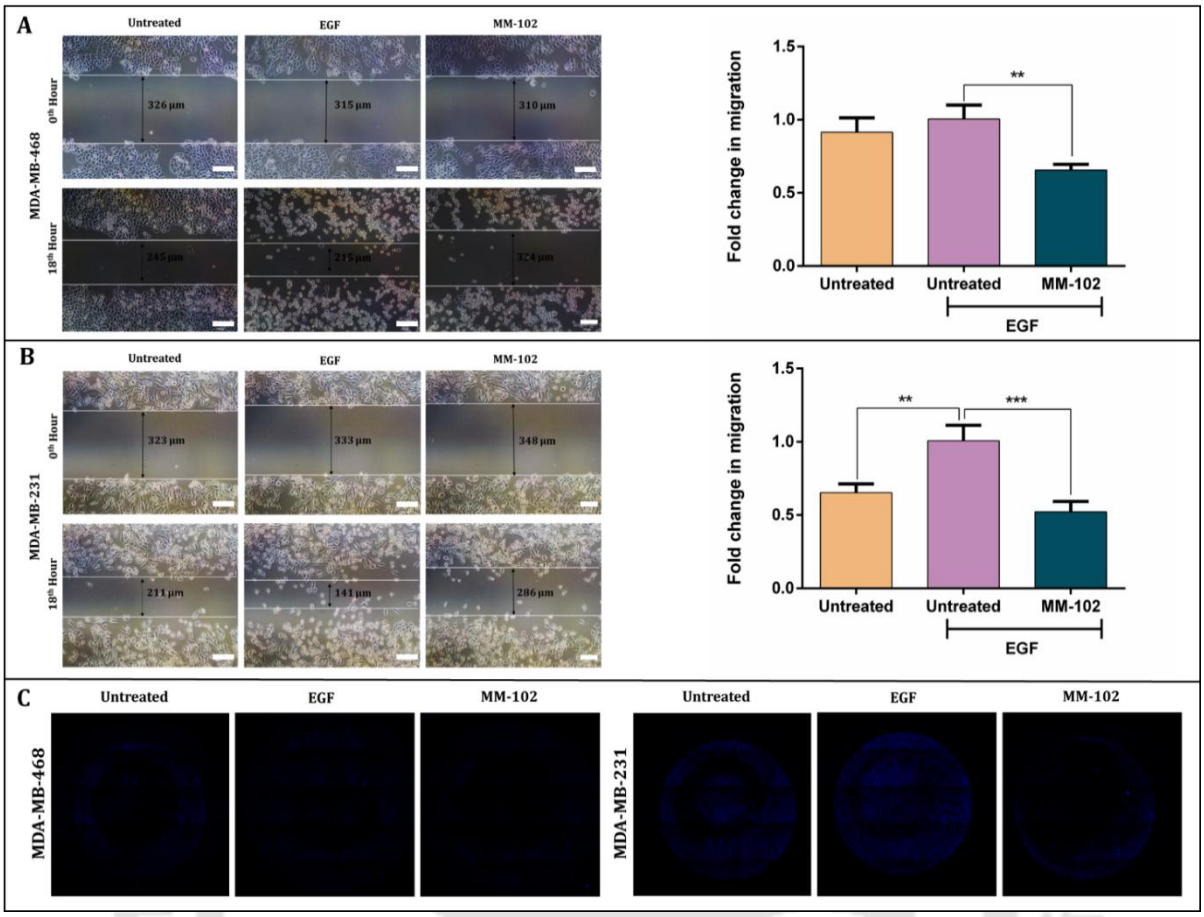

Figure 3.8: *Scratch wound healing assay demonstrating the significant reduction in cell migration in MM-102-treated **A)** MDA-MB-468 cells and **B)** in MDA-MB-231 cells compared to EGF-treated controls after 18 h. Transwell invasion assay showing a significant reduction in cell invasion in MM-102-treated **C)** MDA-MB-468 and **D)** MDA-MB-231 cells compared to EGF-treated cells, with DAPI staining for visualizing invaded cells.*

3.3.7. Reversal of EMT by MLL1 inhibition alters metabolic reprogramming

EMT is closely interconnected with metabolic reprogramming, where epithelial cells predominantly rely on glucose metabolism, while mesenchymal cells exhibit a shift toward fatty acid metabolism [18]. Since inhibiting MLL1 reverses EMT, it was hypothesized that this reversal might impact the metabolic reprogramming of TNBC cells. To confirm this changes in glucose metabolism were analysed by examining the expression of crucial glycolysis enzymes, including ALDO A, PGK, and ENO1, in MDA-MB-468 cells, given the higher MLL1 expression in this cell line. The gene expression analysis revealed a significant upregulation of glycolytic enzymes by a 5-fold increase in ALDO A, a 2-fold increase in PGK, and a 4-fold increase in ENO1 following 6 h of MM-102 treatment **(Figure 3.9A-C)**. This upregulation suggests an increase in glucose metabolism. To further validate these findings, we performed a colorimetric analysis of glucose utilization in MM-102 treated cells. After 6 h of treatment, the glucose levels in the media were reduced by 1.2-fold compared to EGF-treated cells, further indicating enhanced glycolysis **(Figure 3.9D)**.

TH-3600_196106022

In addition to glucose metabolism, changes in fatty acid metabolism were assessed by evaluating fatty acid uptake and lipid droplet accumulation. Using fluorescently labeled fatty acids and Nile red staining, a dramatic decrease in fatty acid uptake and lipid droplet accumulation was observed in MM-102-treated cells compared to EGF-treated cells **(Figure 3.9E-F)**. EMT-induced cells typically exhibit higher lipid droplet accumulation due to their dependence on fatty acid metabolism, especially when detached from the extracellular matrix [11]. The observed increase in glucose uptake and reduction in fatty acid uptake and storage points toward EMT reversal-driven metabolic reprogramming, favoring glucose metabolism. Moreover, a proteomic analysis of MM-102-treated MDA-MB-468 cells was conducted and compared to EGF-treated cells. The proteomic data further confirmed the upregulation of glycolytic enzymes, supporting the increased glucose metabolism observed in MM-102 treated cells **(Figure 3.10)**. This comprehensive metabolic shift highlights the profound impact of MLL1 inhibition on reversing EMT and associated metabolic reprogramming.

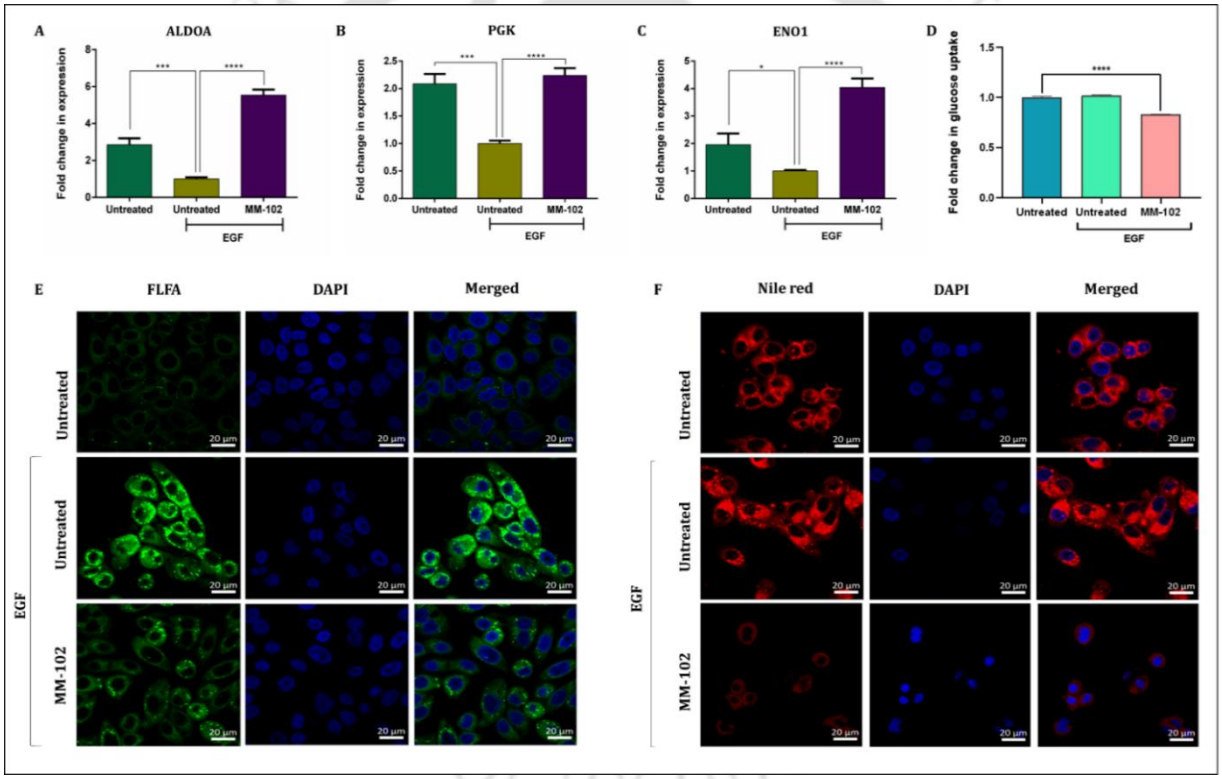

Figure 3.9: Gene expression analysis of glycolytic enzymes *A) ALDO A B) PGK C) ENO1. D) Colorimetric assay for glucose metabolism in MDA-MB-468 cells compared to EGF-treated controls. E) Fatty acid uptake measurement by fluorescently labelled fatty acid and F) Lipid droplet staining by Nile red in MDA-MB-468 cell line.*

TH-3600_196106022

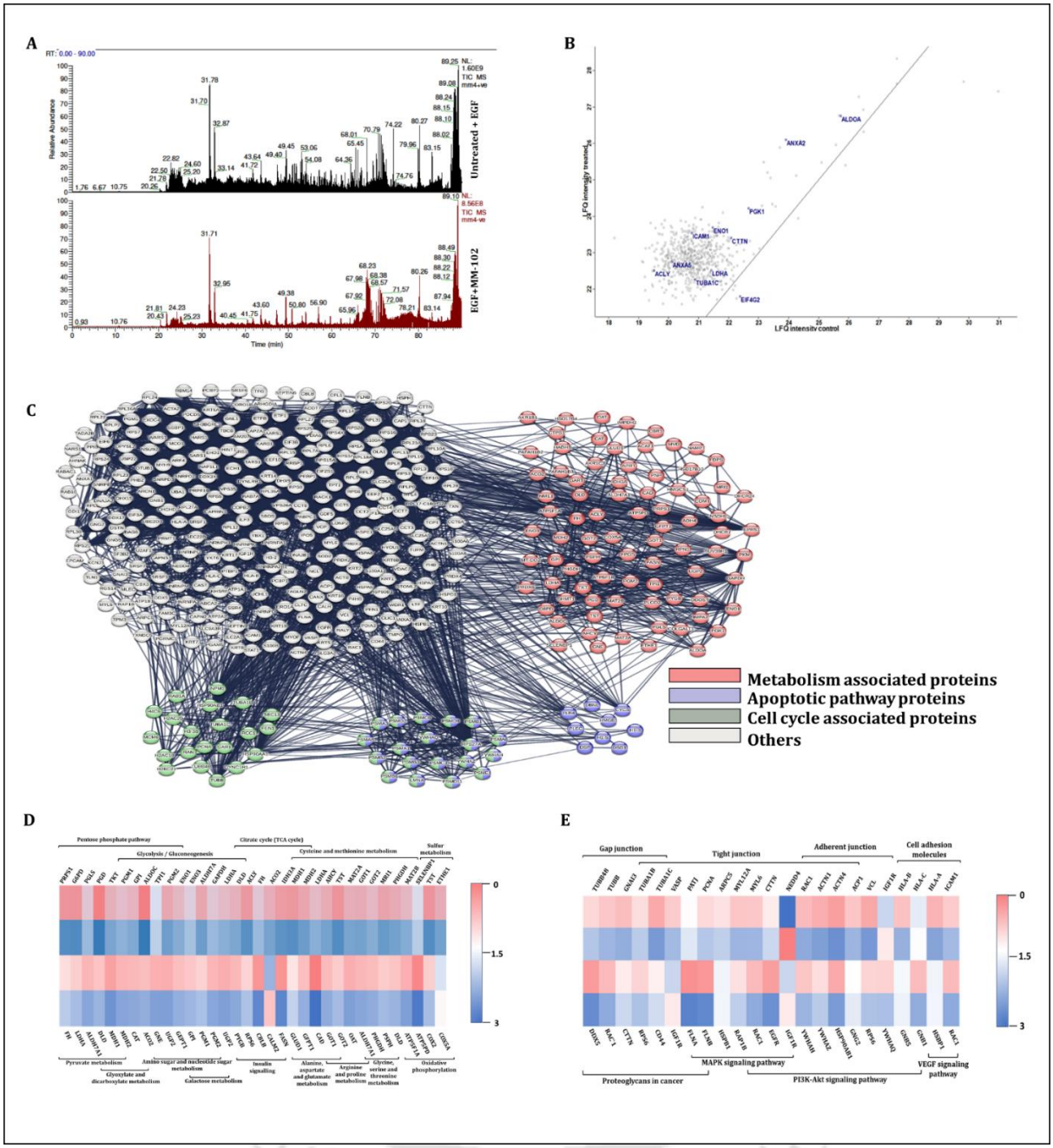

Figure 3.10: *A) MS peaks of protein samples from MDA-MB-468 cells treated with EGF and MM-102. B) Dot plots representing the differentially expressed proteins (DEPs) in MDA-MB-468 after treatment with MM-102 for 48 h. C) Functional interaction network of differentially expressed proteins (DEPs) after treatment with MM-102 for 48 h. D-E) Pathways affected by the DEPs after treatment with MM-102.*

3.3.8. Effect of MLL1 inhibition on 3D tumor spheroids

To assess the therapeutic potential of MLL1 inhibition in a more physiologically relevant model, 3D tumor spheroids were generated using MDA-MB-468 and MDA-MB-231 cell lines. Both spheroid types were treated with MM-102 for 72 h, and cytotoxicity was measured via alamarBlue assay. The IC_{50} concentration for MM-102 was found to be significantly lower in MDA-MB-468 spheroids (23.54 µM) compared to MDA-MB-231 spheroids (69 µM) **(Figure 3.11 A-C)**. This result further supports the

TH-3600_196106022

higher sensitivity of MDA-MB-468 cells to MLL1 inhibition, in line with its elevated MLL1 expression levels. In addition to the cytotoxicity analysis, live/dead cell imaging of the spheroids was performed using Calcein AM and PI staining. Confocal microscopy images revealed a marked increase in red fluorescence (indicative of cell death) in MM-102-treated spheroids compared to EGF-treated controls **(Figure 3.11 D-E)**. These findings suggest that MLL1 inhibition induces significant cell death in EMT-activated TNBC cells. These findings reinforce the therapeutic potential of targeting MLL1 in TNBC, particularly in cells with high MLL1 expression.

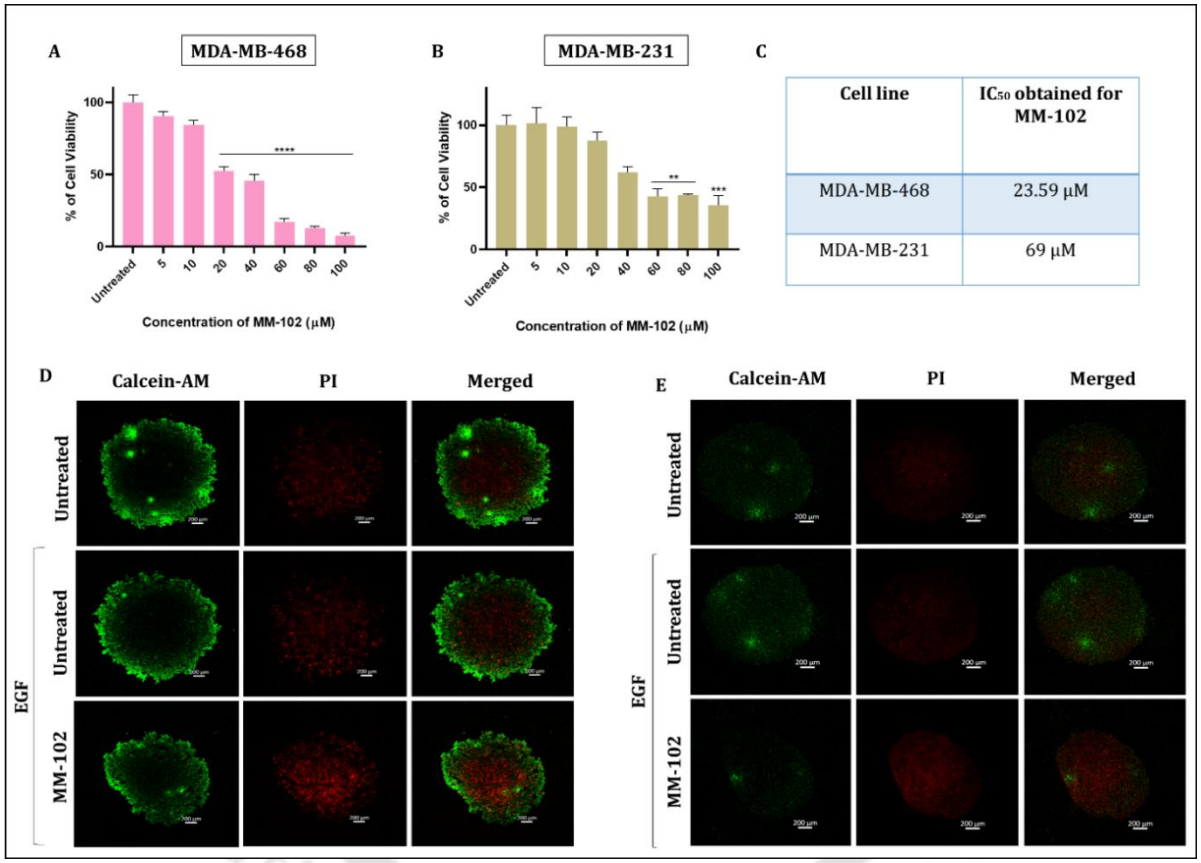

Figure 3.11: *alamarBlue assay showing the reduction in cell viability of A) MDA-MB-468 and B) MDA-MB-231 spheroids treated with MM-102 under EMT-induced conditions. C) IC_{50} values of MM-102 in MDA-MB-468 and MDA-MB-231 spheroids. Live/dead assay confirming increased cell death in MM-102 treated D) MDA-MB-468 and E) MDA-MB-231 spheroids.*

3.4. Discussion

Enzymes responsible for depositing posttranslational modifications on the core histones (H2A, H2B, H3, and H4) are vital in transcriptional regulation. Among these, the histone methyltransferase MLL1 plays a crucial role in the transcription of cell cycle–promoting genes, encouraging proliferation and oncogenesis through the methylation of histone H3 at lysine 4 (H3K4) [2, 3]. The current study provides significant insights into the therapeutic potential of MLL1 inhibition in breast cancer, particularly in the context of EMT and metabolic reprogramming in TNBC. The study initially focused

TH-3600_196106022

on investigating the role of MLL1 and WDR5, a key component of the complex responsible for histone methylation in the EMT process. Significant upregulation of MLL1 and WDR5 was observed in cells undergoing EMT, highlighting their potential involvement in driving this process. Specifically, EGF treatment, which induces EMT, led to a notable increase in the expression of MLL1 and WDR5 in both MDA-MB-231 and MDA-MB-468 cells, with the upregulation being more pronounced in MDA-MB-468. This suggests a key role for MLL1-WDR5 in maintaining the EMT phenotype, which contributes to cancer progression and poor survival outcomes, as supported by the survival analysis. The STRING analysis further reinforced the functional significance of this complex, identifying multiple potential interactors. The consistent upregulation of MLL1 and WDR5 in EMT conditions highlights the MLL1-WDR5 complex as a potential therapeutic target for TNBC treatment.

Inhibition of MLL1 using MM-102 resulted in a significant reduction in cell viability, with a marked difference in IC_{50} values between the two cell lines, correlating with their differential expression of MLL1. The lower IC_{50} observed in MDA-MB-468, which had higher MLL1 expression, suggests that cells with elevated MLL1 levels are more susceptible to MLL1 inhibition. This is further validated by live/dead staining, confirming increased cell death in MM-102-treated cells. This supports the therapeutic potential of MLL1 inhibition, particularly in aggressive subtypes of TNBC where EMT is prevalent. The distinct difference in the sensitivity of the two cell lines underscores the importance of MLL1 expression levels in determining the efficacy of MLL1-targeted therapy. Subsequent analyses demonstrated that MM-102 induces intrinsic apoptosis, as evidenced by a significant increase in intracellular ROS levels and downregulation of the antioxidant enzyme SOD2 in both cell lines [19]. The reduction in SOD2 expression suggests that MLL1 inhibition promotes oxidative stress, which likely contributes to the observed apoptosis [20]. This finding is corroborated by Annexin V/PI staining, which showed a marked increase in apoptotic cell populations in both MDA-MB-468 and MDA-MB-231 after MM-102 treatment. This highlights the role of ROS-mediated apoptosis in the cytotoxic effect of MLL1 inhibition, further supporting its therapeutic potential.

Given that MLL1 is a crucial regulator of histone methylation, specifically H3K4me3, the impact of MM-102 on this epigenetic modification was also explored. The results demonstrated a significant reduction in H3K4me3 levels in both cell lines following MM-102 treatment. The decrease in H3K4me3 has been associated with the downregulation of genes involved in EMT, including key transcription factors that drive this process. This epigenetic modulation likely contributes to the reversal of EMT and the induction of apoptosis, indicating that MLL1 plays a pivotal role in regulating both EMT and cell survival pathways [16]. In line with this, the expression of key EMT markers was analysed, and a reversal of the mesenchymal phenotype upon MM-102 treatment was observed. Notably, the expression of EMT-TFs such as β-catenin and Slug were significantly reduced. At the same time, epithelial markers like claudin and E-cadherin were differentially regulated in the two cell lines. MDA-MB-468 exhibited an increase in claudin expression, while MDA-MB-231 showed elevated E-cadherin levels.

Further investigation into mesenchymal markers, such as caveolin and fibronectin, revealed a significant reduction in caveolin expression in MDA-MB-468 but not in MDA-MB-231, while fibronectin levels decreased in both cell lines. This differential regulation of EMT markers reflects the

TH-3600_196106022

complex role of MLL1 in modulating EMT, which appears to vary between different TNBC subtypes. The observed reduction in mesenchymal markers and increased epithelial marker expression indicate a reversal of EMT, further supporting the therapeutic potential of MLL1 inhibition in controlling cancer cell invasiveness. Since EMT is closely linked to cellular migration and invasion, functional assays were performed to assess these properties. Both scratch wound healing and transwell invasion assays demonstrated a significant reduction in migration and invasion in MM102-treated cells compared to EGF-treated cells. This reduction in the invasive and migratory capabilities of TNBC cells further confirms the role of MLL1 in maintaining the EMT phenotype, and its inhibition presents a promising avenue for reducing metastasis in aggressive breast cancer.

Metabolic reprogramming is a key feature of cancer cells and plays a crucial role in EMT regulation and drug resistance. During EMT, cells shift towards glycolysis to meet their increased energy demands, while also altering lipid metabolism to support membrane remodelling and survival [18,21]. Our findings show that inhibiting MLL1 with MM102 enhances glycolysis, as evidenced by the upregulation of key glycolytic enzymes and a reduction in fatty acid uptake. This metabolic shift coincides with EMT reversal, suggesting that MLL1 regulates the metabolic plasticity required for maintaining mesenchymal traits. Furthermore, drug-resistant TNBC cells often rely on metabolic adaptations for survival; therefore, targeting MLL1-induced metabolic pathways may sensitize cells to therapy and hinder disease progression. Proteomic analysis further supports this link, revealing increased glycolytic enzyme expression in MM102-treated cells. These results highlight MLL1 as a critical regulator of EMT-driven metabolic alterations and suggest that targeting its function could disrupt metabolic dependencies associated with drug-resistant TNBC.

Finally, the impact of MLL1 inhibition was evaluated using 3D tumor spheroids, a more physiologically relevant model. MM-102 treatment led to a significant reduction in spheroid viability, with a lower IC_{50} observed in MDA-MB-468 compared to MDA-MB-231. Live/dead cell imaging further confirmed increased cell death in MM-102-treated spheroids. These findings indicate that MLL1 inhibition not only affects monolayer cultures but also retains its efficacy in more complex spheroid tumor models, reinforcing its potential as a therapeutic target in EMT-driven TNBC. Overall, the key finding of this study is the interconnectedness of EMT reversal and metabolic reprogramming upon MLL1 inhibition, highlighting a coordinated shift from a mesenchymal, lipid-dependent phenotype to an epithelial, glucose-driven metabolic state. This metabolic rewiring, evidenced by increased glycolysis and reduced fatty acid metabolism, underscores the impact of MLL1 inhibition on cellular phenotype and metabolic pathways, suggesting a dual role in hindering EMT-associated traits and reinforcing metabolic dependencies in TNBC. Therefore, targeting MLL1 offers a promising therapeutic strategy, particularly in aggressive subtypes where EMT and metabolism play a key role in cancer progression and metastasis.

TH-3600_196106022

3.5. Conclusion

In summary, the present study provides compelling evidence that MLL1 is crucial in promoting EMT and metabolic reprogramming in TNBC. MLL1 inhibition via MM-102 impedes the EMT process and reverses EMT-associated traits such as enhanced cell migration, invasion, and fatty acid metabolism. The downregulation of mesenchymal markers and the upregulation of glycolytic enzymes further confirmed that MLL1 inhibition shifted cells from a mesenchymal to an epithelial phenotype. Additionally, it was found that MM-102 treatment significantly induced intrinsic apoptosis, which was marked by ROS generation and SOD2 downregulation and led to enhanced cell death. The efficacy of MLL1 inhibition was also confirmed in tumor spheroid models, where MM-102 reduced cell viability and increased cytotoxicity. Overall, these findings highlight MLL1 as a promising therapeutic target in EMT-activated TNBC, with its inhibition offering a novel strategy for treating aggressive breast cancer subtypes. Future studies exploring MLL1 inhibitors in combination therapies could further improve outcomes for TNBC patients.

3.6. References

1. Sarkar, S., Venkatesh, D., Kandasamy, T., & Ghosh, S. S. (2024). Epigenetic Modulations in Breast Cancer: An Emerging Paradigm in Therapeutic Implications. *Frontiers in Bioscience-Landmark*, 29(8), 287. https://doi.org/10.31083/j.fbl2908287

2. Zhang, T., Cooper, S., & Brockdorff, N. (2015). The interplay of histone modifications–writers that read. *EMBO reports*, 16(11), 1467-1481. https://doi.org/10.15252/embr.201540945

3. Rao, R. C., & Dou, Y. (2015). Hijacked in cancer: the KMT2 (MLL) family of methyltransferases. *Nature reviews.* Cancer, 15(6), 334–346. https://doi.org/10.1038/nrc3929

4. Thakur, C., Qiu, Y., Fu, Y., Bi, Z., Zhang, W., Ji, H., & Chen, F. (2022). Epigenetics and environment in breast cancer: New paradigms for anti-cancer therapies. *Frontiers in oncology*, 12, 971288. https://doi.org/10.3389/fonc.2022.971288

5. Guo, L., Kong, D., Liu, J., Zhan, L., Luo, L., Zheng, W., Zheng, Q., Chen, C., & Sun, S. (2023). Breast cancer heterogeneity and its implication in personalized precision therapy. *Experimental hematology & oncology*, 12(1), 3. https://doi.org/10.1186/s40164-022-00363-1

6. Aysola, K., Desai, A., Welch, C., Xu, J., Qin, Y., Reddy, V., Matthews, R., Owens, C., Okoli, J., Beech, D. J., Piyathilake, C. J., Reddy, S. P., & Rao, V. N. (2013). Triple Negative Breast Cancer - An Overview. *Hereditary genetics: current research*, 2013(Suppl 2), 001. https://doi.org/10.4172/2161-1041.S2-001

7. Huang, Z., Zhang, Z., Zhou, C., Liu, L., & Huang, C. (2022). Epithelial–mesenchymal transition: The history, regulatory mechanism, and cancer therapeutic opportunities. *MedComm*, 3(2), e144. https://doi.org/10.1002/mco2.144

TH-3600_196106022

8. Lin, Y. T., & Wu, K. J. (2020). Epigenetic regulation of epithelial-mesenchymal transition: focusing on hypoxia and TGF-β signaling. *Journal of biomedical science*, 27(1), 39. https://doi.org/10.1186/s12929-020-00632-3

9. Pang, Q. Y., Chiu, Y. C., & Huang, R. Y. J. (2024). Regulating epithelial-mesenchymal plasticity from 3D genome organization. *Communications Biology*, 7(1), 750. https://doi.org/10.1038/s42003-024-06441-w

10. Karatas, H., Townsend, E. C., Cao, F., Chen, Y., Bernard, D., Liu, L., ... & Wang, S. (2013). High-affinity, small-molecule peptidomimetic inhibitors of MLL1/WDR5 protein–protein interaction. *Journal of the American Chemical Society*, 135(2), 669-682. http://dx.doi.org/10.1021/ja306028q

11. Kandasamy, T., Sarkar, S., Sen, P., Venkatesh, D., & Ghosh, S. S. (2024). Concurrent inhibition of IR, ITGB1, and CD36 perturbated the interconnected network of energy metabolism and epithelial-to-mesenchymal transition in breast cancer cells. *Journal of Cellular Biochemistry*. https://doi.org/10.1002/jcb.30574

12. Shome, R., Sen, P., Sarkar, S., & Ghosh, S. S. (2024). Single-cell transcriptomics reveals the intra-tumoral heterogeneity and SQSTM1/P62 and Wnt/β-catenin mediated epithelial to mesenchymal transition and stemness of triple-negative breast cancer. *Experimental Cell Research*, 438(1), 114032. https://doi.org/10.1016/j.yexcr.2024.114032

13. Kim, J., Kong, J., Chang, H., Kim, H., & Kim, A. (2016). EGF induces epithelial-mesenchymal transition through phospho-Smad2/3-Snail signaling pathway in breast cancer cells. *Oncotarget*, 7(51), 85021. https://doi.org/10.18632/oncotarget.13116

14. Wang, H., & Helin, K. (2024). Roles of H3K4 methylation in biology and disease. *Trends in Cell Biology*. https://doi.org/10.1016/j.tcb.2024.06.001

15. Perez-Oquendo, M., & Gibbons, D. L. (2022). Regulation of ZEB1 Function and Molecular Associations in Tumor Progression and Metastasis. Cancers, 14(8), 1864. https://doi.org/10.3390/cancers14081864

16. Lu, W., & Kang, Y. (2019). Epithelial-mesenchymal plasticity in cancer progression and metastasis. *Developmental cell*, 49(3), 361-374. https://doi.org/10.1016/j.devcel.2019.04.010

17. Kim, D., Kim, Y., Lee, B. B., Cho, E. Y., Han, J., Shim, Y. M., & Kim, D. H. (2021). Metformin Reduces Histone H3K4me3 at the Promoter Regions of Positive Cell Cycle Regulatory Genes in Lung Cancer Cells. *Cancers*, 13(4), 739. https://doi.org/10.3390/cancers13040739

18. Sciacovelli, M., & Frezza, C. (2017). Metabolic reprogramming and epithelial-to-mesenchymal transition in cancer. *The FEBS journal*, 284(19), 3132–3144. https://doi.org/10.1111/febs.14090

TH-3600_196106022

19. Nakamura, H., & Takada, K. (2021). Reactive oxygen species in cancer: Current findings and future directions. *Cancer science*, 112(10), 3945–3952. https://doi.org/10.1111/cas.15068

20. Kim, Y. S., Gupta Vallur, P., Phaëton, R., Mythreye, K., & Hempel, N. (2017). Insights into the Dichotomous Regulation of SOD2 in Cancer. *Antioxidants*, 6(4), 86. https://doi.org/10.3390/antiox6040086

21. Dogan, S., Leopold, J., Hoffmann, D. T., Kubitschke, H., Blauth, E., Ficorella, C., ... & Käs, J. A. (2024). Identification of Lipid Droplet-Associated Genes in Breast Cancer Patients. *Lipidology*, 1(1), 52-74. https://doi.org/10.3390/lipidology1010005

TH-3600_196106022

CHAPTER 4

Co-therapeutic strategy to modulate epigenetic and autophagy pathways in TNBC cells

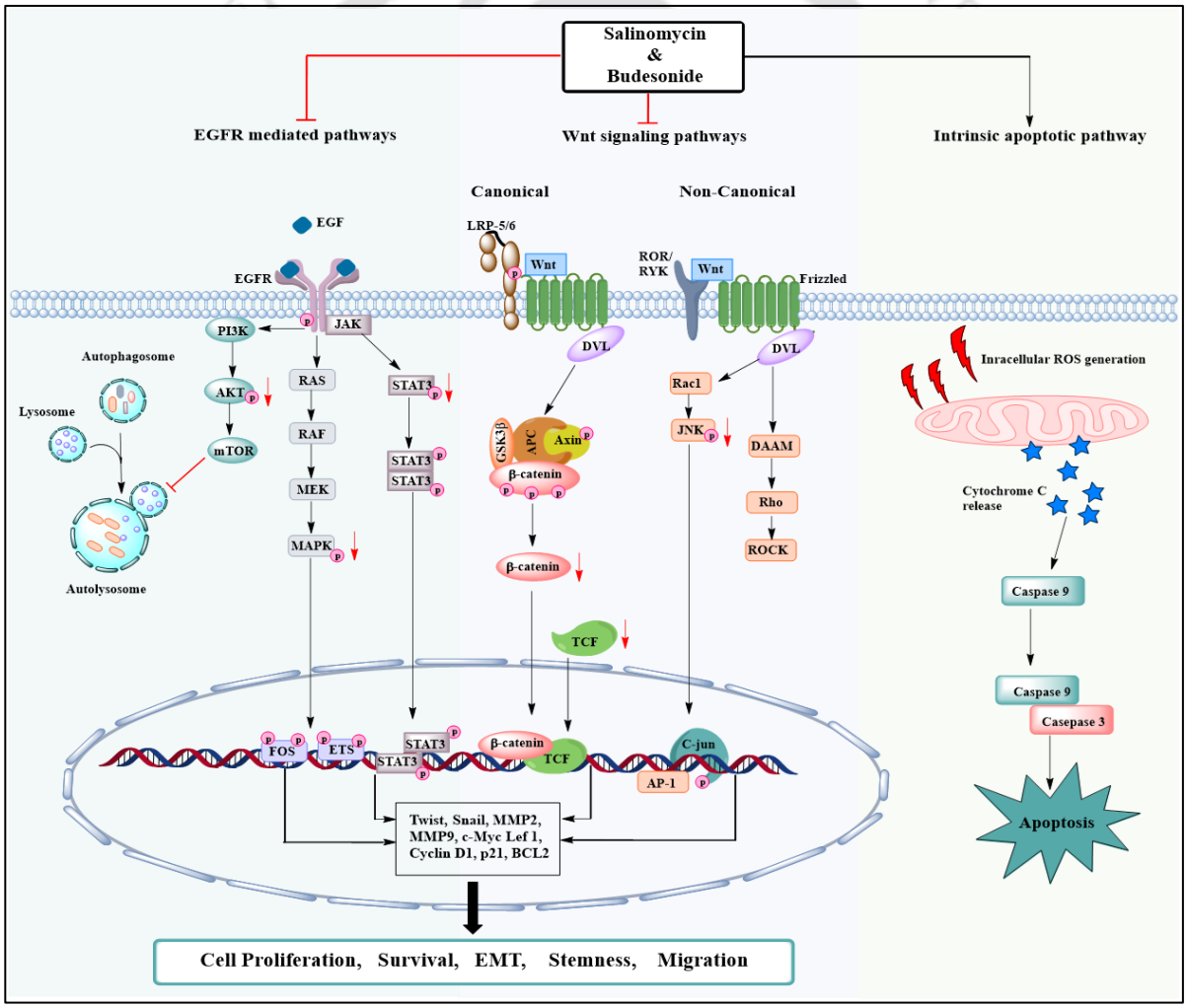

Journal of Biochemical and Molecular Toxicology, 38(11), e70045.

https://doi.org/10.1002/jbt.70045

TH-3600_196106022

Chapter 4

4.1. Introduction

Triple-negative breast cancers (TNBCs) represent a distinct subtype of breast cancer, characterized by the lack of expression of the progesterone receptor (PR), estrogen receptor (ER), and human epidermal growth factor receptor-2 (HER2) [1]. TNBC accounts for approximately 12–17% of all diagnosed breast cancer cases. Unlike other subtypes, such as luminal or HER2-positive tumors, TNBC is associated with early recurrence, aggressiveness, and a poor prognosis [2]. The absence of conventional therapeutic targets (ER, HER2/neu) and the higher risk of metastasis make TNBC particularly challenging to treat and manage. Additionally, TNBC cells have a pronounced ability to undergo epithelial-mesenchymal transition (EMT), which contributes to metastasis and disease progression [3, 4]. EMT also leads to an increase in cancer stem cells (CSCs), which possess dynamic self-renewal capabilities and promote chemotherapy resistance [5].

EMT is regulated by a complex network of signaling pathways, including Wnt, TGF-β, ERK/MAPK, PI3K-AKT, and NF-κB. It is characterized by the overexpression of mesenchymal markers such as vimentin, N-cadherin, and Snail, along with the downregulation of intracellular adhesion markers like E-cadherin [3, 5]. Systemic therapy for TNBC primarily relies on cytotoxic chemotherapy due to the lack of effective targeted or endocrine treatments. As a result, there is an urgent need for more potent chemotherapeutic agents and novel combination therapies to improve TNBC treatment outcomes. Monotherapy often fails to eliminate tumors effectively because cancer cells rapidly develop drug resistance mechanisms [6]. In contrast, combination therapy involving multiple drugs with distinct mechanisms and complementary anti-cancer activities offers better therapeutic efficacy than monotherapy. Combination therapy is also expected to reduce tumor growth, CSC populations, metastatic potential, and drug resistance while inducing apoptosis [7].

Budesonide, a synthetic glucocorticoid, has primarily been used for its anti-inflammatory effects in conditions like asthma and inflammatory bowel diseases [14, 15, 16]. Recently, Budesonide has been explored as a treatment option for colorectal cancer due to its anti-inflammatory properties [17]. Budesonide modulates epigenetic mechanisms, such as DNA methylation, which could impact gene expression and cellular processes in various contexts, including cancer. It has been shown to prevent DNA hypomethylation in mouse lung tumors and inhibit lung cancer cell metastasis by suppressing EMT [18-21]. However, its anticancer activity in TNBC remains largely unexplored.

Salinomycin, a polyether ionophore antibiotic, has attracted significant attention for its potential as an anticancer agent. It exhibits selective toxicity towards CSCs, which are critical for tumor development, relapse, and resistance to conventional cancer treatments [8]. Salinomycin exerts its anti-cancer effects by dysregulating metal ions [9], inducing autophagy-mediated cell death, and impairing CSC survival [10, 11]. Despite its effectiveness against various cancers, the clinical use of

TH-3600_196106022

Salinomycin is limited due to potential organ damage and other adverse effects [12, 13]. Combining Salinomycin with other potent drugs could reduce its side effects without compromising its anticancer efficacy. Therefore, a combination regimen involving Salinomycin and Budesonide represents a promising therapeutic strategy for TNBC.

This study investigates the combined effects of Salinomycin and Budesonide on TNBC cells, focusing on their impact on EMT, stemness, and migratory properties. Additionally, the impact of the combination on key cancer-related signaling pathways and autophagy was evaluated.

4.2. Materials and Methods

4.2.1. Cell lines and chemicals

TNBC cell lines (MDA-MB-468 and MDA-MB-231) were also procured from the National centre for cell science (NCCS) Pune, India. Cells were maintained at 37°C, 5 % CO_2 in Dulbecco's modified eagle's medium (Sigma-Aldrich) added with 10 % fetal bovine serum (Gibco) and 1 % antibiotic (Gibco). Salinomycin and Budesonide with a purity of ≥98% (HPLC) were purchased from Sigma-Aldrich and were prepared in dimethyl sulfoxide (Invitrogen). In culture media, drugs were diluted before being employed at the specified concentrations.

4.2.2. Cytotoxicity and drug combination assays

Cell survival following drug treatment was assessed by alamarBlue assay. In viable cells, the main component of the alamarBlue dye, resazurin, transforms into resorufin, its reduced form. This consequences in a non-fluorescent blue to red fluorescent color change, which can be detected using a fluorescence or absorbance detector to determine cell viability [22]. In a 96-well plate, cells were seeded and incubated for 24h. Following the attachment of cells, varying concentrations of drugs were added and incubated for 48h. Subsequently, AlamarBlue was added to the wells and incubated for 2h in a cell culture environment.

For spheroids, cells were seeded with a density of 20×10^3 cells per well, and spheroids were produced utilizing a forced floating approach [7]. Following 72 h of seeding, spheroids were treated with different drugs. After 72 h of treatment, spheroids were incubated with alamarBlue for 4 h at cell culture conditions. Afterward, the respective incubations and absorbance were noted at 570 nm and 600 nm with a microplate reader (Thermo Fisher Scientific) [7]. Determination of the inhibitory concentration-50 (IC_{50}) was carried out using GraphPad Prism software (www.graphpad.com). Evaluation of the combinative efficacy of Salinomycin and Budesonide was carried out through combination index (CI) analysis with Compasyn software (www.combosyn.com).

4.2.3. Live/dead cell imaging

Monolayer cells were treated with the drugs for 48 h to image live and dead cell populations. Subsequently, cells were incubated for 30 min with 2 µM of Calcein-AM and 4 µM of PI. Afterward, the

TH-3600_196106022

cells were visualized using a ZOE Fluorescent Cell Imager (Bio-Rad). Similarly, MDA-MB-468 and MDA-MB-231 spheroids were treated for 72h. Similarly, the spheroids were also incubated with the same concentrations of Calcein-AM and PI for 1h. Following that, a Zeiss LSM 880 confocal microscope was used for image acquisition of the spheroids after washing with phosphate buffered saline (PBS).

4.2.4. Reactive oxygen species (ROS) detection assay

Intracellular generation of ROS after treatment with drugs was measured by 2'-7'-dichlorodihydrofluorescein diacetate (DCFH-DA) staining. Inside the cells, in the presence of ROS, non-fluorescent DCFH-DA gets converted into DCF, which emits green fluorescence [7]. This detection of fluorescence was carried out using flow cytometry. 3×10^5 cells were plated and allowed to attach in a 6-well plate. After that, cells were incubated with respective concentrations of drugs for 48h. Then, DCFH-DA dye (Sigma-Aldrich) was added to the wells. After 30 min of incubation, trypsinization and PBS washing were performed and further assessed through flow cytometry (Cytoflex, Beckman Coulter).

4.2.5. Mitochondrial membrane potential detection assay

To determine mitochondrial membrane potential changes, JC-1 (Sigma-Aldrich) staining was utilized. After 48 h of the treatment period, cells were incubated with 10 µM of JC-1 for 30 min. 50 µM carbonyl cyanide m-chlorophenylhydrazone (CCCP) treated cells were used as a positive control. Following trypsinization, 2 times PBS washing was carried out, and cells were subjected to flow cytometry for fluorescent detection (Cytoflex, Beckman Coulter).

4.2.6. Apoptotic population determination assay

To estimate the populations of apoptotic cells, Alexa fluor 488 Annexin V/dead Kit (Invitrogen) was utilized. Cells were incubated with the drugs and their combination for 48 h. Subsequently, samples were prepared corresponding with the instructions given by the manufacturer and analyzed through flow cytometry (CytoFLEX, Beckman Coulter). Further analysis was carried out using Cytexpert software.

4.2.7. Scratch wound-healing migration assay

This assay was executed to assess the variation in TNBC cell migratory capacity following treatment in EMT-induced conditions. To induce EMT, MDA-MB-231, and MDA-MB-468 cells were treated with 20 ng/ml hEGF (Sigma-Aldrich) for 48 h. Cells were cultured in DMEM media containing 0.5% FBS in order to enhance the effect of hEGF. The same has been followed for all the experiments employing EMT-induced conditions. MDA-MB-231 and MDA-MB-468 cells were allowed to grow until 60–70% confluency. Subsequently, cells were starved in 0.5% serum media for 24h prior to the linear wound generation. For the removal of cellular debris, PBS washing was implemented. Subsequently, EGF (20 ng/ml) and drugs were added to the cells and treated for 18h. Pre-treatment and post-treatment image acquisition of the wounded area was carried out using a Nikon Eclipse Ti microscope. Using ImageJ

TH-3600_196106022

Software, the wound distance was measured at three different positions inside each wound region, and the average of those measurements was then calculated.

4.2.8. Sphere formation assay

To assess the stem cell population after treatment, sphere formation assay (SFA) is utilized. Cells were treated with the drugs and with respective concentrations of drugs and combination for 48 h. Subsequently, the spheroids of the treated cells were produced via a forced floatation approach. After 72h, the resulting spheroid images were acquired by the Nikon Eclipse Ti microscope.

4.2.9. Colony formation assay

For this assay, MDA-MB-468 and MDA-MB-231 cells were plated and treated with respective drug concentrations for 48 h in 6-well plates. After that, trypsinization was performed to resuspend the cells in fresh DMEM media. In 6 well plates, 2 mL of cell suspension with a cell density of 5000 cells/ml was added and kept in cell culture conditions for 10 days. Ultimately, the generated colonies were stained using 0.5% crystal violet solution after fixing with 4% formaldehyde solution.

4.2.10. Quantitative real-time PCR

After 48h of treatment with the drugs, TRI reagent (Sigma-Aldrich) was used to isolate total RNA from the cells, and the iScript cDNA synthesis kit (Bio-Rad) was used for cDNA synthesis. Further, SYBR Green Master Mix (Bio-Rad) was used to amplify the target cDNA in Rotor-Gene Q real-time PCR cycler (Qiagen). The results were normalized against β-actin and calculated by ΔΔCt process using LinReg PCR software. Primers utilized for amplification are provided in **Table 4.1**.

Table 4.1: *List of primers used for real-time PCR experiments*

Sl.No	Gene name	Forward primer	Reverse primer
1	E-cadherin	TGGGTGAATTCGGGCTTGTT	TGAAGGTGACAGAGCCTCTGGAT
2	N-cadherin	CCATCAAGCCTGTGGGAATC	GCAGATCGGACCGGATACTG
3	Caveolin 1	AACACGTAGCTGCCCTTCAG	GGATGGGAACGGTGTAGAGAT
4	Fibronectin	AACATGTAACCACCAGTCTCATGTG	GGTGACACTTATGAGCGTCCTAAA
5	Vimentin	AGTCCACTGAGTACCGGAGAC	CATTTCACGCATCTGGCGTTC
6	TCF-7	AACTGGCCCGCAAGGAAAG	CTCCGGGTAAGTACCGAATGC
7	c-MYC	GCCACGTCTCCACACATCAG	TGGTGCATTTTCGGTTGTTG
8	ALDH1A3	ATCAACTGCTACAACGCCCT	TATTCGGCCAAAGCGTATTC
9	EpCAM	GCTGGCCGTAAACTGCTTTG	ACATTTGGCAGCCAGCTTTG
4	β-actin	AAGGGACTTCCTGTAACAATGCA	CTGGAACGGTGAAGGTGACA

TH-3600_196106022

4.2.11. Western blotting

After 48h of treatment, total protein from the cells was isolated and quantified using RIPA lysis buffer (Sigma Aldrich) and bicinchoninic acid (BCA) protein assay kit (Thermo Fisher Scientific), respectively. Subsequently, the western blot experiment was performed [7]. Further applying chemiluminescent reagent (Bio-Rad) images were developed using ChemiDoc (Bio-Rad). The image analysis was done through ImageJ software. To evaluate gene expression at the protein level, the acquired data were normalized with respect to expression of β-actin. The antibodies used for protein expression studies are mentioned in **Table 4.2**.

Table 4.2: *The list of antibodies used for protein expression study*

Antibodies	Catalog No	Manufacture
β-actin	8457S	Cell Signaling Technology, USA
β-catenin	C2206	Sigma Aldrich, USA
MAPK	4695	Cell Signaling Technology, USA
p-MAPK	4370	Cell Signaling Technology, USA
STAT-3	12640	Cell Signaling Technology, USA
p-STAT3	9145	Cell Signaling Technology, USA
JNK	8206	Cell Signaling Technology, USA
p-JNK	8206	Cell Signaling Technology, USA
AKT	8200	Cell Signaling Technology, USA
p-AKT (S473)	9271S	Cell Signaling Technology, USA
LC3 A/B	12741	Cell Signaling Technology, USA
Beclin 1	3595T	Cell Signaling Technology, USA
SQSTM1	REF-PA531484	Thermo Fisher Scientific, USA
Vimentin	5741	Cell Signaling Technology, USA

4.2.12. Nile red staining

To detect cellular lipid droplet accumulation, Nile red staining was performed. Subsequent treatment with the drugs for 48 h, cells were fixed using 4% formaldehyde. Afterward, Nile red (0.01 mg/mL) solution was added into cells and incubated under dark conditions for 10 min. Cells were counterstained with DAPI solution (1µg/mL) after PBS washing. Following a thorough PBS wash, pictures were taken with a Zeiss LSM confocal microscope.

4.2.13. Lysotracker staining

The acidotropic dye LysoTracker is used to stain acidic cellular compartments, such as lysosomes and autolysosomes. Thus, Autophagy-related lysosomal activity can be detected using LysoTracker staining [23]. After 48h of treatment, cells were incubated with Lysotracker Deep Red (Invitrogen) for 1h. After that, cells were washed with PBS, and image acquisition was carried out using a ZOE fluorescent cell imager (Bio-Rad). For flow cytometry, following the dye incubation, cells were trypsinized, rinsed with PBS, and analyzed in the flow cytometer (Cytoflex, Beckman Coulter).

TH-3600_196106022

4.2.14. Immunofluorescence analysis

To perform immunocytochemistry, after 48 h of treatment, cells were fixed with 4% formaldehyde and washed with PBS. Further, cells were incubated with a blocking solution for 2 h before incubation with primary antibodies overnight. After washing, secondary antibodies conjugated with Alexa fluor 488 (Invitrogen) were added and incubated for 2h. Subsequently, the cells were counterstained using DAPI and phalloidin 555. Following, rewashing with PBS images was acquired using a Zeiss LSM 880 confocal microscope.

4.2.15. Statistical analysis

GraphPad Prism software was used for all statistical analysis. All the experiments were triplicated, and the data were represented as mean ± SEM. In addition, a one-way ANOVA test was carried out to assess the correlations between the groups. The p-value <0.05 (*) is considered to be statistically significant, whereas p<0.001 (***) and p<0.0001 (****) are considered to be highly significant.

4.3. Results

4.3.1. Salinomycin and Budesonide display synergistic cytotoxic effects on TNBC cells

The cytotoxic effects of Budesonide (a DNA hypomethylating agent) and Salinomycin (a cancer stem cell-targeting agent) were evaluated using the alamarBlue assay. Salinomycin treatment resulted in a concentration-dependent reduction in breast cancer cell viability **(Figures 1A and 1F)**. In contrast, Budesonide alone did not significantly affect cell viability **(Figures 1B and 1G)**. However, the combination of Budesonide and Salinomycin significantly reduced cell viability at lower concentrations in TNBC cells **(Table 4.3) (Figures 4.1C and 4.1H)**. The IC_{50} value of Salinomycin decreased markedly when co-administered with 25 µM Budesonide. The combination index (CI) for both cell lines was less than 1, indicating a dose-dependent synergistic effect of the drugs on TNBC cells. Live/dead cell imaging of TNBC cells in a monolayer further demonstrated the anti-proliferative effects of the drug combination **(Figures 1K and 1L)**.

TH-3600_196106022

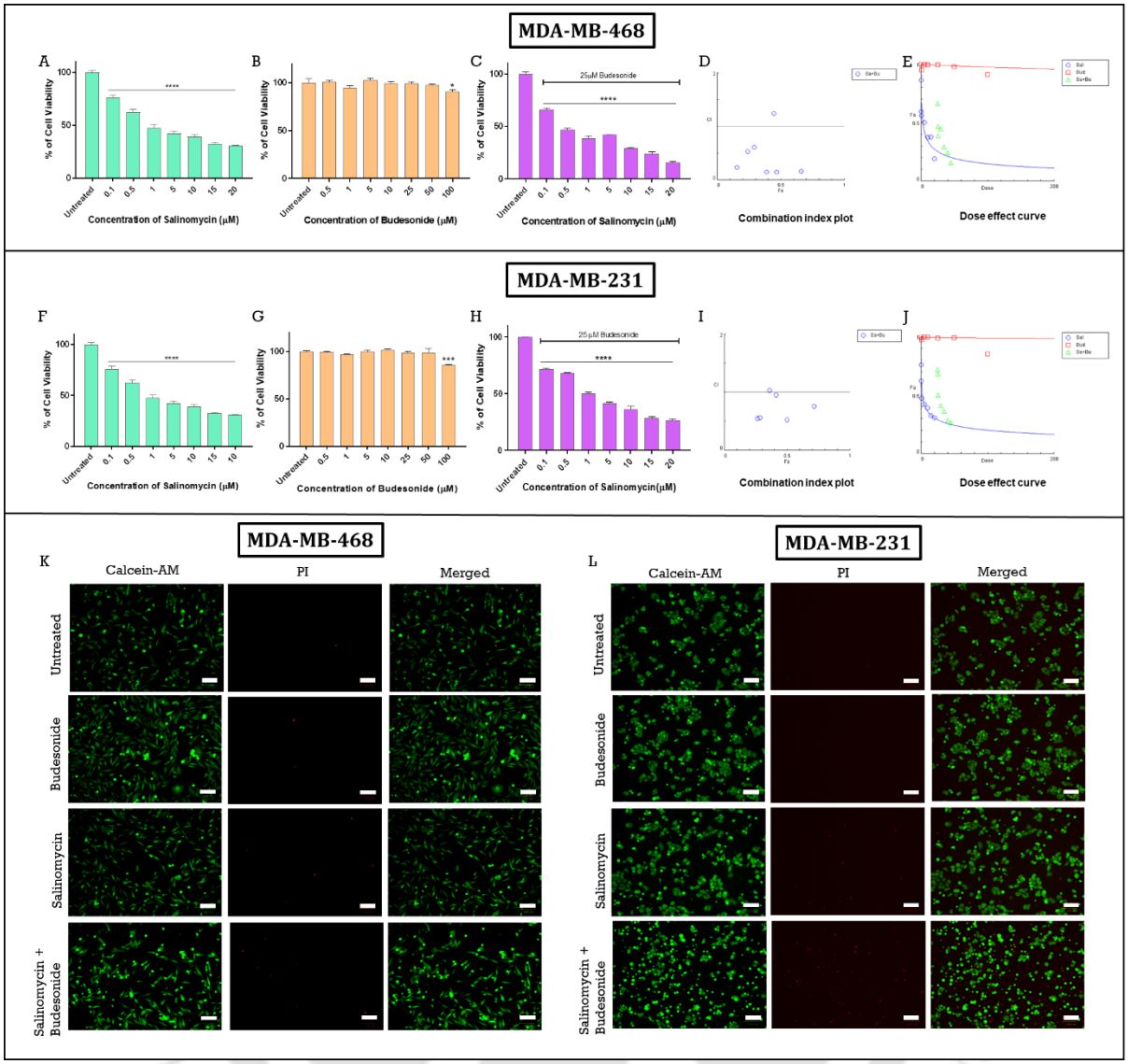

Figure 4.1: *Anti-cell proliferative effect of (A) Salinomycin, (B) Budesonide, C) Budesonide and Salinomycin combination in MDA-MB-468 monolayer, respectively. (D & E) Combination index and dose-response curves of combination treatment in MDA-MB-468, respectively. The anti-cell proliferative effect of (F) Salinomycin, (G) Budesonide, (H) Budesonide, and Salinomycin combination in MDA-MB-231 cells, respectively. (I & J) Combination index and dose-response curves of combination treatment in MDA-MB-231, respectively. Live-dead cell imaging after treatment with drugs and their combination in (K) MDA-MB-468 and (L) MDA-MB-231 cells. The scale bar represents 100 µm. A one-way ANOVA test was carried out to assess the correlations between the groups. The p-value <0.05 (*) is considered to be statistically significant, whereas p<0.001 (***) and p<0.0001 (****) are considered to be highly significant.*

TH-3600_196106022

Table 4.3: *IC_{50} values obtained for different breast cancer monolayers following treatment with drugs by alamarBlue assay.*

DRUG	IC_{50} value obtained for different breast cancer cell line	
	MDA-MB-468	MDA-MB-231
Salinomycin	3.738 µM	2.806 µM
Budesonide	Not attained	Not attained
Salinomycin + Budesonide	0.7431 µM	2.586 µM

4.3.2. Budesonide Enhances Salinomycin-Mediated ROS Generation, Mitochondrial Dysfunction, and Apoptosis Induction in TNBC Cells

The cellular mechanisms underlying the combination treatment-induced cell death were explored by analyzing intracellular ROS generation, mitochondrial membrane depolarization, and the induction of apoptosis. Breast cancer cells were treated with the IC_{50} concentrations of Salinomycin (determined from cotreatment) and 25 µM Budesonide. After 48 h of treatment with either single drugs or their combination, intracellular ROS levels were measured using DCFH-DA-mediated flow cytometry. Compared to untreated cells, ROS levels increased by 2.1-fold in MDA-MB-468 cells **(Figure 4.2C)** and by 2.83-fold in MDA-MB-231 cells **(Figure 4.2D)** following the combination treatment of Budesonide and Salinomycin.

Subsequently, JC-1 staining and flow cytometry were employed to assess the impact of cotreatment on mitochondrial membrane integrity. In MDA-MB-468 cells, cotreatment resulted in a 30.22% increase in green fluorescence, indicating membrane depolarization **(Figure 4.2E)**, while in MDA-MB-231 cells, green fluorescence increased by 25.07% **(Figure 4.2F)**.

The rise in intracellular ROS and mitochondrial membrane depolarization indicates cellular damage, which ultimately leads to programmed cell death. Therefore, the apoptotic cell population after treatment was analyzed using a flow cytometry-based apoptosis assay. After 48 h of cotreatment, apoptosis increased by 25.17% in MDA-MB-468 cells **(Figure 4.2G)** and by 38.59% in MDA-MB-231 cells **(Figure 4.2H)**.

TH-3600_196106022

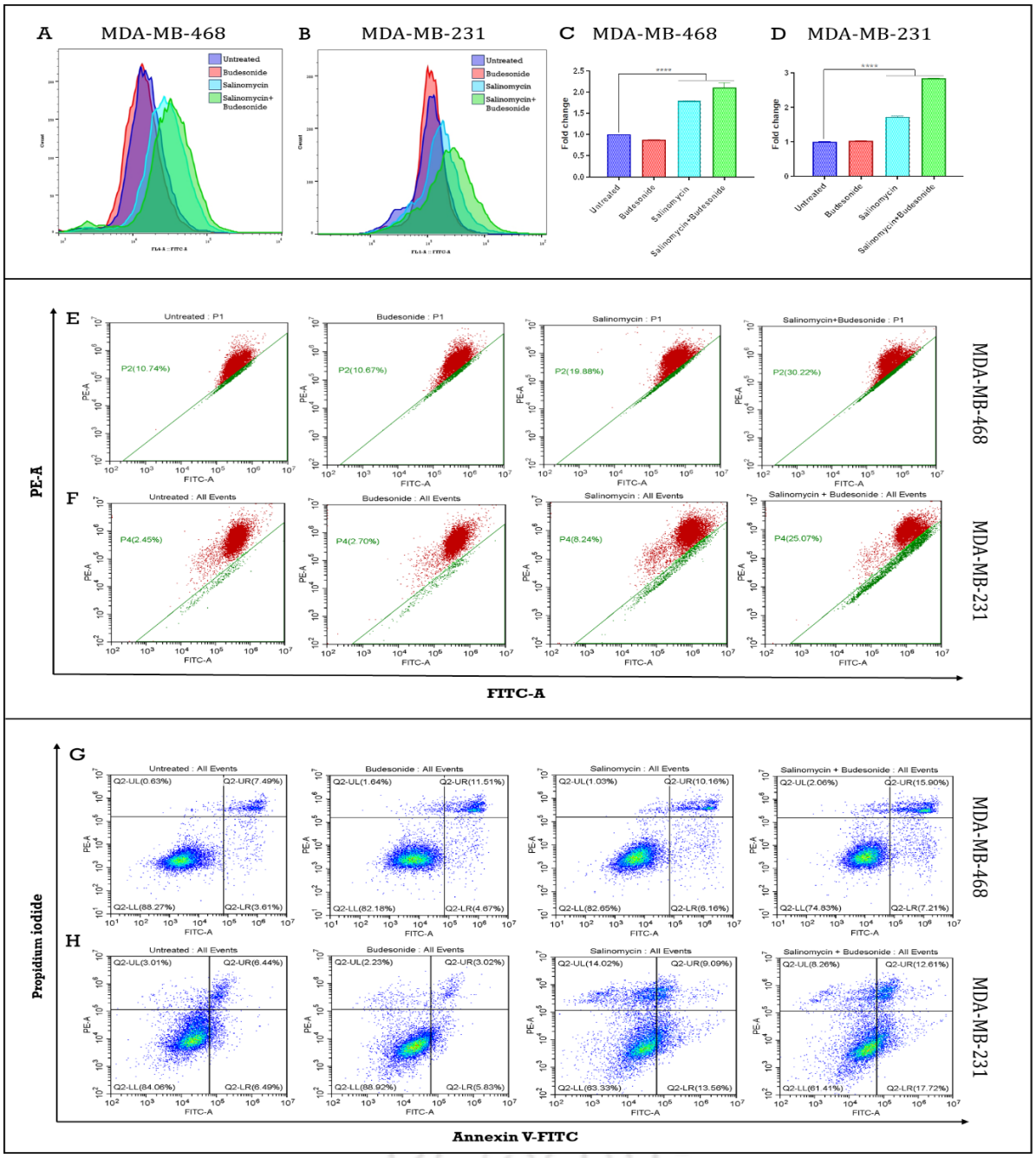

Figure 4.2: *Flow cytometric analysis of intracellular ROS generation in (A) MDA-MB-468 and (B) MDA-MB-231.Graphical representation of change in ROS generation in (C) MDA-MB-468 and (D) MDA-MB-231. MMP analysis of (E) MDA-MB-468 and (F) MDA-MB-231. Flow cytometric determination of apoptotic populations in (G) MDA-MB-468 and (H) MDA-MB-231 after the incubation with drugs and their combination for 48h. A one-way ANOVA test was carried out to assess the correlations between the groups. The p-value <0.05 (*) is considered to be statistically significant, whereas p<0.001 (***) and p<0.0001 (****) are considered to be highly significant.*

TH-3600_196106022

4.3.3. Synergistic Effect of the Drugs in EMT Reversal

The process by which cells acquire a mesenchymal phenotype while losing their epithelial characteristics is known as epithelial-to-mesenchymal transition (EMT). Growing evidence suggests that EMT enables cancer cells to become more migratory and invasive [24]. During EMT, a decrease in epithelial markers (such as E-cadherin and occludin) and an increase in mesenchymal markers (such as fibronectin, vimentin, and N-cadherin) are commonly observed [25]. To evaluate the impact of the combined treatment on EMT regulation, the mRNA expression levels of EMT markers were analysed using qRT-PCR. After 48 h of treatment with the drug combination, E-cadherin expression was upregulated by 2.23-fold in MDA-MB-468 cells **(Figure 4.3A)** and 1.37-fold in MDA-MB-231 cells **(Figure 4.3D)**. Meanwhile, N-cadherin expression was reduced by 2.7-fold in MDA-MB-231 cells **(Figure 4.3A)**, while no significant change was observed in MDA-MB-468 cells **(Figure 4.3D)**. Vimentin expression was reduced by 6.54-fold in MDA-MB-468 cells **(Figure 4.3A)** and by 1.55-fold in MDA-MB-231 cells **(Figure 4.3D)**. In addition, fibronectin expression was downregulated by 3.7-fold in MDA-MB-468 cells **(Figure 4.3B)** and upregulated by 2.33-fold in MDA-MB-231 cells **(Figure 4.3E)**. caveolin-1 expression was downregulated by 1.31-fold in MDA-MB-468 cells **(Figure 4.3B)** and by 1.32-fold in MDA-MB-231 cells **(Figure 4.3E)**.

Additionally, the expression of key EMT transcription factors such as SNAI2 and Twist was studied. Cotreatment led to the downregulation of Twist expression by 1.42-fold in MDA-MB-468 cells **(Figure 4.3C)** and by 1.71-fold in MDA-MB-231 cells **(Figure 4.3F)**. However, SNAI2 expression was upregulated by 2-fold in MDA-MB-468 cells **(Figure 4.3C)** and by 1.75-fold in MDA-MB-231 cells **(Figure 4.3F)**. Further analysis of EMT marker protein expression was conducted through Western blotting after 48 h of treatment. The protein expression level of E-cadherin increased by 3.17-fold in MDA-MB-468 cells **(Figure 4.4A)** and by 1.54-fold in MDA-MB-231 cells **(Figure 4.4B)** after combined treatment. In MDA-MB-468 cells, the protein levels of the mesenchymal markers vimentin and slug were downregulated by 6.5-fold and 2.85-fold, respectively **(Figure 4.4A)**. Similarly, vimentin expression was slightly reduced in MDA-MB-231 cells after co-therapy **(Figure 4.4B)**, while slug expression increased by 2.97-fold in MDA-MB-231 cells **(Figure 4.4B)**.

Immunocytochemistry was used to assess the impact of cotreatment on vimentin protein expression. Compared to untreated cells, a substantial decrease in vimentin expression was observed following the Budesonide and Salinomycin combination treatment **(Figures 4.5)**. Additionally, immunocytochemistry revealed a significant reduction in caveolin-1 protein expression in MDA-MB-468 cells after co-therapy **(Figure 4.6A)**. A slight decrease in caveolin-1 expression was also observed in MDA-MB-231 cells following cotreatment, consistent with the corresponding mRNA expression data **(Figure 4.6B)**. Overall, these results indicate that cotreatment synergistically induces MET in cells undergoing EMT induced by EGF.

TH-3600_196106022

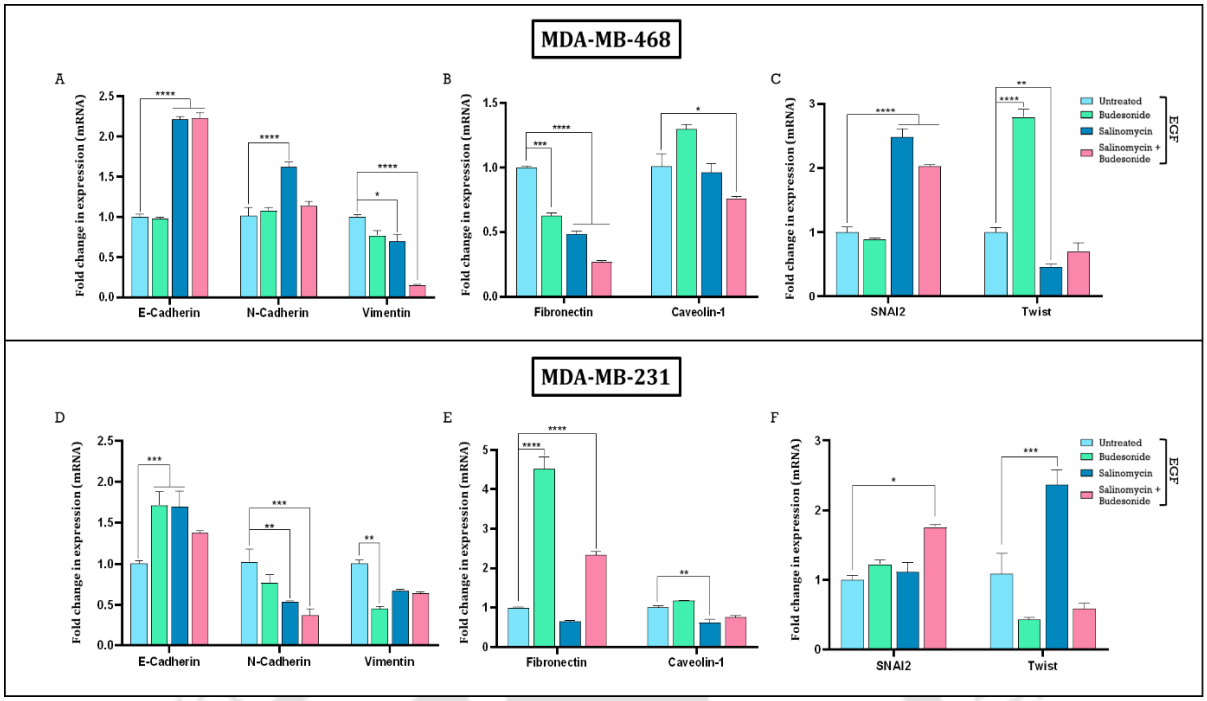

Figure 4.3: *A, B, and C represent the alteration of gene expression in EMT-induced MDA-MB-468, and D, E, and F represents the alteration of gene expression in EMT-induced MDA-MB-231 cells following treatment with drugs and their combination for 48h. One-way ANOVA test was carried out to assess the correlations between the groups. The p-value <0.05 (*) is considered to be statistically significant, whereas p<0.001 (***) and p<0.0001 (****) are considered to be highly significant.*

TH-3600_196106022

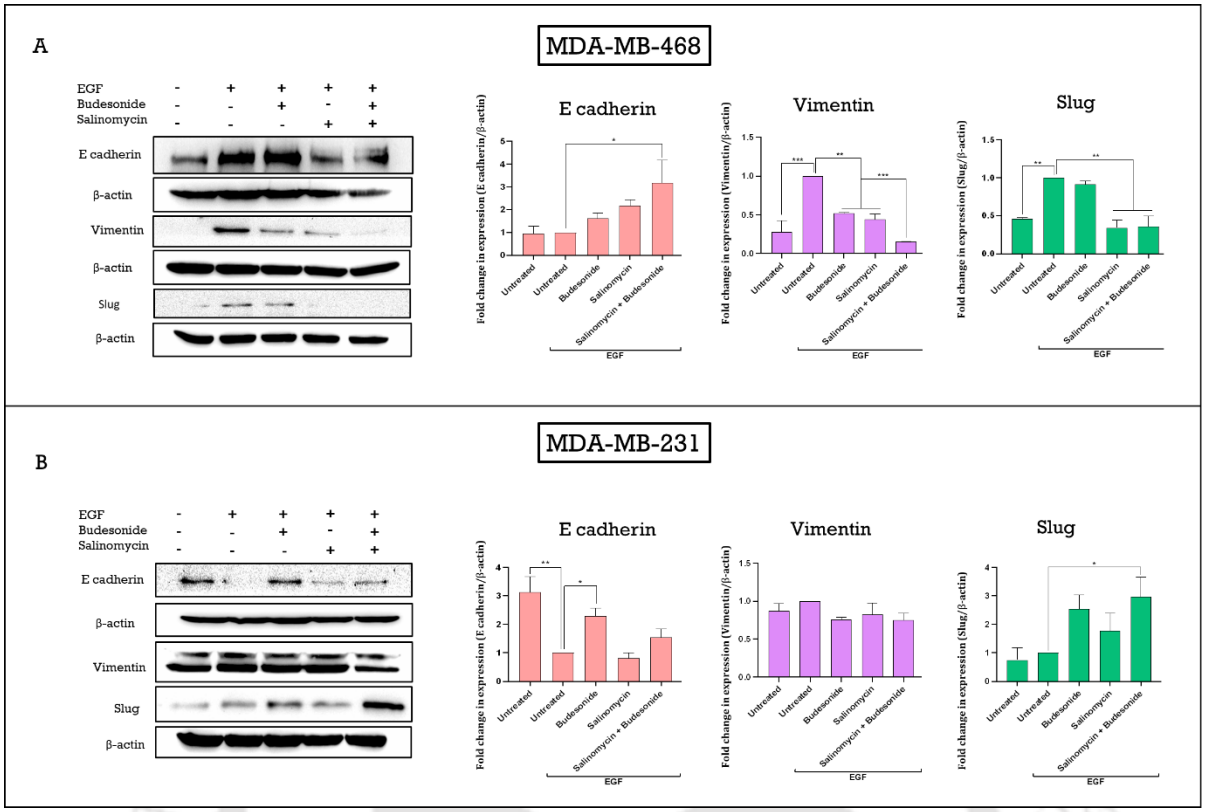

Figure 4.4: *Representative Western blots representing E cadherin, Vimentin, and Slug levels in A) MDA-MB-468 and B) MDA-MB-231 cells treated drugs and their combination for 48h. Visualization of the changes in expression was carried out through the ImageJ software. One-way ANOVA test was carried out to assess the correlations between the groups. The p-value <0.05 (*) is considered to be statistically significant, whereas p<0.001 (***) and p<0.0001 (****) are considered to be highly significant.*

TH-3600_196106022

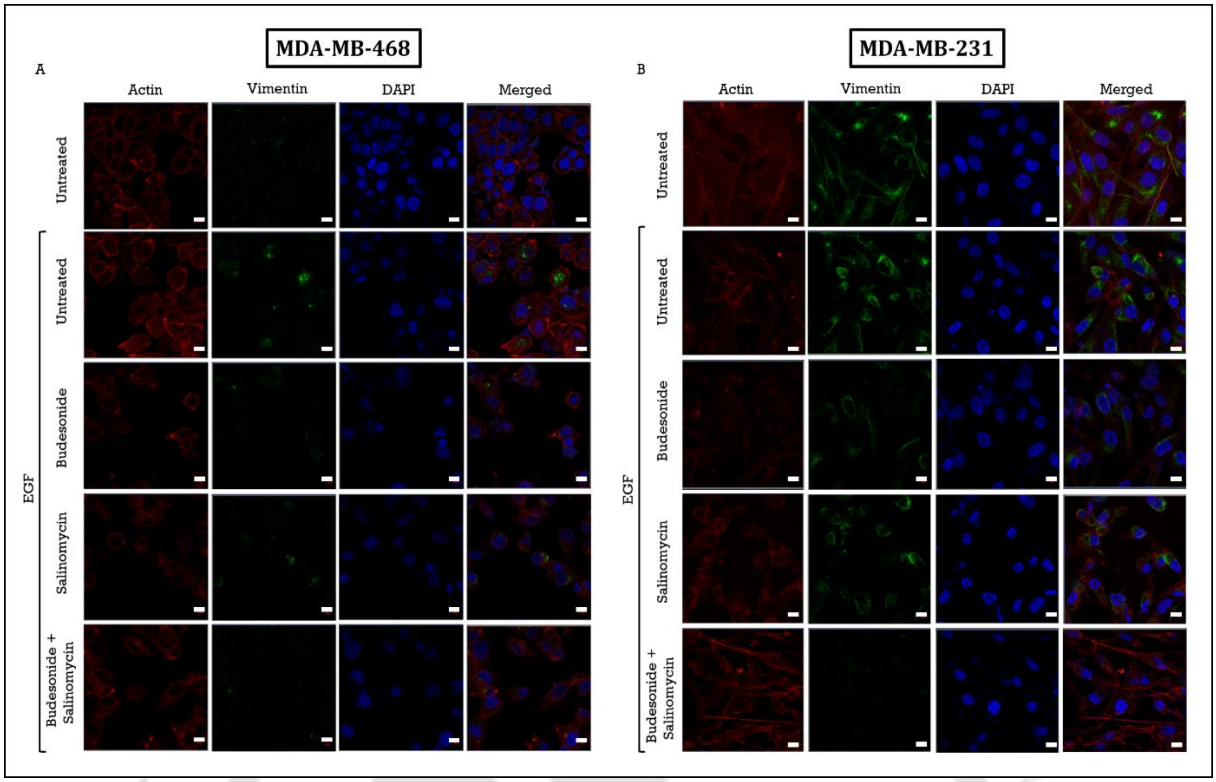

Figure 4.5: *Immunocytochemistry of vimentin in EMT-induced (A)MDA-MB-468 and (B)MDA-MB-231 cells. The scale bar represents 10 µm.*

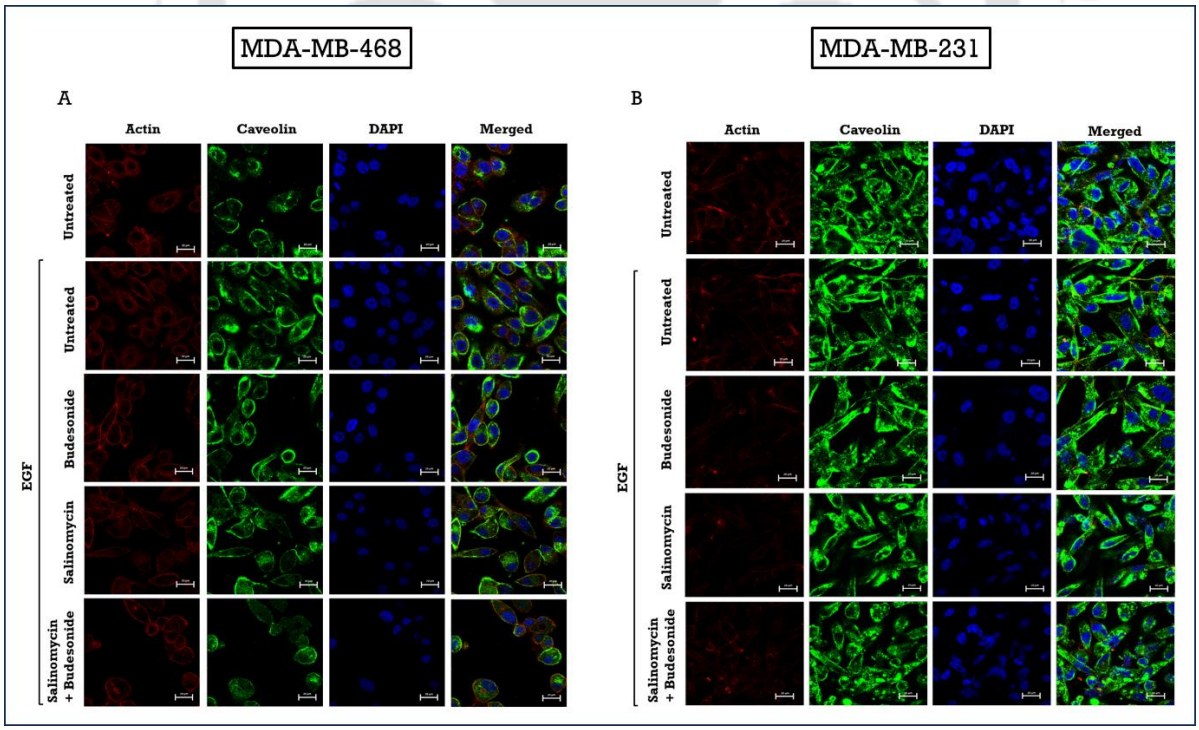

Figure 4.6: *Immunocytochemistry of caveolin-1 in EMT-induced (A)MDA-MB-468 and (B)MDA-MB-231 cells. The scale bar represents 20 µm.*

TH-3600_196106022

4.3.4. Reduction in Stemness and Migration Properties of TNBC through EMT Reversal

Following co-therapy, gene expression studies of stemness markers, including EpCAM and ALDH1A3, were conducted using qRT-PCR. After 48 h of combined drug treatment, ALDH1A3 expression was downregulated by 1.86-fold in MDA-MB-468 cells **(Figure 4.7A)** and slightly upregulated in MDA-MB-231 cells **(Figure 4.7B)**. Additionally, EpCAM expression was downregulated by 1.54-fold in MDA-MB-231 cells **(Figure 4.7B)**, while no significant change was observed in MDA-MB-468 cells **(Figure 4.7A)**.

Subsequently, spheroids of the treated MDA-MB-468 and MDA-MB-231 cells were generated using the force flotation method. A significant reduction in the sphere-forming ability of TNBC cells was noted following treatment with the combination of Salinomycin and Budesonide **(Figures 4.7C and 4.7D)**. Furthermore, a scratch wound-healing assay was performed to assess the impact of cotreatment on the wound-healing ability of TNBC cells. Compared to EGF-treated cells, cotreated cells exhibited a 1.97-fold reduction in wound-healing capacity in MDA-MB-468 cells **(Figures 4.7A and 4.7C)** and a 2.47-fold reduction in MDA-MB-231 cells **(Figures 4.7B and 4.7D)**.

Moreover, the potential of the combined therapy to inhibit the colony-forming capacity of TNBC cells was assessed. Cotreatment resulted in a more substantial reduction in colony formation in both MDA-MB-468 and MDA-MB-231 cells **(Figure 4.8)** compared to monotherapy. Overall, these findings suggest that the combination of Salinomycin and Budesonide inhibits stemness, migration, and tumorigenic potential in TNBC cells.

TH-3600_196106022

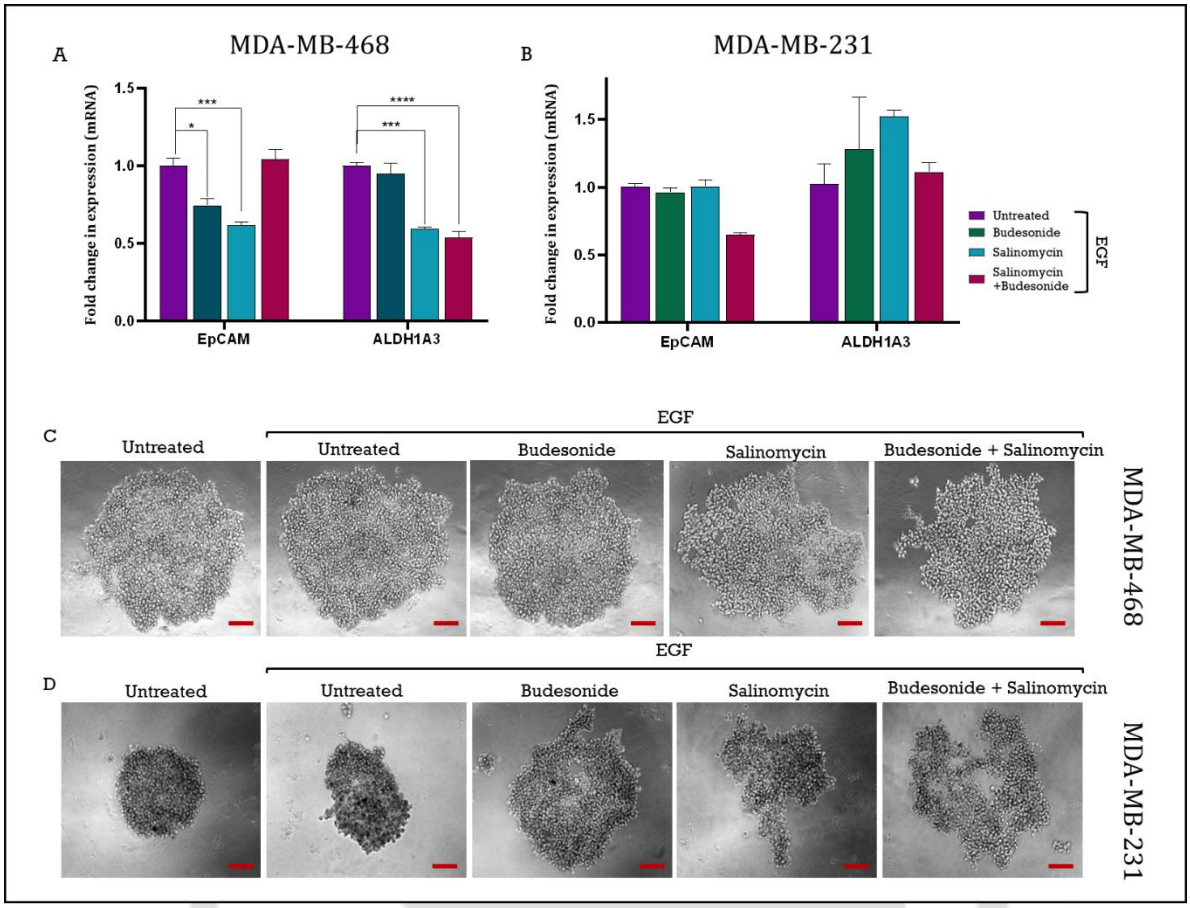

Figure 4.7: *Changes in gene expression of EpCAM and ALDH1A3 in EMT-induced (A) MDA-MB-468 and (B)MDA-MB-231 cells following treatment with drugs and their combination for 48h. Determination of the sphere formation capacity of EMT-induced (C)MDA-MB-468 and (D)MDA-MB-231 cells after 48h of treatment. The scale bar represents 100 µM. One-way ANOVA test was carried out to assess the correlations between the groups. The p-value <0.05 (*) is considered to be statistically significant, whereas p<0.001 (***) and p<0.0001 (****) are considered to be highly significant.*

TH-3600_196106022

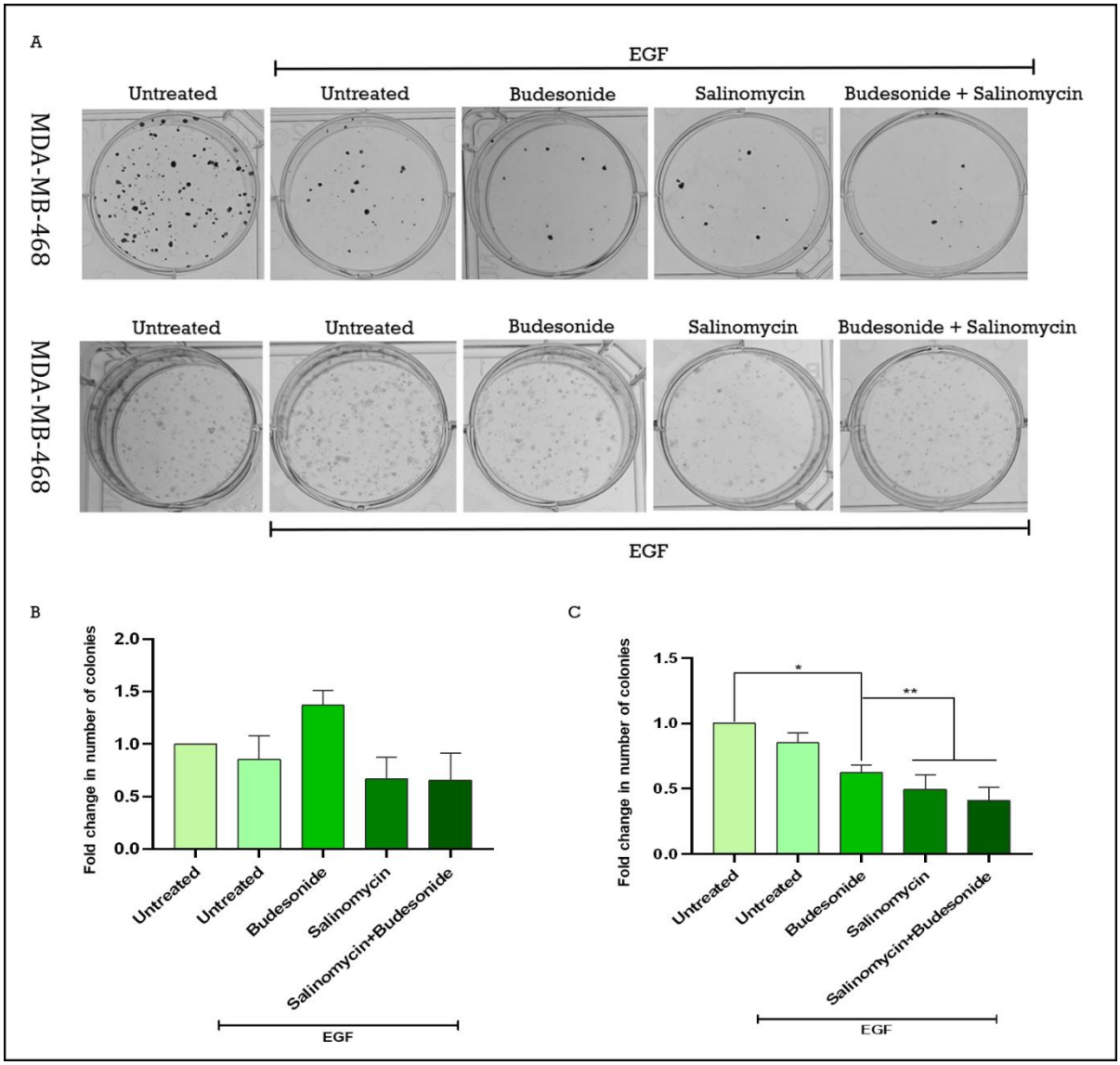

Figure 4.8: Estimation of the colony-forming ability of EMT-induced (A) MDA-MB-468 and MDA-MB-231 cells after 48h of treatment. *Fold change in the number of colonies in EMT-induced (B)MDA-MB-468 and (C)MDA-MB-231 cells after 48h of treatment. One-way ANOVA test was carried out to assess the correlations between the groups. The p-value <0.05 (*) is considered to be statistically significant, whereas p<0.001 (***) and p<0.0001 (****) are considered to be highly significant.*

4.3.5. Inhibition of Wnt/β-catenin Signaling Following Cotreatment with Drugs

TNBC exhibits aberrant Wnt signaling, with both canonical and non-canonical pathways contributing to the development of TNBC malignancies [26]. To assess the impact of cotreatment on the Wnt signaling pathway, gene expression and protein expression studies were conducted. β-catenin, a key coactivator in the canonical Wnt/β-catenin signaling pathway, plays a crucial role in facilitating the transcription of Wnt-responsive genes [27]. After 48 h of cotreatment, Western blot analysis revealed a 10.2-fold reduction in β-catenin expression in MDA-MB-468 cells **(Figure 4.9G)** and a 1.85-fold reduction in MDA-MB-231 cells compared to untreated cells **(Figure 4.9H)**.

TH-3600_196106022

Transcription factors TCF/LEF (T-cell factor/lymphoid enhancer factor) interact with β-catenin, acting as major end-node mediators of the WNT signaling pathway [28]. This interaction activates various oncogenes, including c-Myc, which promotes chemoresistance and TNBC survival [26]. Therefore, the gene expression of TCF7 and c-Myc was evaluated using qRT-PCR following cotreatment. TCF-7 expression was downregulated by 6.26-fold in MDA-MB-468 and by 2.54-fold in MDA-MB-231 cells. Furthermore, c-Myc expression was reduced by 8.22-fold in MDA-MB-468 cells after cotreatment, while in MDA-MB-231 cells, c-Myc expression was upregulated by 1.41-fold **(Figures 4.9I and 4.9J)**.

The planar cell polarity (PCP) pathway, a form of non-canonical Wnt signaling, also contributes to TNBC tumorigenesis [29]. In Wnt–PCP signaling, Wnt binds to multiple receptors, including FZD and co-receptors ROR and Ryk, leading to the activation of JNK (c-Jun N-terminal kinase), which promotes actin cytoskeleton rearrangement and cell polarity [30]. Western blot analysis revealed a 2.19-fold reduction in p-JNK levels in cotreated MDA-MB-468 cells compared to untreated cells. However, no significant alteration in p-JNK levels was observed in MDA-MB-231 cells following cotreatment **(Figures 4.10A and 4.10B)**. These results indicate that both canonical and non-canonical Wnt signaling pathways are negatively regulated by the combination of Salinomycin and Budesonide.

TH-3600_196106022

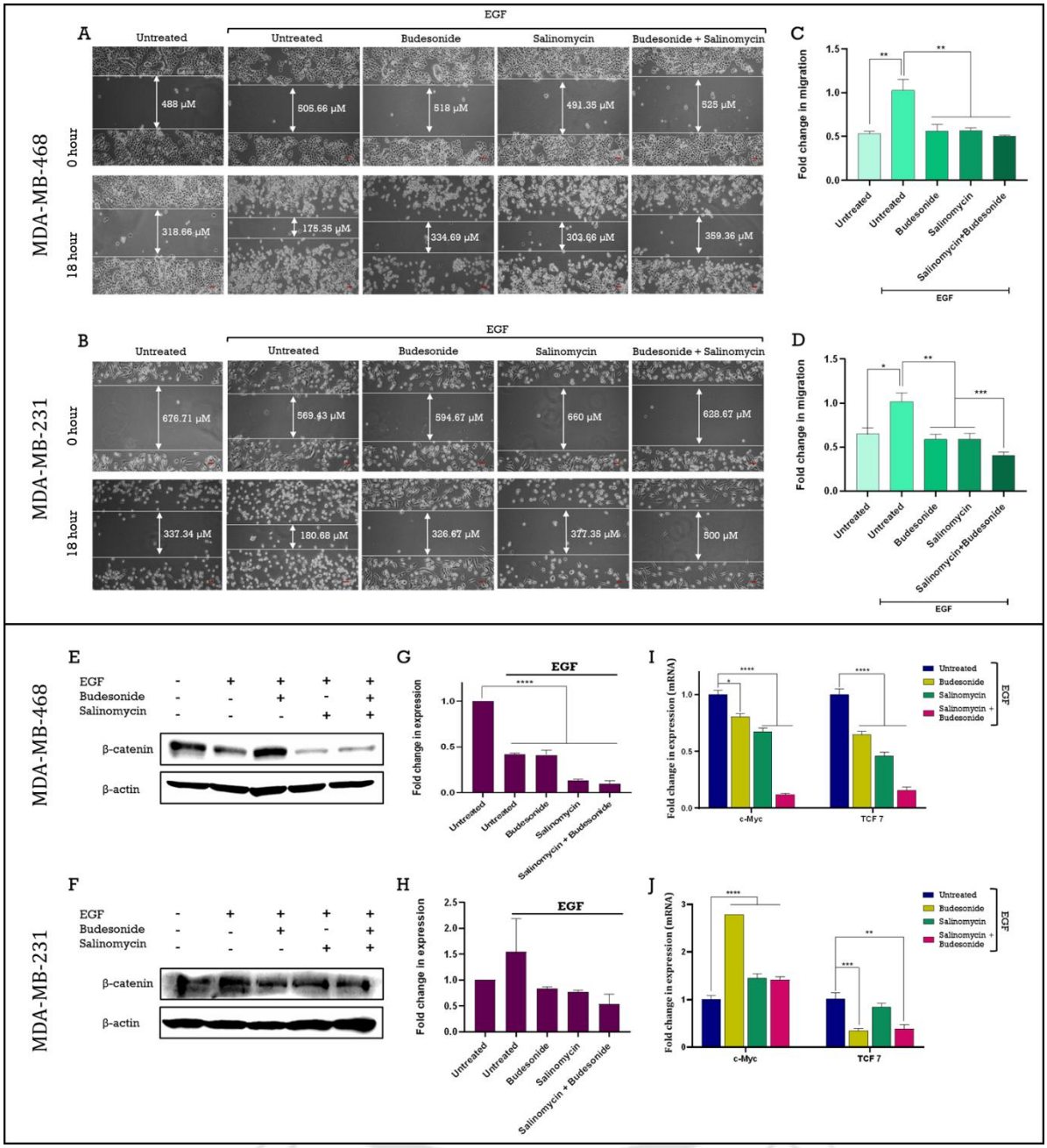

Figure 4.9: *Scratch wound-healing assays of EMT-induced (A) MDA-MB-468 and (B) MDA-MB-231 cells. The scale bar represents 50 µm. Graphical representation of changes in the migration ability following treatment with the drugs and their combination, compared to the untreated cells in (C) MDA-MB-468 and (D) MDA-MB-231 cells. Representative Western blots representing β-catenin levels in (E) MDA-MB-468 and (F) MDA-MB-231 cells and fold change in expression determined in (G) MDA-MB-468 and (H) MDA-MB-231 following treatment with drugs and their combination for 48h. Alteration in gene expression of c-Myc and TCF-7 in EMT-induced (I) MDA-MB-468 and (J)MDA-MB-231 cells following treatment. One-way ANOVA test was carried out to assess the correlations between the groups. The p-value <0.05 (*) is considered to be statistically significant, whereas p<0.001 (***) and p<0.0001 (****) are considered to be highly significant.*

TH-3600_196106022

4.3.6. Salinomycin in Combination with Budesonide Downregulates Pro-Survival Signals in TNBC

During TNBC progression, EGFR overexpression leads to the hyperactivation of multiple signaling pathways, such as mitogen-activated protein kinases (MAPK), signal transducer and activator of transcription-3 (STAT-3), and phosphoinositide 3-kinase (PI3K)/Akt pathways, which facilitate tumor angiogenesis, proliferation, invasion, and metastasis [31]. The effects of the drugs and their combination on various pro-survival signaling pathways were assessed through Western blot analysis. A key signal transduction pathway involved in TNBC development is the MAPK signaling pathway [32]. Following cotreatment, the expression levels of phosphorylated MAPK and total MAPK were analyzed. The expression of phosphorylated MAPK was reduced by 2.54-fold in MDA-MB-468 cells. In contrast, MDA-MB-231 cells exhibited a slight increase in both phosphorylated MAPK **(Figure 4.10A and 4.10B)** and total MAPK.

Further, after cotreatment, we evaluated the levels of phosphorylated STAT3, which regulates genes associated with cell survival, inflammation, angiogenesis, and tumor metastasis [33]. Phosphorylated STAT3 expression was reduced by 2-fold in MDA-MB-468 and by 2.95-fold in MDA-MB-231 cells following cotreatment. Similarly, MDA-MB-468 cells treated with the drug combination showed a 5.13-fold reduction in phospho-AKT levels compared to untreated cells **(Figures 4.10A and 4.10B)**. In MDA-MB-231 cells, no significant change was observed in phosphorylated AKT levels, though a notable reduction in total AKT was seen after cotreatment **(Figure 4.11)**. Additionally, the expression of the cyclin-dependent kinase inhibitor p21, a negative regulator of the cell cycle, was studied after combined treatment [34]. It was found that p21 expression was upregulated by 12.92-fold in MDA-MB-468 cells **(Figure 4.10A)** and by 3.4-fold in MDA-MB-231 cells **(Figure 4.10B)**. These findings suggest that cotreatment can effectively inhibit cell growth through p21 activation.

TH-3600_196106022

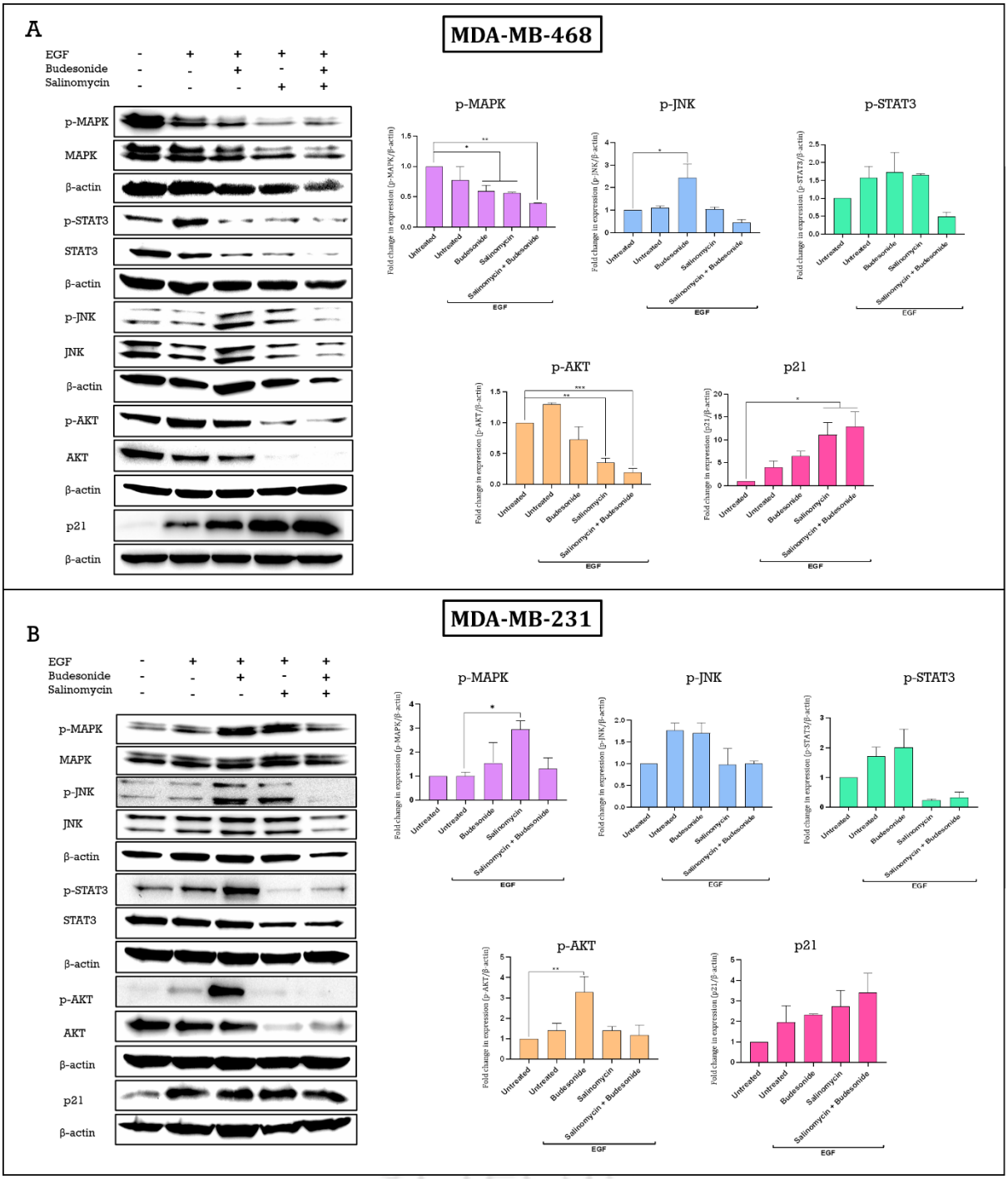

Figure 4.10: *Representative Western blots representing p-MAPK/MAPK, p-STAT3/STAT3, p-JNK/JNK, p-AKT/AKT, and p21 levels in A) MDA-MB-468 and B) MDA-MB-231 cells treated drugs and their combination for 48h. Visualization of the changes in expression was carried out using the ImageJ software. One-way ANOVA test was carried out to assess the correlations between the groups. The p-value <0.05 (*) is considered to be statistically significant, whereas p<0.001 (***) and p<0.0001 (****) are considered to be highly significant.*

TH-3600_196106022

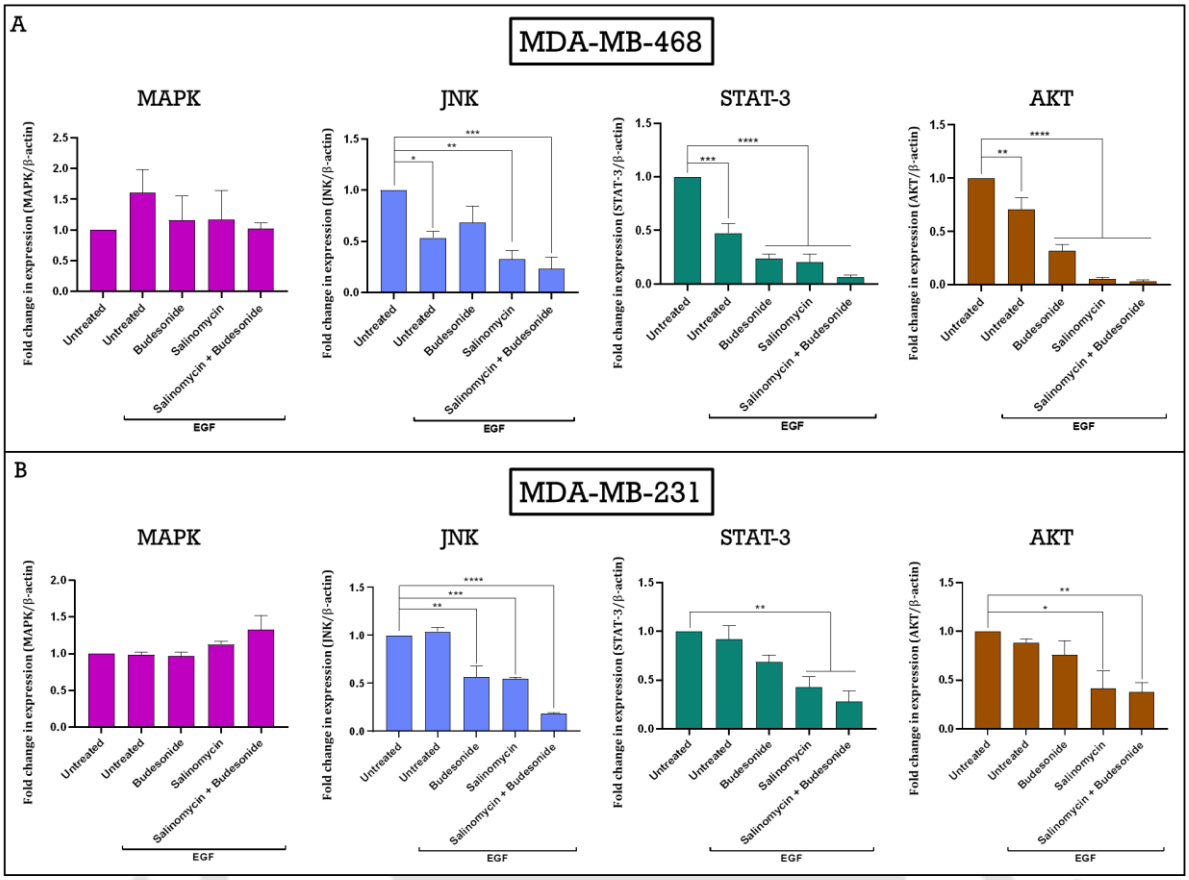

Figure 4.11: *Fold change in protein expression level of total MAPK, JNK, STAT-3 and AKT in (A) MDA-MB-468 and (B) MDA-MB-231 cells treated with drugs and their combination for 48h. One-way ANOVA test was carried out to assess the correlations between the groups. The p-value <0.05 (*) is considered to be statistically significant, whereas p<0.001 (***) and p<0.0001 (****) are considered to be highly significant.*

4.3.7. Upsurge in the Expression of Autophagy Markers Reveals Enhanced Autophagic Activity in TNBC Cells

Autophagy is an essential cellular process that plays a critical role in degrading misfolded proteins and eliminating dysfunctional organelles through lysosomes. Disruptions in autophagy can significantly influence cancer development and progression [35]. To assess the effect of cotreatment on the autophagic activity of TNBC cells, autophagy-related lysosomal activity was detected using LysoTracker staining followed by flow cytometry. In comparison to untreated cells, red fluorescence increased by 5.77-fold in MDA-MB-468 cells and by 2.54-fold in MDA-MB-231 cells following cotreatment. Imaging results also demonstrated an increase in red fluorescence in both cell lines after treatment with the drug combination.

TH-3600_196106022

Autophagy is a critical cellular mechanism involved in the renewal of cellular components and maintaining homeostasis. The relationship between autophagy and cancer is complex and context-dependent, varying by cancer type, tumor stage, and genetic makeup of the cancer cells [36]. Autophagy can serve a protective role by recycling macromolecular precursors to provide nutrients and building blocks. However, excessive and prolonged autophagic activation can lead to cellular degradation and eventual cell death [37]. In this study, we investigated the effect of the drug combination on the autophagy process by analyzing autophagy marker expression via Western blot. The expression of the autophagy marker microtubule-associated protein light chain LC3 A/B was evaluated in treated cells. LC3 I expression was upregulated by 6.54-fold in MDA-MB-468 and by 2.13-fold in MDA-MB-231 **(Figures 4.12A and 4.12B)**. LC3 II expression was upregulated by 17.16-fold in MDA-MB-468 **(Figure 4.12A)** and by 9.61-fold in MDA-MB-231 **(Figure 4.12B)**. These results suggest enhanced LC3 I to LC3 II conversion in co-treated cells, indicating increased autophagic activity [38].

Another marker linked to autophagy induction is SQSTM1 (Sequestosome or p62), which acts as a substrate for autophagy and serves as a reporter of autophagy activity [39]. Cotreatment led to a 9.89-fold increase in SQSTM1 expression in MDA-MB-468 and an 8.15-fold increase in MDA-MB-231. Beclin1, another protein closely associated with autophagic activity and tumorigenesis [38], exhibited a 1.93-fold reduction in expression in MDA-MB-468 cells after cotreatment **(Figure 7A)**, while its expression was enhanced by 1.32-fold in MDA-MB-231 cells **(Figure 4.12B)**. Additionally, LysoTracker red staining indicated that cotreatment induced the formation of acidic lysosomal vacuoles in treated cells, displaying enhanced red fluorescence compared to untreated cells **(Figure 4.12E)**. Overall, these findings suggest that the combination of Salinomycin and Budesonide promotes autophagic activity in TNBC cells.

TH-3600_196106022

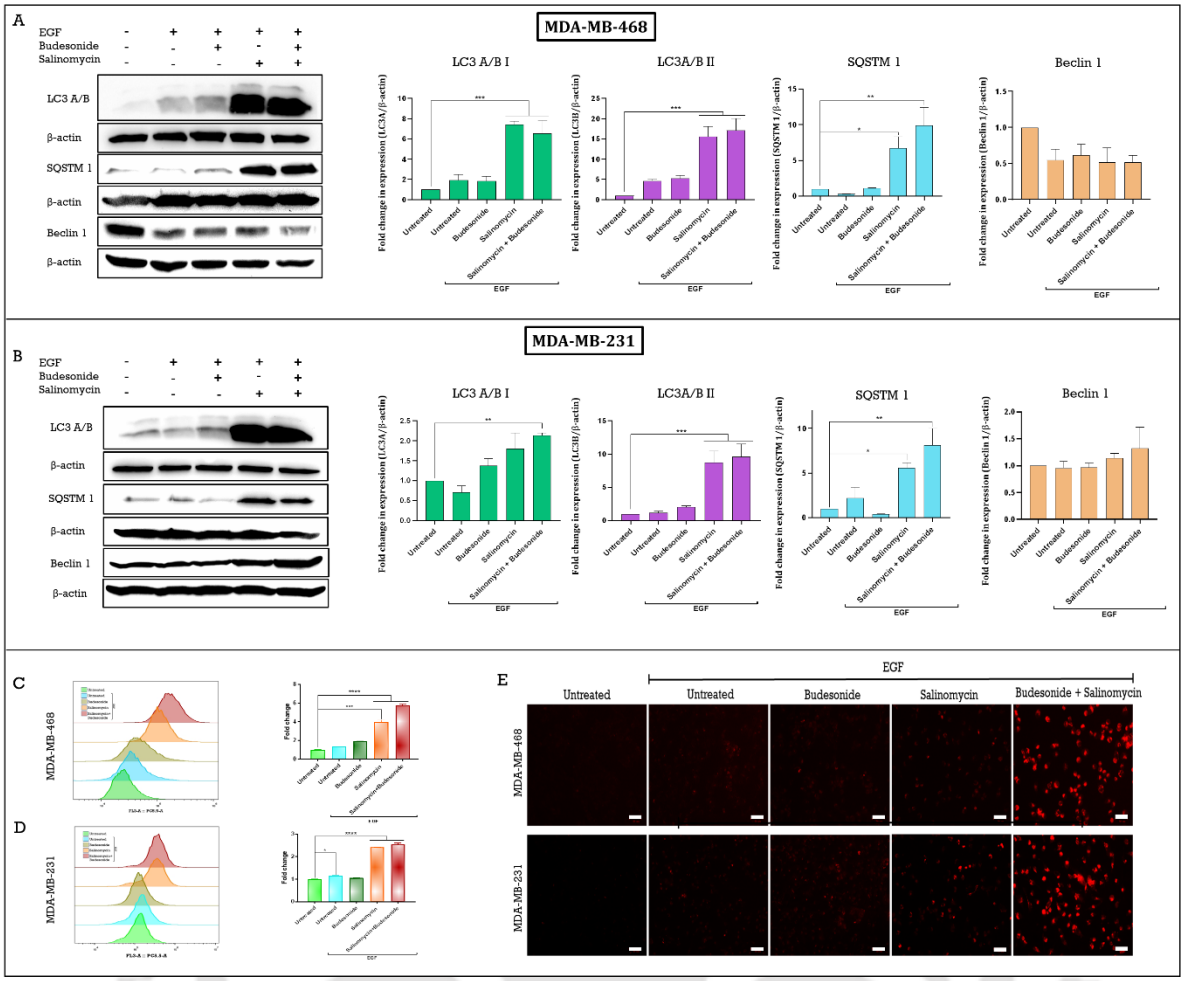

Figure 4.12: *Representative Western blots representing LC3 A/B, SQSTM1, and Beclin-1 levels in (A) MDA-MB-468 and (B) MDA-MB-231 cells treated with drugs andtheir combination for 48h. flow cytometric detection of acidic lysosomal vacuole formation in (C) MDA-MB-468 and (D) MDA-MB-231 cells. (E) Imaging of MDA-MB-468 and MDA-MB-231 cells with Lysotracker deep red after the treatment with drugs and their combination for 48h. The scale bar represents 100 µm. One-way ANOVA test was carried out to assess the correlations between the groups. The p-value <0.05 (*) is considered to be statistically significant, whereas p<0.001 (***) and p<0.0001 (****) are considered to be highly significant.*

4.3.8. Alteration in the Accumulation of Lipid Droplets in EMT-Induced TNBC Cells

Lipid droplets are responsible for storing neutral lipids, primarily triacylglycerol (TAG) and sterol esters, and play a crucial role in regulating lipid uptake, dispersal, and consumption. The accumulation of lipid droplets has been observed in various cancers, particularly in cancer cells exposed to hypoxia or nutrient starvation, which exhibit elevated levels of these droplets. Recent studies have revealed that lipid droplet accumulation promotes cancer cell survival and growth by suppressing nutrient depletion

TH-3600_196106022

and oxidative stress [40]. Following treatment, Nile Red staining was performed to assess lipid droplet accumulation. Upon EMT induction, a substantial increase in the accumulation of lipid droplets was noted. Additionally, Salinomycin-treated EMT-induced cells exhibited the highest levels of lipid droplet accumulation. In contrast, Budesonide treatment reduced the accumulation of lipid droplets within the cells. Interestingly, the combination treatment of Budesonide and Salinomycin resulted in a significant reduction in lipid droplet accumulation in EMT-induced TNBC cells compared to those treated with EGF alone **(Figures 4.13A and 4.13B)**. These findings indicate that cotreatment has a substantial impact on the lipid metabolism processes in TNBC cells.

TH-3600_196106022

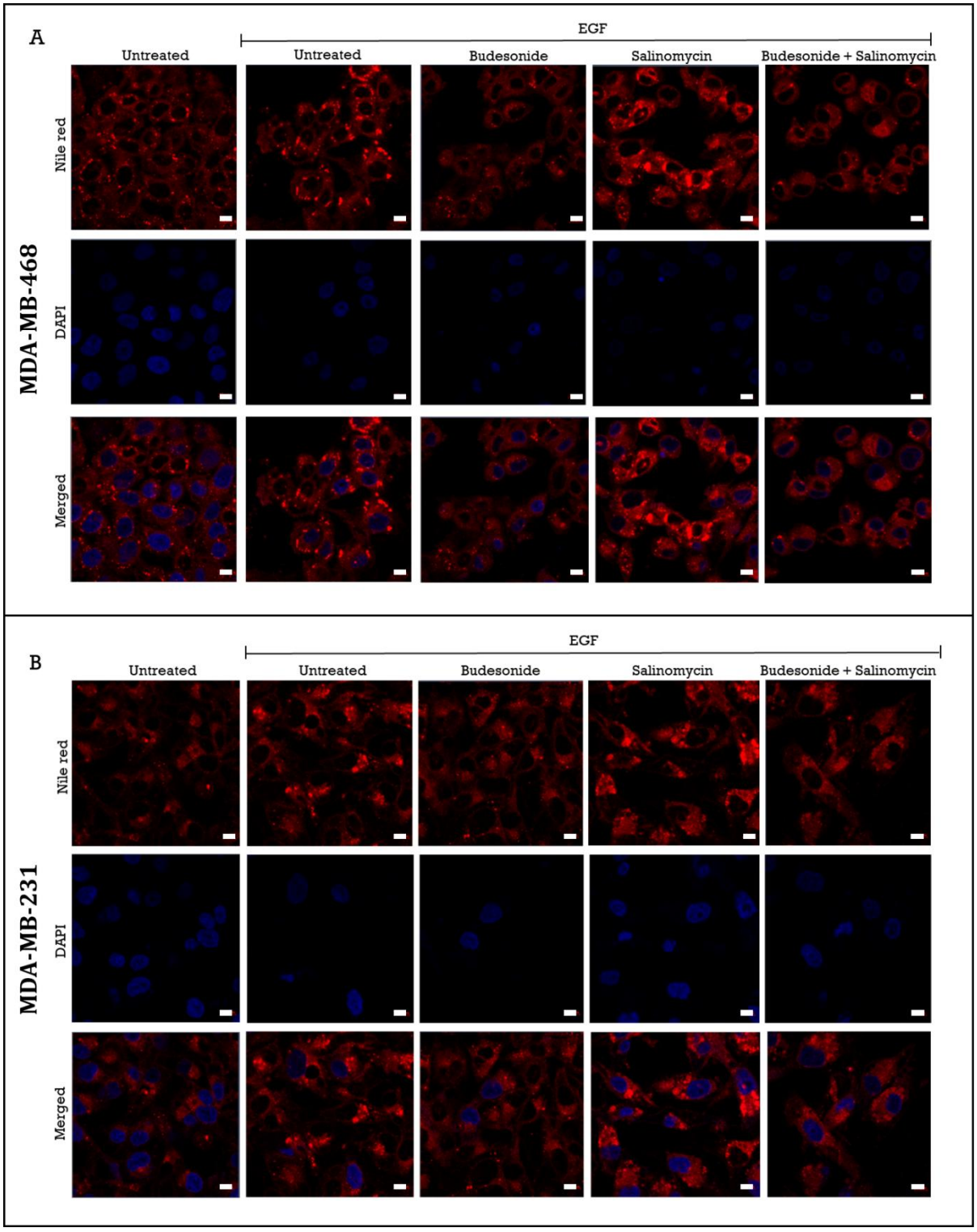

Figure 4.13: *Nile Red staining of (A) MDA-MB-468 and (B) MDA-MB-231 cells. The scale bar represents 10 µm.*

TH-3600_196106022

4.3.9. Salinomycin in Combination with Budesonide Enhances Cytotoxicity in TNBC Spheroids

To ascertain the effects of the drug combination in a 3D multicellular tumor environment, spheroids of MDA-MB-468 and MDA-MB-231 cells were treated with increasing concentrations of single drugs and their combination. In monolayer cultures, Budesonide showed no effect on the cell viability of spheroids, even at higher concentrations. Surprisingly, the combination of Budesonide and Salinomycin demonstrated a significant reduction in spheroid cell viability in a dose-dependent manner, even at lower concentrations **(Table 4.4 and Figure 4.14)**. Furthermore, the impact of cotreatment was visualized through live-dead cell imaging of MDA-MB-468 and MDA-MB-231 spheroids following treatment. Compared to untreated spheroids, drug-treated spheroids exhibited a marked increase in red fluorescence and a decrease in green fluorescence in viable cells **(Figure 4.15)**. This observation indicates the detrimental effect of cotreatment on the survival of the spheroids.

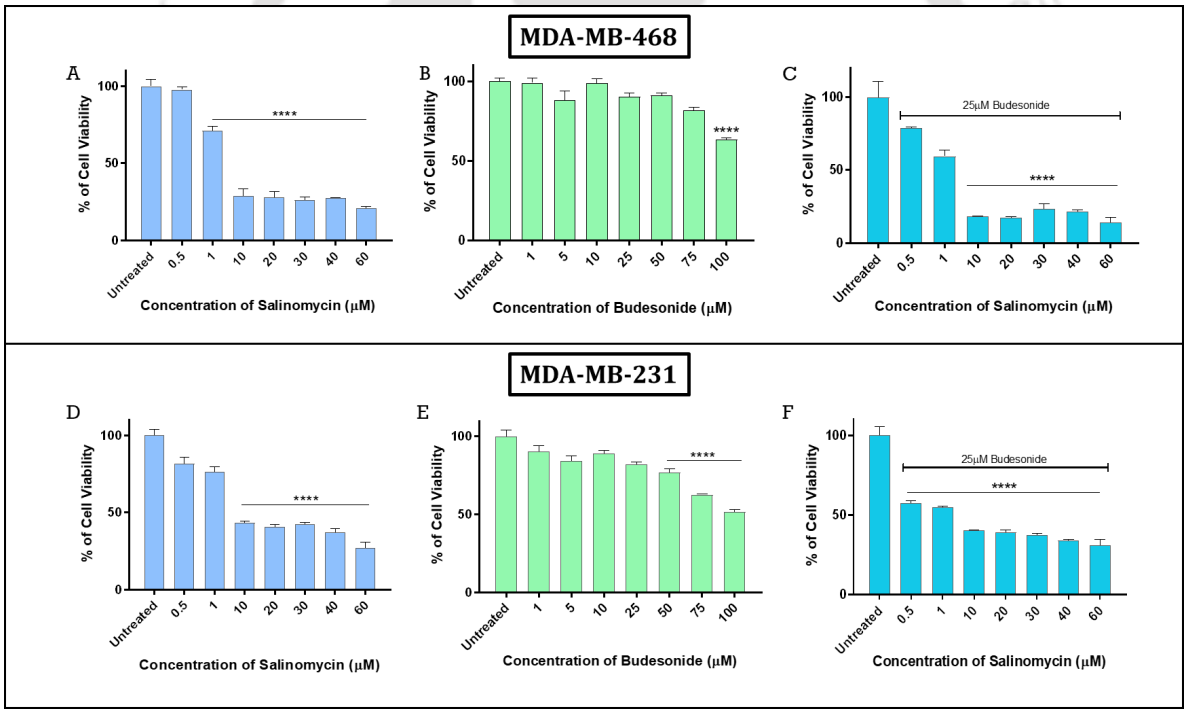

Figure 4.14: *Effect of (A) Salinomycin, (B) Budesonide, C) Budesonide and Salinomycin combination on the viability of MDA-MB-468 spheroids, respectively. Effect of (E) Salinomycin, (F) Budesonide, (G) Budesonide, and Salinomycin combination on the viability of MDA-MB-231 spheroids, respectively, One-way ANOVA test was carried out to assess the correlations between the groups. The p-value <0.05 (*) is considered to be statistically significant, whereas p<0.001 (***) and p<0.0001 (****) are considered to be highly significant.*

TH-3600_196106022

Table 4.4: IC_{50} value obtained for spheroids of different breast cancer cell lines by alamarBlue assay.

DRUG	IC_{50} value obtained for spheroids of different breast cancer cell line	
	MDA-MB-468	MDA-MB-231
Salinomycin	6.685 µM	14.32 µM
Budesonide	Not attained	Not attained
Salinomycin + Budesonide	2.456 µM	10.76 µM

TH-3600_196106022

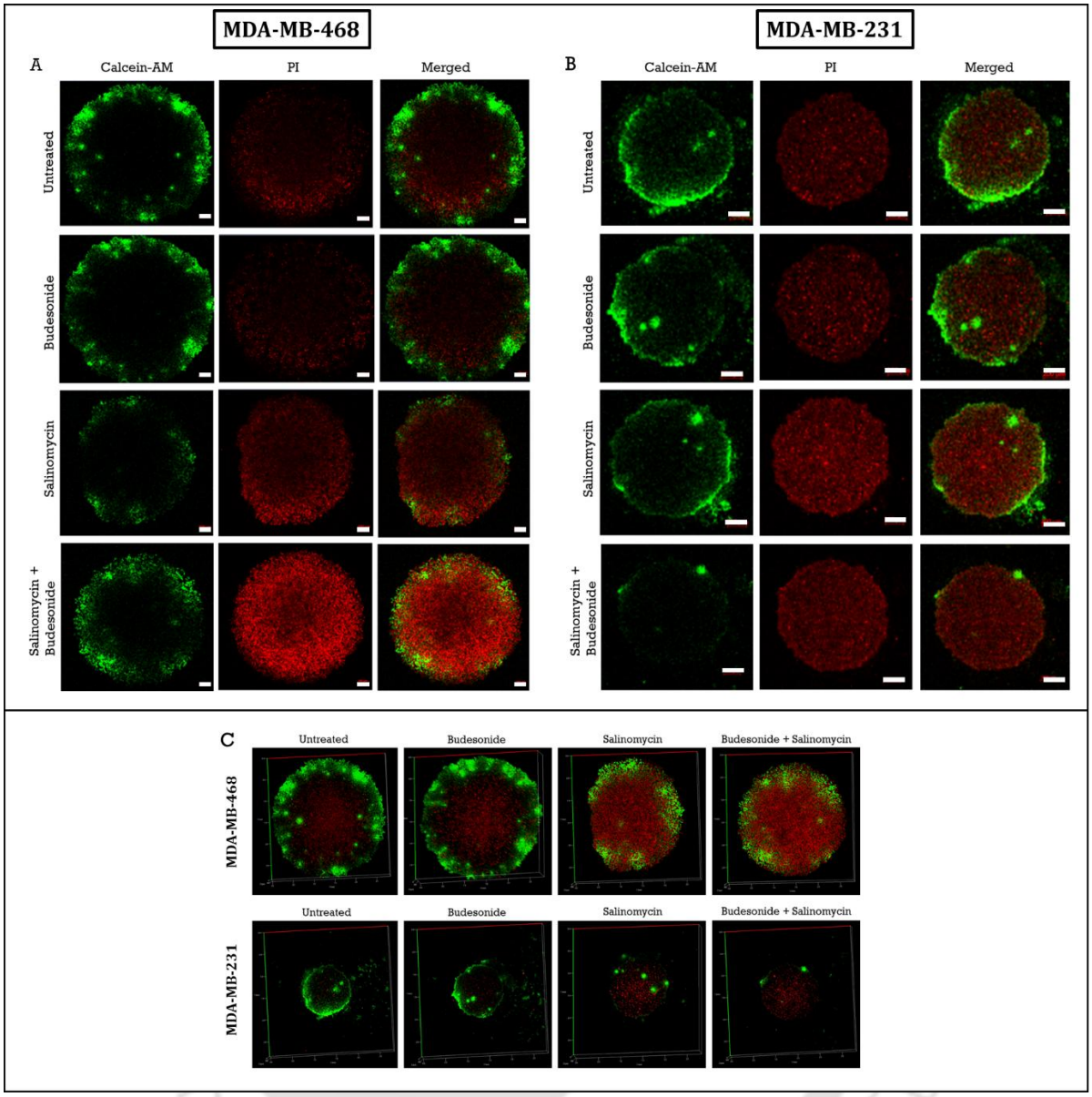

Figure 4.15: *Live/dead cell imaging of (A) MDA-MB-468 and (B) MDA-MB-231 spheroids after treatment with drugs and their combination 72h. The scale bar represents 200 µm. Z-stacking images of (C) MDA-MB-468 and MDA-MB-231 spheroids.*

4.4. Discussion

In this study, it was demonstrated that the co-administration of Budesonide and Salinomycin constitutes an effective combination treatment strategy targeting TNBC cells. The findings from the present study reveal a concentration-dependent inhibitory effect of Salinomycin on triple-negative breast cancer cells, whereas Budesonide had no significant impact on cell viability. Cytotoxicity and live/dead imaging studies explicitly indicate that the combination treatment of Budesonide and Salinomycin yields the most potent effect. Drug combination studies depict a synergistic inhibitory

TH-3600_196106022

effect of the two drugs on TNBC cell proliferation. The cellular mechanisms underlying co-treatment-mediated cell death were further elucidated through various flow cytometric studies, revealing that co-therapy activates the intrinsic pathway of apoptosis via the generation of reactive oxygen species (ROS) and mitochondrial membrane depolarization.

During the progression of TNBC, cells acquire invasive and migratory properties through the EMT process. EMT also enhances TNBC cell survival by activating anti-apoptotic signals and conferring stem cell properties and drug resistance. Therefore, impeding EMT, in addition to facilitating cancer cell death, can be a key therapeutic approach for inhibiting tumorigenesis in TNBC. In the current study, it was found that Budesonide effectively enhances Salinomycin-induced TNBC cell death while inhibiting EGF-induced EMT in TNBC cells. Quantification of mRNA and protein expression clearly indicates that co-treatment reverses the EMT process by enhancing the expression of epithelial markers and downregulating the expression of mesenchymal markers. The reversal of EMT via drug treatment can ultimately contribute to reduced stemness and invasive properties. The effect of co-treatment on stemness and migratory properties was also evaluated. In MDA-MB-468 cells, the expression of the stemness marker ALDH1A3 was reduced, whereas in MDA-MB-231 cells, the expression of another stemness marker, EpCAM, was significantly decreased. These differences may arise from the heterogeneity and diverse mutations in key genes regulating the tumorigenicity of these two cell lines. Co-treated cells exhibited a significant reduction in sphere-forming and colony-forming abilities, further confirming the decrease in stemness resulting from co-treatment. Additionally, the co-treatment significantly impaired the migration ability of TNBC cells.

Moreover, the co-treatment inhibited the Wnt signaling pathway, which promotes EMT in TNBC. WNT/β-catenin signaling influences various cellular mechanisms, such as cell survival, migration, and invasion in breast cancer. Differentiation of epithelial cells and stem cell renewal have been shown to correlate with aberrant WNT/β-catenin signaling. Expression analysis of several genes linked to the Wnt pathway demonstrated that the combined use of Salinomycin and Budesonide results in the suppression of Wnt signaling in TNBC cells. Recent studies have reported that the overexpression of EGFR in TNBC activates the Ras/MAPK (extracellular signal-regulated kinase) pathway. The aberrant activation of the MAPK pathway is known to be associated with EMT progression, cancer cell proliferation, survival, migration, and angiogenesis. The immunoblot results for MDA-MB-468 and MDA-MB-231 revealed a substantial downregulation of phosphorylated MAPK following co-treatment. The pro-oncogenic STAT-3 and AKT pathways, activated by EGFR stimulation, are also notably dysregulated in TNBC. The findings from the protein expression studies indicate that co-treatment significantly downregulates the expression of phospho-STAT3 and phospho-AKT in TNBC

TH-3600_196106022

cells. This suggests that the anti-cancer effects of the drug combination in TNBC cells may potentially involve the downregulation of STAT3 and AKT signaling. Thus, the reversal of EMT, reduction in stemness, and decreased migration due to co-treatment were achieved through the inhibition of these pathways.

Additionally, enhanced autophagic activity following Salinomycin and Budesonide co-treatment was confirmed through LysoTracker red staining and protein expression analysis of autophagy markers. After co-therapy, there was an increase in the conversion of LC3-I to its lipidated form, LC3-II, indicating a significant upregulation of autophagic activity. The reduction in phospho-AKT and total AKT levels after co-treatment underscores the downregulation of the PI3K/AKT/mTOR axis, which leads to autophagy induction. Various studies have revealed a complex relationship between autophagy-related and EMT-related signaling pathways, with evidence suggesting that autophagy can inhibit EMT. Increasing autophagosome production has been linked to reduced Twist1 expression, which suppresses N-cadherin and enhances E-cadherin, ultimately constraining EMT. Thus, the enhanced autophagy-mediated downregulation of Twist1 following co-treatment may contribute to the circumvention of EMT. Furthermore, lipid droplets engage in complex crosstalk with autophagy. Lipid droplets facilitate the formation of autophagosomal membranes, regulate ER stress, and drive signaling mechanisms that induce autophagy. Conversely, autophagy promotes cell survival by driving lipid droplet formation under stress conditions. In this study, co-treatment increased autophagic activity while concomitantly reducing lipid droplet accumulation. This suggests that co-treatment-induced autophagy in TNBC cells does not serve a protective role; rather, it limits cell survival by enhancing self-digesting autophagosomal activity.

The cell survival studies of tumor spheroids containing TNBC cells demonstrated superior efficacy of the drug combination in multicellular tumor conditions compared to monotherapy. Collectively, these results indicate that the co-treatment of Salinomycin and Budesonide triggers autophagy while suppressing TNBC growth, highlighting its therapeutic efficacy as a novel anticancer approach.

4.5. Conclusion

Owing to its higher efficacy compared to monotherapy, combination treatment has become increasingly common in cancer management. The use of drugs with distinct mechanisms of action reduces the risk of drug resistance and relapse. In this study, the therapeutic potential of a combination regimen consisting of the selective anti-cancer stem cell (CSC) agent, Salinomycin, and the DNA methylating agent, Budesonide was explored. The findings from the present study clearly demonstrate that the co-administration of Salinomycin and Budesonide significantly inhibits TNBC cell growth in

TH-3600_196106022

both monolayer cultures and spheroids. Budesonide enhances the anti-proliferative effects of Salinomycin, resulting in synergistic therapeutic activity. The combined treatment promotes the generation of intracellular ROS and mitochondrial membrane depolarization, ultimately leading to enhanced apoptosis in TNBC cells. The observed upregulation of epithelial markers and concurrent downregulation of mesenchymal markers suggest that the co-treatment effectively inhibits the EMT process. Additionally, it suppresses TNBC cell migration and reduces the stem cell-like properties of TNBC cells. The molecular mechanisms underlying the drug combination's efficacy were further elucidated through signaling studies, revealing disruptions in several cancer-associated pathways, including WNT/β-catenin, MAPK, STAT-3, and PI3K-AKT. Furthermore, increased expression of autophagy markers indicates heightened autophagic activity following combined treatment, suggesting that the cytotoxic effects of this regimen may be mediated through autophagy modulation. A notable reduction in lipid droplet accumulation was also observed, highlighting an impact on lipid metabolism. In summary, the combination of Budesonide and Salinomycin offers new insights into the treatment and prognosis of TNBC, demonstrating its potential as an effective therapeutic strategy. However, further *in vivo* studies are necessary to evaluate systemic effects, optimal dosing, and safety profiles for future clinical applications.

4.6. References

1. Yin, L., Duan, J. J., Bian, X. W., & Yu, S. C. (2020). Triple-negative breast cancer molecular subtyping and treatment progress. *Breast Cancer Research*, 22, 1-13. https://doi.org/10.1186/s13058-020-01296-5

2. Almansour, N. M. (2022). Triple-negative breast cancer: a brief review about epidemiology, risk factors, signaling pathways, treatment and role of artificial intelligence. *Frontiers in Molecular Biosciences*, 9, 836417. https://doi.org/10.3389/fmolb.2022.836417

3. Acloque, H., Adams, M. S., Fishwick, K., Bronner-Fraser, M., & Nieto, M. A. (2009). Epithelial-mesenchymal transitions: the importance of changing cell state in development and disease. *The Journal of clinical investigation*, *119*(6), 1438-1449. https://doi.org/10.1172/jci38019

4. Kvokačková, B., Remšík, J., Jolly, M. K., & Souček, K. (2021). Phenotypic heterogeneity of triple-negative breast cancer mediated by epithelial–mesenchymal plasticity. *Cancers*, *13*(9), 2188. https://doi.org/10.3390/cancers13092188

TH-3600_196106022

5. Ishiwata, T. (2016). Cancer stem cells and epithelial-mesenchymal transition: Novel therapeutic targets for cancer. *Pathology International*, *66*(11), 601-608. https://doi.org/10.1111/pin.12447

6. Mansoori, B., Mohammadi, A., Davudian, S., Shirjang, S., & Baradaran, B. (2017). The different mechanisms of cancer drug resistance: a brief review. *Advanced pharmaceutical bulletin*, *7*(3), 339. https://doi.org/10.15171/apb.2017.041

7. Shome, R., & Ghosh, S. S. (2021). Tweaking EMT and MDR dynamics to constrain triple-negative breast cancer invasiveness by EGFR and Wnt/β-catenin signaling regulation. *Cellular Oncology*, *44*, 405-422. https://doi.org/10.1007/s13402-020-00576-8

8. Gupta, P. B., Onder, T. T., Jiang, G., Tao, K., Kuperwasser, C., Weinberg, R. A., & Lander, E. S. (2009). Identification of selective inhibitors of cancer stem cells by high-throughput screening. *Cell*, *138*(4), 645-659. https://doi.org/10.1016/j.cell.2009.06.034

9. Paulus, E. F., Kurz, M., Matter, H., & Vértesy, L. (1998). Solid-state and solution structure of the Salinomycin- sodium complex: Stabilization of different conformers for an ionophore in different environments. *Journal of the American Chemical Society*, *120*(32), 8209-8221.

10. Mai, T. T., Hamaï, A., Hienzsch, A., Cañeque, T., Müller, S., Wicinski, J., ... & Rodriguez, R. (2017). Salinomycin kills cancer stem cells by sequestering iron in lysosomes. *Nature chemistry*, *9*(10), 1025-1033. https://doi.org/10.1038/nchem.2778

11. Liu, Y., Hao, Y., Li, Y., Zheng, Y., Dai, J., Zhong, F., ... & Fang, Z. (2020). Salinomycin induces autophagic cell death in salinomycin-sensitive melanoma cells through inhibition of autophagic flux. *Scientific Reports*, *10*(1), 18515. https://doi.org/10.1038/s41598-020-75598-1

12. Boehmerle, W., & Endres, M. (2011). Salinomycin induces calpain and cytochrome c-mediated neuronal cell death. *Cell death & disease*, *2*(6), e168-e168. https://doi.org/10.1038/cddis.2011.46

13. Story, P., & Doube, A. (2004). A case of human poisoning by Salinomycin, an agricultural antibiotic. *NZ Med j*, *117*(1190), U799.

14. Zappavigna, S., Cossu, A. M., Grimaldi, A., Bocchetti, M., Ferraro, G. A., Nicoletti, G. F., ... & Caraglia, M. (2020). Anti-inflammatory drugs as anticancer agents. International journal of molecular sciences, 21(7), 2605. https://doi.org/10.3390/ijms21072605

TH-3600_196106022

15. Banov, C. H. (2004). The role of Budesonide in adults and children with mild-to-moderate persistent asthma. *Journal of Asthma*, *41*(1), 5-17. https://doi.org/10.1081/jas-120026092

16. Greenberg, G. R., Feagan, B. G., Martin, F., Sutherland, L. R., Thomson, A., Williams, C. N., ... & Canadian Inflammatory Bowel Disease Study Group. (1994). Oral Budesonide for active Crohn's disease. *New England Journal of Medicine*, *331*(13), 836-841. https://doi.org/10.1056/nejm199409293311303

17. Lee, C. S., Ryan, E. J., & Doherty, G. A. (2014). Gastro-intestinal toxicity of chemotherapeutics in colorectal cancer: the role of inflammation. *World journal of gastroenterology: WJG*, *20*(14), 3751. https://doi.org/10.3748/wjg.v20.i14.3751

18. Pereira, M. A., Li, Y., Gunning, W. T., Kramer, P. M., Al-Yaqoub, F., Lubet, R. A., ... & Tao, L. (2002). Prevention of mouse lung tumors by Budesonide and its modulation of biomarkers. *Carcinogenesis*, *23*(7), 1185-1192. https://doi.org/10.1093/carcin/23.7.1185

19. Pereira, M. A., Tao, L. H., Wang, W., Gunning, W. T., & Lubet, R. (2005). Chemoprevention: mouse colon and lung tumor bioassay and modulation of DNA methylation as a biomarker. *Experimental lung research*, *31*(2), 145-163. https://doi.org/10.1080/01902140490495534

20. Yao, R., Wang, Y., Lemon, W. J., Lubet, R. A., & You, M. (2004). Budesonide exerts its chemopreventive efficacy during mouse lung tumorigenesis by modulating gene expressions. *Oncogene*, *23*(46), 7746-7752. https://doi.org/10.1038/sj.onc.1207985

21. D'Aniello, C., Cermola, F., Palamidessi, A., Wanderlingh, L. G., Gagliardi, M., Migliaccio, A., ... & Minchiotti, G. (2019). Collagen prolyl hydroxylation–dependent metabolic perturbation governs epigenetic remodeling and mesenchymal transition in pluripotent and cancer cells. *Cancer research*, *79*(13), 3235-3250. https://doi.org/10.1158/0008-5472.can-18-2070

22. Longhin, E. M., El Yamani, N., Rundén-Pran, E., & Dusinska, M. (2022). The alamar blue assay in the context of safety testing of nanomaterials. *Frontiers in Toxicology*, *4*, 981701. https://doi.org/10.3389/ftox.2022.981701

23. DeVorkin, L., & Gorski, S. M. (2014). LysoTracker staining to aid in monitoring autophagy in Drosophila. *Cold Spring Harbor Protocols*, *2014*(9), 951-958.Felipe Lima, J., Nofech-Mozes, S., Bayani, J., & Bartlett, J. M. (2016). EMT in breast carcinoma—a review. *Journal of clinical medicine*, *5*(7), 65. https://doi.org/10.1101/pdb.prot080325

TH-3600_196106022

24. Felipe Lima, J., Nofech-Mozes, S., Bayani, J., & Bartlett, J. M. (2016). EMT in breast carcinoma—a review. *Journal of clinical medicine*, *5*(7), 65. https://doi.org/10.3390/jcm5070065

25. Elzamly, S., Badri, N., Padilla, O., Dwivedi, A. K., Alvarado, L. A., Hamilton, M., ... & Nahleh, Z. (2018). Epithelial-mesenchymal transition markers in breast cancer and pathological responseafter neoadjuvant chemotherapy. *Breast cancer: basic and clinical research*, *12*, 1178223418788074. https://doi.org/10.1177/1178223418788074

26. Pohl, S. G., Brook, N., Agostino, M., Arfuso, F., Kumar, A. P., & Dharmarajan, A. (2017). Wnt signaling in triple-negative breast cancer. *Oncogenesis*, *6*(4), e310-e310. https://doi.org/10.1038/oncsis.2017.14

27. Yu, W. K., Xu, Z. Y., Yuan, L., Mo, S., Xu, B., Cheng, X. D., & Qin, J. J. (2020). Targeting β-catenin signaling by natural products for cancer prevention and therapy. *Frontiers in Pharmacology*, *11*, 984. https://doi.org/10.3389/fphar.2020.00984

28. Fodde, R., & Brabletz, T. (2007). Wnt/β-catenin signaling in cancer stemness and malignant behavior. *Current opinion in cell biology*, *19*(2), 150-158. https://doi.org/10.1016/j.ceb.2007.02.007

29. Xu, X., Zhang, M., Xu, F., & Jiang, S. (2020). Wnt signaling in breast cancer: biological mechanisms, challenges and opportunities. *Molecular cancer*, *19*, 1-35. https://doi.org/10.1186/s12943-020-01276-5

30. Merikhian, P., Eisavand, M. R., & Farahmand, L. (2021). Triple-negative breast cancer: Understanding Wnt signaling in drug resistance. *Cancer Cell International*, *21*(1), 1-8. https://doi.org/10.1186/s12935-021-02107-3

31. Lee, C. H. (2019). Reversal of epithelial–mesenchymal transition by natural anti-inflammatory and pro-resolving lipids. *Cancers*, *11*(12), 1841. https://doi.org/10.3390/cancers11121841

32. Jiang, W., Wang, X., Zhang, C., Xue, L., & Yang, L. (2020). Expression and clinical significance of MAPK and EGFR in triple-negative breast cancer. *Oncology letters*, *19*(3), 1842-1848. https://doi.org/10.3892/ol.2020.11274

33. Marginean, E. C., Gotfrit, J., Marginean, H., Yokom, D. W., Bateman, J. J., Daneshmand, M., ... & Goodwin, R. A. (2021). Phosphorylated transducer and activator of transcription-3 (pSTAT3) immunohistochemical expression in paired primary and metastatic colorectal cancer. *Translational Oncology*, *14*(2), 100996. https://doi.org/10.1016/j.tranon.2020.100996

TH-3600_196106022

34. Abbas, T., & Dutta, A. (2009). p21 in cancer: intricate networks and multiple activities. *Nature Reviews Cancer*, *9*(6), 400-414. https://doi.org/10.1038/nrc2657

35. Yun, C. W., & Lee, S. H. (2018). The roles of autophagy in cancer. *International journal of molecular sciences*, *19*(11), 3466. https://doi.org/10.3390/ijms19113466

36. Salimi-Jeda, A., Ghabeshi, S., Jazaeri, E. O., Araiinejad, M., Sheikholeslami, F., Abdoli, M., ... & Abdoli, A. (2022). Autophagy modulation and cancer combination therapy: a smart approach in cancer therapy. *Cancer Treatment and Research Communications*, *30*, 100512. https://doi.org/10.1016/j.ctarc.2022.100512

37. Lim, S. M., Mohamad Hanif, E. A., & Chin, S. F. (2021). Is targeting autophagy mechanism in cancer a good approach? The possible double-edge sword effect. *Cell & bioscience*, *11*(1), 1-13. https://doi.org/10.1186/s13578-021-00570-z

38. Ji, Y., Okuno, M. N., Shogren, K. L., Fritchie, K., Okuno, S. H., Yaszemski, M. J., & Maran, A. (2020). Autophagy markers and RNA-dependent protein kinase (PKR) activity in osteosarcoma diagnosis and treatment. *Annals of Joint*, *5*. http://doi.org/10.21037/aoj.2020.02.07

39. Liu, W. J., Ye, L., Huang, W. F., Guo, L. J., Xu, Z. G., Wu, H. L., ... & Liu, H. F. (2016). p62 links the autophagy pathway and the ubiqutin–proteasome system upon ubiquitinated protein degradation. *Cellular & molecular biology letters*, *21*, 1-14. https://doi.org/10.1186/s11658-016-0031-z

40. Petan, T., Jarc, E., & Jusović, M. (2018). Lipid droplets in cancer: guardians of fat in a stressful world. *Molecules*, *23*(8), 1941. https://doi.org/10.3390/molecules23081941

41. Elzamly, S., Badri, N., Padilla, O., Dwivedi, A. K., Alvarado, L. A., Hamilton, M., ... & Nahleh, Z. (2018). Epithelial-mesenchymal transition markers in breast cancer and pathological responseafter neoadjuvant chemotherapy. *Breast cancer: basic and clinical research*, *12*, 1178223418788074. https://doi.org/10.1177/1178223418788074

42. Lee, C. H. (2019). Reversal of epithelial–mesenchymal transition by natural anti-inflammatory and pro-resolving lipids. *Cancers*, *11*(12), 1841. https://doi.org/10.3390/cancers11121841

43. Shome, R., & Ghosh, S. S. (2021). Transferrin Coated d-penicillamine–Au-Cu Nanocluster PLGA Nanocomposite Reverses Hypoxia-Induced EMT and MDR of Triple-Negative Breast Cancers. *ACS Applied Bio Materials*, *4*(6), 5033-5048. https://doi.org/10.1021/acsabm.1c00296

TH-3600_196106022

44. Khramtsov, A. I., Khramtsova, G. F., Tretiakova, M., Huo, D., Olopade, O. I., & Goss, K. H. (2010). Wnt/β-catenin pathway activation is enriched in basal-like breast cancers and predicts poor outcome. *The American journal of pathology*, *176*(6), 2911-2920. https://doi.org/10.2353/ajpath.2010.091125

45. Ehmsen, S., & Ditzel, H. J. (2021). Signaling pathways essential for triple-negative breast cancer stem-like cells. *Stem Cells*, *39*(2), 133-143. https://doi.org/10.1002/stem.3301

46. Ryu, W. J., Lee, J. D., Park, J. C., Cha, P. H., Cho, Y. H., Kim, J. Y., ... & Choi, K. Y. (2020). Destabilization of β-catenin and RAS by targeting the Wnt/β-catenin pathway as a potential treatment for triple-negative breast cancer. *Experimental & Molecular Medicine*, *52*(5), 832-842. https://doi.org/10.1038/s12276-020-0440-y

47. Xie, L., Law, B. K., Chytil, A. M., Brown, K. A., Aakre, M. E., & Moses, H. L. (2004). Activation of the Erk pathway is required for TGF-β1-induced EMT in vitro. *Neoplasia*, *6*(5), 603-610. https://doi.org/10.1593/neo.04241

48. Huang, J., Luo, Q., Xiao, Y., Li, H., Kong, L., & Ren, G. (2017). The implication from RAS/RAF/ERK signaling pathway increased activation in epirubicin treated triple negative breast cancer. *Oncotarget*, *8*(64), 108249. https://doi.org/10.18632/oncotarget.22604

49. Lee, M. M. L., Chan, B. D., Wong, W. Y., Qu, Z., Chan, M. S., Leung, T. W., ... & Tai, W. C. S. (2020). Anti-cancer activity of Centipeda minima extract in triple negative breast cancer via inhibition of AKT, NF-κB, and STAT3 signaling pathways. *Frontiers in oncology*, *10*, 491. https://doi.org/10.3389/fonc.2020.00491

50. Qiang, L., & He, Y. Y. (2014). Autophagy deficiency stabilizes TWIST1 to promote epithelial-mesenchymal transition. Autophagy, 10(10), 1864-1865. https://doi.org/10.4161%2Fauto.32171

51. Roa-Mansergas, X., Fadó, R., Atari, M., Mir, J. F., Muley, H., Serra, D., & Casals, N. (2018). CPT1C promotes human mesenchymal stem cells survival under glucose deprivation through the modulation of autophagy. *Scientific reports*, *8*(1), 6997. https://doi.org/10.1038/s41598-018-25485-7

TH-3600_196106022

CHAPTER 5

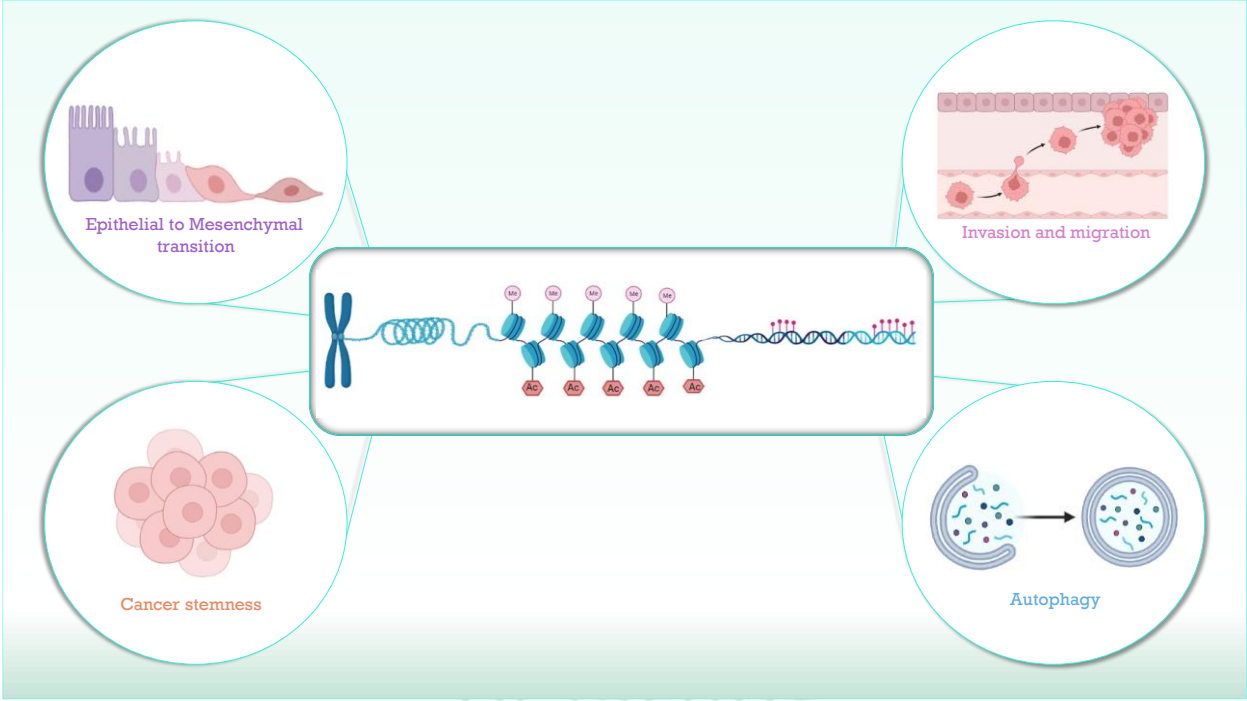

Conclusion and future prospects

TH-3600_196106022

Conclusion and future prospects

Breast cancer remains a significant global health challenge, with TNBC standing out as one of the most aggressive subtypes due to its heterogeneity and lack of targeted therapies. Recent advancements in cancer biology emphasize the role of epigenetic regulators in driving malignancy, offering new avenues for therapeutic intervention. Emerging knowledge on epigenetic regulation of cancer progression has unveiled promising therapeutic targets, including histone acetyltransferases and methyltransferases. This study investigated novel therapeutic approaches by targeting two critical epigenetic regulators, p300 and MLL1, alongside with a combinatorial regimen targeting CSCs and oncogenic pathways.

Histone acetylation, primarily mediated by histone acetyltransferases (HATs) like p300, is pivotal in transcriptional activation and tumorigenesis. Leveraging a series of *in silico* studies, including virtual screening, molecular dynamics simulations (MDS), and binding free energy analysis, Imatinib, a tyrosine kinase inhibitor, was identified as a potent p300 inhibitor. Subsequent *in vitro* studies demonstrated that Imatinib exhibits superior anti-proliferative activity compared to conventional p300 inhibitors. Mechanistically, Imatinib inhibited p300 HAT activity, reduced histone H3K18 and H3K27 acetylation, and downregulated p300 expression. Moreover, Imatinib induced apoptosis through ROS generation and mitochondrial membrane depolarization suppressed EMT and impaired the invasive and migratory abilities of TNBC cells. The downregulation of Notch pathway proteins, including HES1, AKT, and p21, further underscores its therapeutic potential. These findings position Imatinib as a promising repurposed drug for TNBC treatment.

The subsequent study identified MLL1 as a key player in EMT and metabolic reprogramming in TNBC. MLL1 inhibition via MM-102 effectively reverses EMT, shifting cells to an epithelial phenotype marked by upregulation of epithelial markers and downregulation of mesenchymal markers. MM-102 also induced intrinsic apoptosis through ROS generation and SOD2 suppression, leading to enhanced cell death. Furthermore, MLL1 inhibition induced significant metabolic alterations in TNBC cells, characterized by increased glycolysis and decreased lipid metabolism. In 3D spheroid models, MM-102 significantly reduced cell viability and increased cytotoxicity, further validating its efficacy. The inhibition of MLL1 highlights its potential as a novel therapeutic target in aggressive breast cancer subtypes, offering new opportunities for targeted therapy.

Given the increasing reliance on combination therapies to enhance efficacy and minimize drug resistance, the potential of combining Salinomycin with Budesonide, a DNA methylating agent, was explored. The findings revealed that the combined treatment significantly inhibits TNBC cell growth in monolayer and spheroid cultures. Budesonide amplified the anti-proliferative effects of Salinomycin, resulting in synergistic activity. Mechanistically, the combined treatment induced ROS generation, mitochondrial membrane depolarization, and heightened apoptosis. It disrupted EMT by upregulating epithelial markers and downregulating mesenchymal markers, suppressed cell migration, and reduced stem cell-like properties in TNBC cells. Furthermore, signaling studies showed

TH-3600_196106022

that the combination therapy targets multiple cancer-associated pathways, including WNT/β-catenin, MAPK, STAT-3, and PI3K-AKT. Increased autophagic activity and reduced lipid droplet accumulation suggests additional impacts on autophagy and lipid metabolism.

While our findings offer a strong basis for targeting epigenetic modifications in TNBC, several resistance mechanisms need to be addressed:

- **Compensatory Pathways:** Inhibiting one epigenetic target may trigger alternative signaling routes, allowing cancer cells to sustain proliferation and invasion.
- **Microenvironment-Mediated Resistance:** Secreted factors from stromal and immune cells can activate survival pathways in tumor cells, reducing the effectiveness of epigenetic inhibitors.
- **Adaptive Epigenetic Plasticity:** Cancer cells may reprogram their epigenetic landscape in response to therapy, switching to alternative modifications to maintain oncogenic programs.
- **Altered Drug Metabolism:** Upregulation of drug efflux pumps and metabolic changes can lower intracellular drug concentrations, leading to resistance.

Overall, the present study underscores the importance of targeting epigenetic regulators and leveraging combination therapies in TNBC treatment. Imatinib demonstrates significant potential in targeting p300 while using MM-102, and the role of MML1 in TNBC progression was established. Further, the combination of Salinomycin and Budesonide offers a robust strategy to combat TNBC by addressing cancer stemness, survival, and autophagy pathways.

Future Prospects

The potential scopes of the present findings include:

- Future research should explore combinatorial approaches involving Imatinib and MM-102 with existing chemotherapeutics to enhance therapeutic efficacy. These combinatorial strategies could potentially target multiple pathways simultaneously, improving outcomes and minimizing resistance.

- A comprehensive analysis of how these therapies affect the tumor microenvironment is crucial. This includes examining immune cell infiltration, angiogenesis, and stromal interactions, as these components play significant roles in tumor progression and therapy resistance.

- Utilizing patient-derived organoids and xenograft models, the therapeutic efficacy of the proposed treatments can be further validated under conditions that mimic human TNBC.

- *In vivo* investigations might help to improve the efficacy of the therapeutic modules.

- The role of the epigenetic regulators in other signaling pathways contributing to EMT may be studied in detail. This could uncover additional targets or mechanisms that contribute to TNBC progression.

TH-3600_196106022

- The proposed therapeutic strategies may be applicable to other aggressive cancers characterized by similar epigenetic dysregulation, such as pancreatic, ovarian, and lung cancers. Furthermore, establishing the role of crucial regulators like p300 and MLL1 in these cancers could provide a broader understanding of their contribution to EMT-driven cancer progression.

भारतीय प्रौद्योगिकी संस्थान गुवाहाटी • Indian Institute of Technology Guwahati •

TH-3600_196106022

Publications

Publications from the thesis work

1. **Shilpi Sarkar**, Dheepika Venkatesh, Thirukumaran Kandasamy, & Siddhartha Sankar Ghosh (2024). Epigenetic Modulations in Breast Cancer: An Emerging Paradigm in Therapeutic Implications. *Frontiers in Bioscience-Landmark*, 29(8), 287. https://doi.org/10.31083/j.fbl2908287

2. **Shilpi Sarkar**, Thirukumaran Kandasamy, Rajib Shome, & Siddhartha Sankar Ghosh (2023). In silico screening and identification of potential drug against p300 acetyltransferase activity in breast cancer via drug repurposing approach. Journal of *Biomolecular Structure and Dynamics*, 1-12. https://doi.org/10.1080/07391102.2023.2270086

3. **Shilpi Sarkar,** Thirukumaran Kandasamy, & Siddhartha Sankar Ghosh (2024). Imatinib Impedes EMT and Notch Signalling by Inhibiting p300 Acetyltransferase in Breast Cancer Cells. *Molecular Carcinogenesis*, 10.1002/mc.23848. Advance online publication. https://doi.org/10.1002/mc.23848

4. **Shilpi Sarkar,** Thirukumaran Kandasamy, & Siddhartha Sankar Ghosh (2025). Inhibition of the MLL1-WDR5 interaction modulates Epithelial to mesenchymal transition and metabolic pathways in triple-negative breast cancer cells. Biochemical and Biophysical Research Communications, 151559. https://doi.org/10.1016/j.bbrc.2025.151559

5. **Shilpi Sarkar,** & Siddhartha Sankar Ghosh (2024). Synergistic Effect of Salinomycin with Budesonide on TNBC Regression via EMT Reversal and Autophagy Induction. *Journal of Biochemical and Molecular Toxicology*, 38(11), e70045. https://doi.org/10.1002/jbt.70045

TH-3600_196106022

Other Publication

1. Book chapter: **Shilpi Sarkar**, Thirukumaran Kandasamy, Arisha Arora & Siddhartha Sankar Ghosh (2024). Covid 19 vaccine classification, development, and clinical status. (Chapter 17, *Springer Nature*, Book: Pathogenesis, Management and Socio-Economic Impact of COVID-19 Pandemic)

Publications from collaborative work

1. Santa Mondal, **Shilpi Sarkar**, Siddhartha Sankar Ghosh, & Abu Taleb Khan (2022). Regioselective Ring-Opening of Epoxide and N-Tosylaziridine with 4-Hydroxydithiocoumarin: Key Precursors for 2, 3-Dihydro-1, 4-oxathiin and 2, 3-Dihydro-1, 4-thiazine Derivatives. *European Journal of Organic Chemistry*, 2022(18), e202200355. https://doi.org/10.1002/ejoc.202200355

2. Anjela Xalxo, Ujjwal Jyoti Goswami, **Shilpi Sarkar**, Thirukumaran Kandasamy, Kriti Mehta, Siddhartha Sankar Ghosh, Prasad V. Bharatam & Abu Taleb Khan (2023). Synthesis of 3-sulfenylindole derivatives from 4-hydroxy-2H-chromene-2-thione and indole using oxidative cross-dehydrogenative coupling reaction and anti-proliferative activity study of some of their sulfone derivatives. *Bioorganic Chemistry*, *141*, 106900. https://doi.org/10.1016/j.bioorg.2023.106900

3. Rajib Shome, Plaboni Sen, **Shilpi Sarkar**, & Siddhartha Sankar Ghosh (2024). Single-cell transcriptomics reveals the intra-tumoral heterogeneity and SQSTM1/P62 and Wnt/β-catenin mediated epithelial to mesenchymal transition and stemness of triple-negative breast cancer. *Experimental Cell Research*, 114032. https://doi.org/10.1016/j.yexcr.2024.114032

4. Thirukumaran Kandasamy, **Shilpi Sarkar**, Plaboni Sen, Dheepika Venkatesh, & Siddhartha Sankar Ghosh (2024). Concurrent inhibition of IR, ITGB1, and CD36 perturbated the interconnected network of energy metabolism and epithelial-to-mesenchymal transition in breast cancer cells. *Journal of Cellular Biochemistry*. https://doi.org/10.1002/jcb.30574

TH-3600_196106022

5. Thirukumaran Kandasamy, **Shilpi Sarkar**, & Siddhartha Sankar Ghosh (2024). Harnessing Drug Repurposing to Combat Breast Cancer by Targeting Altered Metabolism and Epithelial-to-Mesenchymal Transition Pathways. *ACS Pharmacology & Translational Science.* https://pubs.acs.org/doi/10.1021/acsptsci.4c00545

6. Pallavi Barman, Roopjyoti Misra, Nikita Pal, **Shilpi Sarkar**, & Krishna P. Bhabak (2024). Synthetic Benzylic Diselenides and Disulfides: Potential Anticancer Activities via Modulation of the ROS-Dependent Akt/β-Catenin Signaling Pathway. *ChemMedChem*, e202400358. https://doi.org/10.1002/cmdc.202400358

7. Nikita Pal, Kaustav Banerjee, **Shilpi Sarkar,** Tapas K. Mandal & Krishna P. Bhabak (2024). Synthesis of Thiazolidinedione-and Triazole-Linked Organoselenocyanates and Evaluation of Anticancer Activities Against Breast Cancer with Mechanistic Investigations. Chemistry–A European Journal, e202403026. https://doi.org/10.1002/chem.202403026

8. Dheepika Venkatesh, Shilpi Sarkar, Thirukumaran Kandasamy, & Siddhartha Sankar Ghosh (2025). In-silico identification and validation of Silibinin as a dual inhibitor for ENO1 and GLUT4 to curtail EMT signaling and TNBC progression. Computational Biology and Chemistry, 115, 108312. https://doi.org/10.1016/j.compbiolchem.2024.108312

9. Thirukumaran Kandasamy, **Shilpi Sarkar**, & Siddhartha Sankar Ghosh (2024). The synergistic effects of Epirubicin-SAHA-Pimozide (ESP) drug cocktail: A promising strategy for effective breast cancer treatment. (Manuscript communicated)

10. Thirukumaran Kandasamy, **Shilpi Sarkar**, & Siddhartha Sankar Ghosh (2024). Synergistic Therapeutic Effects of Zn ions and Pimozide in Breast Cancer Cells. (Manuscript communicated)

11. Arisha Arora, **Shilpi Sarkar**, and Siddhartha Sankar Ghosh (2024). Targeting MELK with Repurposed Drugs for TNBC Therapy: Insights on Molecular Simulation and Experimental Validations. (Manuscript communicated)

TH-3600_196106022

Conferences

1. Presented poster on "Targeting p300 acetyltransferase activity in breast cancer via drug repurposing approach" in the poster session of 8th World Cancer Congress-2024, which has been scheduled from 18th to 20th march, 2024, at JNU convention center, New Delhi

2. Presented oral presentation on "Virtual screening and *in vitro* validation of potential repurposed drug against p300 acetyltransferase activity in breast cancer" in Research and Industrial conclave-integration'24 organized by students' academic board, IIT Guwahati, and IIT Guwahati research park. This has been scheduled from 09th to 11th august, 2024, at IIT Guwahati, assam, India.

3. Participated in the 7th international conference on advanced nanomaterials and nanotechnology (ICANN2021), organized by the centre for nanotechnology, IIT Guwahati, assam, India, during 14-17th december,2021.

4. Resource person in the offline workshop of "Hands-on Workshop on Basic Flow Cytometry" organized by BioNEST IIT Guwahati technology innovation and development foundation on January 18th ,2023.

TH-3600_196106022

Permissions

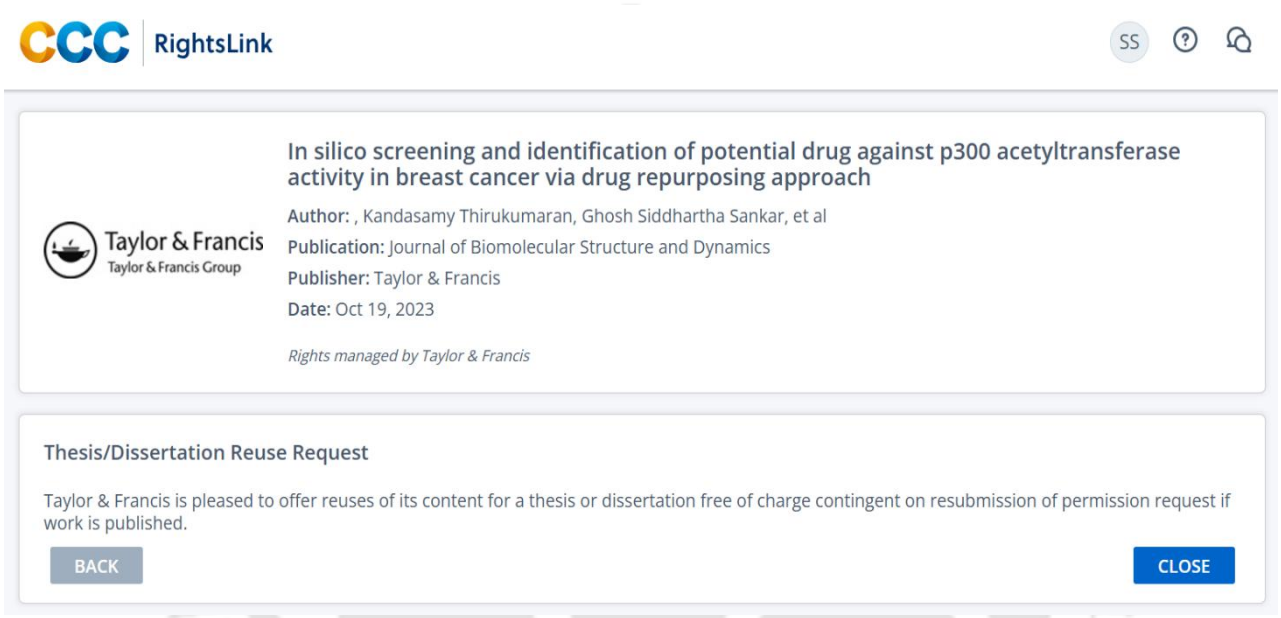

CCC RightsLink

SS

In silico screening and identification of potential drug against p300 acetyltransferase activity in breast cancer via drug repurposing approach

Taylor & Francis
Taylor & Francis Group

Author: , Kandasamy Thirukumaran, Ghosh Siddhartha Sankar, et al
Publication: Journal of Biomolecular Structure and Dynamics
Publisher: Taylor & Francis
Date: Oct 19, 2023

Rights managed by Taylor & Francis

Thesis/Dissertation Reuse Request

Taylor & Francis is pleased to offer reuses of its content for a thesis or dissertation free of charge contingent on resubmission of permission request if work is published.

BACK CLOSE

Indian Institute of Technology Guwahati

TH-3600_196106022

Dec 02, 2024

This Agreement between Shilpi Sarkar ("You") and John Wiley and Sons ("John Wiley and Sons") consists of your license details and the terms and conditions provided by John Wiley and Sons and Copyright Clearance Center.

License Number	5920710497117
License date	Dec 02, 2024
Licensed Content Publisher	John Wiley and Sons
Licensed Content Publication	Molecular Carcinogenesis
Licensed Content Title	Imatinib Impedes EMT and Notch Signalling by Inhibiting p300 Acetyltransferase in Breast Cancer Cells
Licensed Content Author	Shilpi Sarkar, Thirukumaran Kandasamy, Siddhartha Sankar Ghosh
Licensed Content Date	Nov 19, 2024
Licensed Content Volume	0
Licensed Content Issue	0
Licensed Content Pages	13
Type of use	Dissertation/Thesis
Requestor type	Author of this Wiley article
Format	Print and electronic

https://s100.copyright.com/AppDispatchServlet

TH-3600_196106022

Portion	Full article
Will you be translating?	No
Title of new work	phd thesis
Institution name	IIT Guwahati
Expected presentation date	Jan 2025
The Requesting Person / Organization to Appear on the License	Shilpi Sarkar
Requestor Location	Ms. Shilpi Sarkar IIT Guwahati Guwahati, ASSAM 781039 India
Publisher Tax ID	EU826007151
Total	0.00 USD

Terms and Conditions

Institute of Technology G

TH-3600_196106022

JOHN WILEY AND SONS LICENSE
TERMS AND CONDITIONS

Dec 02, 2024

This Agreement between Shilpi Sarkar ("You") and John Wiley and Sons ("John Wiley and Sons") consists of your license details and the terms and conditions provided by John Wiley and Sons and Copyright Clearance Center.

License Number	5920701198980
License date	Dec 02, 2024
Licensed Content Publisher	John Wiley and Sons
Licensed Content Publication	Journal of Biochemical and Molecular Toxicology
Licensed Content Title	Synergistic Effect of Salinomycin With Budesonide on TNBC Regression via EMT Reversal and Autophagy Induction
Licensed Content Author	Siddhartha Sankar Ghosh, Shilpi Sarkar
Licensed Content Date	Nov 11, 2024
Licensed Content Volume	38
Licensed Content Issue	11
Licensed Content Pages	18
Type of use	Dissertation/Thesis
Requestor type	Author of this Wiley article
Format	Print and electronic

TH-3600_196106022

Portion	Full article
Will you be translating?	No
Title of new work	phd thesis
Institution name	IIT Guwahati
Expected presentation date	Jan 2025
The Requesting Person / Organization to Appear on the License	Shilpi Sarkar
Requestor Location	Ms. Shilpi Sarkar IIT Guwahati Guwahati, ASSAM 781039 India
Publisher Tax ID	EU826007151
Total	0.00 USD
Terms and Conditions	

stitute of Technology

TH-3600_196106022